

Drivers of plant nutrient acquisition and allocation strategies and their influence
on plant responses to environmental change

by

Evan A. Perkowski, B.S.

A Dissertation

In

Biological Sciences

Submitted to the Graduate Faculty
of Texas Tech University in
Partial Fulfillment of
the Requirements for
the Degree of

Doctor of Philosophy

Approved

Nicholas G. Smith, Ph.D.
Chair of Committee

Aimée T. Classen, Ph.D.

Natasja van Gestel, Ph.D.

Lindsey C. Slaughter, Ph.D.

Dylan W. Schwilk, Ph.D.

Mark Sheridan, Ph.D.
Dean of the Graduate School

May 2023

Copyright 2023, Evan A. Perkowski

Acknowledgements

This dissertation was made possible by the mentorship, collaboration, and friendship of many people. I am so thankful to be surrounded by such supportive and helpful mentors, peers, and friends that have made navigating through graduate school and finishing this dissertation an enjoyable experience. Specifically, I am thankful for the incredible mentorship of my advisor and committee chair, Dr. Nick Smith, who provided invaluable insight and tools that have helped shape me into the plant ecophysiological I claim to be today. I am also indebted to my committee members, Drs. Aimée Classen, Natasja van Gestel, Dylan Schwilk, and Lindsey Slaughter, for useful feedback, invaluable support, and encouragement as I planned and implemented experiments.

I am also thankful for past and present members of the EcoHealth lab for encouragement, support, and extracurricular activities that made time inside and outside the lab enjoyable and memorable. Particular thanks go to Dr. Lizz Waring, Dr. Xiulin Gao, Helen Scott, and Risa McNellis, Billi Jean Petermann, and the late Dr. Kris Petterson, all of whom were invaluable to helping me navigate my first year. I am especially thankful for the mentorship and friendship of Dr. Lizz Waring, as our weekly coffee chats were instrumental for helping me feel welcome in Lubbock and acclimate to life as a graduate student. I am also grateful for the friendship of Billi Jean Petermann and the late Dr. Kris Petterson for their encouragement and willingness to discuss microbial symbioses over coffee on random Saturday mornings.

Additional thanks go out to Isa Beltran, Snehanjana Chatterjee, Jeff Chi-

eppa, Peter Eludini, Zinny Ezekannagha, Hannah German, Eve Gray, Monika Kelley, Azaj Mahmud, Jorge Ochoa, Brad Posch, Avery Schoenherr, Christine Vanginault, and Jose Villeda for help with experiments or for lending an ear over puzzling results. I am also thankful for collaborators Dr. Christy Goodale and Dave Frey, who provided invaluable insight for the second experimental chapter.

I would like to thank my undergraduate advisor, Dr. Janice Krumm, for continued mentorship and friendship and for insightful advice about navigating graduate school, but most of all for helping me realize my career aspirations and pushing me to pursue this endeavor. Additional thanks go out to my family, particularly my parents, partner, and dog for continued support and distractions outside the lab. The experiments included here would not have been possible without their emotional and monetary support.

This work was made possible from funding by the NSF, USDA, Braun and Gresham, PLLC., and was a contribution to the LEMONTREE (Land Ecosystem Models based On New Theory, obseRvations and ExperimEnts) project. The LEMONTREE project is funded through the generosity of Eric and Wendy Schmidt by recommendation of the Schmidt Futures programme and the Imperial College initiative on Grand Challenges in Ecosystems and the Environment. This work was also funded by graduate student research awards from Texas Tech University and the Botanical Society of America.

I have inevitably missed mentioning folks that were instrumental to the completion of these experiments and contributed to my development as a plant ecophysiological. Please know that I am grateful and appreciative of our interactions.

Table of Contents

Acknowledgements	ii
Abstract	ix
List of Tables	xi
List of Figures	xv
1. Introduction	1
2. Structural carbon costs to acquire nitrogen are determined by nitrogen and light availability in two species with different nitrogen acquisition strategies	7
2.1 Introduction	7
2.2 Methods	11
2.2.1 <i>Experiment setup</i>	11
2.2.2 <i>Plant measurements and calculations</i>	12
2.2.3 <i>Statistical analyses</i>	13
2.3 Results	15
2.3.1 <i>Carbon costs to acquire nitrogen</i>	15
2.3.2 <i>Whole plant nitrogen biomass</i>	18
2.3.3 <i>Root carbon biomass</i>	20
2.3.4 <i>Root nodule biomass</i>	22
2.4 Discussion	26
2.4.1 <i>Carbon costs to acquire nitrogen increase with light availability and decrease with fertilization</i>	26
2.4.2 <i>Modeling implications</i>	28
2.4.3 <i>Study limitations</i>	30
2.4.4 <i>Conclusions</i>	32
3. Soil nitrogen availability modifies leaf nitrogen economies in mature temperate deciduous forests: a direct test of photosynthetic least-cost theory	34
3.1 Introduction	34

3.2 Methods	38
3.2.1 <i>Study site description</i>	38
3.2.2 <i>Experimental design</i>	39
3.2.3 <i>Leaf gas exchange and trait measurements</i>	39
3.2.4 A_{net}/C_i curve-fitting and parameter estimation	42
3.2.5 Proportion of leaf nitrogen allocated to photosynthesis and structure	44
3.2.6 Tradeoffs between nitrogen and water use	45
3.2.7 Soil nitrogen availability and pH	46
3.2.8 Statistical analyses	48
3.3 Results	50
3.3.1 Leaf nitrogen content	50
3.3.2 Net photosynthesis and leaf biochemistry	53
3.3.3 Leaf nitrogen allocation	56
3.3.4 Tradeoffs between nitrogen and water use	59
3.4 Discussion	62
3.4.1 Soil nitrogen availability modifies tradeoffs between nitrogen and water use	63
3.4.2 Soil pH did not modify tradeoffs between nitrogen and water usage	65
3.4.3 Species identity explains a large amount of variation in leaf and whole plant traits	66
3.4.4 Implications for photosynthetic least-cost theory model development	67
3.4.5 Conclusions	69
4. The relative cost of resource use for photosynthesis drives variance in leaf nitrogen content across a climate and soil resource availability gradient	70
4.1 Introduction	70
4.2 Methods	76
4.2.1 Site descriptions and sampling methodology	76

4.2.2	<i>Leaf trait measurements</i>	77
4.2.3	<i>Site climate data</i>	82
4.2.4	<i>Site edaphic characteristics</i>	82
4.2.5	<i>Plant functional group assignments</i>	84
4.2.6	<i>Data analysis</i>	85
4.3	Results	88
4.3.1	<i>Cost to acquire nitrogen relative to water</i>	88
4.3.2	<i>Leaf $C_i:C_a$</i>	91
4.3.3	<i>Leaf nitrogen content</i>	94
4.3.4	<i>Structural equation model</i>	98
4.4	Discussion	101
4.4.1	<i>Negative effects of leaf $C_i:C_a$ on N_{area} are driven by reductions in M_{area}, not N_{mass}</i>	101
4.4.2	<i>Soil nitrogen availability increases N_{area} through changes in β</i>	103
4.4.3	<i>Soil moisture increases N_{area} by facilitating increases in soil nitrogen availability</i>	104
4.4.4	<i>Indirect effects of climate on N_{area} are mediated through changes in leaf $C_i:C_a$ and β</i>	105
4.4.5	<i>Species identity traits modify effects of the environment on β, leaf $C_i:C_a$, and N_{area}</i>	106
4.4.6	<i>Next steps for optimality model development</i>	107
4.4.7	<i>Conclusions</i>	108
5.	Optimal resource investment to photosynthetic capacity maximizes nutrient allocation to whole plant growth under elevated CO₂	110
5.1	Introduction	110
5.2	Methods	115
5.2.1	<i>Seed treatments and experimental design</i>	115
5.2.2	<i>Growth chamber conditions</i>	116
5.2.3	<i>Leaf gas exchange measurements</i>	118

5.2.4 <i>Leaf trait measurements</i>	119
5.2.5 <i>A/C_i curve fitting and parameter estimation</i>	121
5.2.6 <i>Stomatal limitation</i>	122
5.2.7 <i>Proportion of leaf nitrogen allocated to photosynthesis and structure</i>	122
5.2.8 <i>Whole plant traits</i>	124
5.2.9 <i>Statistical analyses</i>	126
5.3 Results	128
5.3.1 <i>Leaf nitrogen and chlorophyll content</i>	128
5.3.2 <i>Leaf biochemistry and stomatal conductance</i>	132
5.3.3 <i>Leaf nitrogen allocation</i>	136
5.3.4 <i>Whole plant traits</i>	140
5.3.5 <i>Nitrogen fixation</i>	144
5.4 Discussion	148
5.4.1 <i>Soil nitrogen fertilization has divergent effects on leaf and whole plant acclimation responses to CO₂</i>	149
5.4.2 <i>Implications for future model development</i>	152
5.4.3 <i>Study limitations and future directions</i>	154
5.4.4 <i>Conclusions</i>	155
6. Conclusions	157
References	167
Appendix A: Supplemental material for "Structural carbon costs to acquire nitrogen are determined by nitrogen and light availability in two species with different nitrogen acquisition strategies"	204
Appendix B: Supplemental material for "Soil nitrogen availability modifies leaf nitrogen economies in mature temperate deciduous forests: a direct test of photosynthetic least-cost theory"	208

Appendix C: Supplemental material for "The relative cost of resource use for photosynthesis drives variance in leaf nitrogen content across a climate and soil resource availability gradient"	213
Appendix D: Supplemental material for "Optimal resource investment to photosynthetic capacity maximizes nutrient allocation to whole plant growth under elevated CO₂" . . .	220

Abstract

Photosynthesis is the largest carbon flux between the atmosphere and is constrained by ecosystem carbon and nutrient cycle dynamics, which causes terrestrial biosphere models to be sensitive to the formulation of photosynthetic processes. Terrestrial biosphere models exhibit high divergence in simulated carbon and nitrogen fluxes under future environmental conditions, which may be due to uncertainty in the acclimation response of photosynthetic processes to environmental change. Photosynthetic least-cost theory provides a promising framework for understanding effects of climatic and edaphic factors on photosynthetic acclimation responses to changing environments. Yet, empirical tests of the theory are rare, limiting our ability to assess whether the theory is suitable for implementation in next-generation terrestrial biosphere models.

Here, I present four experiments designed to test assumptions of photosynthetic least-cost theory. Experiment chapters are flanked by a general introduction chapter and conclusions chapter. The first experimental chapter quantifies structural carbon costs to acquire nitrogen in *Glycine max* and *Gossypium hirsutum* grown under four nitrogen fertilization levels and four light availability levels in a full factorial greenhouse experiment. I find that carbon costs to acquire nitrogen in both species increase with increasing light availability and decrease with increasing fertilization, though responses to fertilization in *G. max* were markedly less than *G. hirsutum*. The second experimental chapter quantifies leaf nitrogen and photosynthetic traits in upper canopy leaves of deciduous trees growing in a 9-year nitrogen-by-sulfur field manipulation experiment. I find strong evi-

dence for nitrogen-water use tradeoffs with increasing soil nitrogen availability, evidenced through a strong negative relationship between leaf nitrogen content and leaf $C_i:C_a$ and stronger increase in leaf nitrogen content with increasing soil nitrogen availability than leaf $C_i:C_a$. The third experiment investigates variance in leaf nitrogen content across a climate and soil resource availability gradient in Texan grasslands, showing that effects of soil resource availability and climate on leaf nitrogen content are driven by changes in leaf $C_i:C_a$. Finally, the fourth experiment quantifies leaf and whole plant acclimation responses in *G. max* grown under two atmospheric CO₂ levels, with and without inoculation with *Bradyrhizobium japonicum*, and across nine nitrogen fertilization treatments in a full factorial growth chamber experiment. I find that leaf acclimation responses to CO₂ were independent of soil nitrogen fertilization or inoculation treatment, though stimulations in whole plant growth under elevated CO₂ were enhanced with increasing soil nitrogen fertilization and in inoculated pots under low nitrogen fertilization.

Experiments included in this dissertation provide consistent support for patterns expected from photosynthetic least-cost theory. The use of multiple experimental approaches allowed me to examine mechanisms driving patterns expected from the theory and investigate whether these patterns occur in the field across environmental gradients. Findings from these chapters challenge common paradigms in plant ecophysiology, providing empirical evidence suggesting that including photosynthetic least-cost frameworks in terrestrial biosphere models may improve the longstanding observed divergence in simulated outcomes across terrestrial biosphere model products.

List of Tables

2.1	Analysis of variance results exploring species-specific effects of light availability, nitrogen fertilization, and their interactions on carbon costs to acquire nitrogen, whole-plant nitrogen biomass, and root carbon biomass	16
2.2	Analysis of variance results exploring effects of light availability, nitrogen fertilization, and their interactions on <i>G. max</i> root nodule biomass and the ratio of root nodule biomass to root biomass	23
2.3	Slopes of the regression line describing the relationship between each dependent variable and nitrogen fertilization at each light level	24
3.1	Effects of soil nitrogen availability, soil pH, and species on leaf nitrogen content per unit leaf area, leaf nitrogen content per unit leaf mass, and leaf mass per unit leaf area	51
3.2	Effects of soil nitrogen availability, soil pH, species, and N_{area} on net photosynthesis, the maximum rate of Rubisco carboxylation, the maximum rate of RuBP regeneration, and the ratio of the maximum rate of RuBP regeneration to the maximum rate of Rubisco carboxylation	54
3.3	Effects of soil nitrogen availability, soil pH, and species on the proportion of leaf nitrogen content allocated to photosynthesis, Rubisco, bioenergetics, and structure	57

3.4 Effects of soil nitrogen availability, soil pH, species, and N_{area} on χ , photosynthetic nitrogen use efficiency, leaf nitrogen content per unit χ , and maximum Rubisco carboxylation rate per unit χ	60
4.1 Site locality information, sampling year, 2006-2020 mean annual precipitation, mean annual temperature, and water holding capacity	80
4.2 Effects of soil moisture, soil nitrogen availability, and plant functional group on β	89
4.3 Effects of soil moisture, soil nitrogen availability, and plant functional group on leaf $C_i:C_a$	92
4.4 Effects of soil moisture, soil nitrogen availability, plant functional group, and leaf $C_i:C_a$ on leaf nitrogen content per unit leaf area, leaf nitrogen content per unit leaf biomass, and leaf biomass per unit leaf area	96
4.5 Structural equation model results investigating direct effects of climatic and soil resource availability on leaf nitrogen content	99
5.1 Effects of soil nitrogen fertilization, inoculation, and CO ₂ treatments on leaf nitrogen content per unit leaf area, leaf nitrogen content per unit leaf mass, leaf mass per unit leaf area, and chlorophyll content per unit leaf area	130

5.2	Effects of soil nitrogen fertilization, inoculation, and CO ₂ on the maximum rate of Rubisco carboxylation, the maximum rate of RuBP regeneration, dark respiration, the ratio of the maximum rate of RuBP regeneration to the maximum rate of Rubisco carboxylation, stomatal conductance, and stomatal limitation	134
5.3	Effects of soil nitrogen fertilization, inoculation, and CO ₂ on the fraction of leaf nitrogen allocated to Rubisco, bioenergetics, light harvesting proteins, photosynthesis, and structure	138
5.4	Effects of CO ₂ , fertilization, and inoculation on total leaf area, whole plant biomass, carbon costs to acquire nitrogen, belowground carbon biomass, and whole plant nitrogen biomass	142
5.5	Effects of CO ₂ , fertilization, and inoculation on root nodule biomass, plant investments in symbiotic nitrogen fixation, and percent nitrogen fixed from the atmosphere	146
A1	Summary table containing volumes of compounds used to create modified Hoagland's solutions for each soil nitrogen fertilization treatment	204
A2	Analysis of variance results exploring species-specific effects of light availability, nitrogen fertilization, and their interactions on the ratio of whole plant biomass to pot volume	205
A3	Slopes of the regression line describing the relationship between each dependent variable and nitrogen fertilization at each light level	206

B1	Sample sizes of each species, abbreviated by their USDA NRCS PLANTS database code, within each plot at each site	208
B2	Analysis of variance results exploring the linear effect of leaf temperature on net photosynthesis rate and stomatal conductance measured at 400 $\mu\text{mol mol}^{-1}$ CO ₂	209
B3	Second order log-polynomial regression coefficients that described the effect of leaf temperature on net photosynthesis and stomatal conductance measured at 400 $\mu\text{mol mol}^{-1}$ CO ₂	210
B4	Mean, standard error, and 95% confidence interval ranges of soil nitrogen availability estimates across all measured plots	211
C1	List of sampled species and their plant functional group assignment	215
C2	List of sampled species and their plant functional group assignment (cont.)	216
C3	List of sampled species and their plant functional group assignment (cont.)	217
C4	Model selection results for soil moisture and vapor pressure deficit	218
D1	Summary table containing volumes of compounds used to create modified Hoagland's solutions for each soil nitrogen fertilization treatment	220
D2	Summary of the daily growth chamber growing condition program	221
D3	Effects of CO ₂ , fertilization, and inoculation on whole plant biomass: pot volume	222

List of Figures

2.1 Relationships between soil nitrogen fertilization and light availability on carbon costs to acquire nitrogen in <i>G. hirsutum</i> and <i>G. max</i>	17
2.2 Relationships between soil nitrogen fertilization and light availability on whole-plant nitrogen biomass in <i>G. hirsutum</i> and <i>G. max</i>	19
2.3 Relationships between soil nitrogen fertilization and light availability on root carbon biomass in <i>G. hirsutum</i> and <i>G. max</i>	21
2.4 Effects of shade cover and nitrogen fertilization on root nodule biomass and the ratio of root nodule biomass to root biomass in <i>G. max</i>	25
3.1 Effects of soil nitrogen availability and species on leaf nitrogen content per unit leaf area, leaf nitrogen content per unit leaf biomass, and leaf mass per leaf area	52
3.2 Effects of soil nitrogen availability, species, and leaf nitrogen content on net photosynthesis, maximum Rubisco carboxylation rate, and maximum RuBP regeneration rate	55
3.3 Effects of soil nitrogen availability, species, and leaf nitrogen content on the fraction of leaf nitrogen allocated to photosynthesis and structure	58
3.4 Effects of soil N availability, species, and leaf N content on tradeoffs between nitrogen and water use	61

4.1	Site locations along 2006-2020 mean annual precipitation and mean annual temperature gradients in Texas, USA.	81
4.2	Effects of soil nitrogen availability and soil moisture on the cost of acquiring and using nitrogen	90
4.3	Effects of 4-day mean vapor pressure deficit, 2-day soil moisture (per water holding capacity), and soil nitrogen availability on leaf $C_i:C_a$	93
4.4	Effects of leaf $C_i:C_a$, soil nitrogen availability, and soil moisture on leaf nitrogen content per unit leaf area, leaf nitrogen content per unit leaf biomass, and leaf mass per area.	97
4.5	Structural equation model results exploring drivers of N_{area}	100
5.1	Effects of CO_2 , fertilization, and inoculation on leaf nitrogen per unit leaf area, leaf nitrogen content, leaf mass per unit leaf area, and chlorophyll content per unit leaf area	131
5.2	Effects of CO_2 , fertilization, and inoculation on maximum rate of Rubisco carboxylation, the maximum rate of RuBP regeneration, and the ratio of the maximum rate of RuBP regeneration to the maximum rate of Rubisco carboxylation leaf mass per unit leaf area, dark respiration, stomatal conductance, and stomatal limitation .	135
5.3	Effects of CO_2 , fertilization, and inoculation on the relative fraction of leaf nitrogen allocated to photosynthesis and the fraction of leaf nitrogen allocated to structure	139

5.4	Effects of CO ₂ , fertilization, and inoculation on total leaf area, total biomass, and structural carbon costs to acquire nitrogen	143
5.5	Effects of CO ₂ , fertilization, and inoculation on nodule biomass, nodule biomass: root biomass, and percent nitrogen fixed from the atmosphere	147
A1	Effects of shade cover and nitrogen fertilization on the ratio of plant biomass to rooting volume in <i>G. hirsutum</i> and <i>G. max</i>	207
B1	Effects of leaf temperature on net photosynthesis rate and stomatal conductance values when measured at 400 μmol mol ⁻¹ CO ₂ . . .	212
C1	Model selection results exploring relevant timescales for soil moisture and vapor pressure deficit	219
D1	Relationships between area-based leaf nitrogen content, mass-based leaf nitrogen content, and leaf mass per unit leaf area measured on the focal leaf used to generate A_{net}/C_i curves and leaf nitrogen content measured on the leaf used for chlorophyll extractions . . .	223
D2	Effects of CO ₂ , fertilization, and inoculation on the ratio of whole plant biomass to pot volume	224

1 Chapter 1

2 Introduction

3 Photosynthesis represents the largest carbon flux between the atmosphere
4 and biosphere, and is regulated by complex ecosystem carbon and nutrient cy-
5 cles (Hungate et al. 2003; IPCC 2021). As a result, the inclusion of robust,
6 empirically tested representations of photosynthetic processes is critical in order
7 for terrestrial biosphere models to accurately and reliably simulate carbon and
8 nutrient fluxes between the atmosphere and terrestrial biosphere (Oreskes et al.
9 1994; Smith and Dukes 2013; Prentice et al. 2015; Wieder et al. 2015). Despite
10 evidence that the inclusion of coupled carbon and nutrient cycles can improve
11 model uncertainty, widespread divergence in predicted carbon and nutrient fluxes
12 is still apparent across model products (Friedlingstein et al. 2014; Arora et al.
13 2020; Davies-Barnard et al. 2020). Divergence in predicted carbon and nutrient
14 fluxes across terrestrial biosphere models may be due to an incomplete under-
15 standing of how plants acclimate to changing environments (Smith and Dukes
16 2013; Davies-Barnard et al. 2020), as terrestrial biosphere models are sensitive to
17 the formulation of photosynthetic processes (Bonan et al. 2011; Ziehn et al. 2011;
18 Booth et al. 2012; Smith et al. 2016; Smith et al. 2017; Rogers et al. 2017).

Many terrestrial biosphere models predict leaf-level photosynthesis through linear relationships between area-based leaf nitrogen content and the maximum rate of Ribulose-1,5-bisphosphate carboxylase/oxygenase (“Rubisco”), following the idea that large fractions of leaf nitrogen content are allocated to the construction and maintenance of Rubisco and other photosynthetic enzymes (Evans

24 1989). The inclusion of coupled carbon and nutrient cycles in terrestrial bio-
25 sphere models (Shi et al. 2016; Braghieri et al. 2022) allows for the prediction
26 of leaf nitrogen content through soil nitrogen availability, which causes models to
27 indirectly predict photosynthetic processes through shifts in soil nitrogen avail-
28 ability (Smith et al. 2014; Lawrence et al. 2019). While these patterns are
29 commonly observed in ecosystems globally (Brix 1971; Evans 1989; Firn et al.
30 2019; Liang et al. 2020), this formulation does not allow for the prediction of
31 leaf and whole plant acclimation responses to changing environments (Smith and
32 Dukes 2013; Rogers et al. 2017; Harrison et al. 2021), and suggests that constant
33 leaf nitrogen-photosynthesis relationships are ubiquitous across ecosystems.

34 Photosynthetic least-cost theory (Prentice et al. 2014; Wang et al. 2017;
35 Smith et al. 2019; Paillassa et al. 2020; Scott and Smith 2022; Harrison et al.
36 2021) provides a contemporary framework for predicting leaf and whole plant ac-
37 climation responses to environmental change. The theory, which unifies optimal
38 coordination (Chen et al. 1993; Maire et al. 2012) and least-cost (Wright et al.
39 2003) theories, posits that plants optimize photosynthetic processes by minimizing
40 the summed cost of nutrient and water use (i.e., β). The summed cost of nutrient
41 and water use is predicted to be positively correlated with the ratio of intercellular
42 CO₂ to atmospheric CO₂ (leaf $C_i:C_a$). Leaf $C_i:C_a$ is determined by factors that
43 influence leaf nutrient demand, such as CO₂, temperature, vapor pressure deficit,
44 and light availability (Prentice et al. 2014; Wang et al. 2017; Smith et al. 2019;
45 Stocker et al. 2020), and may change in response to changing edaphic charac-
46 teristics through changes in β (Paillassa et al. 2020). Photosynthetic processes
47 are optimized such that nutrients and water are allocated to photosynthetic en-

48 zymes to allow net photosynthesis rates to be equally co-limited by the maximum
49 rate of Rubisco carboxylation and the maximum rate of Ribulose-1,5-bisphosphate
50 (RuBP) regeneration (Chen et al. 1993; Maire et al. 2012). The theory indicates
51 that costs of nutrient and water use are substitutable such that, in a given en-
52 vironment, optimal photosynthesis rates can be achieved by sacrificing inefficient
53 use of a relatively more abundant (and less costly to acquire) resource for more
54 efficient use of a relatively less abundant (and more costly to acquire) resource.

55 Optimality models leveraging patterns expected from photosynthetic least-
56 cost theory have been developed for both C₃ (Wang et al. 2017; Smith et al. 2019;
57 Stocker et al. 2020) and more recently for C₄ species (Scott and Smith 2022).
58 Such models show broad agreement with patterns observed across environmental
59 gradients (Smith et al. 2019; Stocker et al. 2020; Paillassa et al. 2020; Querejeta
60 et al. 2022; Westerband et al. 2023), and are capable of reconciling dynamic
61 leaf nitrogen-photosynthesis relationships and acclimation responses to elevated
62 CO₂, temperature, light availability, and vapor pressure deficit (Dong et al. 2017;
63 Dong et al. 2020; Smith and Keenan 2020; Luo et al. 2021; Peng et al. 2021;
64 Dong et al. 2022; Dong et al. 2022; Querejeta et al. 2022; Westerband et al.
65 2023). Current versions of optimality models that invoke patterns expected from
66 photosynthetic least-cost theory hold β constant across growing environments.
67 As growing evidence suggests that costs of nutrient use change across resource
68 availability and climatic gradients in species with different nutrient acquisition
69 strategies (Fisher et al. 2010; Brzostek et al. 2014; Terrer et al. 2018; Allen et al.
70 2020), one might expect that β should dynamically change across environments
71 and in species with different nutrient acquisition strategies.

72 Despite recent recognition that patterns expected from photosynthetic
73 least-cost theory occur across broad environmental gradients, a limited number
74 of studies have investigated how β varies across edaphic and climatic gradients
75 and how variance in β might scale to influence leaf nutrient-water use tradeoffs
76 (Lavergne et al. 2020; Paillassa et al. 2020). Furthermore, no previous study has
77 investigated whether β varies in species with different nutrient acquisition strate-
78 gies, or if changes in β due to changes in edaphic characteristics scale to influence
79 leaf or whole plant acclimation responses to changing environments. The lack of
80 such studies provided motivation for the experimental chapters included in this
81 dissertation.

82 In this dissertation, I use a combination of greenhouse, field manipulation,
83 environmental gradient, and growth chamber experiments to quantify leaf and
84 whole plant acclimation responses across various climatic and edaphic conditions
85 and different nutrient acquisition strategies. Together, these experiments eval-
86 uated patterns expected from photosynthetic least-cost theory and test mechanisms
87 predicted to drive responses expected from theory. The empirical data collected
88 in these experiments provide important information needed to refine existing opti-
89 mality models that include photosynthetic least-cost frameworks, and could help
90 determine whether such models are suitable for implementing in next-generation
91 terrestrial biosphere models. While theory suggests that plants acclimate across
92 environments by minimizing the summed cost of nutrients relative to water, I chose
93 to isolate effects of soil nitrogen availability on costs of nitrogen acquisition rela-
94 tive to water for the sake of brevity. I acknowledge that patterns expected from
95 theory may be modified by other nutrients (e.g., phosphorus) or other edaphic

96 characteristics (Smith et al. 2019; Paillassa et al. 2020; Westerband et al. 2023),
97 and, though not included here, should also be investigated.

98 In the first experimental chapter, I re-analyze data from a greenhouse ex-
99 periment that grew *Glycine max* and *Gossypium hirsutum* seedlings under full-
100 factorial combinations of four light treatments and four fertilization treatments
101 to examine effects of nitrogen and light availability on structural carbon costs to
102 acquire nitrogen. In the second experimental chapter, I measure leaf physiological
103 traits in the upper canopy of mature trees growing in a 9-year nitrogen-by-pH
104 field manipulation experiment to assess whether changes in soil nitrogen availabil-
105 ity or soil pH modify nitrogen-water use trade-offs expected from photosynthetic
106 least-cost theory. The third experimental chapter leverages a broad precipitation
107 and soil nitrogen availability gradient in Texan grasslands to investigate primary
108 drivers of leaf nitrogen content. In the fourth experimental chapter, I use growth
109 chambers to quantify leaf and whole plant acclimation responses to CO₂ across
110 a soil nitrogen fertilization gradient, while also manipulating nutrient acquisition
111 strategy by controlling whether seedlings were able to form associations with sym-
112 biotic nitrogen-fixing bacteria.

113 Across experiments, I find strong and consistent support for patterns ex-
114 pected from photosynthetic least-cost theory, showing that shifts in edaphic char-
115 acteristics predictably alter β , and that shifts in β facilitate changes in leaf
116 nitrogen-water use tradeoffs and leaf nitrogen-photosynthesis relationships. I also
117 show that costs of nitrogen acquisition vary in species with different nitrogen
118 acquisition strategies. Finally, I show strong evidence suggesting that leaf accli-
119 mation responses to elevated CO₂ are decoupled from soil nitrogen availability and

120 inoculation with symbiotic nitrogen-fixing bacteria. It is my hope that these ex-
121 periments will encourage future iterations of optimality models that adopt photo-
122 synthetic least-cost frameworks to consider frameworks for implementing dynamic
123 β values across soil resource availability gradients and in species with different nu-
124 trient acquisition strategies.

125 The four experimental chapters included in this dissertation are presented
126 either as previously published journal articles or as manuscript drafts currently
127 in preparation for journal submission. Specifically, the first experimental chapter
128 was published in *Journal of Experimental Botany* in 2021 and the second chapter
129 is currently in review, while the third and fourth chapters are each in preparation
130 for journal submission. The dissertation concludes with a sixth chapter that sum-
131 marizes experiment findings, briefly synthesizes common themes observed across
132 experiments, and provides some suggestions for future experimentation.

133

Chapter 2

134

Structural carbon costs to acquire nitrogen are determined by
135 nitrogen and light availability in two species with different nitrogen
136 acquisition strategies

137 Perkowski EA, EF Waring, NG Smith, "Root mass carbon costs to acquire nitro-
138 gen are determined by nitrogen and light availability in two species with different
139 nitrogen acquisition strategies", *Journal of Experimental Botany*, 2021, Volume
140 72, Issue 15, Pages 5766-5776, by permission of Oxford University Press

141 2.1 Introduction

142 Carbon and nitrogen cycles are tightly coupled in terrestrial ecosystems. This
143 tight coupling influences photosynthesis (Walker et al. 2014; Rogers et al. 2017),
144 net primary productivity (LeBauer and Treseder 2008; Thomas et al. 2013), de-
145 composition (Cornwell et al. 2008; Bonan et al. 2013; Sulman et al. 2019), and
146 plant resource competition (Gill and Finzi 2016; Xu-Ri and Prentice 2017). Ter-
147 restrial biosphere models are beginning to include connected carbon and nitrogen
148 cycles to improve the realism of their simulations (Fisher et al. 2010; Brzostek
149 et al. 2014; Wieder et al. 2015; Shi et al. 2016; Zhu et al. 2019). Simula-
150 tions from these models indicate that coupling carbon and nitrogen cycles can
151 drastically influence future biosphere-atmosphere feedbacks under global change,
152 such as elevated carbon dioxide or nitrogen deposition (Thornton et al. 2007;
153 Goll et al. 2012; Wieder et al. 2015; Wieder et al. 2019). Nonetheless, there
154 are still limitations in our quantitative understanding of connected carbon and
155 nitrogen dynamics (Thomas et al. 2015; Meyerholt et al. 2016; Rogers et al.
156 2017; Exbrayat et al. 2018; Shi et al. 2019), forcing models to make potentially
157 unreliable assumptions.

158 Plant nitrogen acquisition is a process in terrestrial ecosystems by which
159 carbon and nitrogen are tightly coupled (Vitousek and Howarth 1991; Delaire
160 et al. 2005; Brzostek et al. 2014). Plants must allocate photosynthetically de-
161 rived carbon belowground to produce and maintain root systems or exchange with
162 symbiotic soil microbes in order to acquire nitrogen (Högberg et al. 2008; Hög-
163 berg et al. 2010). Thus, plants have an inherent carbon cost associated with
164 acquiring nitrogen, which can include both direct energetic costs associated with
165 nitrogen acquisition and indirect costs associated with building structures that
166 support nitrogen acquisition (Gutschick 1981; Rastetter et al. 2001; Vitousek
167 et al. 2002; Menge et al. 2008). Model simulations (Fisher et al. 2010; Brzostek
168 et al. 2014; Shi et al. 2016; Allen et al. 2020) and meta-analyses (Terrer et al.
169 2018) suggest that these carbon costs vary between species, particularly those
170 with different nitrogen acquisition strategies. For example, simulations using iter-
171 ations of the Fixation and Uptake of Nitrogen (FUN) model indicate that species
172 that acquire nitrogen from non-symbiotic active uptake pathways (e.g. mass flow)
173 generally have larger carbon costs to acquire nitrogen than species that acquire
174 nitrogen through symbiotic associations with nitrogen-fixing bacteria (Brzostek
175 et al. 2014; Allen et al. 2020).

176 Carbon costs to acquire nitrogen likely vary in response to changes in soil
177 nitrogen availability. For example, if the primary mode of nitrogen acquisition
178 is through non-symbiotic active uptake, then nitrogen availability could decrease
179 carbon costs to acquire nitrogen as a result of increased per-root nitrogen up-
180 take (Franklin et al. 2009; Wang et al. 2018). However, if the primary mode of
181 nitrogen acquisition is through symbiotic active uptake, then nitrogen availabil-

182 ity may incur additional carbon costs to acquire nitrogen if it causes microbial
183 symbionts to shift toward parasitism along the parasitism–mutualism continuum
184 (Johnson et al. 1997; Hoek et al. 2016; Friel and Friesen 2019) or if it reduces
185 the nitrogen acquisition capacity of a microbial symbiont (van Diepen et al. 2007;
186 Soudzilovskaia et al. 2015; Muñoz et al. 2016). Species may respond to shifts in
187 soil nitrogen availability by switching their primary mode of nitrogen acquisition
188 to a strategy with lower carbon costs to acquire nitrogen in order to maximize
189 the magnitude of nitrogen acquired from a belowground carbon investment and
190 outcompete other individuals for soil resources (Rastetter et al. 2001; Menge et al.
191 2008).

192 Environmental conditions that affect demand to acquire nitrogen to sup-
193 port new and existing tissues could also be a source of variance in plant carbon
194 costs to acquire nitrogen. For example, an increase in plant nitrogen demand could
195 increase carbon costs to acquire nitrogen if this increases the carbon that must be
196 allocated belowground to acquire a proportional amount of nitrogen (Kulmatiski
197 et al. 2017; Noyce et al. 2019). This could be driven by a temporary state of
198 diminishing return associated with investing carbon toward building and main-
199 taining structures that are necessary to support enhanced nitrogen uptake, such
200 as fine roots (Matamala and Schlesinger 2000; Norby et al. 2004; Arndal et al.
201 2018), mycorrhizal hyphae (Saleh et al. 2020), or root nodules (Parvin et al.
202 2020). Alternatively, if the environmental factor that increases plant nitrogen de-
203 mand causes nitrogen to become more limiting in the system (e.g. atmospheric
204 CO₂) (Luo et al. 2004; LeBauer and Treseder 2008; Vitousek et al. 2010; Liang
205 et al. 2016), species might switch their primary mode of nitrogen acquisition to

206 a strategy with lower relative carbon costs to acquire nitrogen in order to gain a
207 competitive advantage over species with either different or more limited modes of
208 nitrogen acquisition (Ainsworth and Long 2005; Taylor and Menge 2018).

209 Using a plant economics approach, I examined the influence of plant ni-
210 trogen demand and soil nitrogen availability on plant carbon costs to acquire
211 nitrogen. This was done by growing a species capable of forming associations
212 with nitrogen-fixing bacteria (*Glycine max* L. (Merr)) and a species not capable
213 of forming these associations (*Gossypium hirsutum* L.) under four levels of light
214 availability (plant nitrogen demand proxy) and four levels of soil nitrogen fertil-
215 ization (soil nitrogen availability proxy) in a full-factorial, controlled greenhouse
216 experiment. I used this experimental set-up to test the following hypotheses:

- 217 1. An increase in plant nitrogen demand due to increasing light availability will
218 increase carbon costs to acquire nitrogen through a proportionally larger
219 increase in belowground carbon than whole-plant nitrogen acquisition. This
220 will be the result of an increased investment of carbon toward belowground
221 structures that support enhanced nitrogen uptake, but at a lower nitrogen
222 return.
- 223 2. An increase in soil nitrogen availability will decrease carbon costs to acquire
224 nitrogen as a result of increased per root nitrogen uptake in *G. hirsutum*.
225 However, soil nitrogen availability will not affect carbon costs to acquire
226 nitrogen in *G. max* because of the already high return of nitrogen supplied
227 through nitrogen fixation.

228 2.2 Methods

229 2.2.1 *Experiment setup*

230 *Gossypium hirsutum* and *G. max* were planted in individual 3 liter pots (NS-300; **231** Nursery Supplies, Orange, CA, USA) containing a 3:1 mix of unfertilized potting **232** mix (Sungro Sunshine Mix #2, Agawam, MA, USA) to native soil extracted from **233** an agricultural field most recently planted with *G. max* at the USDA-ARS Lab-**234** oratory in Lubbock, TX, USA (33.59°N, -101.90°W). The field soil was classified **235** as Amarillo fine sandy loam (75% sand, 10% silt, 15% clay). Upon planting, **236** all *G. max* pots were inoculated with *Bradyrhizobium japonicum* (Verdesian N-**237** Dure™ Soybean, Cary, NC, USA) to stimulate root nodulation. Individuals of **238** both species were grown under similar, unshaded, ambient greenhouse conditions **239** for 2 weeks to germinate and begin vegetative growth.

240 Three blocks were set up in the greenhouse, each containing four light **241** treatments created using shade cloth that reduced incoming radiation by either 0 **242** (full sun), 30, 50, or 80%. Two weeks post-germination, individuals were randomly **243** placed in the four light treatments in each block. Individuals received one of four **244** nitrogen fertilization doses as 100mL of a modified Hoagland solution (Hoagland **245** and Arnon 1950) equivalent to either 0, 70, 210, or 630 ppm N twice per week **246** within each light treatment. Nitrogen fertilization doses were received as topical **247** agents to the soil surface. Each Hoagland solution was modified to keep concen-**248** trations of other macro- and micronutrients equivalent (Table A1). Plants were **249** routinely well watered to eliminate water stress.

250 2.2.2 *Plant measurements and calculations*

251 Each individual was harvested after 5 weeks of treatment, and biomass was sepa-
252 rated by organ type (leaves, stems, and roots). Nodules on *G. max* roots were also
253 harvested. Except for the 0% shade cover and 630 ppm N treatment combination,
254 all treatment combinations in both species had lower average dry biomass:pot vol-
255 ume ratios than the 1:1 ratio recommended by Poorter et al. (2012) to minimize
256 the likelihood of pot volume-induced growth limitation (Table A2, A3; Fig. A1).

257 All harvested material was dried, weighed, and ground by organ type.
258 Carbon and nitrogen content (g g^{-1}) was determined by subsampling from ground
259 and homogenized biomass of each organ type using an elemental analyzer (Costech
260 4010; Costech, Inc., Valencia, CA, USA). I scaled these values to total leaf, stem,
261 and root carbon and nitrogen biomass (g) by multiplying dry biomass of each
262 organ type by carbon or nitrogen content of each corresponding organ type. Whole
263 plant nitrogen biomass (g) was calculated as the sum of total leaf (g), stem (g),
264 and root (g) nitrogen biomass. Root nodule carbon biomass was not included in
265 the calculation of root carbon biomass; however, relative plant investment toward
266 root or root nodule standing stock was estimated as the ratio of root biomass to
267 root nodule biomass (g g^{-1}), following similar metrics to those adopted by Dovrat
268 et al. (2018) and Dovrat et al. (2020).

269 Carbon costs to acquire nitrogen (N_{cost} ; gC gN^{-1}) were estimated as the
270 ratio of total root carbon biomass (C_{bg} ; gC) to whole-plant nitrogen biomass
271 (N_{wp} ; gN). This calculation quantifies the relationship between carbon spent on
272 nitrogen acquisition and whole plant nitrogen acquisition by using root carbon
273 biomass as a proxy for estimating the magnitude of carbon allocated toward ni-

274 trogen acquisition. This calculation therefore assumes that the magnitude of root
275 carbon standing stock is proportional to carbon transferred to root nodules or my-
276 corrhizae, or lost through root exudation or turnover. The assumption has been
277 supported in species that associate with ectomycorrhizal fungi (Hobbie 2006; Hob-
278 bie and Hobbie 2008), but is less clear in species that acquire nitrogen through
279 non-symbiotic active uptake or symbiotic nitrogen fixation. It is also unclear
280 whether relationships between root carbon standing stock and carbon transfer to
281 root nodules are similar in magnitude to carbon lost through exudation or when
282 allocated toward other active uptake pathways. Thus, because of the way mea-
283 surements were calculated, proximal values of carbon costs to acquire nitrogen are
284 underestimates.

285 2.2.3 *Statistical analyses*

286 I explored the effects of light and nitrogen availability on carbon costs to acquire
287 nitrogen using separate linear mixed-effects models for each species. Models in-
288 cluded shade cover, nitrogen fertilization, and interactions between shade cover
289 and nitrogen fertilization as continuous fixed effects, and also included block as a
290 random intercept term. Three separate models for each species were built with
291 this independent variable structure for three different dependent variables: (i)
292 carbon costs to acquire nitrogen (gC gN^{-1}); (ii) whole plant nitrogen biomass
293 (denominator of carbon cost to acquire nitrogen; gN); and (iii) belowground car-
294 bon biomass (numerator of carbon cost to acquire nitrogen; gC). I constructed two
295 additional models for *G. max* with the same model structure described above to
296 investigate the effects of light availability and nitrogen fertilization on root nodule

297 biomass (g) and the ratio of root nodule biomass to root biomass (unitless).

298 I used Shapiro–Wilk tests of normality to determine whether species spe-
299 cific linear mixed-effects model residuals followed a normal distribution. Zero
300 models satisfied residual normality assumptions when models were fit using un-
301 transformed data (Shapiro–Wilk: $p < 0.05$ in all cases). I attempted to satisfy
302 residual normality assumptions by first fitting models using dependent variables
303 that were natural-log transformed. If residual normality assumptions were still
304 not met (Shapiro–Wilk: $p > 0.05$), then models were fit using dependent variables
305 that were square root transformed. All residual normality assumptions were satis-
306 fied when models were fit with either a natural-log or square root transformation
307 (Shapiro–Wilk: $p > 0.05$ in all cases). Specifically, I natural-log transformed *G.*
308 *hirsutum* carbon costs to acquire nitrogen and *G. hirsutum* whole-plant nitrogen
309 biomass. I also square root transformed *G. max* carbon costs to acquire nitrogen,
310 *G. max* whole-plant nitrogen biomass, root carbon biomass in both species, *G.*
311 *max* root nodule biomass, and the *G. max* ratio of root nodule biomass to root
312 biomass. I used the ‘lmer’ function in the ‘lme4’ R package (Bates et al. 2015) to
313 fit each model and the ‘Anova’ function in the ‘car’ R package (Fox and Weisberg
314 2019) to calculate Wald’s χ^2 to determine the significance ($\alpha = 0.05$) of each fixed
315 effect coefficient. Finally, I used the ‘emmeans’ R package (Lenth 2019) to conduct
316 post-hoc comparisons of our treatment combinations using Tukey’s tests. Degrees
317 of freedom for all Tukey’s tests were approximated using the Kenward–Roger ap-
318 proach (Kenward and Roger 1997). All analyses and plots were conducted in R
319 version 4.0.1 (R Core Team 2021).

320 2.3 Results

321 2.3.1 *Carbon costs to acquire nitrogen*

322 Carbon costs to acquire nitrogen in *G. hirsutum* increased with increasing light
323 availability ($p<0.001$; Table 2.1; Fig. 2.1) and decreased with increasing nitrogen
324 fertilization ($p<0.001$; Table 2.1; Fig. 2.1). There was no interaction between
325 light availability and nitrogen fertilization ($p=0.486$, Table 2.1; Fig. 2.1).

326 Carbon costs to acquire nitrogen in *G. max* also increased with increasing
327 light availability ($p<0.001$, Table 2.1; Fig. 2.1) and decreased with increasing
328 nitrogen fertilization ($p<0.001$; Table 2.1; Fig. 2.1). There was no interaction
329 between light availability and nitrogen fertilization ($p=0.261$, Table 2.1; Fig. 2.1).

Table 2.1. Analysis of variance results exploring species-specific effects of light availability, nitrogen fertilization, and their interactions on carbon costs to acquire nitrogen (N_{cost} ; gC gN $^{-1}$), whole plant nitrogen biomass (N_{wp} ; gN), and root carbon biomass (C_{bg} ; gC)

	N_{cost}			N_{wp}			C_{bg}			
	df	Coefficient	χ^2	p	Coefficient	χ^2	p	Coefficient	χ^2	p
<i>G. hirsutum</i>										
Intercept		1.594	-	-	-3.232	-	-	0.432	-	-
Light (L)	1	-1.09E-02	56.494	<0.001	-6.41E-03	91.275	<0.001	-2.62E-03	169.608	<0.001
Nitrogen (N)	1	-1.34E-03	54.925	<0.001	1.83E-03	118.784	<0.001	1.15E-04	2.901	0.089
L*N	1	3.88E-06	0.485	0.486	-1.34E-05	10.721	0.001	-1.67E-06	3.140	0.076
<i>G. max</i>										
Intercept		1.877	-	-	0.239	-	-	0.438	-	-
Light (L)	1	-7.67E-03	174.156	<0.001	-6.72E-04	39.799	<0.001	-2.55E-03	194.548	<0.001
Nitrogen (N)	1	-2.35E-04	21.948	<0.001	1.55E-04	70.771	<0.001	2.52E-04	19.458	<0.001
L*N	1	-2.89E-06	1.262	0.261	-6.32E-07	1.435	0.231	-3.16E-06	10.803	0.001

16

330 *Significance determined using Wald's χ^2 tests ($p=0.05$). P -values less than 0.05 are in bold and p -values between
 331 0.05 and 0.1 are italicized. Negative coefficients for light treatments indicate a positive effect of increasing light
 332 availability on all response variables, as light availability is treated as percent shade cover in all linear mixed-effects
 333 models.

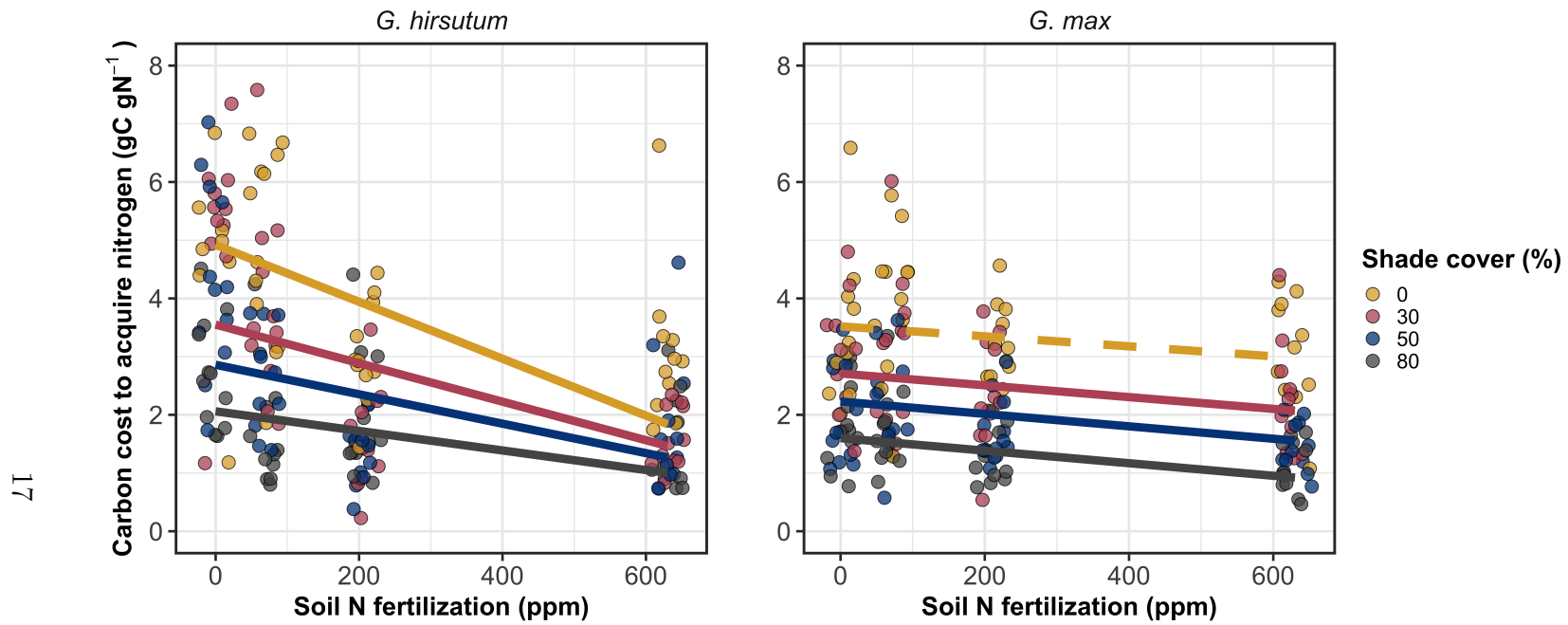


Figure 2.1. Relationships between soil nutrient fertilization and light availability on carbon costs to acquire nitrogen in *G. hirsutum* and *G. max*. Nitrogen fertilization treatments are represented on the x-axis. Shade cover treatments are represented through colored points and trendlines. Trendlines were created by back-transforming marginal mean slopes and intercepts from species-specific linear mixed-effects models. These values were calculated using the ‘emtrends’ and ‘emmeans’ functions in the ‘emmeans’ R package (Lenth, 2019). Yellow points and trendlines represent the 0% shade cover treatment, red points and trendlines represent the 30% shade cover treatment, blue points and trendlines represent the 50% shade cover treatment, and gray points and trendlines represent the 80% shade cover treatment. Solid trendlines indicate slopes that are significantly different from zero (Tukey: $p < 0.05$), while dashed trendlines indicate slopes that are not statistically different from zero.

334 2.3.2 *Whole plant nitrogen biomass*

335 Whole plant nitrogen biomass in *G. hirsutum* was driven by an interaction between
336 light availability and nitrogen fertilization ($p=0.001$; Table 2.1; Fig. 2.2). This
337 interaction indicated a greater stimulation of whole-plant nitrogen biomass by
338 nitrogen fertilization as light levels increased (Table 2.1; Fig. 2.2).

339 Whole plant nitrogen biomass in *G. max* increased with increasing light
340 availability ($p<0.001$) and nitrogen fertilization ($p<0.001$), with no interaction
341 between light availability and nitrogen fertilization ($p=0.231$; Table 2.1; Fig. 2.2).

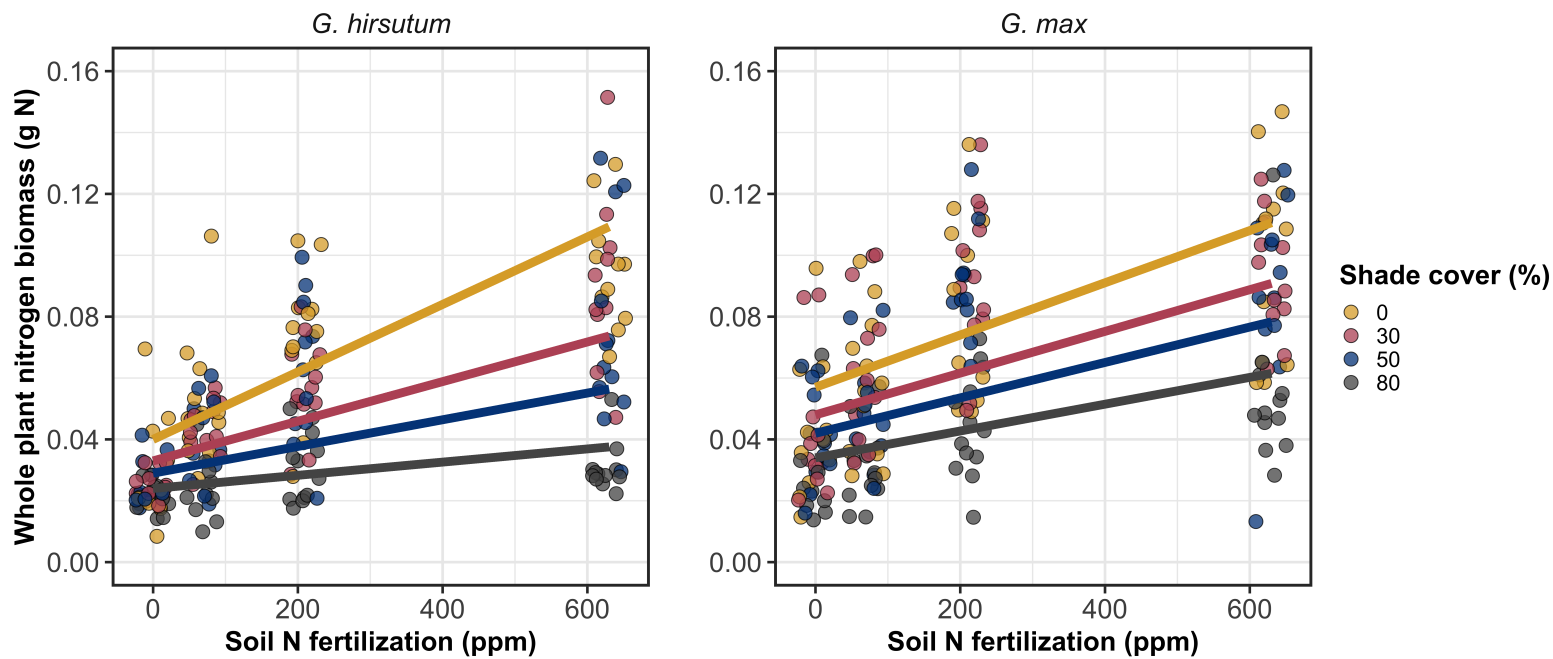


Figure 2.2. Relationships between soil nutrient fertilization and light availability on whole-plant nitrogen biomass in *G. hirsutum* and *G. max*. Whole-plant nitrogen biomass is the denominator of the carbon cost to acquire nitrogen calculation. Nitrogen fertilization treatments are represented on the x-axis. Shade cover treatments are represented through colored points and trendlines. Trendlines were created by back-transforming marginal mean slopes and intercepts from species-specific linear mixed-effects models. These values were calculated using the ‘emtrends’ and ‘emmeans’ functions in the ‘emmeans’ R package (Lenth 2019). Points are jittered for visibility. Colored points and trendlines are as explained in Fig. 2.1. Solid trendlines indicate slopes that are significantly different from zero (Tukey: $p < 0.05$), while dashed trendlines indicate slopes that are not statistically different from zero.

342 2.3.3 *Root carbon biomass*

343 Root carbon biomass in *G. hirsutum* significantly increased with increasing light availability ($p<0.001$; Table 2.1; Fig. 2.3) and marginally increased with nitrogen fertilization ($p=0.089$; Table 2.1; Fig. 2.3). There was also a marginal interaction between light availability and nitrogen fertilization ($p=0.076$; Table 2.1), driven by an increase in the positive response of root carbon biomass to increasing nitrogen fertilization as light availability increased (Table 2.3). This resulted in significantly positive trends between root carbon biomass and nitrogen fertilization in the two highest light treatments (Tukey: $p<0.05$ in both cases; Table 2.3; Fig. 2.3) and no effect of nitrogen fertilization in the two lowest light treatments (Tukey: $p>0.05$ in both cases; Table 2.3; Fig. 2.3).

353 There was an interaction between light availability and nitrogen fertilization on root carbon biomass in *G. max* ($p=0.001$; Table 2.1; Fig. 2.3). Post-hoc analyses indicated that the positive effects of nitrogen fertilization on *G. max* root carbon biomass increased with increasing light availability (Table 2.3; Fig. 2.3). There were also positive individual effects of increasing nitrogen fertilization ($p<0.001$; Table 2.3) and light availability ($p<0.001$; Table 2.3) on *G. max* root carbon biomass (Table 2.1; Fig. 2.3).

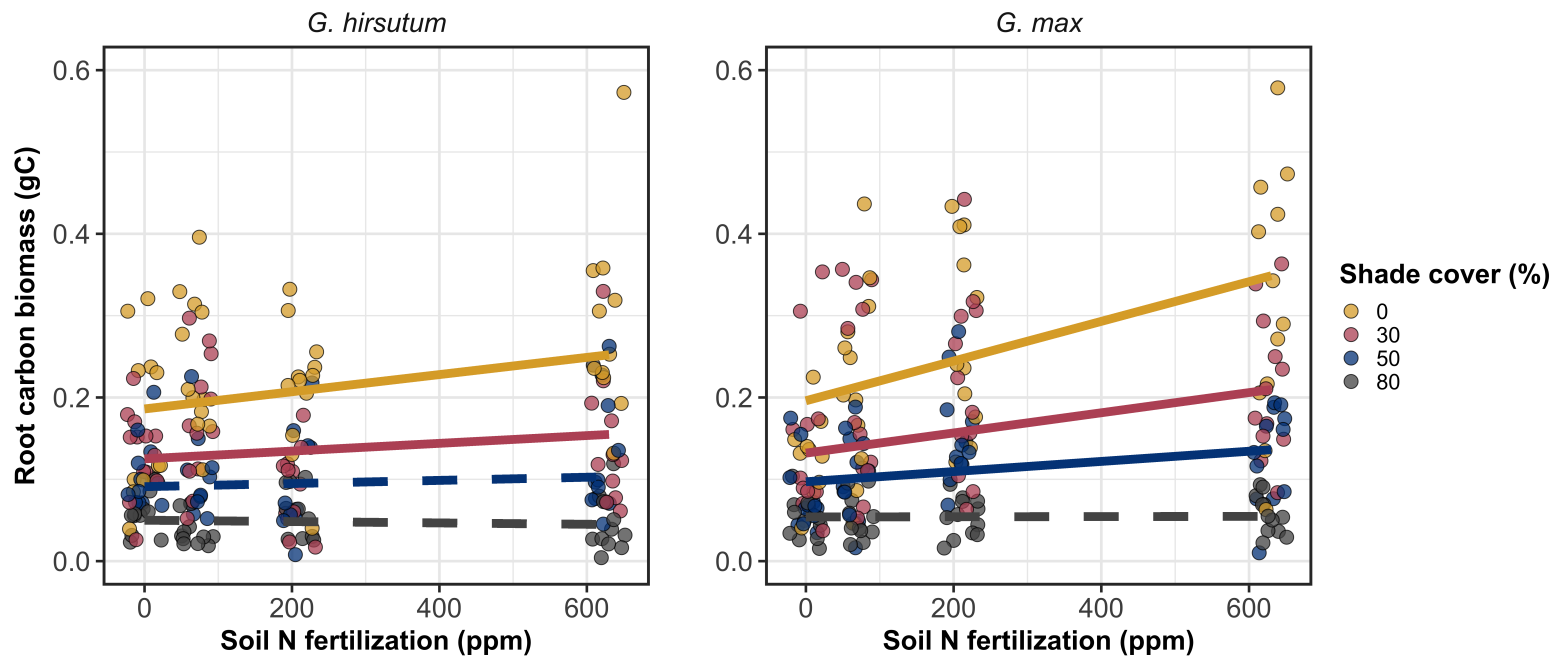


Figure 2.3. Relationships between soil nutrient fertilization and light availability on root carbon biomass in *G. hirsutum* and *G. max*. Root carbon biomass is the numerator of the carbon cost to acquire nitrogen calculation. Nitrogen fertilization treatments are represented on the x-axis. Colored points and trendlines are as explained in Fig. 2.1. Trendlines were created by back-transforming marginal mean slopes and intercepts from species-specific linear mixed-effects models. These values were calculated using the ‘emtrends’ and ‘emmeans’ functions in the ‘emmeans’ R package (Lenth 2019). Points are jittered for visibility. Colored points and trendlines are as explained in Fig. 2.1.

360 2.3.4 *Root nodule biomass*

361 Root nodule biomass in *G. max* increased with increasing light availability ($p <$
362 0.001; Table 2.2; Fig. 2.4a) and decreased with increasing nitrogen fertilization
363 ($p < 0.001$; Table 2.2; Fig. 2.4a). There was no interaction between nitrogen
364 fertilization and light availability ($p = 0.133$; Table 2.2; Fig. 2.4a). The ratio of
365 root nodule biomass to root biomass did not change in response to light availability
366 ($p = 0.481$; Table 2.2; Fig. 2.4b) but decreased with increasing nitrogen fertilization
367 ($p < 0.001$; Table 2.2; Fig. 2.4b). There was no interaction between nitrogen
368 fertilization and light availability on the ratio of root nodule biomass to root
369 biomass ($p = 0.621$; Table 2.2; Fig. 2.4b).

Table 2.2. Analysis of variance results exploring effects of light availability, nitrogen fertilization, and their interactions on *G. max* root nodule biomass (g) and the ratio of root nodule biomass to root biomass (g g⁻¹)*

	Nodule biomass			Nodule biomass: root biomass			<i>p</i>
	df	Coefficient	χ^2	<i>p</i>	Coefficient	χ^2	
(Intercept)		0.302	-	-	0.448	-	-
Light (L)	1	-1.81E-03	72.964	<0.001	-8.76E-05	0.496	0.481
Nitrogen (N)	1	-2.83E-04	115.377	<0.001	-5.09E-04	156.476	<0.001
L*N	1	1.14E-06	2.226	0.133	-7.30E-07	0.244	0.621

370 *Significance determined using Wald's χ^2 tests ($\alpha=0.05$). *P*-values less than 0.05 are in bold. Negative coefficients for
 371 light treatments indicate a positive effect of increasing light availability on all response variables, as light availability
 372 is treated as percent shade cover in all linear mixed-effects models. Root nodule biomass and nodule biomass: root
 373 biomass models were only constructed for *G. max* because *G. hirsutum* was not inoculated with *B. japonicum* and
 374 is not capable of forming root nodules.

Table 2.3. Slopes of the regression line describing the relationship between each dependent variable and nitrogen fertilization at each light level*

Shade cover	Carbon cost to acquire nitrogen	Whole plant nitrogen biomass	Belowground carbon biomass	Root nodule biomass	Nodule biomass: root biomass
<i>G. hirsutum</i>					
0%	-1.34E-03^a	1.83E-03^a	1.15E-04^b	-	-
30%	-1.22E-03^a	1.43E-03^a	1.17E-04^b	-	-
50%	-1.14E-03^a	1.17E-03^a	3.12E-05 ^b	-	-
80%	-1.02E-03^a	7.66E-04^a	-1.89E-06 ^b	-	-
<i>G. max</i>					
0%	-2.35E-04 ^b	1.55E-05^b	2.51E-04^b	-2.83E-04^b	-5.09E-04^b
30%	-3.22E-04^b	1.35E-05^b	1.57E-04^b	-2.49E-04^b	-5.31E-04^b
50%	-3.80E-04^b	1.23E-05^b	9.37E-05^b	-2.26E-04^b	-5.45E-04^b
80%	-4.66E-04^b	1.04E-05^b	-9.95E-07 ^b	-1.92E-04^b	-5.67E-04^b

24

375 * Slopes represent estimated marginal mean slopes from linear mixed-effects models described in the Methods. Slopes
 376 were calculated using the ‘emmeans’ R package (Lenth 2019). Superscripts indicate slopes fit to natural-log (^a) or
 377 square root (^b) transformed data. Slopes statistically different from zero (Tukey: $p<0.05$) are indicated in bold.
 378 Marginally significant slopes (Tukey: $0.05< p<0.1$) are italicized.

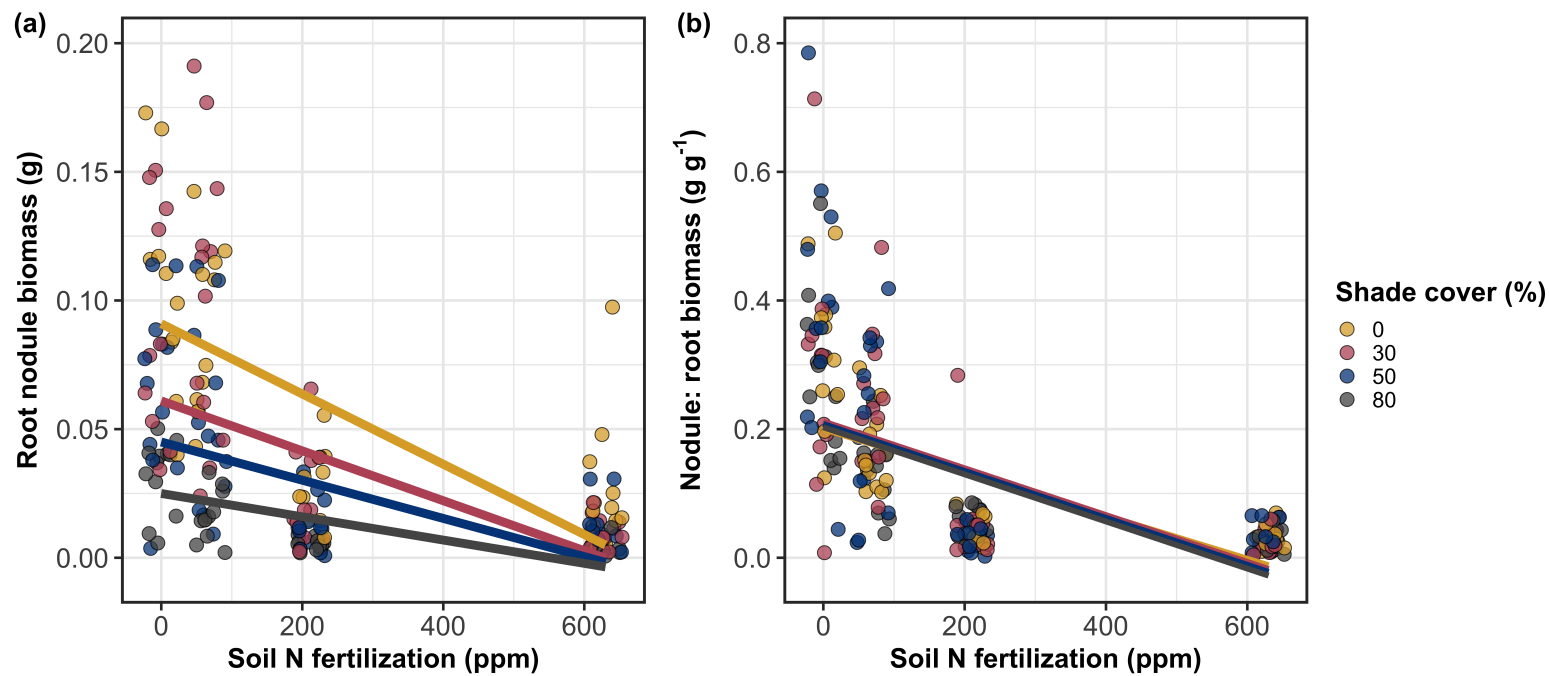


Figure 2.4. Effects of shade cover and nitrogen fertilization on root nodule biomass (a) and the ratio of root nodule biomass to root biomass (b) in *G. max*. Nitrogen fertilization treatments are represented on the x-axis. Shade cover treatments are represented through colored points and trendlines. Trendlines were created by back-transforming marginal mean slopes and intercepts from species-specific linear mixed-effects models. These values were calculated using the ‘emtrends’ and ‘emmeans’ functions in the ‘emmeans’ R package (Lenth 2019). Points are jittered for visibility. Yellow points and trendlines represent the 0% shade cover treatment, blue points and trendlines represent the 30% shade cover treatment, green points and trendlines represent the 50% shade cover treatment, and purple points and trendlines represent the 80% shade cover treatment. Solid trendlines indicate slopes that are significantly different from zero (Tukey: $p < 0.05$), while dashed trendlines indicate slopes that are not statistically different from zero.

379 2.4 Discussion

380 In this chapter, I determined the effects of light availability and soil nitrogen
381 fertilization on root mass carbon costs to acquire nitrogen in *G. hirsutum* and *G.*
382 *max*. In support of my hypotheses, I found that carbon costs to acquire nitrogen
383 generally increased with increasing light availability and decreased with increasing
384 soil nitrogen fertilization in both species. These findings suggest that carbon costs
385 to acquire nitrogen are determined by factors that influence plant nitrogen demand
386 and soil nitrogen availability. In contrast to my second hypothesis, root nodulation
387 data suggested that *G. max* and *G. hirsutum* achieved similar directional carbon
388 cost responses to nitrogen fertilization despite a likely shift in *G. max* allocation
389 from nodulation to root biomass along the nitrogen fertilization gradient.

390 2.4.1 *Carbon costs to acquire nitrogen increase with light availability and*
391 *decrease with fertilization*

392 Both *G. max* and *G. hirsutum* experienced an increase in carbon costs to ac-
393 quire nitrogen due to increasing light availability. These patterns were driven by
394 a larger increase in root carbon biomass than whole-plant nitrogen biomass. In-
395 creases in root carbon biomass due to factors that increase plant nitrogen demand
396 are a commonly observed pattern, as carbon allocated belowground provides sub-
397 strate needed to produce and maintain structures that satisfy aboveground plant
398 nitrogen demand (Nadelhoffer and Raich 1992; Giardina et al. 2005; Raich et al.
399 2014). Findings suggest that plants allocate relatively more carbon for acquiring
400 nitrogen when demand increases over short temporal scales, which may cause a
401 temporary state of diminishing return due to asynchrony between belowground

402 carbon and whole-plant nitrogen responses to plant nitrogen demand (Kulmatiski
403 et al. 2017; Noyce et al. 2019). These responses might be attributed to a temporal
404 lag associated with producing structures that enhance nitrogen acquisition. For
405 example, fine roots (Matamala and Schlesinger 2000; Norby et al. 2004; Arndal
406 et al. 2018) and root nodules (Parvin et al. 2020) take time to build and first
407 require the construction of coarse roots. Thus, full nitrogen returns from these
408 investments may not occur immediately (Kayler et al. 2010; Kayler et al. 2017),
409 and may vary by species acquisition strategy. I speculate that increases in ni-
410 trogen acquisition from a given carbon investment may occur beyond the 5-week
411 scope of this experiment. A similar study conducted over a longer temporal scale
412 would address this.

413 Increasing soil nitrogen fertilization generally decreased carbon costs to
414 acquire nitrogen in both species. These patterns were driven by a larger increase
415 in whole-plant nitrogen biomass than root carbon biomass. In *G. hirsutum*, re-
416 ductions in carbon costs to acquire nitrogen may have been due to an increase in
417 per-root nitrogen uptake, allowing individuals to maximize the amount of nitro-
418 gen acquired from a belowground carbon investment. Interestingly, increased soil
419 nitrogen fertilization increased whole-plant nitrogen biomass in *G. max* despite
420 reductions in root nodule biomass that likely reduced the nitrogen-fixing capac-
421 ity of *G. max* (Andersen et al. 2005; Muñoz et al. 2016). While reductions in
422 root nodulation due to increased soil nitrogen availability are commonly observed
423 (Gibson and Harper 1985; Fujikake et al. 2003), root nodulation responses were
424 observed in tandem with increased root carbon biomass, implying that *G. max*
425 shifted relative carbon allocation from nitrogen fixation to soil nitrogen acquisition

426 (Markham and Zekveld 2007; Dovrat et al. 2020). This was likely because there
427 was a reduction in the carbon cost advantage of acquiring fixed nitrogen relative
428 to soil nitrogen, and suggests that species capable of associating with symbiotic
429 nitrogen-fixing bacteria shift their relative nitrogen acquisition pathway to opti-
430 mize nitrogen uptake (Rastetter et al. 2001). Future studies should investigate
431 these patterns with a larger quantity of phylogenetically related species, or differ-
432 ent varieties of a single species that differ in their ability to form associations with
433 symbiotic nitrogen-fixing bacteria to more directly test the impact of nitrogen
434 fixation on the patterns observed in this study.

435 2.4.2 *Modeling implications*

436 Carbon costs to acquire nitrogen are subsumed in the general discussion of eco-
437 nomic analogies to plant resource uptake (Bloom et al. 1985; Rastetter et al.
438 2001; Vitousek et al. 2002; Phillips et al. 2013; Terrer et al. 2018; Henneron
439 et al. 2020). Despite this, terrestrial biosphere models rarely include costs of
440 nitrogen acquisition within their framework for predicting plant nitrogen uptake.
441 There is currently one plant resource uptake model, FUN, that quantitatively
442 predicts carbon costs to acquire nitrogen within a framework for predicting plant
443 nitrogen uptake for different nitrogen acquisition strategies (Fisher et al. 2010;
444 Brzostek et al. 2014). Iterations of FUN are currently coupled to two terrestrial
445 biosphere models: the Community Land Model 5.0 and the Joint UK Land En-
446 vironment Simulator (Clark et al. 2011; Shi et al. 2016; Lawrence et al. 2019).
447 Recent work suggests that coupling FUN to CLM 5.0 caused a large overpredic-
448 tion of plant nitrogen uptake associated with nitrogen fixation (Davies-Barnard

449 et al. 2020) compared to other terrestrial biosphere model products. Thus, em-
450 pirical data from manipulative experiments that explicitly quantify carbon costs
451 to acquire nitrogen in species capable of associating with nitrogen-fixing bacteria
452 across different environmental contexts is an important step toward identifying
453 potential biases in models such as FUN.

454 These findings broadly support the FUN formulation of carbon costs to
455 acquire nitrogen in response to soil nitrogen availability. FUN calculates carbon
456 costs to acquire nitrogen based on the sum of carbon costs to acquire nitrogen
457 via nitrogen fixation, mycorrhizal active uptake, non-mycorrhizal active uptake,
458 and retranslocation (Fisher et al. 2010; Brzostek et al. 2014). Carbon costs to
459 acquire nitrogen via mycorrhizal or non-mycorrhizal active uptake pathways are
460 derived as a function of nitrogen availability, root biomass, and two parameterized
461 values based on nitrogen acquisition strategy (Brzostek et al. 2014). Due to this,
462 FUN simulates a net decrease in carbon costs to acquire nitrogen with increasing
463 nitrogen availability for mycorrhizal and non-mycorrhizal active uptake pathways,
464 assuming constant root biomass. This was a pattern I observed in *G. hirsutum* re-
465 gardless of light availability. In contrast, FUN would not simulate a net change in
466 carbon costs to acquire nitrogen via nitrogen fixation due to nitrogen availability.
467 This is because carbon costs to acquire nitrogen via nitrogen fixation are derived
468 from a well established function of soil temperature, which is independent of soil
469 nitrogen availability (Houlton et al. 2008; Fisher et al. 2010). I observed a net
470 reduction in carbon costs to acquire nitrogen in *G. max*, except when individu-
471 als were grown under 0% shade cover. While a net reduction of carbon costs in
472 response to nitrogen fertilization runs counter to nitrogen fixation carbon costs

473 simulated by FUN, these patterns were likely because *G. max* individuals switched
474 their primary mode of nitrogen acquisition from symbiotic nitrogen fixation to a
475 non-symbiotic active uptake pathway.

476 2.4.3 *Study limitations*

477 It should be noted that the metric used in this study to determine carbon costs
478 to acquire nitrogen has several limitations. Most notably, this metric uses root
479 carbon biomass as a proxy for estimating the amount of carbon spent on nitrogen
480 acquisition. While it is true that most carbon allocated belowground has at least
481 an indirect structural role in acquiring soil resources, it remains unclear whether
482 this assumption holds true for species that acquire nitrogen via symbiotic nitro-
483 gen fixation. I also cannot quantify carbon lost through root exudates or root
484 turnover, which may increase due to factors that increase plant nitrogen demand
485 (Tingey et al. 2000; Phillips et al. 2011), and can increase the magnitude of
486 available nitrogen from soil organic matter through priming effects on soil micro-
487 bial communities (Uselman et al. 2000; Bengtson et al. 2012). It is also not
488 clear whether these assumptions hold under all environmental conditions, such
489 as those that shift belowground carbon allocation toward a different mode of ni-
490 trogen acquisition (Taylor and Menge 2018; Friel and Friesen 2019) or between
491 species with different acquisition strategies. In this study, increasing soil nitrogen
492 fertilization increased carbon investment to roots relative to carbon transferred to
493 root nodules. By assuming that carbon allocated to root carbon was proportional
494 to carbon allocated to root nodules across all treatment combinations, these ob-
495 served responses to soil nitrogen fertilization were likely to be overestimated in *G.*

496 *max*. I encourage future research to quantify these carbon fates independently.

497 Researchers conducting pot experiments must carefully choose pot volume
498 to minimize the likelihood of growth limitations induced by pot volume (Poorter
499 et al. 2012). Poorter et al. (2012) indicate that researchers are likely to avoid
500 growth limitations associated with pot volume if measurements are collected when
501 the plant biomass:pot volume ratio is less than 1 g L^{-1} . In this experiment, all
502 treatment combinations in both species had biomass:pot volume ratios less than
503 1 g L^{-1} except for *G. max* and *G. hirsutum* that were grown under 0% shade
504 cover and had received 630 ppm N. Specifically, *G. max* and *G. hirsutum* had
505 average respective biomass:pot volume ratios of $1.24 \pm 0.07 \text{ g L}^{-1}$ and 1.34 ± 0.13
506 g L^{-1} , when grown under 0% shade cover and received 630 ppm N (Table A2,
507 A3; Fig. A1). If growth in this treatment combination was limited by pot vol-
508 ume, then individuals may have had larger carbon costs to acquire nitrogen than
509 would be expected if they were grown in larger pots. This pot volume induced
510 growth limitation could cause a reduction in per-root nitrogen uptake associated
511 with more densely packed roots, which could reduce the positive effect of nitro-
512 gen fertilization on whole-plant nitrogen biomass relative to root carbon biomass
513 (Poorter et al. 2012).

514 Growth limitation associated with pot volume provides a possible expla-
515 nation for the marginally insignificant effect of increasing nitrogen fertilization on
516 *G. max* carbon costs to acquire nitrogen when grown under 0% shade cover. This
517 is because the regression line describing the relationship between carbon costs to
518 acquire nitrogen and nitrogen fertilization in *G. max* grown under 0% shade cover
519 would have flattened if growth limitation had caused larger than expected carbon

520 costs to acquire nitrogen in the 0% shade cover, 630 ppm N treatment combi-
521 nation. This may have been exacerbated by the fact that *G. max* likely shifted
522 relative carbon allocation from nitrogen fixation to soil nitrogen acquisition, which
523 could have increased the negative effect of more densely packed roots on nitrogen
524 uptake. These patterns could have also occurred in *G. hirsutum* grown under 0%
525 shade cover; however, there was no change in the effect of nitrogen fertilization on
526 *G. hirsutum* carbon costs to acquire nitrogen grown under 0% shade cover relative
527 to other shade cover treatments. Regardless, the possibility of growth limitation
528 due to pot volume suggests that effects of increasing nitrogen fertilization on car-
529 bon costs to acquire nitrogen in both species grown under 0% shade cover could
530 have been underestimated. Follow-up studies using a similar experimental design
531 with a larger pot volume would be necessary in order to determine whether these
532 patterns were impacted by pot volume-induced growth limitation.

533 2.4.4 *Conclusions*

534 In conclusion, this chapter provides empirical evidence that carbon costs to ac-
535 quire nitrogen are influenced by light availability and soil nitrogen fertilization
536 in a species capable of acquiring nitrogen via symbiotic nitrogen fixation and a
537 species not capable of forming such associations. We show that carbon costs to
538 acquire nitrogen generally increase with increasing light availability and decrease
539 with increasing nitrogen fertilization. This chapter provides important empirical
540 data needed to evaluate the formulation of carbon costs to acquire nitrogen in
541 terrestrial biosphere models, particularly carbon costs to acquire nitrogen that
542 are associated with symbiotic nitrogen fixation. Findings broadly support the

543 general formulation of these carbon costs in the FUN biogeochemical model in
544 response to shifts in nitrogen availability. However, there is a need for future
545 studies to explicitly quantify carbon costs to acquire nitrogen under different en-
546 vironmental contexts, over longer temporal scales, and using larger selections of
547 phylogenetically related species. In addition, I suggest that future studies mini-
548 mize the limitations associated with the metric used here by explicitly measuring
549 belowground carbon fates independently.

550 Chapter 3

551 Soil nitrogen availability modifies leaf nitrogen economies in mature
552 temperate deciduous forests: a direct test of photosynthetic least-cost
553 theory

554 3.1 Introduction

Photosynthesis represents the largest carbon flux between the atmosphere and land surface (IPCC 2021), and plays a central role in biogeochemical cycling at multiple spatial and temporal scales (Vitousek and Howarth 1991; LeBauer and Treseder 2008; Kaiser et al. 2015; Wieder et al. 2015). Therefore, carbon and energy fluxes simulated by terrestrial biosphere models are sensitive to the formulation of photosynthetic processes (Ziehn et al. 2011; Bonan et al. 2011; Booth et al. 2012; Smith et al. 2016; Smith et al. 2017) and must be represented using robust, empirically tested processes (Prentice et al. 2015; Wieder et al. 2019). Current formulations of photosynthesis vary across terrestrial biosphere models (Smith and Dukes 2013; Rogers et al. 2017), which causes variation in modeled ecosystem processes (Knorr 2000; Knorr and Heimann 2001; Bonan et al. 2011; Friedlingstein et al. 2014) and casts uncertainty on the ability of these models to accurately predict terrestrial ecosystem responses and feedbacks to global change (Zaehle et al. 2005; Schaefer et al. 2012; Davies-Barnard et al. 2020).

Terrestrial biosphere models commonly represent C₃ photosynthesis through variants of the Farquhar et al. (1980) biochemical model (Smith and Dukes 2013; Rogers 2014; Rogers et al. 2017). This well-tested photosynthesis model estimates leaf-level carbon assimilation, or photosynthetic capacity, as a function of the maximum rate of Ribulose-1,5-bisphosphate carboxylase-oxygenase (Ru-

574 bisco) carboxylation (V_{cmax}) and the maximum rate of Ribulose-1,5-bisphosphate
575 (RuBP) regeneration (J_{max}) (Farquhar et al. 1980). Many terrestrial biosphere
576 models predict these model inputs based on plant functional group specific lin-
577 ear relationships between leaf nutrient content and V_{cmax} (Smith and Dukes 2013;
578 Rogers 2014; Rogers et al. 2017) under the tenet that a large fraction of leaf nutri-
579 ents, and nitrogen in particular, are partitioned toward building and maintaining
580 enzymes that support photosynthetic capacity, such as Rubisco (Brix 1971; Gul-
581 mon and Chu 1981; Evans 1989; Kattge et al. 2009; Walker et al. 2014). Terres-
582 trial biosphere models predict leaf nutrient content from soil nutrient availability
583 based on the assumption that increasing soil nutrients generally increases leaf nu-
584 trients (Firn et al. 2019; Li et al. 2020; Liang et al. 2020) which, in the case of
585 nitrogen, generally corresponds with an increase in photosynthetic processes (Li
586 et al. 2020; Liang et al. 2020).

587 Recent work calls the generality of relationships between soil nutrient avail-
588 ability, leaf nutrient content, and photosynthetic capacity into question, suggest-
589 ing instead that leaf nutrients and photosynthetic capacity are better predicted as
590 an integrated product of aboveground climate, leaf traits, and soil nutrient avail-
591 ability, rather than soil nutrient availability alone (Dong et al. 2017; Dong et al.
592 2020; Dong et al. 2022; Firn et al. 2019; Smith et al. 2019; Peng et al. 2021).
593 It has been reasoned that this result is because plants allocate added nutrients to
594 growth and storage rather than alterations in leaf chemistry (Smith et al. 2019),
595 perhaps as a result of nutrient limitation of primary productivity (LeBauer and
596 Treseder 2008; Fay et al. 2015). Additionally, recent work suggests that relation-
597 ships between leaf nutrient content and photosynthesis vary across environments,

598 and that the proportion of leaf nutrient content allocated to photosynthetic tis-
599 sue varies over space and time with plant acclimation and adaptation responses
600 to light availability, vapor pressure deficit, soil pH, soil nutrient availability, and
601 environmental factors that influence leaf mass per area (Pons and Pearcy 1994;
602 Niinemets and Tenhunen 1997; Evans and Poorter 2001; Hikosaka and Shigeno
603 2009; Ghimire et al. 2017; Onoda et al. 2017; Luo et al. 2021). The use of linear
604 relationships between leaf nutrient content and V_{cmax} to predict photosynthetic
605 capacity, as commonly used in terrestrial biosphere models (Rogers 2014), is not
606 capable of detecting such responses.

607 Photosynthetic least-cost theory provides an alternative framework for un-
608 derstanding relationships between soil nutrient availability, leaf nutrient content,
609 and photosynthetic capacity (Harrison et al. 2021). Leveraging a two-input mi-
610 croeconomics approach (Wright et al. 2003), the theory posits that plants accli-
611 mate to a given environment by optimizing leaf photosynthesis rates at the lowest
612 summed cost of using nutrients and water (Prentice et al. 2014; Wang et al. 2017;
613 Smith et al. 2019; Paillassa et al. 2020). Across resource availability gradients,
614 the theory predicts that optimal photosynthetic rates can be achieved by trading
615 less efficient use of a resource that is less costly to acquire (or more abundant)
616 for more efficient use of a resource more costly to acquire (or less abundant). For
617 example, an increase in soil nutrient availability should reduce the cost of acquir-
618 ing and using nutrients (Bae et al. 2015; Eastman et al. 2021; Perkowski et al.
619 2021), which could increase leaf nutrient investments in photosynthetic proteins to
620 allow similar photosynthetic rates to be achieved with higher nutrient use (lower
621 nutrient use efficiency) but lower water use (greater water use efficiency). The

622 theory suggests similar tradeoffs in response to increasing soil pH (Paillassa et al.
623 2020), specifically, that increasing soil pH should reduce the cost of acquiring soil
624 nutrients due to an increase in plant-available nutrient concentration (Paillassa
625 et al. 2020; Dong et al. 2022). The theory is also capable of reconciling dynamic
626 leaf nutrient-photosynthesis relationships at global scales (Luo et al. 2021).

627 Patterns expected from photosynthetic least-cost theory have recently re-
628 ceived empirical support both in global environmental gradient (Smith et al.
629 2019; Paillassa et al. 2020; Luo et al. 2021; Querejeta et al. 2022; Wester-
630 band et al. 2023) and local manipulative invasion (Bialic-Murphy et al. 2021)
631 studies. However, nutrient addition experiments that directly examine nutrient-
632 water use tradeoffs expected from the theory are rare (but see Guerrieri et al.
633 2011), and only global gradient studies testing the theory have considered soil pH
634 in their analyses. As a result, there is a need to use nutrient addition and soil pH
635 manipulation experiments to test mechanisms driving responses predicted by the
636 theory.

637 In this study, I measured leaf responses to soil nitrogen availability in five
638 deciduous tree species growing in the upper canopy of mature closed canopy tem-
639 perate forests in the northeastern United States. Soil nitrogen availability and pH
640 were manipulated through a nitrogen-by-pH field manipulation experiment with
641 treatments applied since 2011, eight years prior to measurement. Two different soil
642 nitrogen treatments were applied to increase nitrogen availability with opposing
643 effects on soil pH. An additional nitrogen-free acidifying treatment was expected
644 to decrease soil pH. I hypothesized that increased soil nitrogen availability would
645 enable plants to increase nutrient uptake and create more photosynthetic enzymes

646 per leaf, allowing similar photosynthetic rates achieved with lower leaf C_i:C_a and
647 increased leaf nitrogen content allocated to photosynthetic leaf tissue. I expected
648 that this response would be driven by a reduction in the cost of acquiring nitrogen,
649 which would cause trees to sacrifice efficient nitrogen use to enable more efficient
650 use of other limiting resources (i.e., water). Finally, I hypothesized similar leaf
651 responses to increasing soil pH.

652 3.2 Methods

653 3.2.1 *Study site description*

654 I conducted this study in summer 2019 at three stands located within a 20-km ra-
655 dius of Ithaca, NY, USA (42.444 °N, 76.502 °W). All stands contain mature,
656 closed-canopy forests dominated by deciduous tree species. Stands contained
657 abundant sugar maple (*Acer saccharum* Marshall), American beech (*Fagus gran-*
658 *difolia* Ehrh.), and white ash (*Fraxinus americana* L.), accounting for 43%, 15%,
659 and 17% of the total aboveground biomass across the three stands, respectively,
660 with less frequent red maple (*Acer rubrum* L.; 9% of total aboveground biomass)
661 and red oak occurrences (*Quercus rubra* L.; 10% of total aboveground biomass).
662 Soils at each site were broadly classified as a channery silt loam Inceptisols using
663 the USDA NRCS Web Soil Survey data product (Soil Survey Staff 2022). Between
664 2006 and 2020, study sites averaged 972 mm of precipitation per year and had an
665 average temperature of 7.9 °C per a weather station located near the Cornell Uni-
666 versity campus (42.449 °N, 76.449 °W) part of the NOAA NCEI Global Historical
667 Climatology Network (Menne et al. 2012).

668 3.2.2 *Experimental design*

669 Four 40 m x 40 m plots were set up at each site in 2009, each with an additional
670 10 m buffer along plot perimeters (60 m x 60 m total). The plots were set up as a
671 nitrogen-by-pH field manipulation experiment, with one each of four treatments
672 at each site. Two nitrogen treatments were applied, both at $50 \text{ kg N ha}^{-1} \text{ yr}^{-1}$, as
673 either sodium nitrate (NaNO_3) to raise soil pH, or ammonium sulfate ($(\text{NH}_4)_2\text{SO}_4$)
674 to acidify; an elemental sulfur treatment was selected to acidify without nitrogen,
675 applied at the same rate of S addition ($57 \text{ kg S ha}^{-1} \text{ yr}^{-1}$); and control plots
676 received no additions. All amendments were added in pelletized form using hand-
677 held fertilizer spreaders to both the main plots and buffers. Amendments were
678 divided into three equal doses distributed across the growing season from 2011-
679 2017 and added as a single dose from 2018 onward. During 2019, plots were
680 fertilized during the week of May 20.

681 3.2.3 *Leaf gas exchange and trait measurements*

682 I sampled one leaf each from 6 to 10 individuals per plot between June 25 and July
683 12, 2019 for gas exchange measurements (Table B1). Leaves were collected from
684 deciduous broadleaf trees represented across all sites and plots and were replicated
685 in efforts to mimic the species abundance of each plot at each site. I attempted
686 to collect leaves from the upper canopy to reduce differential shading effects on
687 leaf physiology. Leaves were accessed by pulling down small branches using an
688 arborist's slingshot and weighted beanbag attached to a throw line. Branches
689 were immediately recut under deionized water and remained submerged to reduce
690 stomatal closure and avoid xylem embolism, as done in Smith and Dukes (2018),

691 until gas exchange data were collected.

692 Randomly selected leaves with little to no visible external damage were
693 attached to a Li-COR LI-6800 (Li-COR Bioscience, Lincoln, Nebraska, USA)
694 portable photosynthesis machine to measure net photosynthesis (A_{net} ; $\mu\text{mol m}^{-2}$
695 s^{-1}), stomatal conductance (g_{sw} ; $\text{mol m}^{-2} \text{s}^{-1}$), and intercellular CO_2 concentra-
696 tion (C_i ; $\mu\text{mol mol}^{-1}$) at different reference CO_2 concentrations (C_a ; $\mu\text{mol mol}^{-1}$)
697 concentrations (i.e., an A_{net}/C_i curve) under saturating light conditions (2,000
698 $\mu\text{mol m}^{-2} \text{s}^{-1}$). Reference CO_2 concentrations followed the sequence: 400, 300,
699 200, 100, 50, 400, 400, 600, 800, 1000, 1200, 1500, and 2000 $\mu\text{mol mol}^{-1} \text{CO}_2$. Leaf
700 temperatures were not controlled in the cuvette and ranged from 21.8 °C to 31.7
701 °C (mean±SD: 27.2±2.2 °C). A linear and second order log-polynomial nonlinear
702 regression suggested no effect of temperature on stomatal conductance measured
703 at 400 $\mu\text{mol mol}^{-1} \text{CO}_2$ or net photosynthesis measured at 400 $\mu\text{mol mol}^{-1} \text{CO}_2$
704 (Table B2, B3; Fig. B1). All A_{net}/C_i curves were generated within one hour of
705 branch severance.

706 Leaf morphological and chemical traits were collected on the same leaf used
707 to generate each A_{net}/C_i curve. Images of each leaf were taken using a flat-bed
708 scanner to determine fresh leaf area using the ‘LeafArea’ R package (Katabuchi
709 2015), which automates leaf area calculations using ImageJ software (Schneider
710 et al. 2012). Each leaf was dried at 65°C for at least 48 hours, weighed, and
711 ground using a Retsch MM200 ball mill grinder (Verder Scientific, Inc., Newtown,
712 PA, USA) until homogenized. Leaf mass per unit leaf area (M_{area} , g m^{-2}) was
713 calculated as the ratio of dry leaf biomass to fresh leaf area. Using a subsample
714 of ground and homogenized leaf biomass, leaf nitrogen content (N_{mass} ; gN g^{-1})

715 and leaf $\delta^{13}\text{C}$ (‰, relative to Vienna Pee Dee Belemnite international reference
 716 standard) were measured at the Cornell Stable Isotope Lab with an elemental
 717 analyzer (NC 2500, CE Instruments, Wigan, UK) interfaced to an isotope ratio
 718 mass spectrometer (Delta V Isotope Ratio Mass Spectrometer, ThermoFisher Sci-
 719 entific, Waltham, MA, USA). Leaf nitrogen content per unit leaf area (N_{area} ; g N
 720 m^{-2}) was calculated by multiplying N_{mass} by M_{area} .

721 I used leaf $\delta^{13}\text{C}$ values to estimate χ (unitless), which is an isotope-derived
 722 estimate of the leaf $C_i:C_a$ ratio. While intercellular and atmospheric CO_2 concen-
 723 trations were directly measured during each A_{net}/C_i curve, deriving χ from $\delta^{13}\text{C}$
 724 provides a more integrative estimate of the leaf $C_i:C_a$ over an individual leaf's
 725 lifespan. I derived χ following the approach of Farquhar et al. (1989) described
 726 in Cernusak et al. (2013):

$$\chi = \frac{\Delta^{13}\text{C} - a}{b - a} \quad (3.1)$$

727 where $\Delta^{13}\text{C}$ represents the relative difference between leaf $\delta^{13}\text{C}$ (‰) and air $\delta^{13}\text{C}$
 728 (‰), and is calculated from the following equation:

$$\Delta^{13}\text{C} = \frac{\delta^{13}\text{C}_{\text{air}} - \delta^{13}\text{C}_{\text{leaf}}}{1 + \delta^{13}\text{C}_{\text{leaf}}} \quad (3.2)$$

729 where $\delta^{13}\text{C}_{\text{air}}$ is assumed to be -8‰ (Keeling et al. 1979; Farquhar et al. 1989), a
 730 represents the fractionation between ^{12}C and ^{13}C due to diffusion in air, assumed
 731 to be 4.4‰, and b represents the fractionation caused by Rubisco carboxylation,
 732 assumed to be 27‰ (Farquhar et al. 1989).

733 3.2.4 A_{net}/C_i curve-fitting and parameter estimation

734 I fit A_{net}/C_i curves of each individual using the ‘fitaci’ function in the ‘plante-
735 cophys’ R package (Duursma 2015). This function estimates the maximum rate
736 of Rubisco carboxylation (V_{cmax} ; $\mu\text{mol m}^{-2} \text{s}^{-1}$) and maximum rate of electron
737 transport for RuBP regeneration (J_{max} ; $\mu\text{mol m}^{-2} \text{s}^{-1}$) based on the Farquhar,
738 von Caemmerer, and Berry biochemical model of C₃ photosynthesis (Farquhar
739 et al. 1980). For each curve fit, I included triose phosphate utilization (TPU)
740 limitation to avoid underestimating J_{max} (Gregory et al. 2021). Curves were
741 visually examined to confirm the likely presence of TPU limitation.

742 I determined Michaelis-Menten coefficients for Rubisco affinity to CO₂ (K_c ;
743 $\mu\text{mol mol}^{-1}$) and O₂ (K_o ; $\mu\text{mol mol}^{-1}$), and the CO₂ compensation point (Γ^* ;
744 $\mu\text{mol mol}^{-1}$) using leaf temperature and equations described in Medlyn et al.
745 (2002) and derived in Bernacchi et al. (2001). Specifically, K_c and K_o were
746 calculated as:

$$K_c = 404.9 * \exp^{\frac{79430(T_k - 298)}{298RT_k}} \quad (3.3)$$

747 and

$$K_o = 278.4 * \exp^{\frac{36380(T_k - 298)}{298RT_k}} \quad (3.4)$$

748 while Γ^* was calculated as:

$$\Gamma^* = 42.75 * \exp^{\frac{37830(T_k - 298)}{298RT_k}} \quad (3.5)$$

749 In all three equations, T_k is the leaf temperature (in Kelvin) during each A_{net}/C_i

750 curve and R is the universal gas constant ($8.314 \text{ J mol}^{-1} \text{ K}^{-1}$).

751 I standardized V_{cmax} and J_{max} estimates to 25°C using a modified Arrhe-

752 nius equation (Kattge and Knorr 2007):

$$k_{25} = \frac{k_{\text{obs}}}{e^{\frac{H_a(T_{\text{obs}} - T_{\text{ref}})}{T_{\text{ref}}RT_{\text{obs}}}} * \frac{1+e^{\frac{T_{\text{ref}}\Delta S - H_d}{T_{\text{obs}}\Delta S - H_d}}}{1+e^{\frac{T_{\text{obs}}\Delta S - H_d}{T_{\text{obs}}}}}} \quad (3.6)$$

753 k_{25} represents the standardized V_{cmax} or J_{max} rate at 25°C , k_{obs} represents the

754 V_{cmax} or J_{max} estimate at the average leaf temperature measured inside the cuvette

755 during the A_{net}/C_i curve. H_a is the activation energy of V_{cmax} ($71,513 \text{ J mol}^{-1}$)

756 Kattge and Knorr (2007) or J_{max} ($49,884 \text{ J mol}^{-1}$) (Kattge and Knorr 2007).

757 H_d represents the deactivation energy of both V_{cmax} and J_{max} ($200,000 \text{ J mol}^{-1}$)

758 (Medlyn et al. 2002), and R represents the universal gas constant (8.314 J mol^{-1}

759 K^{-1}). T_{ref} represents the standardized temperature of 298.15 K (25°C) and T_{obs}

760 represents the mean leaf temperature (in K) during each A_{net}/C_i curve. ΔS is an

761 entropy term that (Kattge and Knorr 2007) derived as a linear relationship with

762 average growing season temperature (T_g ; $^\circ\text{C}$), where:

$$\Delta S_{v_{\text{cmax}}} = -1.07 T_g + 668.39 \quad (3.7)$$

763 and

$$\Delta S_{j_{\text{max}}} = -0.75 T_g + 659.70 \quad (3.8)$$

764 I estimated T_g in Equations 3.7 and 3.8 based on mean daily (24-hour) air tem-
765 perature of the 30 days leading up to the day of each sample collection using the
766 same weather station reported in the site description. I used V_{cmax25} and J_{max25}
767 estimates to calculate the ratio of J_{max25} to V_{cmax25} ($J_{max25}:V_{cmax25}$; unitless).

768 3.2.5 *Proportion of leaf nitrogen allocated to photosynthesis and structure*

769 I used equations from Niinemets and Tenhunen (1997) to estimate the proportion
770 of leaf nitrogen content allocated to Rubisco and bioenergetics. The proportion of
771 leaf nitrogen allocated to Rubisco ($\rho_{rubisco}$; gN gN⁻¹) was calculated as a function
772 of V_{cmax25} and N_{area} :

$$\rho_{rubisco} = \frac{V_{cmax25} N_r}{V_{cr} N_{area}} \quad (3.9)$$

773 where N_r is the amount of nitrogen in Rubisco, set to 0.16 gN (gN in Rubisco)⁻¹
774 and V_{cr} is the maximum rate of RuBP carboxylation per unit Rubisco protein,
775 set to 20.5 μmol CO₂ (g Rubisco)⁻¹. The proportion of leaf nitrogen allocated to
776 bioenergetics (ρ_{bioe} ; gN gN⁻¹) was similarly calculated as a function of J_{max25} and
777 N_{area} :

$$\rho_{bioe} = \frac{J_{max25} N_b}{J_{mc} N_{area}} \quad (3.10)$$

778 where N_b is the amount of nitrogen in cytochrome f, set to 0.12407 gN (μmol
779 cytochrome f)⁻¹ assuming a constant 1: 1: 1.2 cytochrome f: ferredoxin NADP
780 reductase: coupling factor molar ratio (Evans and Seemann 1989; Niinemets and
781 Tenhunen 1997), and J_{mc} is the capacity of electron transport per cytochrome f,

782 set to 156 μmol electron (μmol cytochrome f) $^{-1}\text{s}^{-1}$.

783 I estimated the proportion of leaf nitrogen content allocated to photosynthetic tissue (ρ_{photo} ; gN gN^{-1}) as the sum of ρ_{rubisco} and ρ_{bioe} . This calculation
784 is an underestimate of the proportion of leaf nitrogen allocated to photosynthetic
785 tissue because it does not include nitrogen allocated to light harvesting proteins.
786 This leaf nitrogen pool was not included because I did not perform chlorophyll
787 extractions on focal leaves. However, the proportion of leaf nitrogen content al-
788 located to light harvesting proteins tends to be small relative to ρ_{rubisco} and ρ_{bioe} ,
789 and may scale with changes in ρ_{rubisco} and ρ_{bioe} (Niinemets and Tenhunen 1997).

791 Finally, the proportion of leaf nitrogen content allocated to structural tissue
792 ($\rho_{\text{structure}}$; gN gN^{-1}) was estimated as:

$$\rho_{\text{structure}} = \frac{N_{\text{cw}}}{N_{\text{area}}} \quad (3.11)$$

793 where N_{cw} is the leaf nitrogen content allocated to cell walls (gN m^{-2}), calculated
794 as a function of M_{area} using an empirical equation from Onoda et al. (2017):

$$N_{\text{cw}} = 0.000355 * M_{\text{area}}^{1.39} \quad (3.12)$$

795 3.2.6 *Tradeoffs between nitrogen and water use*

796 Photosynthetic nitrogen use efficiency (PNUE; $\mu\text{mol CO}_2 \text{ mol}^{-1} \text{ N s}^{-1}$) was cal-
797 culated by dividing A_{net} by N_{area} , first converting N_{area} to mol N m^{-2} using the
798 molar mass of nitrogen (14 g mol^{-1}). I used χ as an indicator of water use effi-
799 ciency, which exploratory analyses suggest had similar responses to soil nitrogen

800 availability and pH as intrinsic water use efficiency measured from gas exchange
801 ($A_{\text{net}}/g_{\text{sw}}$). Tradeoffs between nitrogen and water use were determined by cal-
802 culating the ratio of N_{area} to χ ($N_{\text{area}}:\chi$; gN m⁻²) and V_{cmax25} to χ ($V_{\text{cmax25}}:\chi$;
803 $\mu\text{mol m}^{-2} \text{ s}^{-1}$). This approach is similar to tradeoff calculations in which nitrogen-
804 water use tradeoffs are measured as the ratio of N_{area} or V_{cmax25} to g_{sw} (Paillassa
805 et al. 2020; Bialic-Murphy et al. 2021). In this chapter, I quantify these rela-
806 tionships using χ in lieu of g_{sw} because g_{sw} rapidly changes with environmental
807 conditions and therefore may have been altered by recent tree branch severance
808 and/or placement in the cuvette.

809 3.2.7 *Soil nitrogen availability and pH*

810 To characterize soil nitrogen availability at the time of our leaf gas exchange
811 measurements, I used mixed bed resin bags to quantify mobile ammonium-N and
812 nitrate-N concentrations in each plot. Lycra mesh bags were filled with 5 g of
813 Dowex® Marathon MR-3 hydrogen and hydroxide form resin (MilliporeSigma,
814 Burlington, MA USA) and sealed with a zip tie. Each bag was activated by
815 soaking in 0.5 M HCl for 20 minutes, then in 2 M NaCl until pH of the saline
816 solution stabilized, as described in Allison et al. (2008). Five resin bags were
817 inserted about 10 cm below the soil surface at each plot on June 25, 2019: one
818 near each of the four plot corners and one near the plot center. All resin bags
819 were collected 24 days later on July 19, 2019 and were frozen until extracted.

820 Prior to anion and cation extraction, each resin bag was rinsed with ul-
821 trapure water (MilliQ IQ 7000; Millipore Sigma, Burlington, MA) to remove any
822 surface soil residues. Anions and cations were extracted from surface-cleaned

823 resin bags by individually soaking and shaking each bag in 100 mL of a 0.1 M
824 HCl/2.0 M NaCl matrix for one hour. Using a microplate reader (Biotek Synergy
825 H1; Biotek Instruments, Winooski, VT USA), I quantified nitrate-N concentra-
826 tions spectrophotometrically at 540 nm with the end product of a single reagent
827 vanadium (III) chloride reaction (Doane and Horwáth 2003), and ammonium-N
828 concentrations quantified at 650 nm with the end product of a modified phenol-
829 hypochlorite reaction (Weatherburn 1967; Rhine et al. 1998). Both the single
830 reagent vanadium (III) chloride and modified phenol-hypochlorite methodologies
831 are well established for determining nitrate-N and ammonium-N concentrations
832 in resin bag extracts (Arnone 1997; Allison et al. 2008). I used a series of nega-
833 tive and positive controls throughout each well plate to verify the accuracy and
834 precision of our measurements, assaying each resin bag extract and control in
835 triplicate. Soil nitrogen availability was estimated as the sum of the nitrate-N
836 and ammonium-N concentration in each resin bag, normalized per g of resin and
837 duration in the field ($\mu\text{g N g}^{-1} \text{ resin d}^{-1}$), then subsequently averaged across all
838 resin bags in a plot for a plot-level mean.

839 Soil pH was measured on 0-10 cm mineral soil samples collected prior to
840 fertilization in 2019. Near each of the four plot corners, three 5.5 cm diameter soil
841 cores were collected after first removing the forest floor where present. Each set
842 of three cores was placed in a plastic bag, and later composited by hand mixing
843 and sieved to 4mm. Soil pH was determined for a 1:2 soil:water slurry (10 g field-
844 moist soil to 20 mL DI water) of each sample using an Accumet AB15 pH meter
845 with flushable junction probe (Fisher Scientific; Hampton, NH, USA), and was
846 estimated at the plot level as the mean soil pH within each plot.

847 3.2.8 *Statistical analyses*

848 I built two separate series of linear mixed-effects models to explore effects of soil
849 nitrogen availability, soil pH, species, and leaf nitrogen content on leaf physiolog-
850 ical traits. In the first series of linear mixed-effects models, I explored the effect
851 of soil nitrogen availability, soil pH, and species on leaf nitrogen content, leaf
852 photosynthesis, stomatal conductance, and nitrogen-water use tradeoffs. Models
853 included plot-level soil nitrogen availability and plot-level soil pH as continuous
854 fixed effects, species as a categorical fixed effect, and site as a categorical ran-
855 dom intercept term. Interaction terms between fixed effects were not included
856 due to the small number of experimental plots. I built a series of separate mod-
857 els with this independent variable structure to quantify individual effects of soil
858 nitrogen availability, soil pH, and species on N_{area} , M_{area} , N_{mass} , A_{net} , V_{cmax25} ,
859 J_{max25} , $J_{\text{max25}}:V_{\text{cmax25}}$, ρ_{rubisco} , $\rho_{\text{bioenergetics}}$, ρ_{photo} , $\rho_{\text{structure}}$, χ , PNUE, $N_{\text{area}}:\chi$, and
860 $V_{\text{cmax25}}:\chi$.

861 A second series of linear mixed-effects models were built to investigate
862 relationships between leaf nitrogen content and photosynthetic parameters. Sta-
863 tistical models included N_{area} as a single continuous fixed effect with species and
864 site designated as individual random intercept terms. I used this independent
865 variable structure to quantify individual effects of leaf nitrogen content on A_{net} ,
866 V_{cmax25} , J_{max25} , $J_{\text{max25}}:V_{\text{cmax25}}$, and χ .

867 For all linear mixed-effects models, I used Shapiro-Wilk tests of normality
868 to determine whether linear mixed-effects models satisfied residual normality as-
869 sumptions. If residual normality assumptions were not met, then models were fit
870 using dependent variables that were natural log transformed. If residual normal-

871 ity assumptions were still not met (Shapiro-Wilk: $p<0.05$), then models were fit
872 using dependent variables that were square root transformed. All residual nor-
873 mality assumptions for both sets of models that did not originally satisfy residual
874 normality assumptions were met with either a natural log or square root data
875 transformation (Shapiro-Wilk: $p>0.05$ in all cases).

876 In the first series of models, models for N_{area} , M_{area} , N_{mass} , V_{cmax25} , J_{max25} ,
877 χ , $N_{\text{area}}:\chi$, and $V_{\text{cmax25}}:\chi$, ρ_{rubisco} , $\rho_{\text{bioenergetics}}$, ρ_{photo} , $\rho_{\text{structure}}$ satisfied residual
878 normality assumptions without data transformations (Shapiro-Wilk: $p>0.05$ in
879 all cases). The model for $J_{\text{max25}}:V_{\text{cmax25}}$ satisfied residual normality assumptions
880 with a natural log data transformation, while models for A_{net} and PNUE each
881 satisfied residual normality assumptions with square root data transformations.
882 In the second series of models, models for V_{cmax25} , J_{max25} , χ , and $V_{\text{cmax25}}:\chi$ satis-
883 fied residual normality assumptions without data transformations (Shapiro-Wilk:
884 $p>0.05$ in all cases). The model for $J_{\text{max25}}:V_{\text{cmax25}}$ required a natural log data
885 transformation and the model for A_{net} required a square root data transformation
886 (Shapiro-Wilk: $p>0.05$ in both cases).

887 In all models, I used the ‘lmer’ function in the ‘lme4’ R package (Bates
888 et al. 2015) to fit each model and the ‘Anova’ function in the ‘car’ R package
889 (Fox and Weisberg 2019) to calculate Type II Wald’s χ^2 and determine the signif-
890 icance level ($\alpha=0.05$) of each fixed effect coefficient. Finally, I used the ‘emmeans’
891 R package (Lenth, 2019) to conduct post-hoc comparisons using Tukey’s tests,
892 where degrees of freedom were approximated using the Kenward-Roger approach
893 (Kenward and Roger 1997). All analyses and plots were conducted in R version
894 4.1.1 (R Core Team 2021). All figure regression lines and associated 95% confi-

895 dence interval error bars were plotted using predictions generated across the soil
896 nitrogen availability gradient using the ‘emmeans’ R package (Lenth 2019).

897 3.3 Results

898 3.3.1 *Leaf nitrogen content*

899 Increasing soil nitrogen availability generally increased N_{area} (Table 3.1; Fig. 3.1a).
900 This pattern was driven by an increase in N_{mass} (Table 3.1; Fig. 3.1c) and a
901 marginal increase in M_{area} (Table 3.1; Fig. 3.1e) with increasing soil nitrogen
902 availability. There was no effect of soil pH on N_{area} , N_{mass} , or M_{area} (Table 3.1);
903 however, I also observed strong differences in N_{area} (Fig. 3.1b), N_{mass} (Fig. 3.1d),
904 and M_{area} (Fig. 3.1e) between species (Table 3.1).

Table 3.1. Effects of soil nitrogen availability, soil pH, and species on leaf nitrogen content per unit leaf area (N_{area} ; gN m⁻²), leaf nitrogen content per unit leaf mass (N_{mass} ; gN g⁻¹), and leaf mass per unit leaf area (M_{area} ; g m⁻²)*

	N_{area}			N_{mass}			M_{area}			
	df	Coefficient	χ^2	p	Coefficient	χ^2	p	Coefficient	χ^2	p
Intercept	-	9.03E-01	-	-	1.68E+00	-	-	4.60E+01	-	-
Soil N	1	1.68E-02	11.990	0.001	1.25E-02	6.902	0.009	4.87E-01	4.143	0.042
Soil pH	1	9.28E-02	0.836	0.361	8.08E-02	0.663	0.415	4.05E+00	0.653	0.419
Species	4	-	72.128	<0.001	-	35.074	<0.001	-	29.869	<0.001

905 *Significance determined using Type II Wald χ^2 tests ($\alpha=0.05$). P-values<0.05 are in bold.

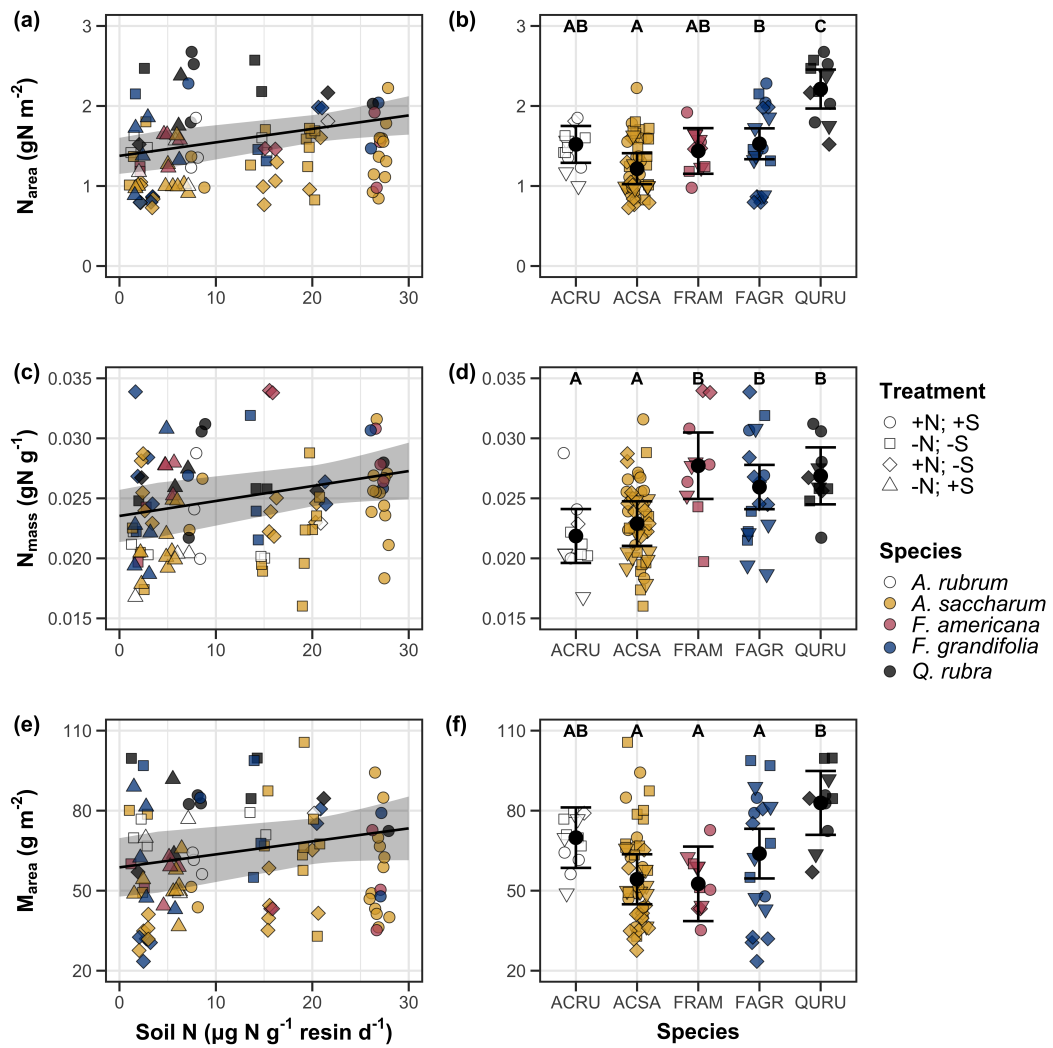


Figure 3.1. Effects of soil N availability and species on leaf nitrogen content per unit leaf area (a-b), leaf nitrogen content per unit leaf biomass (c-d), and leaf mass per unit leaf area (e-f). Soil nitrogen availability is represented on the x-axis in the left column of panels, while species is represented on the x-axis in the right column of panels. Tree species are represented as colored points and treatment plots are represented as shaped points, jittered for visibility. Species are abbreviated in the right column of panels through their assigned NRCS PLANTS Database symbol (USDA NRCS 2022), grouped along the x-axis per common mycorrhizal association, where the first three species commonly associate with arbuscular mycorrhizae (ACRU, ACSA, FAGR) and the second two species with ectomycorrhizae (FAGR, QURU). Trendlines are only included when the regression slope is statistically different from zero ($p < 0.05$).

906 3.3.2 *Net photosynthesis and leaf biochemistry*

907 Increasing soil nitrogen availability generally had no effect on A_{net} , V_{cmax25} , J_{max25} ,
908 or $J_{\text{max25}}:V_{\text{cmax25}}$ (Table 3.2, Figs. 3.2a, 3.2d, 3.2g). I also observed strong species
909 effects on all measured leaf photosynthetic traits (Table 3.2; Figs. 3.2b, 3.2e, 3.2h).
910 Increasing soil pH had a marginal negative effect on A_{net} , but had no effect on
911 V_{cmax25} , J_{max25} , or $J_{\text{max25}}:V_{\text{cmax25}}$ (Table 3.2). There was a weak positive effect of
912 increasing N_{area} on A_{net} (Fig. 3.2c), but quite strong positive effects of increasing
913 N_{area} on V_{cmax25} and J_{max25} (Table 3.2; Fig. 3.2f and 3.2i).

Table 3.2. Effects of soil nitrogen availability, soil pH, species, and N_{area} on net photosynthesis (A_{net} ; $\mu\text{mol m}^{-2} \text{s}^{-1}$), the maximum rate of Rubisco carboxylation (V_{cmax25} ; $\mu\text{mol m}^{-2} \text{s}^{-1}$), the maximum rate of RuBP regeneration (J_{max25} ; $\mu\text{mol m}^{-2} \text{s}^{-1}$), and the ratio of the maximum rate of RuBP regeneration to the maximum rate of Rubisco carboxylation ($J_{\text{max25}}:V_{\text{cmax25}}$; unitless)*

	A_{net}			V_{cmax25}			J_{max25}			
	df	Coefficient	χ^2	p	Coefficient	χ^2	p	Coefficient	χ^2	p
(Intercept)	-	3.29E+00 ^b	-	-	6.38E+01	-	-	1.12E+02	-	-
Soil N	1	-1.23E-03 ^b	1.798	0.180	-3.84E-01	1.745	0.187	-6.70E-01	2.172	0.141
Soil pH	1	-3.09E-01 ^b	3.312	0.069	-4.91E+00	0.655	0.418	-8.18E+00	0.742	0.389
Species	4	-	11.838	0.019	-	31.748	<0.001	-	27.291	<0.001
(N_{area} int.)	-	6.59E-01 ^b	-	-	1.45E-01	-	-	2.86E+01	-	-
N_{area}	4	3.13E-01 ^b	4.790	0.029	2.43E+01	22.616	<0.001	4.04E+01	28.259	<0.001

	$J_{\text{max25}}:V_{\text{cmax25}}$			
	df	Coefficient	χ^2	p
(Intercept)	-	6.59E-01 ^a	-	-
Soil N	1	7.04E-04 ^a	0.088	0.767
Soil pH	1	-7.84E-03 ^a	0.025	0.874
Species	4	-	12.745	0.013
(N_{area} int.)	-	6.69E-01 ^a	-	-
N_{area}	4	-4.69E-02 ^a	1.142	0.285

54

914 *Significance determined using Type II Wald χ^2 tests ($\alpha=0.05$). P-values less than 0.05 are in bold, while p-values
 915 between 0.05 and 0.1 are italicized. Superscript letters indicate model coefficients fit to natural-log (^a) or square-root
 916 (^b) transformed data. Relationships between N_{area} and each response variable were fit using the second series of
 917 bivariate mixed-effects models, so model coefficients and results are independent of model coefficients and results
 918 reported for relationships between soil nitrogen, soil pH, and species for each response variable.

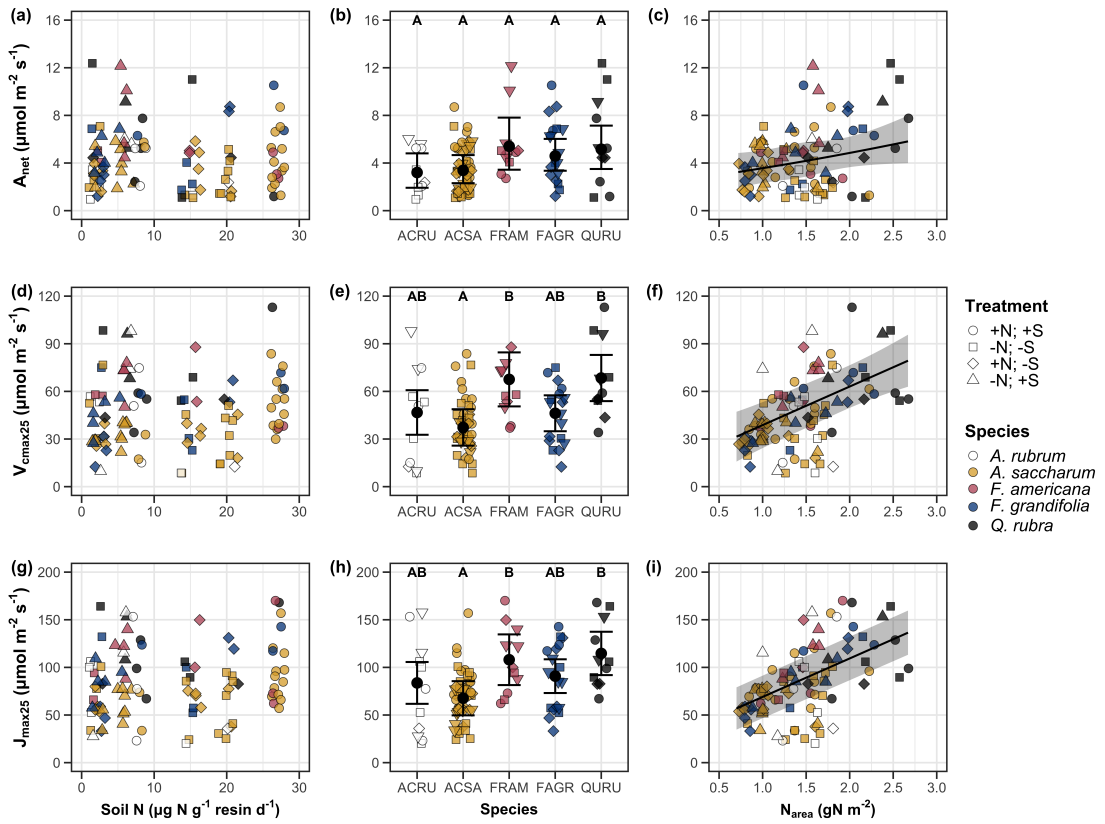


Figure 3.2. Effects of soil nitrogen availability (left column of panels), species (middle column of panels), and leaf nitrogen content per unit leaf area (right column of panels) on net photosynthesis (a-c), maximum Rubisco carboxylation rate (d-f), and maximum RuBP regeneration rate (g-i). Soil nitrogen availability is represented on the x-axis in the left column of panels, species is represented on the x-axis in the middle column of panels, and leaf nitrogen content per unit leaf area is represented continuously on the x-axis in the right column of panels. Species abbreviations and position along the x-axis in the middle column of panels, colored points, shapes, and trendlines are as explained in Figure 3.1.

919 3.3.3 *Leaf nitrogen allocation*

920 Neither soil nitrogen availability nor soil pH affected the proportion of leaf nitrogen
921 allocated to Rubisco or bioenergetics (Table 3.3; Fig. 3.3a, Fig. 3.3c). There was
922 also no effect of soil nitrogen availability or soil pH on the proportion of leaf
923 nitrogen allocated to photosynthesis (Table 3.3; Fig. 3.3f). I found no effect of
924 soil nitrogen availability or soil pH on the proportion of leaf nitrogen allocated to
925 structure (Table 3.3; Fig 3.3g). Species varied in the proportion of leaf nitrogen
926 allocated to Rubisco, photosynthesis, and structure (Fig 3.3b, Fig. 3.3f, Fig 3.3h),
927 with no detectable species effect on the proportion of leaf nitrogen allocated to
928 bioenergetics (Table 3.3, Fig. 3.3d).

Table 3.3. Effects of soil nitrogen availability, soil pH, and species on the proportion of leaf nitrogen content allocated to photosynthesis (ρ_{photo} ; gN gN⁻¹), Rubisco (ρ_{rubisco} ; gN gN⁻¹), bioenergetics (ρ_{bioe} ; gN gN⁻¹), and structure ($\rho_{\text{structure}}$; gN gN⁻¹)*

	ρ_{photo}			ρ_{rubisco}			ρ_{bioe}			
	df	Coefficient	χ^2	p	Coefficient	χ^2	p	Coefficient	χ^2	p
Intercept	-	4.93E-01	-	-	4.17E-01	-	-	7.64E-02	-	-
Soil N	1	-1.23E-03	0.521	0.470	-1.04E-03	0.501	0.479	-1.77E-04	0.557	0.455
Soil pH	1	-4.37E-02	1.581	0.209	-3.70E-02	1.511	0.219	-6.84E-03	1.941	0.164
Species	4	-	13.106	0.011	-	14.152	0.007	-	7.300	0.121

	$\rho_{\text{structure}}$			
	df	Coefficient	χ^2	p
Intercept	-	9.77E-02	-	-
Soil N	1	-2.29E-04	1.165	0.280
Soil pH	1	-1.87E-03	0.179	0.672
Species	4	-	16.428	0.002

929 *Significance determined using Type II Wald χ^2 tests ($\alpha=0.05$). P-values less than 0.05 are in bold.

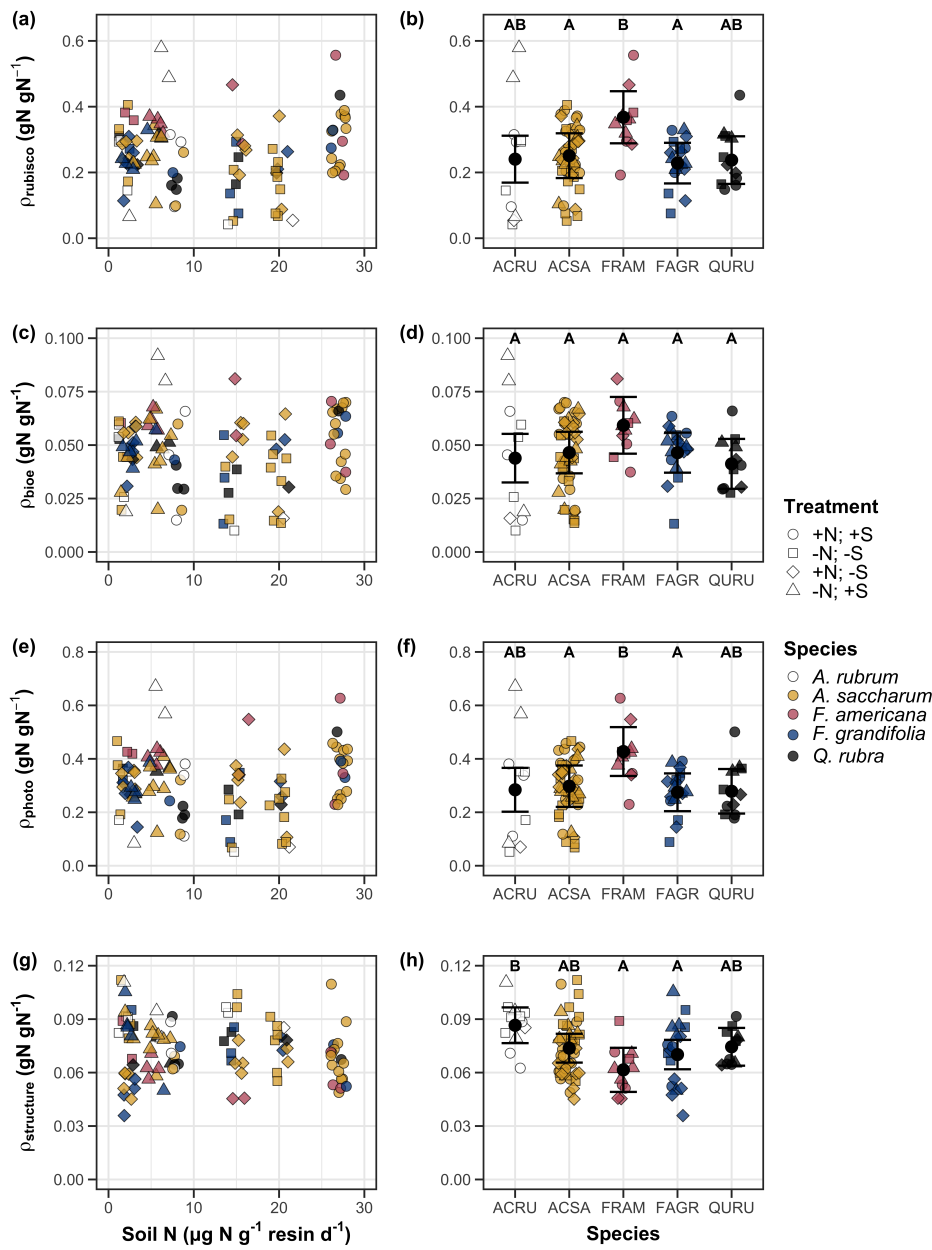


Figure 3.3. Effects of soil nitrogen availability and species on the proportion of leaf nitrogen content allocated to Rubisco (a-b), bioenergetics (c-d), photosynthesis (e-f), and structure (g-h). Soil nitrogen availability is represented on the x-axis in the left column of panels and species are represented on the x-axis in the right column of panels. Species abbreviations and position along the x-axis in the middle column of panels, colored points, shapes, trendlines, error bars, and compact lettering are as explained in Figure 3.1.

930 3.3.4 *Tradeoffs between nitrogen and water use*

931 Although soil nitrogen availability did not affect χ (Table 3.4; Fig. 3.4a), increasing
932 soil nitrogen availability decreased PNUE (Table 3.4; Fig. 3.4d) and increased
933 the ratio of $N_{\text{area}}:\chi$ (Table 3.4; Fig. 3.4f). Specifically, this response yielded a
934 26% reduction in PNUE and 37% stimulation in $N_{\text{area}}:\chi$ across the soil nitrogen
935 availability gradient. There was no apparent effect of soil nitrogen availability on
936 $V_{\text{cmax25}}:\chi$ (Table 3.4; Fig. 3.4h). Increasing soil pH had a weak marginal nega-
937 tive effect on PNUE, but did not influence χ , $N_{\text{area}}:\chi$, or $V_{\text{cmax25}}:\chi$ (Table 3.4). I
938 observed differences in χ (Fig. 3.4b), PNUE (Fig. 3.4e), $N_{\text{area}}:\chi$ (Fig. 3.4g), and
939 $V_{\text{cmax25}}:\chi$ (Fig. 3.4i) between species (Table 3.4). Finally, increasing N_{area} had a
940 strong negative effect on χ (Table 3.4; Fig. 3.4c) and a strong positive effect on
941 $V_{\text{cmax25}}:\chi$ (Table 3.4; Fig. 3.4j).

Table 3.4. Effects of soil nitrogen availability, soil pH, species, and N_{area} on χ (unitless), photosynthetic nitrogen use efficiency (PNUE; $\mu\text{mol CO}_2 \text{ mol}^{-1} \text{ N s}^{-1}$), leaf nitrogen content per unit χ ($N_{\text{area}}:\chi$; gN m^{-2}), and maximum Rubisco carboxylation rate per unit χ ($V_{\text{cmax25}}:\chi$; $\mu\text{mol m}^{-2} \text{ s}^{-1}$)^{*}

	χ			PNUE			$N_{\text{area}}:\chi$			
	df	Coefficient	χ^2	p	Coefficient	χ^2	p	Coefficient	χ^2	p
(Intercept)	-	8.12E-01	-	-	9.57E+00 ^b	-	-	9.19E-01	-	-
Soil N	1	-1.14E-03	1.698	0.193	-6.63E-02 ^b	6.396	0.011	2.60E-02	9.533	0.002
Soil pH	1	-1.91E-02	1.087	0.297	-9.25E-01 ^b	2.843	<i>0.092</i>	2.03E-01	1.321	0.250
Species	4	-	18.843	0.001	-	13.454	0.009	-	52.983	<0.001
(N_{area} int.)	-	8.93E-01	-	-	-	-	-	-	-	-
N_{area}	1	-1.11E-01	80.606	<0.001	-	-	-	-	-	-

	$V_{\text{cmax25}}:\chi$			
	df	Coefficient	χ^2	p
(Intercept)	-	7.20E+01	-	-
Soil N	1	3.99E-01	0.963	0.326
Soil pH	1	-3.12E+00	0.138	0.711
Species	4	-	31.450	<0.001
(N_{area} int.)	-	1.18E+01	-	-
N_{area}	4	3.87E+01	32.797	<0.001

60

942 *Significance determined using Type II Wald χ^2 tests ($\alpha = 0.05$). P-values less than 0.05 are in bold, while p-values
 943 between 0.05 and 0.1 are italicized. Superscript letters indicate model coefficients fit to natural-log (^a) or square-root
 944 (^b) transformed data. Relationships between N_{area} and each response variable were fit using the second series of
 945 bivariate mixed-effects models, so model coefficients and results are independent of model coefficients and results
 946 reported for relationships between soil nitrogen, soil pH, and species for each response variable.

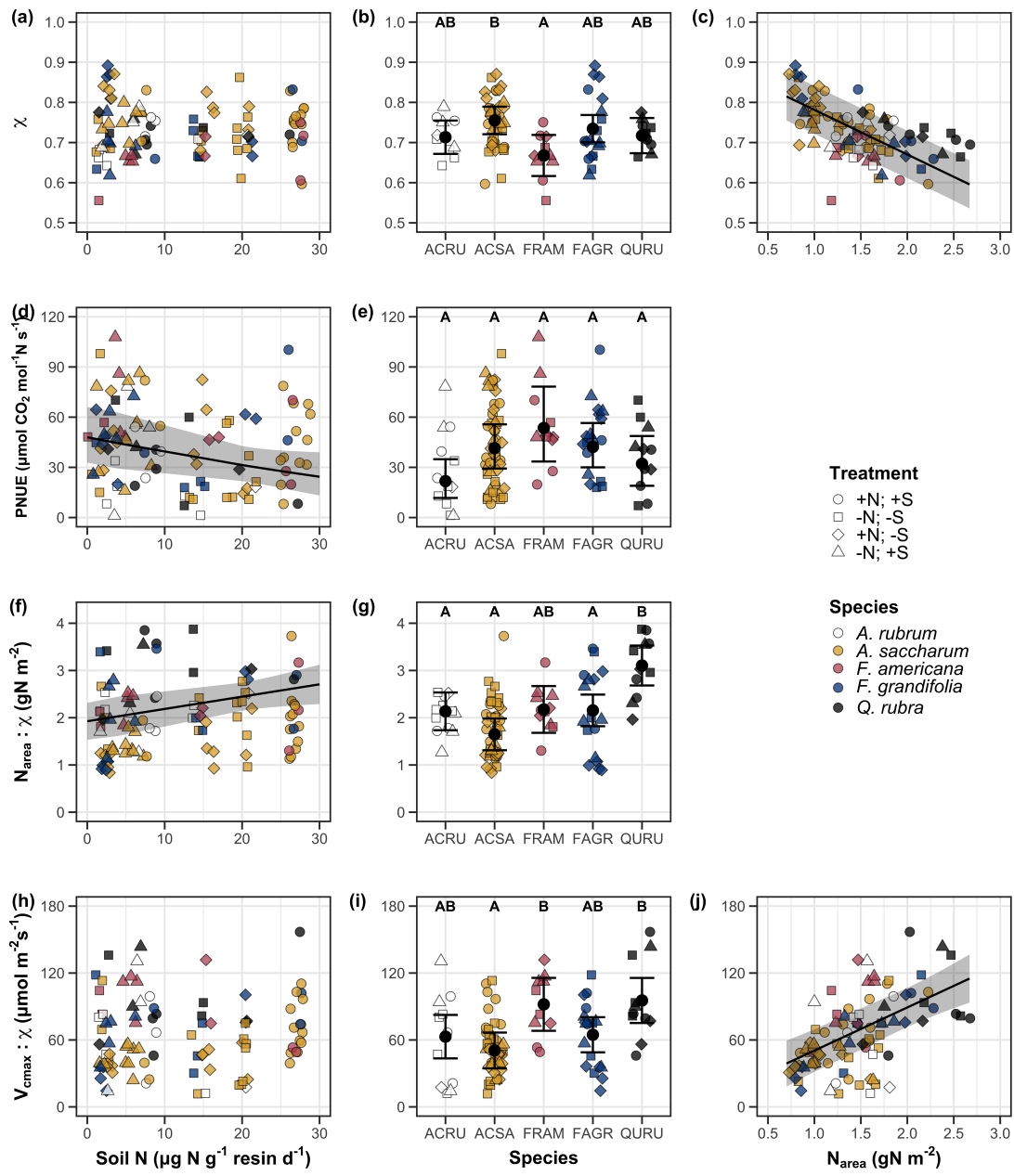


Figure 3.4. Effects of soil nitrogen availability and species on the proportion of leaf nitrogen content allocated to Rubisco (a-b), bioenergetics (c-d), photosynthesis (Rubisco + bioenergetics; e-f), and structure (g-h). Soil nitrogen availability is represented on the x-axis in the left column of panels and species are represented on the x-axis in the right column of panels. Species abbreviations and position along the x-axis in the middle column of panels, colored points, shapes, trendlines, error bars, and compact lettering are as explained in Figure 3.1.

947 3.4 Discussion

948 Photosynthetic least-cost theory provides an explanation for understanding rela-
949 tionships between soil nutrient availability, leaf nutrient allocation, and photosyn-
950 thetic capacity. The theory suggests that plants acclimate to a given environment
951 by optimizing leaf photosynthesis rates at the lowest summed cost of using nu-
952 trients and water (Prentice et al. 2014; Wang et al. 2017; Smith et al. 2019;
953 Paillassa et al. 2020). The theory predicts that an increase in soil nutrient avail-
954 ability should allow similar photosynthesis rates to be achieved with increased leaf
955 nutrient content and photosynthetic capacity (i.e., V_{cmax25} and J_{max25}) at lower
956 leaf $C_i:C_a$ (χ), resulting in an increase in water use efficiency, decrease in nutri-
957 ent use efficiency, and increase in both leaf nutrient content and photosynthetic
958 capacity per unit χ . The theory predicts similar leaf responses to increasing soil
959 pH under acidic conditions, presumably due to generally faster nutrient cycle dy-
960 namics and consequent reductions in the cost of acquiring nutrients relative to
961 water with increasing soil pH (Wang et al. 2017; Paillassa et al. 2020; Dong et al.
962 2020).

963 Supporting the theory, increasing soil nitrogen availability was associated
964 with increased leaf nitrogen content, a pattern that reduced photosynthetic nitro-
965 gen use efficiency and increased leaf nitrogen content per unit χ . Increasing soil
966 nitrogen coincided with slight, but non-significant decreases in χ and increases
967 in V_{cmax25} and J_{max25} ($p<0.2$, Table 3.2). The positive trend between soil ni-
968 trogen availability and photosynthetic capacity was supported by the concurrent
969 strong increase in leaf nitrogen content with increasing soil nitrogen availability,
970 which resulted in no change in the proportion of leaf nitrogen content allocated to

971 photosynthesis across the soil nitrogen availability gradient. Additionally, leaf ni-
972 trogen content exhibited a strong negative correlation with χ , indicative of strong
973 nitrogen-water use tradeoffs at the leaf level. Responses tended to vary more due
974 to soil nitrogen availability than soil pH. Overall, these findings are consistent
975 with the nutrient-water use tradeoffs predicted from theory.

976 3.4.1 *Soil nitrogen availability modifies tradeoffs between nitrogen and water use*
977 In support of expected least-cost outcomes and past environmental gradient stud-
978 ies (Dong et al. 2017; Paillassa et al. 2020), increasing soil nitrogen availability
979 was associated with increased leaf nitrogen content. Soil nitrogen availability had
980 smaller impacts on measures of net photosynthesis and χ , which led to reductions
981 in PNUE and increases in leaf nitrogen content per unit χ , as expected from the-
982 ory. Photosynthetic least-cost theory suggests that reductions in PNUE should
983 be driven by an increase in the proportion of leaf nitrogen allocated to photosyn-
984 thetic tissue, a pattern that should allow plants to achieve optimal photosynthetic
985 rates with greater photosynthetic capacity to make better use of available light.
986 Contrasting theory predictions, I found no effect of soil nitrogen availability on
987 photosynthetic capacity. However, photosynthetic capacity did tend to increase
988 with increasing soil nitrogen availability ($p<0.20$; Table 3.2) resulting in no effect
989 of soil nitrogen availability on the relative fraction of leaf nitrogen allocated to
990 photosynthesis, Rubisco, or bioenergetics. These lines of evidence support the
991 idea that trees use additional nitrogen to support increased leaf nitrogen alloca-
992 tion toward photosynthetic tissue and enhance photosynthetic capacity (Wright
993 et al. 2003).

994 Soil nitrogen availability had a stronger effect on leaf nitrogen than photo-
995 synthetic capacity. This pattern suggests that additional plant nitrogen up-
996 take due to increased soil nitrogen availability was also being used to support
997 non-photosynthetic nitrogen pools, possibly to structural tissue or stress-induced
998 amino acid and polyamine synthesis (Minocha et al. 2000; Onoda et al. 2004;
999 Bubier et al. 2011). While I found no change in the proportion of leaf nitrogen
1000 allocated to leaf structural tissue, the overall stimulation in leaf nitrogen content
1001 with increasing soil nitrogen availability suggests an increase in the net amount of
1002 nitrogen invested in leaf structural tissue along the nitrogen availability gradient.
1003 Importantly, leaf nitrogen allocated to structure was calculated using an empiri-
1004 cal relationship between M_{area} and the amount of leaf nitrogen allocated to cell
1005 walls (Onoda et al. 2017). As the generality of relationships between M_{area} and
1006 the amount of leaf nitrogen allocated to cell walls has been called into question
1007 (Harrison et al. 2009), future work should consider explicitly measuring nitrogen
1008 allocation to cell wall tissue and stress-induced amino acid synthesis to confirm
1009 these patterns.

1010 In opposition to patterns expected from least-cost theory, increasing soil
1011 nitrogen availability had no apparent effect on χ . Interestingly, despite the null
1012 effect of soil nitrogen availability on χ , I observed a strong negative effect of in-
1013 creasing N_{area} on χ , consistent with the nitrogen-water use tradeoffs expected from
1014 theory. The null response of χ to increasing soil nitrogen availability may have
1015 been due to a lack of water limitation in the system, given that the area received
1016 approximately 20% more precipitation (1167 mm) during the 12-month period
1017 leading up to our measurement period than normally expected (972 mm). How-

1018 ever, droughts can and do occur in temperate forests of the northeastern United
1019 States (Sweet et al. 2017), so the observed increase in leaf nitrogen content with
1020 increasing soil nitrogen availability could be a strategy that allows trees to hedge
1021 bets against drier than normal growing seasons (Onoda et al. 2004; Onoda et al.
1022 2017; Hallik et al. 2009). As was suggested in Paillassa et al. (2020), and more
1023 recently by Querejeta et al. (2022), negative effects of soil nitrogen availabil-
1024 ity on χ may increase with increasing aridity. This strategy would be especially
1025 advantageous if it allows individuals growing in arid regions to maintain carbon
1026 assimilation rates with reduced water loss. Future work should attempt to quan-
1027 tify interactive roles of climate and soil nitrogen availability on nitrogen-water use
1028 tradeoffs, which could be done by leveraging coordinated and multifactor nutrient
1029 (Borer et al. 2014) and water (Knapp et al. 2017) manipulation experiments
1030 across broad climatic gradients.

1031 3.4.2 *Soil pH did not modify tradeoffs between nitrogen and water usage*

1032 While the primary purpose of this study was to examine the role of soil nitrogen
1033 availability on nitrogen-water use tradeoffs, this experimental design manipulated
1034 both soil nitrogen and pH, providing an opportunity to isolate the roles of these
1035 variables. Previous correlational studies along environmental gradients have iden-
1036 tified soil pH as a particularly important factor that can modify tradeoffs between
1037 nutrient and water use (Smith et al. 2019; Paillassa et al. 2020; Westerband et al.
1038 2023) and the proportion of leaf nitrogen allocated to photosynthesis (Luo et al.
1039 2021). Such studies implied that these patterns may be driven by reductions in
1040 the cost of acquiring nutrients relative to water with increasing pH, which may

1041 be exacerbated in acidic soils.

1042 Consistent with theory (Wright et al. 2003; Prentice et al. 2014), results
1043 indicate that increasing soil pH was negatively associated with PNUE. However,
1044 there was no effect of soil pH on leaf nitrogen content, χ , or leaf nitrogen content
1045 per unit χ , most likely because the experimental nitrogen additions increased soil
1046 nitrogen supply while both increasing (sodium nitrate) and decreasing (ammo-
1047 nium sulfate) soil pH. These results suggest that soil pH did not play a major
1048 role in modifying expected photosynthetic least-cost theory patterns, contrasting
1049 findings from Paillassa et al. (2020) and other gradient studies that note positive
1050 effects of increasing soil pH on leaf nitrogen content, Rubisco carboxylation, and
1051 χ (Viet et al. 2013; Cornwell et al. 2018; Luo et al. 2021). Instead, null responses
1052 to soil pH show that leaf photosynthetic parameters depend more on soil nitrogen
1053 availability than pH per se, and that inferences from gradient studies might be
1054 confounding covariation between nitrogen availability and soil acidity.

1055 3.4.3 *Species identity explains a large amount of variation in leaf and whole*
1056 *plant traits*

1057 Species generally explained a larger amount of variation in measured leaf traits
1058 than soil nitrogen availability or soil pH. Interspecies variation is an important
1059 factor to consider when deducing mechanisms that drive photosynthetic least-
1060 cost theory, particularly for species that form distinct mycorrhizal associations or
1061 have different photosynthetic pathways, growth forms, or leaf habit (Espelta et al.
1062 2005; Adams et al. 2016; Bialic-Murphy et al. 2021; Scott and Smith 2022). The
1063 need to consider species may also be important when comparing nutrient-water

1064 use tradeoffs in early and late successional species, or in species with different
1065 resource economic strategies (Abrams and Mostoller 1995; Ellsworth and Reich
1066 1996; Wright et al. 2004; Reich 2014; Onoda et al. 2017; Ziegler et al. 2020).

1067 A strength of the study design and sampling effort is that it controls for
1068 many species differences that should modify nitrogen-water use tradeoffs expected
1069 from theory. All tree species measured in this study shared the leaf habit of de-
1070 ciduous broadleaves, were growing in forests of similar successional stage, but
1071 differed in mycorrhizal association and consequent resource economic strategies.
1072 As stands tended to be dominated by trees that associate with arbuscular myc-
1073 orrhizae (*Fraxinus* and both *Acer* species made up roughly 70% of total above-
1074 ground biomass across stands), ecosystem biogeochemical cycle dynamics may be
1075 more closely aligned to the inorganic nutrient economy proposed in Phillips et al.
1076 (2013), which may promote stronger nitrogen-water use tradeoffs in tree species
1077 that associate with arbuscular mycorrhizae. This result was not observed here,
1078 as photosynthetic properties varied as much within as across the two mycorrhizal
1079 associations represented. Given the high variability in measured photosynthetic
1080 traits within and across species, effects of mycorrhizal association likely require
1081 more intensive sampling efforts to detect than were possible here.

1082 3.4.4 *Implications for photosynthetic least-cost theory model development*

1083 In the field, soil nutrient availability is heterogeneous across time and space (Ta-
1084 ble B4). Unaccounted within-plot heterogeneity may have contributed to the low
1085 amount of variation explained by soil nitrogen availability in statistical models,
1086 as resin bags are a coarse surrogate for soil nitrogen availability. Despite this, I

1087 still observed evidence for nutrient-water use tradeoffs, suggesting that observed
1088 responses reported here may be an underestimate toward the net effect of soil ni-
1089 trogen availability on these tradeoffs. While I urge caution in the interpretation of
1090 these results, they do provide a promising baseline for future studies investigating
1091 patterns expected from photosynthetic least-cost theory at finer spatiotemporal
1092 resolutions.

1093 The general stronger relationship between leaf nitrogen content and photo-
1094 synthetic parameters versus between leaf nitrogen content and soil nitrogen avail-
1095 ability suggests that leaf nitrogen content is more directly tied to photosynthesis
1096 than soil nitrogen availability. While this could be due to the high spatiotemporal
1097 heterogeneity of soil nitrogen availability, principles from photosynthetic least-
1098 cost theory suggest that leaf nitrogen content is the downstream product of leaf
1099 nutrient demand to build and maintain photosynthetic machinery, which is set by
1100 aboveground environmental conditions such as light availability, CO₂, tempera-
1101 ture, or vapor pressure deficit (Smith et al. 2019; Paillassa et al. 2020; Peng et al.
1102 2021; Westerband et al. 2023). The stronger relationship between leaf nitrogen
1103 and photosynthetic parameters, paired with the strong negative relationship be-
1104 tween leaf nitrogen and χ , could indicate a relatively stronger effect of climate on
1105 leaf nitrogen-photosynthesis relationships than soil resource availability. However,
1106 the short distance between plots and across sites limited my ability to test this
1107 mechanism.

1108 Variation in soil pH affected least cost responses less than variations in soil
1109 nitrogen availability, in part because experimental treatments directly increased
1110 soil nitrogen and affected soil pH in opposite directions. While soil pH has been

1111 shown to drive nitrogen-water tradeoffs in global gradient analyses (Viet et al.
1112 2013; Paillassa et al. 2020), these responses may be due to covariations between
1113 soil pH and nutrient cycling rather than a role of pH per se. The direct manipula-
1114 tions of soil pH and soil nitrogen availability in this study partly disentangle these
1115 factors and show that variation in nitrogen availability matters more for least-cost
1116 tradeoffs than pH alone.

1117 3.4.5 *Conclusions*

1118 Increasing soil nitrogen availability generally increased leaf nitrogen content (both
1119 area- and mass-based), but did not significantly influence χ . This shift in leaf ni-
1120 trogen led to a reduction in PNUE, and an increase in leaf nitrogen per unit
1121 χ with increasing soil nitrogen availability. Despite null effects of soil nitrogen
1122 availability on χ , I observed a strong negative relationship between leaf nitrogen
1123 content and χ . These results provide empirical support for the nutrient-water use
1124 tradeoffs expected from photosynthetic least-cost theory in response to increas-
1125 ing soil nutrient availability, but suggest that all tenets of the theory may not
1126 hold in every environment. These results experimentally test previous work sug-
1127 gesting that leaf nitrogen-water economies vary across gradients of soil nutrient
1128 availability and pH, and show that variations in nutrient availability matter more
1129 for determining variation in leaf photosynthetic traits than soil pH.

1130

Chapter 4

1131 The relative cost of resource use for photosynthesis drives variance in
1132 leaf nitrogen content across a climate and soil resource availability
1133 gradient

1134 4.1 Introduction

1135 Terrestrial biosphere models, which comprise the land surface component of Earth
1136 system models, are sensitive to the formulation of photosynthetic processes (Knorr
1137 and Heimann 2001; Ziehn et al. 2011; Booth et al. 2012; Walker et al. 2021).
1138 This is because photosynthesis is the largest carbon flux between the atmosphere
1139 and terrestrial biosphere (IPCC 2021), and is constrained by ecosystem carbon
1140 and nutrient cycles (Hungate et al. 2003; LeBauer and Treseder 2008; Fay et al.
1141 2015). Many terrestrial biosphere models formulate photosynthesis by parame-
1142 terizing photosynthetic capacity within plant functional groups through empiri-
1143 cal linear relationships between area-based leaf nitrogen content (N_{area}) and the
1144 maximum carboxylation rate of Ribulose-1,5-bisphosphate carboxylase/oxygenase
1145 (V_{cmax}) (Kattge et al. 2009; Rogers 2014; Rogers et al. 2017). Models are also
1146 beginning to include connected carbon-nitrogen cycles (Wieder et al. 2015; Shi
1147 et al. 2016; Davies-Barnard et al. 2020; Braghieri et al. 2022), which allows leaf
1148 photosynthesis to be predicted directly through changes in N_{area} and indirectly
1149 through changes in soil nitrogen availability (e.g., LPJ-GUESS, CLM5.0) (Smith
1150 et al. 2014; Lawrence et al. 2019). Despite recent model developments, open
1151 questions remain regarding the generality of ecological relationships between soil
1152 nitrogen availability, leaf nitrogen content, and leaf photosynthesis across edaphic
1153 and climatic gradients.

1154 Empirical support for positive relationships between soil nitrogen availabil-
1155 ity and N_{area} is abundant (Firn et al. 2019; Liang et al. 2020), and is a result
1156 often attributed to the high nitrogen cost of building and maintaining Rubisco
1157 (Evans 1989; Evans and Seemann 1989; Onoda et al. 2004; Walker et al. 2014;
1158 Onoda et al. 2017; Dong et al. 2020). Such patterns imply that positive relation-
1159 ships between soil nitrogen availability and N_{area} should increase leaf photosyn-
1160 thesis and photosynthetic capacity by increasing the maximum rate of Rubisco
1161 carboxylation through increased investments to Rubisco construction and mainte-
1162 nance. This integrated N_{area} -photosynthesis response to soil nitrogen availability
1163 has been observed both in manipulative experiments and across environmental
1164 gradients (Field and Mooney 1986; Evans 1989; Walker et al. 2014; Li et al.
1165 2020), and is thought to be driven by ecosystem nitrogen limitation, which lim-
1166 its primary productivity globally (LeBauer and Treseder 2008; Fay et al. 2015).
1167 However, this response is not consistently observed, as recent studies note variable
1168 N_{area} -photosynthesis relationships across edaphic and climatic gradients (Liang
1169 et al. 2020; Luo et al. 2021) and that aboveground growing conditions (e.g., light
1170 availability, temperature, vapor pressure deficit) or species identity traits (e.g.,
1171 photosynthetic pathway, nitrogen acquisition strategy) may be more important
1172 for explaining variance in N_{area} and photosynthetic capacity across environmental
1173 gradients (Adams et al. 2016; Dong et al. 2017; Smith et al. 2019; Dong et al.
1174 2020; Peng et al. 2021; Dong et al. 2022; Westerband et al. 2023).

1175 One hypothesized mechanism to explain variance in N_{area} across environ-
1176 mental gradients has been proposed via photosynthetic least-cost theory (Wright
1177 et al. 2003; Prentice et al. 2014; Paillassa et al. 2020; Harrison et al. 2021).

1178 The theory predicts that plants acclimate to environments by optimizing photo-
1179 synthetic assimilation rates at the lowest summed cost of nitrogen and water use
1180 (Wright et al. 2003; Prentice et al. 2014). In a given environment, the theory
1181 suggests that nitrogen and water use can be substituted for each other to maintain
1182 the lowest summed cost of resource use, such that optimal photosynthetic rates
1183 are achieved with less efficient use of the more abundant and less costly resource
1184 to acquire in exchange for more efficient use of the less abundant and more costly
1185 resource to acquire.

1186 Photosynthetic least-cost theory predicts that, all else equal, an increase in
1187 soil nitrogen availability should decrease the cost of acquiring and using nitrogen
1188 relative to water (a ratio referred to herein as β), resulting in optimal photosyn-
1189 thetic rates achieved with greater N_{area} at lower stomatal conductance and lower
1190 leaf $C_i:C_a$ (Wright et al. 2003; Prentice et al. 2014; Paillassa et al. 2020). Alter-
1191 natively, an increase in soil moisture should reduce costs of water acquisition and
1192 use, increasing β (Lavergne et al. 2020), stomatal conductance, and leaf $C_i:C_a$,
1193 resulting in optimal photosynthetic rates achieved with decreased N_{area} . The the-
1194 ory also predicts variability in stomatal conductance and N_{area} in response to
1195 climatic factors, suggesting that the optimal response to increased vapor pressure
1196 deficit (VPD) should be a reduction in stomatal conductance and leaf $C_i:C_a$ that
1197 is counterbalanced by an increase in N_{area} to support the greater photosynthetic
1198 capacity needed to maintain high assimilation at lower conductance (Grossiord
1199 et al. 2020; Dong et al. 2020; López et al. 2021; Westerband et al. 2023).

1200 Leaf nitrogen allocation responses to changing climates or soil resource
1201 availability may also depend on their mode of nutrient acquisition or photo-

1202 synthetic pathway. For example, species that form associations with symbiotic
1203 nitrogen-fixing bacteria (referred as “N-fixing species” from this point forward)
1204 should, in theory, have access to less finite nitrogen supply than species not capa-
1205 ble of forming such associations (referred as “non-fixing species” from this point
1206 forward), which may result in lower β values in N-fixing species than non-fixing
1207 species. This result was previously shown in a greenhouse experiment, where a
1208 leguminous species generally had lower costs of nitrogen acquisition compared to a
1209 non-leguminous species, although these differences were generally stronger under
1210 increased nitrogen limitation (Perkowski et al. 2021). Lower β values could be an
1211 explanation for why N-fixing species commonly have greater leaf nitrogen content
1212 than non-fixing species (Adams et al. 2016; Dong et al. 2017).

1213 Similarly, leaf nitrogen allocation patterns across environmental gradients
1214 may be dependent on photosynthetic pathway. Lower leaf $C_i:C_a$ values in C₄
1215 species suggests that C₄ species should have lower β values than C₃ species (Scott
1216 and Smith 2022), a pattern that could be the result of increased costs associated
1217 with water acquisition and use or reduced costs of nitrogen acquisition and use
1218 relative to C₃ species. Theory predicts that this response in C₄ species will cause
1219 C₄ species to have higher leaf nitrogen content on average compared to C₃ species,
1220 though ample evidence exists documenting general lower leaf nitrogen content in
1221 C₄ species (Schmitt and Edwards 1981; Sage and Pearcy 1987; Ghannoum et al.
1222 2011). No study to date has directly quantified β in C₄ species aside from the
1223 initial parameterization of β in an optimality model for C₄ species (Scott and
1224 Smith 2022) using a global dataset of leaf $\delta^{13}\text{C}$ values (Cornwell et al. 2018).

1225 While photosynthetic least-cost theory provides a unified framework for

1226 understanding integrated effects of climate and soil resource availability on N_{area} ,
1227 empirical tests of the theory are sparse. Previous work shows that increasing
1228 soil nitrogen availability decreases costs of acquiring nutrients (Bae et al. 2015;
1229 Perkowski et al. 2021; Lu et al. 2022), which can induce predictable nutrient-
1230 water use tradeoffs expected from the theory across broad environmental gradients
1231 (Paillassa et al. 2020; Querejeta et al. 2022; Westerband et al. 2023) and in ma-
1232 nipulation experiments (Bialic-Murphy et al. 2021). Additionally, increasing VPD
1233 has been shown to have a positive effect on N_{area} , which is commonly associated
1234 with reduced leaf $C_i:C_a$ (Dong et al. 2017; Dong et al. 2020; Firn et al. 2019;
1235 López et al. 2021).

1236 Despite evidence for patterns expected from photosynthetic least-cost the-
1237 ory, studies have been restricted to exploring these patterns in C₃ species and,
1238 while variance in N_{area} across environmental gradients has been shown to be driven
1239 by strong negative relationships with leaf $C_i:C_a$ (Dong et al. 2017; Paillassa et al.
1240 2020; Westerband et al. 2023), no study has explicitly investigated effects of soil
1241 resource availability or species identity on N_{area} using β as a direct predictor of leaf
1242 $C_i:C_a$. Furthermore, as N_{area} can be broken down into structural (leaf mass per
1243 area; M_{area} ; g m⁻²) and metabolic (mass-based leaf nitrogen content; N_{mass} ; gN
1244 g⁻¹) components (Dong et al. 2017), no study has investigated which component
1245 of N_{area} drives the hypothesized response of N_{area} to leaf $C_i:C_a$. Understanding
1246 whether changes in N_{area} due to leaf $C_i:C_a$ are driven by changes in leaf morphol-
1247 ogy (i.e. M_{area}), stoichiometry (i.e. N_{mass}), or both, is important, particularly
1248 because N_{mass} may negatively covary with M_{area} across environmental gradients
1249 due to tradeoffs between leaf longevity and leaf productivity (Wright et al. 2004;

1250 Reich 2014; Onoda et al. 2017; Wang et al. 2023).

1251 In this study, I measured N_{area} , N_{mass} , M_{area} , leaf $\delta^{13}\text{C}$ -derived estimates
1252 of leaf $C_i:C_a$, and leaf $\delta^{13}\text{C}$ -derived estimates of β in 520 individuals spanning
1253 57 species scattered across 24 grassland sites in Texas, USA. Texas contains a
1254 diverse climatic gradient, indicated by 2006-2020 mean annual precipitation totals
1255 ranging from 204 to 1803 mm and 2006-2020 mean annual temperature ranging
1256 from 11.8° to 24.6°C. Variability in soil nitrogen availability and soil moisture was
1257 expected across sites, owing to differences in soil texture and aboveground climate
1258 that would drive differential rates of water retention and nitrogen transformations
1259 to plant-available nitrogen substrate. I leveraged the expected climatic and soil
1260 resource variability across sites to test the following hypotheses:

- 1261 1. Soil nitrogen availability will decrease β through a reduction in costs of
1262 nitrogen acquisition and use, while soil moisture will increase β through a
1263 reduction in costs of water acquisition and use. Following previous results, I
1264 expected that N-fixing species would have lower β values and that C₄ species
1265 would have lower β values.
- 1266 2. Leaf $C_i:C_a$ will be positively related to β , a pattern that will result in a
1267 negative indirect effect of increasing soil nitrogen availability on leaf $C_i:C_a$,
1268 a positive indirect effect of increasing soil moisture on leaf $C_i:C_a$, and lower
1269 leaf $C_i:C_a$ in both N-fixing species and C₄ species. I expected that leaf
1270 $C_i:C_a$ would be negatively related to VPD, as increasing atmospheric dryness
1271 would cause plants to close stomata to minimize water loss.
- 1272 3. N_{area} will be negatively related to leaf $C_i:C_a$. This response will result in an

1273 indirect positive and negative effect of increasing soil nitrogen availability
1274 and soil moisture, respectively, on N_{area} , and larger N_{area} values in N-fixing
1275 species. While theory predicts that lower β values in C₄ species should
1276 yield larger N_{area} in C₄ species, I expected that C₄ species would have lower
1277 N_{area} than C₃ species due to greater nitrogen use efficiency in C₄ species.
1278 Additionally, I expected VPD to increase N_{area} , a pattern that would be
1279 directly mediated through the reduction in leaf $C_i:C_a$ with increasing VPD.

1280 4.2 Methods

1281 4.2.1 *Site descriptions and sampling methodology*

1282 I collected leaf and soil samples from 24 open canopy grassland sites scattered
1283 across central and eastern Texas in summer 2020 and summer 2021 (Fig. 4.1).
1284 Twelve sites were visited between June and July 2020 and 14 sites (11 unique from
1285 2020) were visited between May and June 2021 (Table 4.1). I explicitly chose sites
1286 that maximized variability in precipitation and edaphic variability between sites
1287 while minimizing temperature variability across the environmental gradient (Ta-
1288 ble 4.1). No site with personally communicated or anecdotal evidence of grazing
1289 or disturbance (e.g., mowing, feral hog activity, etc.) was used. I collected leaf
1290 material from three individuals each of the five most abundant species at ran-
1291 dom locations at each site, only selecting species that were broadly classified as
1292 graminoid or forb/herb growth habits per the USDA PLANTS database (USDA
1293 NRCS 2022). All collected leaves were fully expanded with no visible herbivory or
1294 other external damage and also free from shading by nearby shrubs or trees. Five
1295 soil samples were collected from 0-15 cm below the soil surface at each site near

1296 the leaf collection sample locations. Soil samples were mixed together by hand to
1297 create one composite soil sample per site.

1298 4.2.2 *Leaf trait measurements*

1299 Images of each leaf were taken immediately following each site visit using a flat-
1300 bed scanner. Fresh leaf area was determined from each image using the ‘LeafArea’
1301 R package (Katabuchi 2015), which automates leaf area calculations using ImageJ
1302 software (Schneider et al. 2012). Each leaf was dried at 65°C for at least 48 hours
1303 to a constant mass, weighed, and manually ground in a mortar and pestle until
1304 homogenized. Leaf mass per area (M_{area} ; g m⁻²) was calculated as the ratio of
1305 dry leaf biomass to fresh leaf area. Subsamples of dried and homogenized leaf
1306 tissue were used to measure leaf nitrogen content (N_{mass} ; gN g⁻¹) through ele-
1307 mental combustion analysis (Costech-4010, Costech Instruments, Valencia, CA).
1308 Leaf nitrogen content per unit leaf area (N_{area} ; gN m⁻²) was calculated as the
1309 product of N_{mass} and M_{area} .

1310 Subsamples of dried and homogenized leaf tissue were sent to the University
1311 of California-Davis Stable Isotope Facility to determine leaf $\delta^{13}\text{C}$. Leaf $\delta^{13}\text{C}$ values
1312 were determined using an elemental analyzer (PDZ Europa ANCA-GSL; Sercon
1313 Ltd., Chestshire, UK) interfaced to an isotope ratio mass spectrometer (PDZ
1314 Europa 20-20 Isotope Ratio Mass Spectrometer, Sercon Ltd., Chestshire, UK).
1315 I used leaf $\delta^{13}\text{C}$ values (‰; relative to Vienna Pee Dee Belemnite international
1316 reference standard) to estimate the ratio of intercellular (C_i) to extracellular (C_a)
1317 CO₂ ratio (leaf $C_i:C_a$; unitless) following the approach of Farquhar et al. (1989)
1318 described in Cernusak et al. (2013). Specifically, I derived leaf $C_i:C_a$ as:

$$C_i : C_a = \frac{\Delta^{13}C - a}{b - a} \quad (4.1)$$

1319 where $\Delta^{13}C$ represents the relative difference between leaf $\delta^{13}\text{C}$ (\textperthousand) and air $\delta^{13}\text{C}$
1320 (\textperthousand), calculated as:

$$\Delta^{13}C = \frac{\delta^{13}C_{air} - \delta^{13}C_{leaf}}{1 + \delta^{13}C_{leaf}} \quad (4.2)$$

1321 $\delta^{13}\text{C}_{air}$, which is commonly assumed to be $-8\text{\textperthousand}$ (Keeling et al. 1979; Farquhar
1322 et al. 1989), was calculated as a function of calendar year t using an empirical
1323 equation derived in Feng (1999):

$$\delta^{13}C_{air} = -6.429 - 0.006e^{0.0217(t-1740)} \quad (4.3)$$

1324 Using this equation, $\delta^{13}\text{C}_{air}$ values were set to $-9.04\text{\textperthousand}$ and $-9.09\text{\textperthousand}$ for 2020 and
1325 2021, respectively. The parameter a represents the fractionation between ^{12}C
1326 and ^{13}C due to diffusion in air, assumed to be $4.4\text{\textperthousand}$, while b represents the
1327 fractionation caused by Rubisco carboxylation, assumed to be $27\text{\textperthousand}$ (Farquhar
1328 et al. 1989). For C_4 species, b in Eqn. 4.1 was set to $6.3\text{\textperthousand}$, and was derived from:

$$b = c + (d \cdot \phi) \quad (4.4)$$

1329 Where c was set to $-5.7\text{\textperthousand}$ and d was set to $30\text{\textperthousand}$ (Farquhar et al. 1989). ϕ , which
1330 is the bundle sheath leakiness term, was set to 0.4. All leaf $C_i:C_a$ values less than
1331 0.1 and greater than 0.95 were assumed to be incorrect and removed from the

1332 analysis.

1333 I derived the unit cost of resource use (β) using leaf $C_i:C_a$ and site climate

1334 data using equations first described in Prentice et al. (2014) and simplified in

1335 Lavergne et al. (2020):

$$\beta = 1.6\eta^*VPD \frac{\chi - (\frac{\Gamma^*}{C_a})^2}{(1 - \chi)^2(K_m + \Gamma^*)} \quad (4.5)$$

1336 where η^* is the viscosity of water relative to 25°C, calculated using elevation and

1337 mean air temperature of the seven days leading up to each site visit following equa-

1338 tions in Huber et al. (2009). VPD (Pa) was set to the mean vapor pressure deficit

1339 of the seven days leading up to each site visit, C_a represents atmospheric CO₂

1340 concentration, arbitrarily set to 420 $\mu\text{mol mol}^{-1}$ CO₂. K_m (Pa) is the Michaelis-

1341 Menten coefficient for Rubisco affinity to CO₂ and O₂, calculated as:

$$K_m = K_c \cdot \left(1 + \frac{O_i}{K_o}\right) \quad (4.6)$$

1342 where K_c (Pa) and K_o (Pa) are the Michaelis-Menten coefficients for Rubisco

1343 affinity to CO₂ and O₂, respectively, and O_i is the intercellular O₂ concentration.

1344 Γ^* (Pa) is the CO₂ compensation point in the absence of dark respiration. K_c , K_o ,

1345 and Γ^* were determined using equations described in Medlyn et al. (2002) and

1346 derived in Bernacchi et al. (2001), invoking an elevation correction for atmospheric

1347 pressure as explained in Stocker et al. (2020).

Table 4.1. Site locality information, sampling year, 2006-2020 mean annual precipitation (MAP; mm), mean annual temperature (MAT; °C), and water holding capacity (WHC; mm)*

Site	Latitude	Longitude	Sampling year	MAP	MAT	WHC
Edwards_2019_17	29.95	-100.36	2020	563.5	19.0	224.7
Uvalde_2020_02	29.59	-100.09	2020, 2021	648.5	19.5	224.7
Menard_2020_01	30.91	-99.59	2020	641.9	18.3	220.2
Kerr_2020_03	30.06	-99.34	2021	672.4	18.3	237.5
Bandera_2020_03	29.85	-99.30	2021	789.4	18.8	235.1
Sansaba_2020_01	31.29	-98.62	2020	733.0	18.8	234.3
Comal_2020_21	29.79	-98.43	2020	878.5	19.9	220.7
Blanco_2019_16	29.99	-98.43	2020	833.0	19.2	222.2
Bexar_2019_13	29.24	-98.43	2020	759.3	21.5	206.0
Burnet_2020_14	30.84	-98.34	2021	763.3	19.5	217.8
Comal_2020_19	30.01	-98.32	2021	845.0	19.3	220.4
Hays_2020_54	29.96	-98.17	2021	861.3	20.0	225.6
Burnet_2020_12	30.82	-98.06	2021	815.1	19.4	245.3
Williamson_2019_09	30.71	-97.86	2020	867.7	19.7	270.2
Williamson_2019_10	30.54	-97.77	2020	819.5	19.9	239.8
Bell_2021_08	31.06	-97.55	2021	937.3	19.6	232.3
Fayette_2021_12	29.86	-97.21	2021	985.7	20.4	165.6
Fayette_2019_04	30.09	-96.78	2020	1017.4	20.6	226.9
Fayette_2020_09	29.86	-96.71	2021	1002.7	20.8	187.6
Washington_2020_08	30.28	-96.41	2021	1077.4	20.4	203.9
Austin_2020_03	29.78	-96.24	2021	1108.7	20.6	253.0
Brazos_2020_16	30.93	-96.23	2021	1078.0	20.1	202.2
Brazos_2020_18	30.52	-96.21	2020, 2021	1099.4	20.4	233.5
Harris_2020_03	29.88	-95.31	2020, 2021	1492.0	21.6	265.6

1348 * Rows are arranged by longitude to visualize precipitation variability across sites

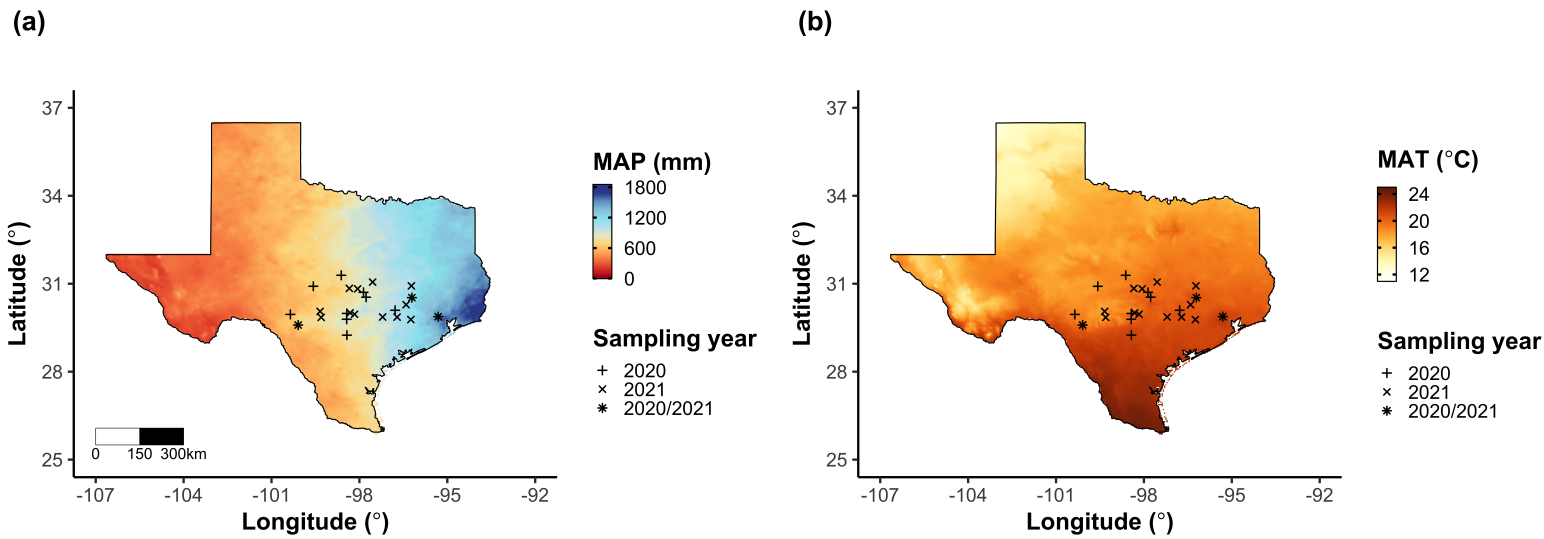


Figure 4.1. Site locations along 2006-2020 mean annual precipitation (a) and mean annual temperature (b) gradients in Texas, USA. Precipitation and temperature data were plotted using PRISM data at a 4-km grid resolution and are masked to include only grid cells that occur within the Texas state boundary of the United States. In both panels, addition signs refer to sites visited in 2020, multiplication signs to sites visited in 2021, and asterisks to sites visited in 2020 and 2021. The scale bar in (a) also applies to (b).

1349 4.2.3 *Site climate data*

1350 I used the Parameter elevation Regressions on Independent Slopes Model (PRISM)
1351 (Daly et al. 2008) climate product to access gridded daily temperature and precip-
1352 itation data for the coterminous United States at a 4-km grid resolution between
1353 January 1, 2006 and July 31, 2021 (PRISM Climate Group, Oregon State Uni-
1354 versity, <https://prism.oregonstate.edu>, data created 4 Feb 2014, accessed 24
1355 Mar 2022). Mean daily air temperature, mean daily VPD, and total daily pre-
1356 cipitation data were extracted from the grid cell that contained the latitude and
1357 longitude of each property using the ‘extract’ function in the ‘terra’ R package
1358 (Hijmans 2022). PRISM data were used in lieu of local weather station data
1359 because several rural sites did not have a local weather station present within a
1360 20-km radius of the site. Daily site climate data were used to estimate mean an-
1361 nual precipitation and mean annual temperature for each site between 2006 and
1362 2020 (Table 4.1). I calculated total precipitation and mean daily VPD for the
1363 prior 1, 2, 3, 4, 5, 6, 7, 8, 9, 10, 15, 20, 25, 30, 60, and 90 days leading up to each
1364 site visit. Temperature was not included in any analysis due to the close range in
1365 mean annual temperature between sites (mean \pm SD: $19.8\pm0.9^{\circ}\text{C}$; Table 4.1).

1366 4.2.4 *Site edaphic characteristics*

1367 Composted soil samples were sent to the Texas A&M Soil, Water and Forage
1368 Laboratory to quantify soil nitrate concentration ($\text{NO}_3\text{-N}$; ppm). Soil $\text{NO}_3\text{-N}$
1369 was determined by extracting composite soil samples in 1 M KCl, measuring
1370 absorbance values of extracts at 520 nm using the end product of a $\text{NO}_3\text{-N}$ to
1371 $\text{NO}_2\text{-N}$ cadmium reduction reaction (Kachurina et al. 2000; Keeney and Nelson

1372 1983). Soil texture data from 0-15 cm below the soil surface were accessed using
1373 the SoilGrids2.0 data product (Poggio et al. 2021) through the ‘fetchSoilGrids’
1374 function in the ‘soilDB’ R package (Beaudette et al. 2022). I used SoilGrids2.0
1375 to access soil texture data in lieu of analyses using the composite soil sample due
1376 to a lack of soil material from some sites after sending samples for soil NO₃-N.

1377 Soil moisture was not measured in the field, but was estimated using the
1378 ‘Simple Process-Led Algorithms for Simulating Habitats’ model (SPLASH) (Davis
1379 et al. 2017). This model, derived from the STASH model (Cramer and Prentice
1380 1988), spins up a bucket model using Priestley-Taylor equations (Priestley and
1381 Taylor 1972) to calculate daily soil moisture (W_n ; mm) as a function of the previous
1382 day’s soil moisture (W_{n-1} ; mm), daily precipitation (P_n ; mm), condensation (C_n ;
1383 mm), actual evapotranspiration (E_n^a ; mm), and runoff (RO; mm):

$$W_n = W_{n-1} + P_n + C_n - E_n^a - RO \quad (4.7)$$

1384 Models were spun up by equilibrating the previous day’s soil moisture using succes-
1385 sive model iterations with daily mean air temperature, daily precipitation total,
1386 the number of daily sunlight hours, and latitude as model inputs (Davis et al.
1387 2017). Daily sunlight hours were estimated for each day at each site using the
1388 ‘getSunlightTimes’ function in the ‘suncalc’ R package, which estimated sunrise
1389 and sunset times of each property using date and site coordinates (Thieurmel and
1390 Elmarhraoui 2019). Water holding capacity (mm), or bucket size, was estimated
1391 as a function of soil texture using pedotransfer equations explained in Saxton and
1392 Rawls (2006), as done in Stocker et al. (2020) and Bloomfield et al. (2023). A

1393 summary of these equations is included in Appendix C.1.

1394 Daily soil moisture outputs from the SPLASH model for each site were
1395 used to calculate mean daily soil moisture for the prior 1, 2, 3, 4, 5, 6, 7, 8, 9,
1396 10, 15, 20, 25, 30, 60, and 90 days leading up to each site visit. Mean daily
1397 soil moisture values were then expressed as a fraction of water holding capacity
1398 to normalize across sites with different bucket depths, as done in Stocker et al.
1399 (2018). Site water holding capacity values are referenced in Table 4.1.

1400 4.2.5 *Plant functional group assignments*

1401 Plant functional group was assigned to each species and used as the primary de-
1402 scriptor of species identity. Specifically, plant functional groups were assigned
1403 based on photosynthetic pathway (C_3 , C_4) and ability to form associations with
1404 symbiotic nitrogen-fixing bacteria (legume, nonlegume). The ability to form as-
1405 sociations with symbiotic nitrogen-fixing bacteria was assigned based on whether
1406 species were in the *Fabaceae* family, and photosynthetic pathway of each species
1407 was determined from past literature and confirmed through leaf $\delta^{13}C$ values. I
1408 chose these plant functional groups based on *a priori* hypotheses regarding the
1409 functional role of nitrogen fixation and photosynthetic pathway on the sensitivity
1410 of plant nitrogen uptake and leaf nitrogen allocation to soil nitrogen availability
1411 and aboveground growing conditions. These plant functional group classifications
1412 resulted in three distinct plant functional groups within our dataset: C_3 legumes
1413 (n=53), C_3 nonlegumes (n=350), and C_4 nonlegumes (n=117).

1414 4.2.6 *Data analysis*

1415 All analyses and plotting were conducted in R version 4.1.1 (R Core Team 2021).

1416 I constructed a series of separate linear mixed-effects models to investigate en-

1417 vironmental drivers of β , leaf $C_i:C_a$, N_{area} , N_{mass} , and M_{area} , followed by a path

1418 analysis using a piecewise structural equation model to investigate direct and

1419 indirect effects of climate and soil resource availability on N_{area} .

1420 To explore environmental drivers of β , I built a linear mixed-effects model

1421 that included soil moisture, soil nitrogen availability, and plant functional group

1422 as fixed effect coefficients. Species were designated as a random intercept term.

1423 Interaction coefficients between all possible combinations of the three fixed effect

1424 coefficients were also included. β was natural log transformed to linearize data.

1425 I used an information-theoretic model selection approach to determine whether

1426 90-, 60-, 30-, 20-, 15-, 10-, 9-, 8-, 7-, 6-, 5-, 4-, 3-, 2-, or 1-day mean daily soil

1427 moisture conferred the best model fit for β . To do this, I constructed 16 separate

1428 linear mixed-effects models where log-transformed β was included as the response

1429 variable and each soil moisture time step was separately included as a single

1430 continuous fixed effect. Species were included as a random intercept term for all

1431 models. I used corrected Akaike Information Criterion (AICc) to select the soil

1432 moisture timescale that conferred the best model fit, indicated by the model with

1433 the lowest AICc score (Table C4; Fig. C1).

1434 To explore environmental drivers of leaf $C_i:C_a$, I constructed a second linear

1435 mixed effects model that included VPD, soil moisture, soil nitrogen availability,

1436 and plant functional group as fixed effect coefficients. Two-way interactions be-

1437 tween plant functional group and VPD, soil nitrogen availability, or soil moisture

1438 were included as additional fixed effect coefficients, in addition to a three-way
1439 interaction between soil moisture, soil nitrogen availability, and plant functional
1440 group. Species were included as a random intercept term. I used an information-
1441 theoretic model selection approach to determine whether 90-, 60-, 30-, 20-, 15-,
1442 10-, 9-, 8-, 7-, 6-, 5-, 4-, 3-, 2-, or 1-day mean daily VPD conferred the best model
1443 fit for leaf $C_i:C_a$ using the same approach explained above for the soil moisture ef-
1444 fect on β . The soil moisture timescale was set to the same timescale that conferred
1445 the best fit for β .

1446 To explore environmental drivers of N_{area} , N_{mass} , and M_{area} , I constructed
1447 a linear mixed effects model for each trait, including leaf $C_i:C_a$, soil nitrogen
1448 availability, soil moisture, and plant functional group as fixed effect coefficients
1449 for each model. Two-way interactions between plant functional group and β , leaf
1450 $C_i:C_a$, soil nitrogen availability, or soil moisture were included as additional fixed
1451 effect coefficients, in addition to a three-way interaction between soil nitrogen
1452 availability, soil moisture, and plant functional group. Species were included as a
1453 random intercept term, with the soil moisture timescale set to the same timescale
1454 that conferred the best fit for β .

1455 In all linear mixed-effects models explained above, including those to select
1456 relevant timescales, I used the ‘lmer’ function in the ‘lme4’ R package (Bates et al.
1457 2015) to fit each model and the ‘Anova’ function in the ‘car’ R package (Fox and
1458 Weisberg 2019) to calculate Type II Wald’s χ^2 and determine the significance
1459 level ($\alpha=0.05$) of each fixed effect coefficient. I used the ‘emmeans’ R package
1460 (Lenth 2019) to conduct post-hoc comparisons using Tukey’s tests, where degrees
1461 of freedom were approximated using the Kenward-Roger approach (Kenward and

1462 Roger 1997). Trendlines and error ribbons for all plots were drawn using a series
1463 of ‘emmeans’ outputs across the range in plotted x-axis values.

1464 Finally, I conducted a path analysis using a piecewise structural equation
1465 model to examine direct and indirect pathways that determined variance in N_{area} .
1466 Six separate linear mixed effects models were loaded into the piecewise structural
1467 equation model. Models were constructed per *a priori* hypotheses following pat-
1468 terns expected from photosynthetic least-cost theory. The first model regressed
1469 N_{area} against N_{mass} and M_{area} . The second model regressed M_{area} against leaf
1470 $C_i:C_a$. The third model regressed N_{mass} against leaf $C_i:C_a$ and M_{area} (Dong et al.
1471 2017; Dong et al. 2020). The fourth model regressed leaf $C_i:C_a$ against β and
1472 VPD. The fifth model regressed β against soil nitrogen availability, soil moisture,
1473 ability to associate with symbiotic nitrogen-fixing bacteria, and photosynthetic
1474 pathway. The sixth model regressed soil nitrogen availability against soil mois-
1475 ture. All models included the relevant timescale selected in the individual linear
1476 mixed effect models explained above. Models included species as a random inter-
1477 cept term, were built using the ‘lme’ function in the ‘nlme’ R package (Pinheiro
1478 and Bates 2022), and subsequently loaded into the piecewise structural equation
1479 model using the ‘psem’ function in the ‘piecewiseSEM’ R package (Lefcheck 2016).

1480 4.3 Results

1481 4.3.1 *Cost to acquire nitrogen relative to water*

1482 Model selection indicated that 90-day mean soil moisture conferred the best model

1483 fit for β (AICc=1429.14; Table C4; Fig. C1).

1484 Increasing soil nitrogen availability generally decreased β ($p<0.001$; Table

1485 4.2; Fig. 4.2a), a pattern driven by a negative effect of increasing soil nitrogen on

1486 β in C₃ nonlegumes (Tukey: $p=0.002$) and C₃ legumes (Tukey: $p=0.031$) despite

1487 a null effect of soil nitrogen on β in C₄ nonlegumes (Tukey: $p=0.905$). There was

1488 no effect of soil moisture on β ($p=0.902$; Table 4.2; Fig. 4.2b). A functional group

1489 effect ($p<0.001$; Table 4.2) indicated that C₄ nonlegumes generally had lower β

1490 values than both C₃ legumes and C₃ non-legumes (Tukey: $p<0.001$ in both cases),

1491 while β values in C₃ legumes did not differ from C₃ nonlegumes (Tukey: $p=0.804$).

Table 4.2. Effects of soil moisture, soil nitrogen availability, and plant functional group on β (unitless)*

	df	Coefficient	χ^2	p
Intercept	-	3.39E+00	-	-
Soil moisture (SM ₉₀)	1	-2.03E-01	0.015	0.902
Soil N (N)	1	-1.49E-02	13.832	<0.001
PFT	2	-	225.049	<0.001
SM ₉₀ *N	1	-8.86E-04	1.016	0.313
SM ₉₀ *PFT	2	-	0.754	0.686
N*PFT	2	-	5.236	0.073
SM ₉₀ *N*PFT	2	-	3.633	0.163

1492 *Significance determined using Type II Wald χ^2 tests ($\alpha=0.05$). P-values<0.05
1493 are in bold. Model coefficients are expressed on the natural-log scale and are only
1494 included for continuous fixed effects. Key: df=degrees of freedom; χ^2 =Wald Type
1495 II chi-square test statistic

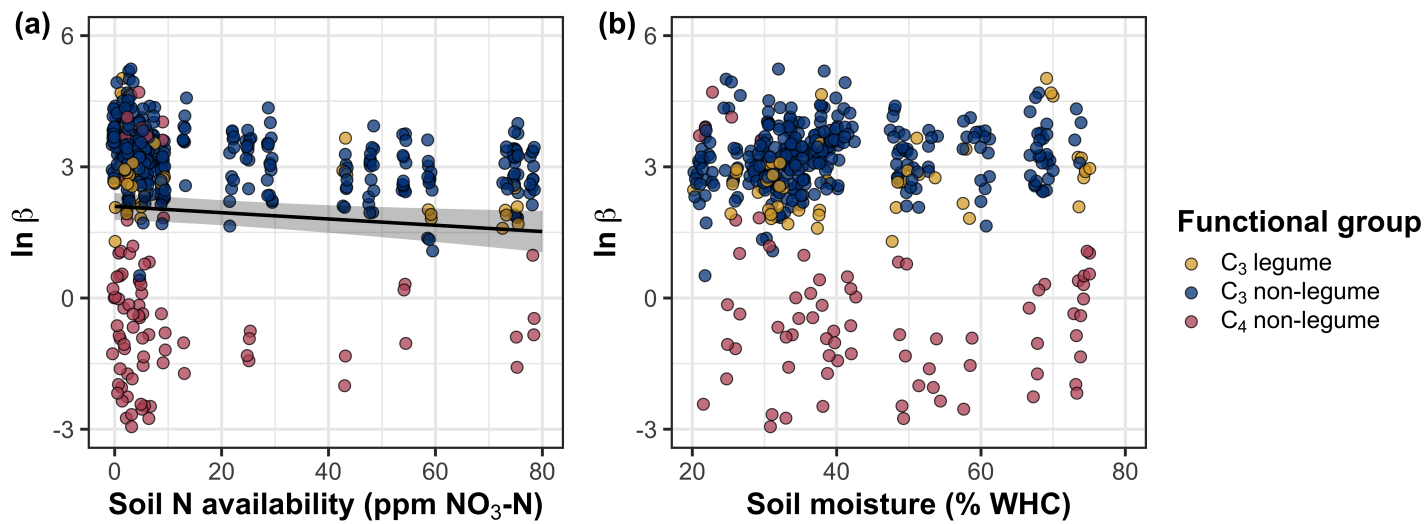


Figure 4.2. Effects of soil nitrogen availability (a) and soil moisture (b) on the cost of acquiring and using nitrogen (β ; unitless). Soil nitrogen availability is represented on the x-axis in (a), soil moisture is represented on the x-axis in (b) as a percent of site water holding capacity, and natural-log transformed β is represented on the y-axis for both panels. Yellow points represent C₃ legumes, blue points represent C₃ nonlegumes, and red points represent C₄ nonlegumes. Throughout, points are jittered for visibility. A black solid trendline is drawn to denote bivariate relationships where the slope is different from zero ($p<0.05$), with error ribbons representing the upper and lower 95% confidence intervals.

1496 4.3.2 *Leaf C_i:C_a*

1497 Model selection indicated that 4-day mean VPD was the timescale that conferred

1498 the best model fit for leaf $C_i:C_a$ (AICc=-793.49; Table C4; Fig. C1).

1499 Model results revealed that increasing VPD generally decreased leaf $C_i:C_a$

1500 ($p<0.001$; Table 4.3; Fig. 4.3a). There was no effect of soil moisture ($p=0.843$;

1501 Table 4.3; Fig. 4.3b) or soil nitrogen availability ($p=0.544$; Table 4.3; Fig. 4.3c) on

1502 leaf $C_i:C_a$. A strong plant functional group effect ($p<0.001$; Table 4.3) indicated

1503 that C₄ nonlegumes had lower leaf $C_i:C_a$ than C₃ legumes and C₃ nonlegumes

1504 (Tukey: $p<0.001$ in both cases), with no difference between C₃ legumes and C₃

1505 nonlegumes (Tukey: $p=0.865$).

Table 4.3. Effects of soil moisture, soil nitrogen availability, and plant functional group on leaf $C_i:C_a$ (unitless)*

	df	Coefficient	χ^2	<i>p</i>
Intercept	-	1.32E+00	-	-
Vapor pressure deficit (VPD_4)	1	-4.53E-01	11.211	<0.001
Soil moisture (SM_{90})	1	-1.71E-01	0.039	0.843
Soil N (N)	1	-3.33E-03	0.369	0.544
PFT	2	-	227.005	<0.001
SM_{90}^*N	1	7.34E-03	2.361	0.124
VPD_4^*PFT	2	-	0.927	0.629
SM_{90}^*PFT	2	-	0.817	0.664
N^*PFT	2	-	4.085	0.130
$SM_{90}^*N^*PFT$	2	-	3.677	0.159

1506 *Significance determined using Type II Wald χ^2 tests ($\alpha=0.05$). *P*-values less
1507 than 0.05 are in bold and *p*-values where $0.05 < p < 0.1$ are italicized. Leaf $C_i:C_a$
1508 was not transformed prior to model fitting, so model coefficients are reported
1509 on the response scale. Model coefficients are only included for continuous fixed
1510 effects. Key: df=degrees of freedom; χ^2 =Wald Type II chi-square test statistic

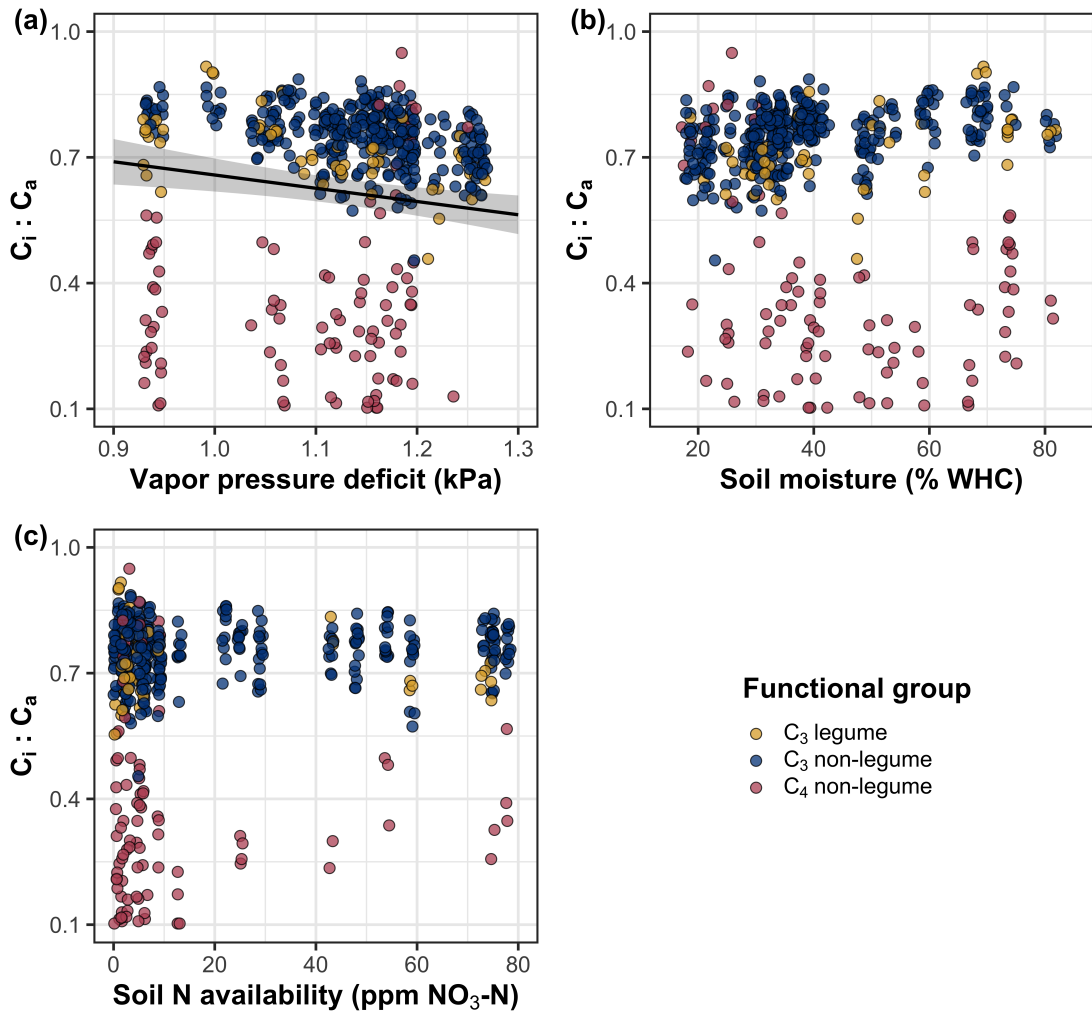


Figure 4.3. Effects of 4-day mean vapor pressure deficit (a), 90-day soil moisture (per water holding capacity; b), and soil nitrogen availability (c) on leaf $C_i:C_a$. Shading and trendlines are as explained in Figure 4.2. Points are jittered for visibility. Variably colored trendlines are only included if there is an interaction between the x-axis and plant functional group, where solid trendlines indicate slopes that are different from zero ($p < 0.05$) and dashed trendlines indicate slopes that are not different from zero ($p > 0.05$). Error ribbons represent the upper and lower 95% confidence intervals of each fitted trendline.

1511 4.3.3 *Leaf nitrogen content*

1512 An interaction between leaf $C_i:C_a$ and plant functional group ($p<0.001$; Table
1513 4.4) revealed that the negative effect of increasing leaf $C_i:C_a$ on N_{area} ($p<0.001$;
1514 Table 4.4) was driven by a negative effect of increasing leaf $C_i:C_a$ on N_{area} in
1515 C_3 nonlegumes (Tukey: $p<0.001$) and C_3 legumes (Tukey: $p=0.002$), but not C_4
1516 nonlegumes (Tukey: $p=0.795$; Fig. 4.4a). An interaction between soil nitrogen
1517 availability and plant functional group ($p=0.041$; Table 4.4) indicated that the
1518 positive effect of increasing soil nitrogen ($p=0.007$; Table 4.4) was only apparent
1519 in C_3 legumes (Tukey: $p<0.001$; Table 4.4; Fig. 4.4d), but not C_3 nonlegumes
1520 (Tukey: $p=0.449$) or C_4 nonlegumes (Tukey: $p=0.680$). Increasing soil moisture
1521 increased N_{area} ($p=0.010$, Table 4.4). A plant functional group effect ($p<0.001$;
1522 Table 4.4) indicated that C_4 nonlegumes had lower N_{area} compared to C_3 legumes
1523 (Tukey: $p<0.001$) and C_3 nonlegumes (Tukey: $p<0.001$), while C_3 legumes had
1524 lower N_{area} compared to C_3 nonlegumes (Tukey: $p=0.030$).

1525 A marginal interaction between soil nitrogen availability and soil moisture
1526 ($p=0.097$; Table 4.4) indicated that the positive effect of increasing soil nitrogen
1527 on N_{mass} ($p<0.001$; Table 4.4; Fig. 4.4e) was only apparent when soil moisture
1528 was less than 50% of the maximum water holding capacity (Tukey: $p<0.05$ in
1529 all cases). There was no effect of leaf $C_i:C_a$ on N_{mass} ($p=0.447$; Table 4.4; Fig.
1530 4.4b). Increasing soil moisture had a positive effect on N_{mass} ($p<0.001$; Table 4.4;
1531 Fig. 4.4h). A plant functional group effect ($p<0.001$; Table 4.4) indicated that
1532 C_4 nonlegumes had lower N_{mass} compared to C_3 legumes (Tukey: $p=0.003$) and
1533 C_3 nonlegumes (Tukey: $p=0.011$), while N_{mass} did not differ between C_3 legumes
1534 and C_3 nonlegumes (Tukey: $p=0.231$).

1535 Variance in M_{area} was driven by a three-way interaction between soil nitro-
1536 gen availability, soil moisture, and plant functional group ($p=0.018$; Table 4.4).
1537 This interaction indicated that increasing soil moisture increased the positive effect
1538 of increasing soil nitrogen availability on M_{area} in C₃ legumes (Tukey: $p=0.030$)
1539 but did not modify the negative effect of increasing soil nitrogen availability on
1540 M_{area} in C₄ nonlegumes (Tukey: $p=0.511$) or C₃ nonlegumes (Tukey: $p>0.999$).
1541 There was otherwise no effect of soil moisture on M_{area} ($p=0.696$; Table 4.4), but
1542 there was a general negative effect of increasing soil nitrogen availability on M_{area}
1543 ($p<0.001$; Table 4.4). An interaction between leaf $C_i:C_a$ and plant functional
1544 group ($p<0.001$; Table 4.4; Fig. 4.4c) indicated that negative effect of increasing
1545 leaf $C_i:C_a$ on M_{area} ($p<0.001$; Table 4.4) was driven by a negative effect of in-
1546 creasing leaf $C_i:C_a$ on M_{area} in C₃ legumes and C₃ nonlegumes (Tukey: $p<0.001$
1547 in both cases), but not C₄ nonlegumes (Tukey: $p=0.343$; Fig. 4.4c).

Table 4.4. Effects of soil moisture, soil nitrogen availability, plant functional group, and leaf $C_i:C_a$ on leaf nitrogen content per unit leaf area (N_{area} ; gN m $^{-2}$), leaf nitrogen content per unit leaf biomass (N_{mass} ; gN g $^{-1}$), and leaf biomass per unit leaf area (M_{area} ; g m $^{-2}$)

		N_{area}			N_{mass}			M_{area}		
	df	Coefficient	χ^2	p	Coefficient	χ^2	p	Coefficient	χ^2	p
(Intercept)	-	2.41E+00	-	-	6.28E-02	-	-	6.90E+00	-	-
$C_i:C_a$	1	-2.32E+00	7.386	0.007	8.04E-01	0.578	0.447	-3.13E+00	15.913	<0.001
Soil N (N)	1	1.26E-02	6.070	0.014	1.12E-02	90.940	<0.001	-2.66E-02	43.529	<0.001
Soil moisture (SM ₉₀)	1	5.60E-01	6.717	0.010	7.81E-01	11.205	<0.001	-2.53E-01	0.153	0.696
PFT	1	-	52.277	<0.001	-	17.184	<0.001	-	7.289	0.026
SM ₉₀ *N	1	5.44E-02	0.444	0.505	-1.91E-02	2.749	0.097	8.16E-02	1.690	0.194
$C_i:C_a$ *PFT	1	-	25.631	<0.001	-	4.864	0.078	-	34.683	<0.001
N*PFT	1	-	6.389	0.041	-	1.219	0.544	-	19.949	<0.001
SM ₉₀ *PFT	1	-	3.548	0.170	-	0.911	0.634	-	3.293	0.193
SM ₉₀ *N*PFT	1	-	3.520	0.172	-	0.092	0.955	-	7.987	0.018

96

1548 *Significance determined using Type II Wald χ^2 tests ($\alpha=0.05$). P-values less than 0.05 are in bold and p-values
 1549 where $0.05 < p < 0.1$ are italicized. Coefficients are reported on the natural-log scale for all traits and are only included
 1550 for continuous fixed effects. Key: df=degrees of freedom; χ^2 =Wald Type II chi-square test statistic

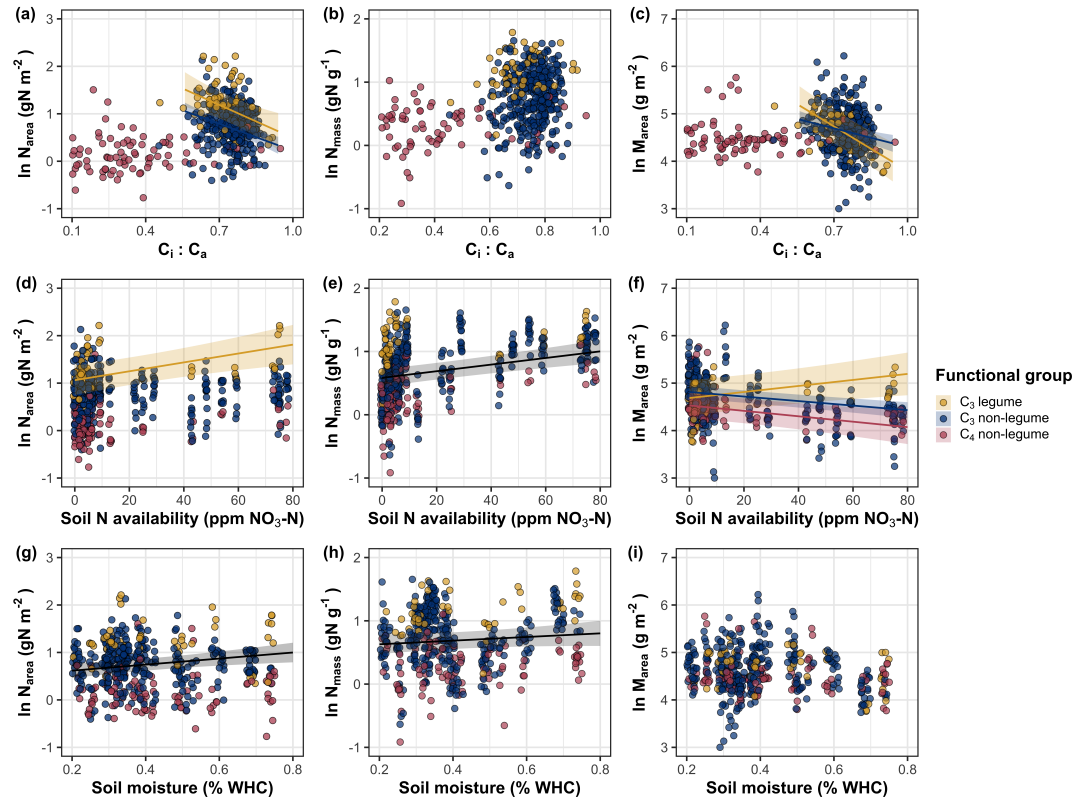


Figure 4.4. Effects of leaf $C_i:C_a$ (a-c), soil nitrogen availability (d-f), and soil moisture (g-i) on leaf nitrogen content per unit leaf area (a, d, g), leaf nitrogen content per unit leaf biomass (b, e, h), and leaf mass per area (c, f, i). Yellow points and trendlines indicate C_3 legumes, blue points and trendlines indicate C_3 nonlegumes, and red points and trendlines indicate C_4 nonlegumes. Points are jittered for visibility. Variably colored trendlines are only included if there is an interaction between plant functional group and the x-axis. Black solid trendlines denote bivariate slopes that are different from zero ($p < 0.05$) where there is no apparent interaction between plant functional group and the x-axis.

1551 4.3.4 *Structural equation model*

1552 The piecewise structural equation model explained 89%, 56%, 77%, 82%, and
1553 37% of variance in N_{area} , N_{mass} , M_{area} , leaf $C_i:C_a$, and β , respectively (Table 4.5; Fig. 4.5). Variance in N_{area} was driven by a positive effect of increasing N_{mass} and M_{area} ($p < 0.001$ in both cases; Table 4.5; Fig. 4.5). Model results indicated that an indirect negative effect of $C_i:C_a$ on N_{area} was driven by a strong reduction in M_{area} with increasing leaf $C_i:C_a$ ($p < 0.001$; Table 4.5) paired with no effect of increasing $C_i:C_a$ on N_{mass} ($p = 0.111$; Table 4.5). However, there was a strong negative effect of increasing M_{area} on N_{mass} ($p < 0.001$; Table 4.5; Fig. 4.5). Leaf $C_i:C_a$ increased with increasing β ($p < 0.001$; Table 4.5) and decreased with increasing VPD ($p < 0.001$; Table 4.5; Fig. 4.5). Variance in β was driven by a negative effect of increasing soil nitrogen availability ($p < 0.001$; Table 4.5) and was generally higher in C₃ species ($p < 0.001$; Table 4.5; Fig. 4.5). However, β did not change with soil moisture ($p = 0.904$; Table 4.5) or with ability to acquire nitrogen via symbiotic nitrogen fixation ($p = 0.495$; Table 4.5). Finally, soil nitrogen availability was positively associated with increasing soil moisture ($p = 0.002$; Table 4.5; Fig. 4.5).

Table 4.5. Structural equation model results investigating direct effects of climatic and soil resource availability on leaf nitrogen content*

Predictor	Coefficient	<i>p</i>
N_{area} ($R^2_c=0.89$)		
M_{area}	0.758	<0.001
N_{mass}	0.781	<0.001
N_{mass} ($R^2_c=0.56$)		
Leaf $C_i:C_a$	0.092	0.111
M_{area}	-0.311	<0.001
M_{area} ($R^2_c=0.77$)		
Leaf $C_i:C_a$	-0.237	<0.001
Leaf $C_i:C_a$ ($R^2_c=0.82$)		
β	0.309	<0.001
VPD_4	-0.110	<0.001
β ($R^2_c=0.37$)		
Soil N	-0.213	<0.001
SM_{90}	-0.006	0.904
Photo. pathway	0.446	<0.001
N-fixing ability	-0.056	0.495
Soil N ($R^2_c=0.35$)		
SM_{90}	-0.154	0.002

1567 *Coefficients are standardized across the structural equation model. *P*-values less
1568 than 0.05 are noted in bold. Positive coefficients for photosynthetic pathway
1569 indicate generally larger values in C₃ species, while positive coefficients for N-
1570 fixing ability indicate generally larger values in N-fixing species. Key: df=degrees
1571 of freedom; χ^2 =Wald Type II chi-square test statistic; R^2_c =conditional R² value;
1572 N_{area} =leaf nitrogen content per unit leaf area (gN m⁻²); M_{area} =leaf mass per
1573 unit leaf biomass (g m⁻²); N_{mass} =leaf nitrogen content per unit leaf biomass (gN
1574 g⁻¹); β =cost of acquiring nitrogen relative to water (unitless); VPD_4 =4-day mean
1575 vapor pressure deficit (kPa); SM_{90} =90-day mean soil moisture (mm)

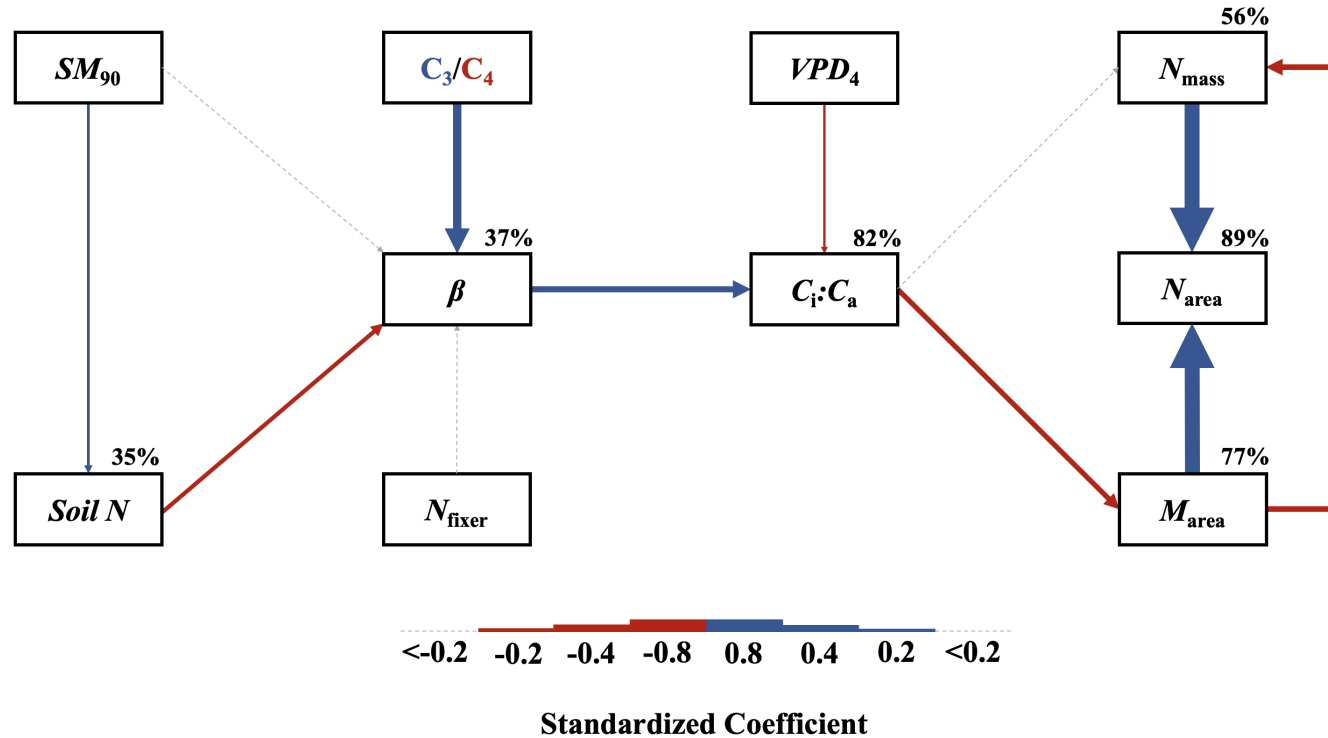


Figure 4.5. Structural equation model results exploring drivers of N_{area} . Boxes indicate measured edaphic factors, climatic factors, and leaf traits. Solid arrows indicate bivariate relationships where $p<0.05$, while dashed arrows indicate relationships where $p>0.05$. Positive model coefficients are indicated through blue arrows, negative model coefficients are indicated through red arrows, and insignificant coefficients are indicated through gray dashed arrows. Arrow thickness scales with the standardized model coefficient of each bivariate relationship. A positive coefficient for photosynthetic pathway indicates larger values in C_3 species, while a positive coefficient for N_{fixer} indicates larger values in N-fixing species. Standardized model coefficients and associated p -values are reported in Table 4.5, with conditional R^2 values for each response variable reported on the top right of each box.

1576 4.4 Discussion

1577 In this study, I quantified direct and indirect effects of edaphic and climatic char-
1578 acteristics on N_{area} and components of N_{area} (N_{mass} and M_{area}) in 520 individuals
1579 spanning across a soil resource availability and climate gradient in Texas, USA.
1580 Strong and consistent patterns emerged in support of those expected from photo-
1581 synthetic least-cost theory, a result driven by a strong direct negative relationship
1582 between leaf $C_i:C_a$ and N_{area} . In further support of patterns expected from theory,
1583 increasing soil nitrogen availability had a strong negative effect on β , resulting in
1584 an indirect stimulation in N_{area} mediated through a positive relationship between
1585 β and $C_i:C_a$. Increasing VPD also indirectly increased N_{area} through a direct
1586 negative effect of increasing VPD on leaf $C_i:C_a$, following hypotheses and pat-
1587 terns expected from theory. Interestingly, a strong positive association between
1588 soil moisture and N_{area} was driven by covariance between soil moisture and soil
1589 nitrogen availability and was not associated with a direct effect of soil moisture
1590 on β . Overall, results provide strong and consistent support for patterns expected
1591 from photosynthetic least-cost theory, showing that both soil resource availability
1592 and climate drive variance in N_{area} through changes in leaf $C_i:C_a$.

1593 4.4.1 *Negative effects of leaf $C_i:C_a$ on N_{area} are driven by reductions in M_{area} ,*
1594 *not N_{mass}*

1595 A strong negative effect of increasing leaf $C_i:C_a$ on N_{area} was detected in both
1596 the linear mixed effect and piecewise structural equation models. The negative
1597 response of N_{area} to increasing leaf $C_i:C_a$ is consistent with previous environmental
1598 gradient (Dong et al. 2017; Querejeta et al. 2022) and manipulation experiments

1599 (3.4c), showing strong support for the nitrogen-water use tradeoffs expected from
1600 photosynthetic least cost theory (Wright et al. 2003; Prentice et al. 2014). Neg-
1601 ative effects of increasing leaf $C_i:C_a$ on N_{area} were driven by a strong negative
1602 effect of increasing $C_i:C_a$ on M_{area} , with no apparent effect of leaf $C_i:C_a$ on N_{mass} ,
1603 suggesting that changes in N_{area} were driven by changes in leaf structure and not
1604 leaf chemistry. However, increasing M_{area} was negatively associated with N_{mass} ,
1605 indicating that an increase in N_{mass} was associated with larger, thinner leaves (i.e.
1606 lower M_{area}). These results are consistent with patterns reported from previous
1607 studies indicating that variance in N_{area} is driven by changes in M_{area} across envi-
1608 ronmental gradients, and that part of this response is due to negative covariance
1609 between M_{area} and N_{mass} (Dong et al. 2017; Dong et al. 2020). Negative co-
1610 variance between M_{area} and N_{mass} could be a response associated with tradeoffs
1611 between leaf longevity and leaf productivity (Wright et al. 2004; Dong et al. 2017;
1612 Dong et al. 2022; Querejeta et al. 2022; Wang et al. 2023).

1613 The negative relationship between leaf $C_i:C_a$ and M_{area} could also be a re-
1614 sponse that allows leaves to maximize productivity in shorter-lived leaves. Trade-
1615 offs between leaf longevity and leaf productivity are commonly observed and are
1616 included in a continuum of coordinated leaf traits that position individuals along
1617 a fast- or slow-growing leaf economics spectrum (Wright et al. 2003; Onoda et al.
1618 2004; Reich 2014; Onoda et al. 2017; Wang et al. 2023). Negative relationships
1619 between leaf $C_i:C_a$ and M_{area} indicate that increased stomatal conductance and
1620 reduced water use efficiency were associated with thinner, larger leaves (i.e., lower
1621 M_{area}). These patterns, combined with the negative covariance between M_{area} and
1622 N_{mass} mentioned above, may have allowed individuals to maximize light intercep-

tion and productivity by exploiting high light environments, though this comes
1624 at the expense of increased water loss and decreased water-use efficiency. This
1625 strategy may be especially advantageous for fast-growing species in open canopy
1626 systems. In this study, C₃ legumes and C₃ nonlegumes dominated the dataset
1627 (78% of total sampling effort), of which 22% (17% of total sampling effort) were
1628 classified as annual species with short growing seasons. We observed no effect of
1629 leaf $C_i:C_a$ on N_{area} or M_{area} in C₄ nonlegumes, which made up 22% of the sampling
1630 effort and were generally classified as warm season graminoid species with slower
1631 growth rates and longer growing seasons. These patterns indicate that stronger
1632 tradeoffs between nitrogen and water use may be more apparent in fast-growing
1633 species with high demand for building and maintaining productive leaf tissues.

1634 4.4.2 *Soil nitrogen availability increases N_{area} through changes in β*

1635 The experimental and statistical approach used in this study allowed for N_{area} and
1636 components of N_{area} to be quantified as direct and indirect products of soil nitrogen
1637 availability. Linear mixed effect models revealed a positive effect of increasing soil
1638 nitrogen availability on N_{area} , a pattern that was driven by a stronger positive
1639 effect of increasing soil nitrogen availability on N_{mass} than the negative effect
1640 of increasing soil nitrogen availability on M_{area} . These patterns were associated
1641 with a reduction in β with increasing soil nitrogen availability. Similar patterns
1642 were observed in the structural equation model, where indirect positive effects
1643 of increasing soil nitrogen availability on N_{area} were driven by negative effects of
1644 increasing soil nitrogen availability on β , positive effects of β and leaf $C_i:C_a$, and
1645 negative relationships between leaf $C_i:C_a$ and M_{area} . However, structural equation

1646 model results revealed a null direct relationship between leaf $C_i:C_a$ and N_{mass} ,
1647 and instead indicated an indirect positive effect of leaf $C_i:C_a$ on N_{mass} mediated
1648 through strong negative covariance between M_{area} and N_{mass} .

1649 Results reported here suggest that positive direct effects of increasing soil
1650 nitrogen availability on N_{area} are not necessarily the direct product of increased
1651 leaf nitrogen concentration, as has been previously suggested (Firn et al. 2019;
1652 Liang et al. 2020). Instead, effects of increasing soil nitrogen availability on leaf
1653 nitrogen concentration may be driven by costs of nitrogen acquisition relative
1654 to water and negative covariance between M_{area} and N_{mass} , following patterns
1655 predicted by photosynthetic least-cost theory. Findings reported here suggest that
1656 studies quantifying variance in leaf nitrogen content across resource availability
1657 gradients may risk confounding covariance between M_{area} and N_{mass} if costs of
1658 nitrogen acquisition relative to water are not also quantified.

1659 4.4.3 *Soil moisture increases N_{area} by facilitating increases in soil nitrogen
1660 availability*

1661 Increasing soil moisture had a positive effect on N_{area} , a response that was asso-
1662 ciated with a null effect of soil moisture on β . These results contrast patterns
1663 expected from theory, where increasing soil moisture is expected to indirectly de-
1664 crease N_{area} through an increase in β due to a reduction in costs associated with
1665 water acquisition and use (Wright et al. 2003; Prentice et al. 2014; Lavergne
1666 et al. 2020). Interestingly, structural equation model results revealed a strong
1667 positive association between soil moisture and soil nitrogen availability, indicat-
1668 ing an indirect positive effect of increasing soil moisture on N_{area} mediated by
1669 the negative effect of increasing soil nitrogen availability on β . In Texan grass-

1670 lands, productivity and nutrient uptake are often co-limited by precipitation and
1671 nutrient availability (Yahdjian et al. 2011; Wang et al. 2017). Thus, increases
1672 in soil moisture may have facilitated more favorable and productive environments
1673 for soil microbial communities (Reichman et al. 1966; Stark and Firestone 1995;
1674 Paul et al. 2003), or alternatively greater nitrogen mobility in soil solution. As
1675 discussed above, the positive indirect response of N_{area} to increasing soil nitrogen
1676 availability as mediated through reductions in β follow patterns expected from
1677 theory.

1678 4.4.4 *Indirect effects of climate on N_{area} are mediated through changes in leaf*
1679 *$C_i:C_a$ and β*

1680 In support of hypotheses and patterns expected from theory, increasing vapor
1681 pressure deficit indirectly increased N_{area} , mediated through the negative effect
1682 of increasing vapor pressure deficit on leaf $C_i:C_a$. These responses are consistent
1683 with previous work noting strong reductions in stomatal conductance with increas-
1684 ing vapor pressure deficit (Oren et al. 1999; Novick et al. 2016; Sulman et al.
1685 2016; Grossiord et al. 2020; López et al. 2021), a response that allows plants
1686 to minimize water loss as a result of high atmospheric water demand. Results
1687 also support findings from previous experiments across environmental gradients,
1688 where increasing vapor pressure deficit generally increases N_{area} at lower stomatal
1689 conductance across environmental gradients (Dong et al. 2017; Dong et al. 2022;
1690 Paillassa et al. 2020; Westerband et al. 2023). These responses provide another
1691 line of evidence that suggests leaf nitrogen content is a deterministic acclima-
1692 tion response to changing aboveground climate, allowing plants to satisfy demand
1693 to build and maintain photosynthetic enzymes and optimize photosynthetic pro-
1694 cesses by maximizing resource use efficiency (Paillassa et al. 2020; Peng et al.

1695 2021; Dong et al. 2022; Westerband et al. 2023).

1696 4.4.5 *Species identity traits modify effects of the environment on β , leaf $C_i:C_a$,*
1697 *and N_{area}*

1698 N-fixing species had greater N_{area} values on average compared to non-fixing species,

1699 a pattern driven by a stronger stimulation in N_{mass} in N-fixing species coupled with

1700 no change in M_{area} between species with different N-fixation ability. There was

1701 no evidence to suggest that N-fixing species had different β or leaf $C_i:C_a$ values

1702 compared to non-fixing species across the environmental gradient. These results

1703 follow patterns from previous environmental gradient experiments that investi-

1704 gate variance in leaf nitrogen allocation in N-fixing species (Adams et al. 2016;

1705 Dong et al. 2017; Dong et al. 2020), and that increases in N_{mass} and N_{area} in

1706 N-fixing species are not necessarily correlated to increases in water use efficiency

1707 or reductions in leaf $C_i:C_a$ (Adams et al. 2016). While results are consistent with

1708 results from previous environmental gradient experiments, they do not support

1709 hypotheses presented here or patterns expected from theory, which predicts that

1710 stimulations in N_{area} by N-fixing species should be driven by a reduction in β

1711 relative to non-fixing species, and that this response should decrease stomatal

1712 conductance and leaf $C_i:C_a$.

1713 C₄ species had reduced β , leaf $C_i:C_a$, and N_{area} than C₃ species. Reduced

1714 β and leaf $C_i:C_a$ values in C₄ species follow hypotheses listed above, a pattern

1715 that could be the result of either reduced costs of nitrogen acquisition and use,

1716 increased costs of water acquisition and use, or both (Wright et al. 2003; Prentice

1717 et al. 2014). Results also indicate that β in C₄ nonlegumes was unresponsive to

1718 changes in soil nitrogen availability despite an apparent negative effect of increas-

1719 ing soil nitrogen availability on β in C₃ legumes and C₃ nonlegumes. Combined
1720 with a general null response of β to soil moisture regardless of plant functional
1721 group, these patterns imply that reduced β values in C₄ species may be the re-
1722 sult of lower costs of nitrogen acquisition and use relative to C₃ species. While
1723 lower β values in C₄ species provides a possible explanation for why C₄ species
1724 often have lower leaf $C_i:C_a$ and greater water use efficiency, theory predicts that
1725 this response should cause C₄ species to have greater N_{area} values compared to
1726 C₃ species, though C₄ species commonly exhibit lower N_{area} and higher nitrogen
1727 use efficiency than C₃ species (Schmitt and Edwards 1981; Sage and Pearcy 1987;
1728 Ghannoum et al. 2011). We speculate that lowered costs of nitrogen acquisition
1729 and use in C₄ species could be driven by more efficient Rubisco carboxylation effi-
1730 ciency in C₄ species associated with CO₂ concentrating mechanisms that eliminate
1731 photorespiration (Ghannoum et al. 2011), which could reduce or eliminate the
1732 need to sacrifice inefficient nitrogen use for efficient water use to achieve optimal
1733 photosynthesis rates.

1734 4.4.6 *Next steps for optimality model development*

1735 Optimality models for both C₃ and C₄ species have been developed using principles
1736 from photosynthetic least-cost theory (Prentice et al. 2014; Wang et al. 2017;
1737 Smith et al. 2019; Stocker et al. 2020; Scott and Smith 2022). In both C₃ and C₄
1738 model variants, β values are held constant using global datasets of leaf $\delta^{13}\text{C}$ (Wang
1739 et al. 2017; Cornwell et al. 2018). Specifically, the C₃ optimality model initially
1740 assumed a constant β value of 240 (Wang et al. 2017), later corrected to 146
1741 (Stocker et al. 2020), while the C₄ optimality model assumes a constant β value of
1742 166 (Scott and Smith 2022). These results, which build on findings from Paillassa

1743 et al. (2020) and Lavergne et al. (2020), demonstrate high variability in calculated
1744 β values across the environmental gradient. Specifically, β values in C₃ species
1745 ranged from 1.7 to 188.0 (mean: 30.2; median: 23.1; standard deviation: 25.4),
1746 while ranged from 0.1 to 110.6 in C₄ species (mean: 7.2; median: 0.7; standard
1747 deviation: 18.6). Mean β values in both C₃ and C₄ species were consistently lower
1748 than values currently implemented in optimality models, though this was likely
1749 the result of increased water limitation across sites relative to global averages.
1750 Regardless, the high degree of β variability across this environmental gradient,
1751 together with findings from Lavergne et al. (2020) and Paillassa et al. (2020),
1752 suggests that the use of constant β values may contribute to erroneous errors when
1753 conducting optimality model simulations. Results from this experiment build
1754 on suggestions from Wang et al. (2017), suggesting that future photosynthetic
1755 least-cost optimality model developments should consider adopting frameworks
1756 for dynamically calculating β .

1757 4.4.7 Conclusions

1758 To summarize, variability in N_{area} across an environmental gradient in Texan
1759 grasslands was driven by indirect effects of climate and soil resource availability
1760 mediated. Results from this experiment provide strong and consistent support for
1761 patterns expected from photosynthetic least-cost theory, demonstrating that neg-
1762 ative relationships between $C_i:C_a$ and N_{area} unify expected effects of climatic and
1763 edaphic characteristics on N_{area} across environmental gradients. Results reported
1764 here also demonstrate a need to consider the dynamic nature of the relative cost
1765 of nitrogen versus water uptake (β) across environmental gradients in optimality

1766 models that leverage principles of photosynthetic least-cost theory.

1767

Chapter 5

1768
1769

Optimal resource investment to photosynthetic capacity maximizes
nutrient allocation to whole plant growth under elevated CO₂

1770 5.1 Introduction

1771 Terrestrial ecosystems are regulated by complex carbon and nitrogen cycles. As
1772 a result, terrestrial biosphere models, which are beginning to include coupled
1773 carbon and nitrogen cycles (Shi et al. 2016; Davies-Barnard et al. 2020; Braghieri
1774 et al. 2022), must accurately represent these cycles under different environmental
1775 scenarios to reliably simulate carbon and nitrogen atmosphere-biosphere fluxes
1776 (Hungate et al. 2003; Prentice et al. 2015). While the inclusion of coupled carbon
1777 and nitrogen cycles tends to reduce model uncertainty (Arora et al. 2020), large
1778 uncertainty in role of soil nitrogen availability and nitrogen acquisition strategy
1779 on leaf and whole plant acclimation responses to CO₂ remains (Smith and Dukes
1780 2013; Terrer et al. 2018; Smith and Keenan 2020). This source of uncertainty
1781 likely contributes to the widespread divergence in future carbon and nitrogen flux
1782 simulations across terrestrial biosphere models (Friedlingstein et al. 2014; Zaehle
1783 et al. 2014; Meyerholt et al. 2020).

1784 Plants grown under elevated CO₂ generally have less leaf nitrogen content
1785 than those grown under ambient CO₂, a response that often corresponds with
1786 reductions in photosynthetic capacity and stomatal conductance at the leaf-level
1787 and biomass stimulation over time at the whole plant level (Curtis 1996; Drake
1788 et al. 1997; Ainsworth et al. 2002; Makino 2003; Morgan et al. 2004; Ainsworth
1789 and Long 2005; Ainsworth and Rogers 2007; Smith and Dukes 2013; Poorter et al.
1790 2022). As net primary productivity is generally limited by nitrogen availability

1791 (Vitousek and Howarth 1991; LeBauer and Treseder 2008; Fay et al. 2015), and
1792 soil nitrogen availability is often positively correlated with leaf nitrogen content
1793 and photosynthetic capacity (Field and Mooney 1986; Evans and Seemann 1989;
1794 Evans 1989; Walker et al. 2014; Firn et al. 2019; Liang et al. 2020), some
1795 have hypothesized that leaf and whole plant acclimation responses to CO₂ are
1796 constrained by soil nitrogen availability.

1797 The progressive nitrogen limitation hypothesis predicts that elevated CO₂
1798 will increase plant nitrogen demand, which will increase plant nitrogen uptake and
1799 progressively deplete soil nitrogen if soil nitrogen supply does not exceed plant
1800 nitrogen demand (Luo et al. 2004). The hypothesis predicts that this response
1801 should result in strong acute stimulations in whole plant growth and primary
1802 productivity that diminish over time as nitrogen becomes more limiting. Assuming
1803 a positive relationship between soil nitrogen availability, leaf nitrogen content, and
1804 photosynthetic capacity, this hypothesis also implies that progressive reductions in
1805 soil nitrogen availability should be the mechanism that drives the downregulation
1806 of leaf nitrogen content and photosynthetic capacity under elevated CO₂. This
1807 hypothesis has received some support from free air CO₂ enrichment experiments
1808 (Reich et al. 2006; Norby et al. 2010), although is not consistently observed across
1809 experiments (Finzi et al. 2006; Moore et al. 2006; Liang et al. 2016).

1810 While possible that progressive nitrogen limitation may determine leaf and
1811 whole plant acclimation responses to CO₂, growing evidence indicates that leaf ni-
1812 trogen and photosynthetic capacity are more strongly determined through above-
1813 ground growing conditions than by soil resource availability (Dong et al. 2017;
1814 Dong et al. 2020; Dong et al. 2022; Smith et al. 2019; Smith and Keenan 2020;

1815 Paillassa et al. 2020; Peng et al. 2021; Querejeta et al. 2022; Westerband et al.
1816 2023), and satellite-derived chlorophyll fluorescence data indicate that increasing
1817 atmospheric CO₂ may decrease leaf and canopy demand for nitrogen (Dong et al.
1818 2022). Together, results from these studies suggest that the downregulation in
1819 leaf nitrogen content and photosynthetic capacity due to increasing CO₂ may not
1820 be as tightly linked to progressive nitrogen limitation as previously hypothesized.

1821 A unification of optimal coordination and least-cost theories predicts that
1822 leaves acclimate to elevated CO₂ by downregulating nitrogen allocation to Ribulose-
1823 1,5-bisphosphate (RuBP) carboxylase/oxygenase (Rubisco) to optimize resource
1824 use efficiencies at the leaf level, which allows for greater resource allocation to
1825 whole plant growth (Drake et al. 1997; Wright et al. 2003; Prentice et al. 2014;
1826 Smith et al. 2019). The theory predicts that the downregulation in nitrogen
1827 allocation to Rubisco results in a stronger downregulation in the maximum rate
1828 of Rubisco carboxylation (V_{cmax}) than the maximum rate of RuBP regeneration
1829 (J_{max}), which maximizes photosynthetic efficiency by allowing net photosynthesis
1830 rates to be equally co-limited by Rubisco carboxylation and RuBP regeneration
1831 (Chen et al. 1993; Maire et al. 2012). This acclimation response allows plants to
1832 make more efficient use of available light while avoiding overinvestment in Rubisco,
1833 which has high nitrogen and energetic costs of building and maintaining (Evans
1834 1989; Evans and Clarke 2019). Instead, additional acquired resources not needed
1835 to optimize leaf photosynthesis are allocated to the maintenance of structures that
1836 support whole plant growth (e.g., total leaf area, whole plant biomass, etc.) or
1837 to allocation processes not related to leaf photosynthesis or growth, such as plant
1838 defense mechanisms. Regardless, optimized resource allocation at the leaf level

1839 should allow for greater resource allocation to whole plant growth. The theory
1840 indicates that leaf acclimation responses to CO₂ should be independent of changes
1841 in soil nitrogen availability. While this leaf acclimation response maximizes nitro-
1842 gen allocation to structures that support whole plant growth, the theory suggests
1843 that the positive effect of elevated CO₂ on whole plant growth may be further
1844 stimulated by soil nitrogen availability through reductions in the cost of acquiring
1845 nitrogen (Bae et al. 2015; Perkowski et al. 2021; Lu et al. 2022).

1846 Plants acquire nitrogen by allocating photosynthetically derived carbon be-
1847 lowground in exchange for nitrogen through different nitrogen acquisition strate-
1848 gies. These nitrogen acquisition strategies can include direct uptake pathways
1849 such as mass flow or diffusion (Barber 1962), symbioses with mycorrhizal fungi or
1850 symbiotic nitrogen-fixing bacteria (Vance and Heichel 1991; Marschner and Dell
1851 1994; Smith and Read 2008; Udvardi and Poole 2013), or through the release
1852 of root exudates that prime free-living soil microbial communities (Phillips et al.
1853 2011; Wen et al. 2022). Plants cannot acquire nitrogen without first allocating
1854 carbon belowground, which implies an inherent carbon cost to the plant for acquir-
1855 ing nitrogen regardless of nitrogen acquisition strategy. Carbon costs to acquire
1856 nitrogen often vary in species with different nitrogen acquisition strategies and
1857 are dependent on external environmental factors such as atmospheric CO₂, light
1858 availability, and soil nitrogen availability (Brzostek et al. 2014; Terrer et al. 2016;
1859 Terrer et al. 2018; Allen et al. 2020; Perkowski et al. 2021; Lu et al. 2022). These
1860 patterns suggest that acquisition strategy may at least partially determine the net
1861 effect of soil nitrogen availability on leaf and whole plant acclimation responses to
1862 elevated CO₂.

1863 A recent meta-analysis using data across 20 grassland and forest CO₂ en-
1864 richment experiments suggested that species which acquire nitrogen from sym-
1865 biotic nitrogen-fixing bacteria had reduced costs of nitrogen acquisition under
1866 elevated CO₂ (Terrer et al. 2018). Though these analyses only included data
1867 from two experimental sites, findings from this meta-analysis indicated that re-
1868 ductions in costs of nitrogen acquisition in species that form associations with
1869 symbiotic nitrogen-fixing bacteria under elevated CO₂ may drive stronger stim-
1870 ulations in whole plant growth and downregulations in V_{cmax} than species that
1871 associate with arbuscular mycorrhizal fungi (Smith and Keenan 2020), which gen-
1872 erally have greater costs of nitrogen acquisition under elevated CO₂ (Terrer et al.
1873 2018). However, plant investments in symbiotic nitrogen fixation generally de-
1874 cline with increasing nitrogen availability (Dovrat et al. 2018; Perkowski et al.
1875 2021), a response that has been previously inferred to be the result of a shift in
1876 the dominant mode of nitrogen acquisition to direct uptake pathways as costs of
1877 direct uptake decrease with increasing soil nitrogen availability (Rastetter et al.
1878 2001; Perkowski et al. 2021). Thus, effects of symbiotic nitrogen fixation on plant
1879 acclimation responses to CO₂ should decline with increasing soil nitrogen avail-
1880 ability, although manipulative experiments that directly test these patterns are
1881 rare.

1882 Here, I conducted a 7-week growth chamber experiment using *Glycine max*
1883 L. (Merr.) to examine the effects of soil nitrogen fertilization and inoculation with
1884 symbiotic nitrogen-fixing bacteria on leaf and whole plant acclimation responses
1885 to elevated CO₂. Following patterns expected from theory, I hypothesized that in-
1886 dividual leaves should acclimate to elevated CO₂ by more strongly downregulating

1887 V_{cmax} relative to J_{max} , allowing leaf photosynthesis to approach optimal coordi-
1888 nation. I expected this response to correspond with a stronger downregulation in
1889 leaf nitrogen content than V_{cmax} and J_{max} , which would increase the fraction of
1890 leaf nitrogen content allocated to photosynthesis and photosynthetic nitrogen use
1891 efficiency. At the whole-plant level, I hypothesized that plants would acclimate
1892 to elevated CO₂ by stimulating whole plant growth and productivity, a response
1893 that would be driven by a strong positive response of total leaf area and above-
1894 ground biomass to elevated CO₂. I predicted that leaf acclimation responses to
1895 elevated CO₂ would be independent of soil nitrogen fertilization and inoculation
1896 with symbiotic nitrogen-fixing bacteria; however, I expected that increasing soil
1897 nitrogen fertilization would increase the positive effect of elevated CO₂ on mea-
1898 sures of whole plant growth due to a stronger reduction in the cost of acquiring
1899 nitrogen under elevated CO₂ with increasing fertilization. I also expected stronger
1900 stimulations in whole plant growth due to inoculation, but that this effect would
1901 only be apparent under low fertilization due to a reduction in root nodulation
1902 with increasing fertilization.

1903 5.2 Methods

1904 5.2.1 *Seed treatments and experimental design*

1905 *Glycine max* L. (Merr) seeds were planted in 144 6-liter surface sterilized pots (NS-
1906 600, Nursery Supplies, Orange, CA, USA) containing a steam-sterilized 70:30 v:v
1907 mix of Sphagnum peat moss (Premier Horticulture, Quakertown, PA, USA) to
1908 sand (Pavestone, subsidiary of Quikrete Companies, Atlanta, GA, USA). Before
1909 planting, all *G. max* seeds were surface sterilized in 2% sodium hypochlorite for 3

1910 minutes, followed by three separate 3-minute washes with ultrapure water (MilliQ
1911 7000; MilliporeSigma, Burlington, MA USA). A subset of surface sterilized seeds
1912 were inoculated with *Bradyrhizobium japonicum* (Verdesian N-DureTM Soybean,
1913 Cary, NC, USA) in a slurry following manufacturer recommendations (3.12 g
1914 inoculant and 241 g deionized water per 1 kg seed).

1915 Seventy-two pots were randomly planted with surface-sterilized seeds inoc-
1916 ulated with *B. japonicum*, while the remaining 72 pots were planted with surface-
1917 sterilized uninoculated seeds. Thirty-six pots within each inoculation treatment
1918 were randomly placed in one of two atmospheric CO₂ treatments (ambient and
1919 1000 $\mu\text{mol mol}^{-1}$ CO₂). Pots within each unique inoculation-by-CO₂ treatment
1920 combination randomly received one of nine soil nitrogen fertilization treatments
1921 equivalent to 0, 35, 70, 105, 140, 210, 280, 350, or 630 ppm N. Nitrogen fertil-
1922 ization treatments were created using a modified Hoagland solution (Hoagland
1923 and Arnon 1950) designed to keep concentrations of other macronutrients and
1924 micronutrients equivalent across treatments (Table D1). Pots received the same
1925 fertilization treatment throughout the entire duration experiment, which were ap-
1926 plied twice per week in 150 mL doses as topical agents to the soil surface. This
1927 experimental design yielded a fully factorial experiment with four replicates per
1928 unique fertilization-by-inoculation-by-CO₂ combination.

1929 5.2.2 *Growth chamber conditions*

1930 Upon experiment initiation, pots were randomly placed in one of six Percival
1931 LED-41L2 growth chambers (Percival Scientific Inc., Perry, IA, USA) over two
1932 experimental iterations due to chamber space limitation. Two iterations were

1933 conducted such that one iteration included all elevated CO₂ pots and the second
1934 iteration included all ambient CO₂ pots. Mean (\pm SD) CO₂ concentrations across
1935 chambers throughout the experiment were $439 \pm 5 \mu\text{mol mol}^{-1}$ CO₂ for the ambient
1936 CO₂ treatment and $989 \pm 4 \mu\text{mol mol}^{-1}$ CO₂ for the elevated CO₂ treatment.

1937 Daytime growing conditions were simulated using a 16-hour photoperiod,
1938 with incoming light radiation set to chamber maximum (mean \pm SD: 1240 ± 32
1939 $\mu\text{mol m}^{-2} \text{s}^{-1}$ across chambers), air temperature set to 25°C, and relative humid-
1940 ity set to 50%. The remaining 8 hours simulated nighttime growing conditions,
1941 with incoming light radiation set to 0 $\mu\text{mol m}^{-2} \text{s}^{-1}$, chamber temperature set
1942 to 17°C, and relative humidity set to 50%. Transitions between daytime and
1943 nighttime growing conditions were simulated by ramping incoming light radiation
1944 in 45-minute increments and temperature in 90-minute increments over a 3-hour
1945 period (Table D2).

1946 Including the two, 3-hour ramping periods, pots grew under average (\pm SD)
1947 daytime light intensity of $1049 \pm 27 \mu\text{mol m}^{-2} \text{s}^{-1}$. In the elevated CO₂ iteration,
1948 pots grew under $24.0 \pm 0.2^\circ\text{C}$ during the day, $16.4 \pm 0.8^\circ\text{C}$ during the night, and
1949 51.6 $\pm 0.4\%$ relative humidity. In the ambient CO₂ iteration, pots grew under
1950 $23.9 \pm 0.2^\circ\text{C}$ during the day, $16.0 \pm 1.4^\circ\text{C}$ during the night, and $50.3 \pm 0.2\%$ relative
1951 humidity. I accounted for any climatic differences across the six chambers by
1952 shuffling the same group of pots daily throughout the growth chambers. This
1953 process was done by iteratively moving the group of pots on the top rack of a
1954 chamber to the bottom rack of the same chamber, while simultaneously moving
1955 the group of pots on the bottom rack of a chamber to the top rack of the adjacent
1956 chamber. I moved pots within and across chambers every day throughout the

1957 course of each experiment iteration.

1958 5.2.3 *Leaf gas exchange measurements*

1959 Gas exchange measurements were collected for all individuals on the seventh week

1960 of development. All gas exchange measurements were collected on the center leaf

1961 of the most recent fully expanded trifoliate leaf set. Specifically, I measured net

1962 photosynthesis (A_{net} ; $\mu\text{mol m}^{-2} \text{s}^{-1}$), stomatal conductance (g_{sw} ; $\text{mol m}^{-2} \text{s}^{-1}$),

1963 and intercellular CO_2 (C_i ; $\mu\text{mol mol}^{-1}$) concentrations across a range of atmo-

1964 spheric CO_2 concentrations (i.e., an A_{net}/C_i curve) using the Dynamic Assimila-

1965 tion TechniqueTM. The Dynamic Assimilation TechniqueTM has been shown to

1966 correspond well with traditional steady-state CO_2 response curves in *G. max*

1967 (Saathoff and Welles 2021). A_{net}/C_i curves were generated along a reference CO_2

1968 ramp down from $420 \mu\text{mol mol}^{-1} \text{CO}_2$ to $20 \mu\text{mol mol}^{-1} \text{CO}_2$, followed by a ramp

1969 up from $420 \mu\text{mol mol}^{-1} \text{CO}_2$ to $1620 \mu\text{mol mol}^{-1} \text{CO}_2$ after a 90-second wait

1970 period at $420 \mu\text{mol mol}^{-1} \text{CO}_2$. The ramp rate for each curve was set to 200

1971 $\mu\text{mol mol}^{-1} \text{min}^{-1}$, logging every five seconds, which generated 96 data points per

1972 response curve. All A_{net}/C_i curves were generated after A_{net} and g_{sw} stabilized

1973 in a LI-6800 cuvette set to a 500 mol s^{-1} , 10,000 rpm mixing fan speed, 1.5 kPa

1974 vapor pressure deficit, 25°C leaf temperature, $2000 \mu\text{mol m}^{-2} \text{s}^{-1}$ incoming light

1975 radiation, and initial reference CO_2 set to $420 \mu\text{mol mol}^{-1}$.

1976 With the same focal leaf used to generate A_{net}/C_i curves, I measured dark

1977 respiration (R_{d25} ; $\mu\text{mol m}^{-2} \text{s}^{-1}$) following at least a 30-minute period of darkness.

1978 Measurements were collected on a 5-second log interval for 60 seconds after stabi-

1979 lizing in a LI-6800 cuvette set to a 500 mol s^{-1} , 10,000 rpm mixing fan speed, 1.5

1980 kPa vapor pressure deficit, 25°C leaf temperature, and 420 $\mu\text{mol mol}^{-1}$ reference
1981 CO₂ concentration (for both CO₂ concentrations), with incoming light radiation
1982 set to 0 $\mu\text{mol m}^{-2} \text{s}^{-1}$. A single dark respiration value was determined for each
1983 focal leaf by calculating the mean dark respiration value (i.e. the absolute value
1984 of A_{net} during the logging period) across the logging interval.

1985 5.2.4 *Leaf trait measurements*

1986 The focal leaf used to generate A_{net}/C_i curves and dark respiration was harvested
1987 immediately following gas exchange measurements. Images of each focal leaf were
1988 curated using a flat-bed scanner to determine wet leaf area using the ‘LeafArea’ R
1989 package (Katabuchi 2015), which automates leaf area calculations using ImageJ
1990 software (Schneider et al. 2012). Each leaf was dried at 65°C for at least 48
1991 hours, and subsequently weighed and ground until homogenized. Leaf mass per
1992 area (M_{area} ; g m⁻²) was calculated as the ratio of dry leaf biomass to fresh leaf
1993 area. Using subsamples of ground and homogenized leaf tissue, I measured leaf
1994 nitrogen content (N_{mass} ; gN g⁻¹) through elemental combustion analysis (Costech-
1995 4010, Costech, Inc., Valencia, CA, USA). Leaf nitrogen content per unit leaf area
1996 (N_{area} ; gN m⁻²) was calculated by multiplying N_{mass} and M_{area} . Subsamples of
1997 ground and homogenized leaf tissue were also sent to the UC-Davis Stable Isotope
1998 Facility to quantify leaf $\delta^{15}\text{N}$, later used to estimate the fraction of leaf nitrogen
1999 derived from the atmosphere.

2000 I extracted chlorophyll content from a second leaf in the same trifoliolate
2001 leaf set as the focal leaf used to generate A_{net}/C_i curves. Prior to chlorophyll
2002 extraction, I used a cork borer to punch between 3 and 5 0.6 cm² disks from the

2003 leaf. Separate images of each punched leaf and set of leaf disks were curated using
2004 a flat-bed scanner to determine wet leaf area, again quantified using the ‘LeafArea’
2005 R package (Katabuchi 2015). The punched leaf was dried and weighed after at
2006 least 65°C in the drying oven to determine M_{area} of the chlorophyll leaf.

2007 Leaf disks were shuttled into a test tube containing 10mL dimethyl sulfoxide, vortexed, and incubated at 65°C for 120 minutes (Barnes et al. 1992). Incubated test tubes were vortexed again before loaded in 150 μL triplicate aliquots to
2010 a 96-well plate. Dimethyl sulfoxide was also loaded in a 150 μL triplicate aliquot
2011 as a blank. Absorbance measurements at 649.1 nm ($A_{649.1}$) and 665.1 nm ($A_{665.1}$)
2012 were read in each well using a plate reader (Bioteck Synergy H1; Bioteck Instruments, Winooski, VT USA) (Wellburn 1994), with triplicates subsequently aver-
2014 aged and corrected by the mean of the blank absorbance value. Blank-corrected
2015 absorbance values were used to estimate Chl_a ($\mu\text{g mL}^{-1}$) and Chl_b ($\mu\text{g mL}^{-1}$)
2016 following equations from Wellburn (1994):

$$Chl_a = 12.47A_{665.1} - 3.62A_{649.1} \quad (5.1)$$

2017 and

$$Chl_b = 25.06A_{665.1} - 6.50A_{649.1} \quad (5.2)$$

2018 Chl_a and Chl_b were converted to mmol mL^{-1} using the molar mass of chlorophyll a
2019 (893.51 g mol^{-1}) and the molar mass of chlorophyll b (907.47 g mol^{-1}), then added
2020 together to calculate total chlorophyll content in the dimethyl sulfoxide extractant
2021 (mmol mL^{-1}). Total chlorophyll content was multiplied by the volume of the
2022 dimethyl sulfoxide extractant (10 mL) and converted to area-based chlorophyll

2023 content by dividing by the total area of the leaf disks (Chl_{area} ; mmol m⁻²). Mass-
2024 based chlorophyll content (Chl_{mass} ; mmol g⁻¹) was calculated by dividing Chl_{area}
2025 by the leaf mass per area of the punched leaf.

2026 5.2.5 *A/C_i curve fitting and parameter estimation*

2027 I fit A_{net}/C_i curves of each individual using the ‘fitaci’ function in the ‘plante-
2028 cophys’ R package (Duursma 2015). This function estimates the maximum rate
2029 of Rubisco carboxylation (V_{cmax} ; $\mu\text{mol m}^{-2} \text{s}^{-1}$) and maximum rate of electron
2030 transport for RuBP regeneration (J_{max} ; $\mu\text{mol m}^{-2} \text{s}^{-1}$) based on the Farquhar
2031 biochemical model of C₃ photosynthesis (Farquhar et al. 1980). Triose phosphate
2032 utilization (TPU) limitation was included in all curve fits, and all curve fits in-
2033 cluded measured dark respiration values. As A_{net}/C_i curves were generated using
2034 a common leaf temperature, curves were fit using Michaelis-Menten coefficients
2035 for Rubisco affinity to CO₂ (K_c ; $\mu\text{mol mol}^{-1}$) and O₂ (K_o ; $\mu\text{mol mol}^{-1}$), and the
2036 CO₂ compensation point (Γ^* ; $\mu\text{mol mol}^{-1}$) reported in Bernacchi et al. (2001).
2037 Specifically, K_c was set to 404.9 $\mu\text{mol mol}^{-1}$, K_o was set to 278.4 $\mu\text{mol mol}^{-1}$,
2038 and Γ^* was set to 42.75 $\mu\text{mol mol}^{-1}$. All curve fits were visually examined for
2039 goodness-of-fit. The use of a common leaf temperature across curves and dark
2040 respiration measurements eliminated the need to temperature standardize rate
2041 estimates. For clarity, I reference V_{cmax} , J_{max} , and R_d estimates throughout the
2042 rest of the chapter as V_{cmax25} , J_{max25} , and R_{d25} .

2043 5.2.6 *Stomatal limitation*

2044 I quantified the extent by which stomatal conductance limited photosynthesis (l ;

2045 unitless) following equations originally described in Farquhar and Sharkey (1982).

2046 Stomatal limitation was calculated as:

$$l = 1 - \frac{A_{net}}{A_{mod}} \quad (5.3)$$

2047 where A_{mod} represents the photosynthetic rate where $C_i = C_a$. A_{mod} was calculated

2048 as:

$$A_{mod} = V_{cmax25} - \frac{420 - \Gamma^*}{420 + K_m} - R_{d25} \quad (5.4)$$

2049 K_m is the Michaelis-Menten coefficient for Rubisco-limited photosynthesis, calcu-

2050 lated as:

$$K_m = K_c \cdot \left(1 + \frac{O_i}{K_o}\right) \quad (5.5)$$

2051 where O_i refers to leaf intercellular O_2 concentrations, set to $210 \mu\text{mol mol}^{-1}$.

2052 5.2.7 *Proportion of leaf nitrogen allocated to photosynthesis and structure*

2053 I used equations from Niinemets and Tenhunen (1997) to estimate the proportion

2054 of leaf nitrogen content allocated to Rubisco, bioenergetics, and light harvesting

2055 proteins. The proportion of leaf nitrogen allocated to Rubisco ($\rho_{rubisco}$; gN gN^{-1})

2056 was calculated as a function of V_{cmax25} and N_{area} :

$$\rho_{rubisco} = \frac{V_{cmax25} N_r}{V_{cr} N_{area}} \quad (5.6)$$

2057 where N_r is the amount of nitrogen in Rubisco, set to 0.16 gN (gN in Rubisco) $^{-1}$
2058 and V_{cr} is the maximum rate of RuBP carboxylation per unit Rubisco protein,
2059 set to 20.5 $\mu\text{mol CO}_2$ (g Rubisco) $^{-1}$. The proportion of leaf nitrogen allocated to
2060 bioenergetics (ρ_{bioe} ; gN gN $^{-1}$) was similarly calculated as a function of J_{max25} and
2061 N_{area} :

$$\rho_{bioe} = \frac{J_{max25} N_b}{J_{mc} N_{area}} \quad (5.7)$$

2062 where N_b is the amount of nitrogen in cytochrome f, set to 0.12407 gN (μmol
2063 cytochrome f) $^{-1}$ assuming a constant 1: 1: 1.2 cytochrome f: ferredoxin NADP
2064 reductase: coupling factor molar ratio (Evans and Seemann 1989; Niinemets and
2065 Tenhunen 1997), and J_{mc} is the capacity of electron transport per cytochrome f,
2066 set to 156 $\mu\text{mol electron}$ ($\mu\text{mol cytochrome f}$) $^{-1}\text{s}^{-1}$.

2067 The proportion of leaf nitrogen allocated to light harvesting proteins (ρ_{light} ;
2068 gN gN $^{-1}$) was calculated as a function of Chl_{mass} and N_{mass} :

$$\rho_{light} = \frac{Chl_{mass}}{N_{mass} c_b} \quad (5.8)$$

2069 where c_b is the stoichiometry of the light-harvesting chlorophyll complexes of
2070 photosystem II, set to 2.75 mmol chlorophyll (gN in chlorophyll) $^{-1}$. I used the
2071 N_{mass} value of the focal leaf used to generate A_{net}/C_i curves instead of the leaf
2072 used to extract chlorophyll content, as the two leaves are from the same trifoliolate
2073 leaf set and are highly correlated (Figure D1).

2074 The proportion of leaf nitrogen content allocated to photosynthetic tissue
2075 (ρ_{photo} ; gN gN $^{-1}$) was estimated as the sum of $\rho_{rubisco}$, ρ_{bioe} , and ρ_{light} . Finally,
2076 the proportion of leaf nitrogen content allocated to structural tissue ($\rho_{structure}$; gN

2077 gN⁻¹) was estimated as:

$$\rho_{structure} = \frac{N_{cw}}{N_{area}} \quad (5.9)$$

2078 where N_{cw} is the leaf nitrogen content allocated to cell walls (gN m⁻²), calculated

2079 as a function of M_{area} using an empirical equation from Onoda et al. (2017):

$$N_{cw} = 0.000355 * M_{area}^{1.39} \quad (5.10)$$

2080 5.2.8 *Whole plant traits*

2081 Seven weeks after experiment initiation and immediately following gas exchange

2082 measurements, I harvested all experimental individuals and separated biomass of

2083 each experimental individual into major organ types (leaves, stems, roots, and

2084 nodules when present). Fresh leaf area of all harvested leaves was measured using

2085 an LI-3100C (Li-COR Biosciences, Lincoln, Nebraska, USA). Total fresh leaf area

2086 (cm²) was calculated as the sum of all leaf areas, including the focal leaf used to

2087 collect gas exchange data and the focal leaf used to extract chlorophyll content. All

2088 harvested material was dried in an oven set to 65°C for at least 48 hours, weighed,

2089 and ground to homogeneity. Leaves and nodules were manually ground with a

2090 mortar and pestle, while stems and roots were ground using a Wiley mill (E3300

2091 Mini Mill; Eberbach Corp., MI, USA). Total dry biomass (g) was calculated as

2092 the sum of dry leaf (including focal leaf for both the A_{net}/C_i curve and leaf used

2093 to extract chlorophyll content), stem, root, and root nodule biomass. I quantified

2094 carbon and nitrogen content of each respective organ type through elemental

2095 combustion (Costech-4010, Costech, Inc., Valencia, CA, USA) using subsamples

2096 of ground and homogenized organ tissue.

2097 Following the approach explained in the first experimental chapter, I calcu-
2098 lated structural carbon costs to acquire nitrogen as the ratio of total belowground
2099 carbon biomass to whole plant nitrogen biomass (N_{cost} ; gC gN⁻¹). Belowground
2100 carbon biomass (C_{bg} ; gC) was calculated as the sum of root carbon biomass
2101 and root nodule carbon biomass. Root carbon biomass and root nodule carbon
2102 biomass was calculated as the product of the organ biomass and the respective
2103 organ carbon content. Whole plant nitrogen biomass (N_{wp} ; gN) was similarly
2104 calculated as the sum of total leaf, stem, root, and root nodule nitrogen biomass,
2105 including the focal leaf used for A_{net}/C_i curve and chlorophyll extractions. Leaf,
2106 stem, root, and root nodule nitrogen biomass was calculated as the product of
2107 the organ biomass and the respective organ nitrogen content. This calculation
2108 only quantifies plant structural carbon costs to acquire nitrogen and does not
2109 include any additional costs of nitrogen acquisition associated with respiration,
2110 root exudation, or root turnover. An explicit explanation of the limitations for
2111 interpreting this calculation can be found in Perkowski et al. (2021) and Terrer
2112 et al. (2018).

2113 Finally, plant investments in nitrogen fixation were calculated as the ratio
2114 of root nodule biomass to root biomass, where increasing values indicate an in-
2115 crease in plant investments to nitrogen fixation (Dovrat et al. 2018; Dovrat et al.
2116 2020; Perkowski et al. 2021). I also calculated the percent of leaf nitrogen ac-
2117 quired from the atmosphere (% N_{dfa} ; %) using leaf $\delta^{15}\text{N}$ and the following equation
2118 from Andrews et al. (2011):

$$\%N_{\text{dfa}} = \frac{\delta^{15}N_{\text{reference}} - \delta^{15}N_{\text{sample}}}{\delta^{15}N_{\text{reference}} - B} \quad (5.11)$$

2119 where $\delta^{15}\text{N}_{\text{reference}}$ refers to a reference plant that exclusively acquires nitrogen via
2120 direct uptake, $\delta^{15}\text{N}_{\text{sample}}$ refers to an individual's leaf $\delta^{15}\text{N}$, and B refers to individuals
2121 that are entirely reliant on nitrogen fixation. Within each unique nitrogen
2122 fertilization treatment-by-CO₂ treatment combination, I calculated the mean leaf
2123 $\delta^{15}\text{N}$ for individuals growing in the non-inoculated treatment for $\delta^{15}\text{N}_{\text{reference}}$. Any
2124 individuals with visual confirmation of root nodule formation were omitted from
2125 the calculation of $\delta^{15}\text{N}_{\text{reference}}$. Following recommendations from Andrews et al.
2126 (2011) I calculated B within each CO₂ treatment using the mean leaf $\delta^{15}\text{N}$ of
2127 inoculated individuals that received 0 ppm N. I did not calculate B within each
2128 unique soil nitrogen-by-CO₂ treatment combination, as previous studies suggest
2129 decreased reliance on nitrogen fixation with increasing soil nitrogen availability
2130 (Perkowski et al. 2021).

2131 5.2.9 *Statistical analyses*

2132 Uninoculated pots that had substantial root nodule formation (nodule biomass:
2133 root biomass values greater than 0.05 g g⁻¹) were removed from all analyses, as
2134 pots were assumed to have been colonized by symbiotic nitrogen-fixing bacteria
2135 from outside sources. This decision resulted in the removal of sixteen pots from
2136 analyses: two pots in the elevated CO₂ treatment that received 35 ppm N, three
2137 pots in the elevated CO₂ treatment that received 70 ppm N, one pot in the elevated
2138 CO₂ treatment that received 210 ppm N, two pots in the elevated CO₂ treatment
2139 that received 280 ppm N, two pots in the ambient CO₂ treatment that received
2140 0 ppm N, three pots in the ambient CO₂ treatment that received 70 ppm N, two
2141 pots in the ambient CO₂ treatment that received 105 ppm N, and one pot in the

2142 ambient CO₂ treatment that received 280 ppm N.

2143 I built a series of linear mixed effects models to investigate the impacts of
2144 CO₂ concentration, soil nitrogen fertilization, and inoculation with *B. japonicum*
2145 on *G. max* gas exchange, tradeoffs between nitrogen and water use, whole plant
2146 growth, and investment in nitrogen fixation. All models included CO₂ treatment
2147 as a categorical fixed effect, inoculation treatment as a categorical fixed effect,
2148 soil nitrogen fertilization as a continuous fixed effect, with interaction terms be-
2149 tween all three fixed effects. All models also accounted for climatic difference
2150 between chambers across experiment iterations by including a random intercept
2151 term that nested starting chamber rack by CO₂ treatment. Models with this
2152 independent variable structure were created for each of the following dependent
2153 variables: N_{area} , M_{area} , N_{mass} , Chl_{area} , V_{cmax25} , J_{max25} , $J_{\text{max25}}:V_{\text{cmax25}}$, R_{d25} , g_{sw} ,
2154 stomatal limitation, ρ_{rubisco} , ρ_{bioe} , ρ_{light} , ρ_{photo} , $\rho_{\text{structure}}$, total biomass, total leaf
2155 area, N_{cost} , C_{bg} , N_{wp} , nodule biomass, the ratio of nodule biomass to root biomass,
2156 and % N_{dfa} .

2157 I used Shapiro-Wilk tests of normality to determine whether linear mixed
2158 effects models satisfied residual normality assumptions. If residual normality as-
2159 sumptions were not met (Shapiro-Wilk: $p < 0.05$), then models were fit using de-
2160 pending variables that were natural log transformed. If residual normality as-
2161 sumptions were still not met (Shapiro-Wilk: $p < 0.05$), then models were fit using
2162 dependent variables that were square root transformed. All residual normality
2163 assumptions that did not originally satisfy residual normality assumptions were
2164 met with either a natural log or square root data transformation (Shapiro-Wilk:
2165 $p > 0.05$ in all cases). Specifically, models for N_{area} , N_{mass} , Chl_{area} , V_{cmax25} , J_{max25} ,

2166 $J_{\max25}$: $V_{\text{cmax}25}$, R_{d25} , g_{sw} , stomatal limitation, ρ_{rubisco} , ρ_{bioe} , ρ_{light} , ρ_{photo} , total leaf
2167 area, N_{cost} satisfied residual normality assumptions without data transformation.
2168 Models for M_{area} , $\rho_{\text{structure}}$, C_{bg} , and total biomass satisfied residual normality as-
2169 sumptions with a natural log data transformation, while models for N_{wp} , nodule
2170 biomass, nodule biomass: root biomass, and $\%N_{dfa}$ satisfied residual normality
2171 assumptions with a square root data transformation.

2172 In all statistical models, I used the ‘lmer’ function in the ‘lme4’ R package
2173 (Bates et al. 2015) to fit each model and the ‘Anova’ function in the ‘car’ R
2174 package (Fox and Weisberg 2019) to calculate Type II Wald’s χ^2 and determine
2175 the significance ($\alpha=0.05$) of each fixed effect coefficient. I used the ‘emmeans’
2176 R package (Lenth 2019) to conduct post-hoc comparisons using Tukey’s tests,
2177 where degrees of freedom were approximated using the Kenward-Roger approach
2178 (Kenward and Roger 1997). All analyses and plots were conducted in R version
2179 4.2.0 (R Core Team 2021).

2180 5.3 Results

2181 5.3.1 Leaf nitrogen and chlorophyll content

2182 Elevated CO₂ reduced N_{area} , N_{mass} , and Chl_{area} by 29%, 50%, and 31%, respec-
2183 tively, and stimulated M_{area} by 44% ($p<0.001$ in all cases; Table 5.1). An inter-
2184 action between fertilization and CO₂ (CO₂-by-fertilization interaction: $p_{N_{\text{area}}}=$
2185 0.017, $p_{N_{\text{mass}}}<0.001$, $p_{Chl_{\text{area}}}=0.083$; Table 5.1) indicated that the positive effect
2186 of increasing fertilization on N_{area} , N_{mass} , and Chl_{area} ($p<0.001$ in all cases; Table
2187 5.1) was stronger under ambient CO₂ (Tukey _{N_{area}} : $p=0.026$; Tukey _{N_{mass}} : $p<0.001$;
2188 Tukey _{Chl_{area}} : $p=0.065$; Table 5.1; Figs. 5.1a, 5.1b, 5.1d). An interaction between

2189 fertilization and CO₂ on M_{area} (CO₂-by-fertilization interaction: $p=0.006$; Ta-
2190 ble 5.1) indicated that the positive effect of increasing fertilization on M_{area} was
2191 stronger under elevated CO₂ (Tukey: $p=0.009$; Fig. 5.1c). Overall, interactions
2192 between fertilization and CO₂ resulted in stronger reductions in N_{area} , N_{mass} , and
2193 Chl_{area} , and a stronger stimulation in M_{area} under elevated CO₂ with increasing
2194 fertilization.

2195 An interaction between inoculation and CO₂ on N_{area} (CO₂-by-inoculation
2196 interaction: $p=0.030$; Table 5.1) indicated that the positive effect of inoculation
2197 on N_{area} ($p<0.001$; Table 5.1) was stronger under elevated CO₂ (45% increase;
2198 Tukey: $p<0.001$) than under ambient CO₂ (18% increase; Tukey: $p<0.001$), a
2199 result that increased the reduction in N_{area} in inoculated pots under elevated
2200 CO₂. Inoculation treatment did not modify the downregulation in N_{mass} (CO₂-
2201 by-inoculation interaction: $p=0.148$; Table 5.1) and Chl_{area} ($p = 0.147$; Table
2202 5.1) or the stimulation in M_{area} ($p=0.866$; Table 5.1) under elevated CO₂. How-
2203 ever, interactions between fertilization and inoculation on N_{area} , N_{mass} , M_{area} ,
2204 and Chl_{area} (fertilization-by-inoculation interaction: $p_{N_{\text{area}}}<0.001$, $p_{N_{\text{mass}}}=0.001$,
2205 $p_{M_{\text{area}}}=0.025$, $p_{Chl_{\text{area}}}=0.083$; Table 5.1) indicated that the positive effect of in-
2206 creasing fertilization on each trait was stronger in uninoculated pots (Tukey _{N_{area}} :
2207 $p<0.001$; Tukey _{N_{mass}} : $p=0.001$; Tukey _{M_{area}} : $p=0.031$; Tukey _{Chl_{area}} : $p<0.001$;
2208 Figs. 5.1a-d).

Table 5.1. Effects of soil nitrogen fertilization, inoculation, and CO₂ treatments on leaf nitrogen content per unit leaf area (N_{area} ; gN m⁻²), leaf nitrogen content per unit leaf mass (N_{mass} , gN g⁻¹), leaf mass per unit leaf area (M_{area} ; g m⁻²), and chlorophyll content per unit leaf area (Chl_{area} ; mmol m⁻²)^{*}

	N_{area}			N_{mass}			M_{area}^a			
	df	Coefficient	χ^2	p	Coefficient	χ^2	p	Coefficient	χ^2	p
(Intercept)	-	1.10E+00	-	-	3.05E-02	-	-	3.64E+00	-	-
CO ₂	1	-5.67E-01	155.908	<0.001	-1.80E-02	272.362	<0.001	3.04E-01	151.319	<0.001
Inoculation (I)	1	6.21E-01	86.029	<0.001	7.54E-03	15.576	<0.001	1.81E-01	19.158	<0.001
Fertilization (N)	1	3.06E-03	316.408	<0.001	5.78E-05	106.659	<0.001	3.10E-04	21.440	<0.001
CO ₂ *I	1	2.63E-01	4.729	0.030	3.96E-03	2.025	0.155	-3.37E-02	0.029	0.866
CO ₂ *N	1	-3.68E-04	5.723	0.017	-2.85E-05	22.542	<0.001	2.80E-04	7.619	0.006
I*N	1	-1.36E-03	43.381	<0.001	-2.00E-05	11.137	0.001	-3.36E-04	5.022	0.025
CO ₂ *I*N	1	-3.23E-04	0.489	0.484	-2.59E-06	0.041	0.839	1.15E-04	0.208	0.649
Chl _{area}										
	df	Coefficient	χ^2	p						
(Intercept)	-	2.13E-02	-	-						
CO ₂	1	-1.33E-02	69.233	<0.001						
Inoculation (I)	1	1.24E-01	136.341	<0.001						
Fertilization (N)	1	3.35E-04	163.111	<0.001						
CO ₂ *I	1	-3.18E-02	2.102	0.147						
CO ₂ *N	1	-8.79E-05	2.999	0.083						
I*N	1	-2.65E-04	75.769	<0.001						
CO ₂ *I*N	1	7.68E-05	2.144	0.147						

2209 *Significance determined using Type II Wald χ^2 tests ($\alpha=0.05$). P-values less than 0.05 are in bold, while p-values
 2210 between 0.05 and 0.1 are italicized. A superscript “a” is included after trait labels to indicate if models were fit with
 2211 natural log transformed response variables. Key: df=degrees of freedom, χ^2 =Wald Type II chi-square test statistic.

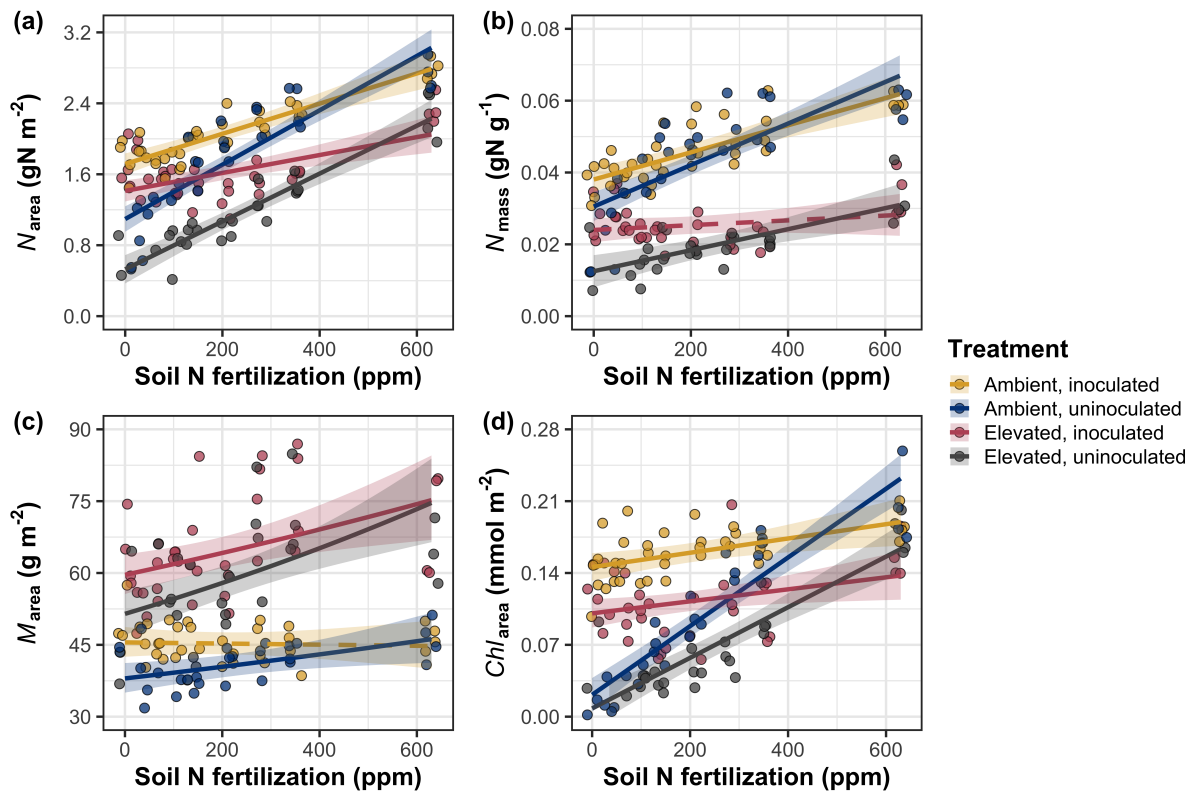


Figure 5.1. Effects of CO_2 , fertilization, and inoculation on leaf nitrogen per unit leaf area (a), leaf nitrogen content (b), leaf mass per unit leaf area (c), and chlorophyll content per unit leaf area (d). Soil nitrogen fertilization is represented on the x-axis in all panels. Yellow points and trendlines indicate inoculated individuals grown under ambient CO_2 , blue points and trendlines indicate uninoculated individuals grown under ambient CO_2 , red points and trendlines indicate inoculated individuals grown under elevated CO_2 , and grey points indicate uninoculated individuals grown under elevated CO_2 . Solid trendlines indicate regression slopes that are different from zero ($p < 0.05$), while dashed trendlines indicate slopes that are not distinguishable from zero ($p > 0.05$).

2212 5.3.2 *Leaf biochemistry and stomatal conductance*

2213 Elevated CO₂ resulted in plants with 16% lower V_{cmax25} ($p<0.001$; Table 5.2) and
2214 10% lower J_{max25} ($p=0.014$; Table 5.2) compared to those grown under ambient
2215 CO₂. However, CO₂ concentration did not influence R_{d25} ($p=0.613$; Table 5.2;
2216 Fig. 5.2d). A relatively stronger downregulation in V_{cmax25} than J_{max25} resulted
2217 in an 8% stimulation in $J_{max25}:V_{cmax25}$ under elevated CO₂ ($p<0.001$; Table 5.2).
2218 The downregulatory effect of CO₂ on V_{cmax25} and J_{max25} was not modified across
2219 the fertilization gradient (CO₂-by-fertilization interaction: $p=0.185$ and $p=0.389$
2220 for V_{cmax25} and J_{max25} , respectively; Table 5.2; Figs. 5.2a, 5.2b) or between in-
2221 oculation treatments (CO₂-by-inoculation interaction: $p=0.799$ and $p=0.714$ for
2222 V_{cmax25} and J_{max25} , respectively; Table 5.2). However, a strong interaction between
2223 fertilization and inoculation (fertilization-by-inoculation interaction: $p\leq0.001$ in
2224 all cases; Table 5.2) indicated that the positive effect of increasing fertilization
2225 on V_{cmax25} ($p<0.001$; Table 5.2), J_{max25} ($p<0.001$; Table 5.2), and R_{d25} ($p=0.015$;
2226 Table 5.2) was only observed in uninoculated pots (Tukey: $p\leq0.001$ in all cases;
2227 Figs. 5.2a, 5.2b). A stronger positive effect of increasing fertilization on V_{cmax25}
2228 than J_{max25} resulted in a reduction in $J_{max25}:V_{cmax25}$ with increasing fertilization
2229 ($p<0.001$; Table 5.2), though this pattern was only observed in uninoculated pots
2230 (fertilization-by-inoculation interaction: $p=0.002$; Table 5.2; Fig. 5.2c).

2231 Elevated CO₂ reduced stomatal conductance by 20% ($p<0.001$; Table 5.2;
2232 Fig. 5.2e), but this downregulation did not influence stomatal limitation of pho-
2233 tosynthesis ($p=0.355$; Table 5.2; Fig. 5.2f). As with V_{cmax25} and J_{max25} , the down-
2234 regulation of stomatal conductance due to elevated CO₂ was not modified across
2235 the fertilization gradient (CO₂-by-fertilization interaction: $p=0.141$; Table 5.2) or

2236 between inoculation treatments (CO_2 -by-inoculation interaction: $p=0.179$; Table
2237 5.2). Fertilization also did not modify the null effect of CO_2 on stomatal limitation
2238 (CO_2 -by-fertilization interaction: $p=0.554$; Table 5.2), although an interaction
2239 between CO_2 and inoculation (CO_2 -by-inoculation interaction: $p=0.043$; Table
2240 5.2) indicated that inoculation increased stomatal limitation under ambient CO_2
2241 (Tukey: $p=0.021$), but not under elevated CO_2 (Tukey: $p>0.999$). An interaction
2242 between inoculation and fertilization on stomatal conductance (fertilization-by-
2243 inoculation interaction: $p<0.001$; Table 5.2) indicated that increasing fertilization
2244 increased stomatal conductance in uninoculated pots (Tukey: $p=0.003$) but de-
2245 creased stomatal conductance in inoculated pots (Tukey: $p=0.021$). The similar
2246 in magnitude, but opposite direction, trend in the effect of increasing fertiliza-
2247 tion on stomatal conductance between inoculation treatments likely drove a null
2248 response of stomatal conductance to increasing fertilization ($p=0.642$; Table 5.2).

Table 5.2. Effects of soil nitrogen fertilization, inoculation, and CO₂ on the maximum rate of Rubisco carboxylation ($V_{\text{cmax}25}$; $\mu\text{mol m}^{-2} \text{s}^{-1}$), the maximum rate of RuBP regeneration ($J_{\text{max}25}$; $\mu\text{mol m}^{-2} \text{s}^{-1}$), dark respiration ($R_{\text{d}25}$; $\mu\text{mol m}^{-2} \text{s}^{-1}$), the ratio of the maximum rate of RuBP regeneration to the maximum rate of Rubisco carboxylation ($J_{\text{max}25}:V_{\text{cmax}25}$; unitless), stomatal conductance (g_{sw} ; $\text{mol m}^{-2} \text{s}^{-1}$), and stomatal limitation (unitless)*

	$V_{\text{cmax}25}$			$J_{\text{max}25}$			$R_{\text{d}25}$			
	df	Coefficient	χ^2	p	Coefficient	χ^2	p	Coefficient	χ^2	p
(Intercept)	-	4.36E+01	-	-	8.30E+01	-	-	1.69E+00	-	-
CO ₂	1	-7.05E+00	18.039	<0.001	-9.11E+00	6.042	0.014	4.53E-01	0.256	0.613
Inoculation (I)	1	5.87E+01	98.579	<0.001	9.62E+01	85.064	<0.001	1.04E+00	3.094	0.079
Fertilization (N)	1	1.32E-01	37.053	<0.001	2.09E-01	25.356	<0.001	2.86E-03	5.965	0.015
CO ₂ *I	1	-4.65E+00	0.065	0.799	7.84E-01	0.667	0.414	-5.71E-01	2.563	0.109
CO ₂ *N	1	-3.58E-02	1.758	0.185	-4.33E-02	0.742	0.389	-1.55E-03	2.675	0.102
I*N	1	-1.35E-01	60.394	<0.001	-2.30E-01	57.410	<0.001	-2.84E-03	12.083	0.001
CO ₂ *I*N	1	2.73E-02	0.748	0.387	3.46E-02	0.377	0.539	7.21E-04	0.244	0.622

134

	$J_{\text{max}25}:V_{\text{cmax}25}$			g_{sw}			Stomatal limitation			
	df	Coefficient	χ^2	p	Coefficient	χ^2	p	Coefficient	χ^2	p
(Intercept)	-	1.92E+00	-	-	1.95E-01	-	-	2.12E-01	-	-
CO ₂	1	5.71E-02	92.010	<0.001	-6.23E-02	9.718	0.002	3.91E-02	0.856	0.355
Inoculation (I)	1	-1.79E-01	27.768	<0.001	1.30E-01	22.351	<0.001	7.87E-02	4.582	0.032
Fertilization (N)	1	-4.61E-04	28.147	<0.001	2.50E-04	0.066	0.797	2.60E-04	32.218	<0.001
CO ₂ *I	1	8.94E-02	2.916	0.088	6.69E-02	1.810	0.179	-7.84E-02	4.093	0.043
CO ₂ *N	1	2.35E-04	3.210	0.073	-8.50E-05	2.165	0.141	-1.24E-04	0.350	0.554
I*N	1	3.27E-04	9.607	0.002	-3.09E-04	14.696	<0.001	-1.67E-04	2.547	0.110
CO ₂ *I*N	1	-1.66E-04	1.102	0.294	-8.89E-05	0.234	0.629	1.67E-04	2.231	0.135

2249 *Significance determined using Type II Wald χ^2 tests ($\alpha=0.05$). P-values less than 0.05 are in bold, while p-values
 2250 between 0.05 and 0.1 are italicized. Key: df=degrees of freedom; χ^2 =Wald Type II chi-square test statistic.

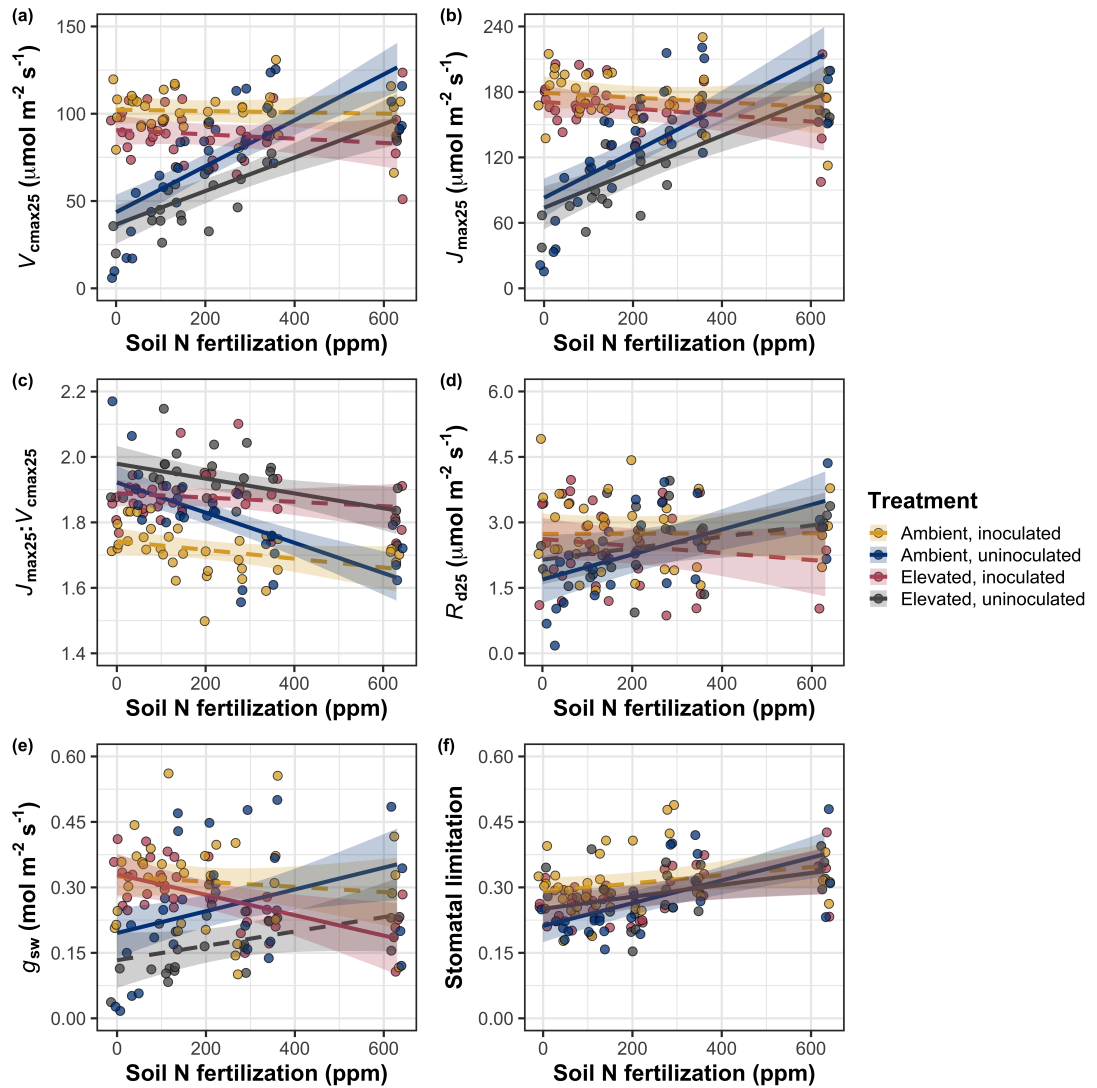


Figure 5.2. Effects of CO₂, fertilization, and inoculation on maximum rate of Rubisco carboxylation (a), the maximum rate of RuBP regeneration (b), and the ratio of the maximum rate of RuBP regeneration to the maximum rate of Rubisco carboxylation leaf mass per unit leaf area (c), dark respiration (d), stomatal conductance (e), and stomatal limitation (f). Soil nitrogen fertilization is represented on the x-axis in all panels. Colored points and trendlines are as explained in Figure 5.1.

2251 5.3.3 *Leaf nitrogen allocation*

2252 A relatively stronger downregulation in N_{area} than $V_{\text{cmax}25}$ and $J_{\text{max}25}$ resulted in
2253 an 20% and 29% respective stimulation in ρ_{rubisco} and ρ_{bioe} under elevated CO₂
2254 ($p<0.001$ in both cases; Table 5.3). There was no effect of CO₂ on ρ_{light} ($p=0.700$;
2255 Table 5.3), but the stimulation in ρ_{rubisco} and ρ_{bioe} resulted in a 21% stimulation
2256 of ρ_{photo} under elevated CO₂ ($p<0.001$; Table 5.3; Fig. 5.3a). The stimulation
2257 of ρ_{rubisco} , ρ_{bioe} , and ρ_{photo} under elevated CO₂ was not modified across the fer-
2258 tilization gradient (CO₂-by-fertilization interaction: $p_{\text{rubisco}}=0.269$, $p_{\text{bioe}}=0.298$,
2259 $p_{\text{photo}}=0.281$; Table 5.3). A marginal interaction between inoculation and CO₂ on
2260 ρ_{rubisco} and ρ_{photo} (CO₂-by-inoculation interaction: $p_{\text{rubisco}}=0.057$, $p_{\text{photo}}=0.055$;
2261 Table 5.3) indicated that the positive effect of inoculation on ρ_{rubisco} and ρ_{photo}
2262 ($p<0.001$ in both cases; Table 5.3) was only apparent under ambient CO₂ (Tukey:
2263 $p<0.001$ in both cases). Inoculation did not modify the stimulation of ρ_{bioe} un-
2264 der elevated CO₂ (CO₂-by-inoculation interaction: $p=0.122$; Table 5.3) or the
2265 null effect of CO₂ on ρ_{bioe} (CO₂-by-inoculation interaction: $p=0.298$; Table 5.3).
2266 An interaction between fertilization and inoculation on ρ_{rubisco} , ρ_{bioe} , and ρ_{photo}
2267 (fertilization-by-inoculation interaction: $p<0.001$ in all cases; Table 5.3) indicated
2268 that the negative effect of increasing fertilization on each trait ($p<0.001$ in all
2269 cases; Table 5.3) was only observed in inoculated pots (Tukey: $p<0.001$ in all
2270 cases). An additional interaction between fertilization and inoculation on ρ_{light}
2271 (fertilization-by-inoculation interaction: $p<0.001$; Table 5.3) indicated a negative
2272 effect of increasing fertilization on ρ_{light} in inoculated pots (Tukey: $p=0.041$), but
2273 a positive effect of increasing fertilization in uninoculated pots (Tukey: $p<0.001$).
2274 The stimulation in M_{area} under elevated CO₂ resulted in an 133% stimu-

2275 lation of $\rho_{\text{structure}}$ ($p<0.001$; Table 5.3; Fig 5.3b). An interaction between fertil-
2276 ization and CO₂ (CO₂-by-fertilization interaction: $p=0.039$; Table 5.3) indicated
2277 that the negative effect of increasing fertilization ($p<0.001$; Table 5.3) on $\rho_{\text{structure}}$
2278 was marginally stronger under ambient CO₂ (Tukey: $p=0.055$). A marginal inter-
2279 action between inoculation and CO₂ (CO₂-by-inoculation interaction: $p=0.057$;
2280 Table 5.3) indicated that the positive effect of inoculation on $\rho_{\text{structure}}$ ($p<0.001$;
2281 Table 5.3) was only observed under elevated CO₂ (Tukey: $p<0.001$), with no ap-
2282 parent inoculation effect observed under ambient CO₂ (Tukey: $p=0.513$). Finally,
2283 an interaction between fertilization and inoculation (fertilization-by-inoculation
2284 interaction: $p<0.001$; Table 5.3) indicated that, while increasing fertilization in-
2285 creased $\rho_{\text{structure}}$ ($p<0.001$; Table 5.3), this response was stronger in uninoculated
2286 pots (Tukey: $p=0.001$; Fig. 5.3b).

Table 5.3. Effects of soil nitrogen fertilization, inoculation, and CO₂ on the fraction of leaf nitrogen allocated to Rubisco (ρ_{rubisco} ; gN gN⁻¹), bioenergetics (ρ_{bioe} ; gN gN⁻¹), light harvesting proteins (ρ_{light} ; gN gN⁻¹), photosynthesis (ρ_{photo} ; gN gN⁻¹), and structure ($\rho_{\text{structure}}$; gN gN⁻¹)*

	ρ_{rubisco}			ρ_{bioe}			ρ_{light}			
	df	Coefficient	χ^2	p	Coefficient	χ^2	p	Coefficient	χ^2	p
(Intercept)	-	2.70E-01	-	-	5.26E-02	-	-	8.48E-03	-	-
CO ₂	1	1.42E-01	23.510	<0.001	3.00E-02	53.899	<0.001	2.03E-03	0.149	0.700
Inoculation (I)	1	1.83E-01	23.475	<0.001	2.80E-02	13.860	<0.001	2.04E-02	147.234	<0.001
Fertilization (N)	1	1.35E-04	16.609	<0.001	1.22E-05	26.827	<0.001	3.22E-05	19.378	<0.001
CO ₂ *I	1	-1.07E-01	3.629	0.057	-1.67E-02	2.390	0.122	-5.33E-03	0.684	0.408
CO ₂ *N	1	-2.16E-04	1.223	0.269	-3.59E-05	1.085	0.298	-7.01E-06	0.351	0.553
I*N	1	-4.26E-04	20.045	<0.001	-6.87E-05	15.458	<0.001	-4.37E-05	64.042	<0.001
CO ₂ *I*N	1	2.50E-04	3.327	0.068	4.08E-05	2.651	0.103	1.74E-05	3.735	0.053

	ρ_{photo}			$\rho_{\text{structure}}^a$			
	df	Coefficient	χ^2	p	Coefficient	χ^2	p
(Intercept)	-	3.32E-01	-	-	-2.93E+00	-	-
CO ₂	1	1.81E-01	27.651	<0.001	8.77E-01	229.571	<0.001
Inoculation (I)	1	2.31E-01	26.238	<0.001	-2.55E-01	13.872	<0.001
Fertilization (N)	1	1.76E-04	15.899	<0.001	-1.51E-03	38.128	<0.001
CO ₂ *I	1	-1.36E-01	3.671	0.055	-2.99E-01	3.622	0.057
CO ₂ *N	1	-2.72E-04	1.163	0.281	3.14E-04	4.266	0.039
I*N	1	-5.37E-04	21.355	<0.001	7.00E-04	11.025	0.001
CO ₂ *I*N	1	3.29E-04	4.009	0.045	4.52E-04	0.669	0.413

2287 *Significance determined using Type II Wald χ^2 tests ($\alpha=0.05$). P-values less than 0.05 are in bold, while p-values
 2288 between 0.05 and 0.1 are italicized. A superscript “a” is included after trait labels to indicate if models were fit with
 2289 natural log transformed response variable. Key: df=degrees of freedom; χ^2 =Wald Type II chi-square test statistic.

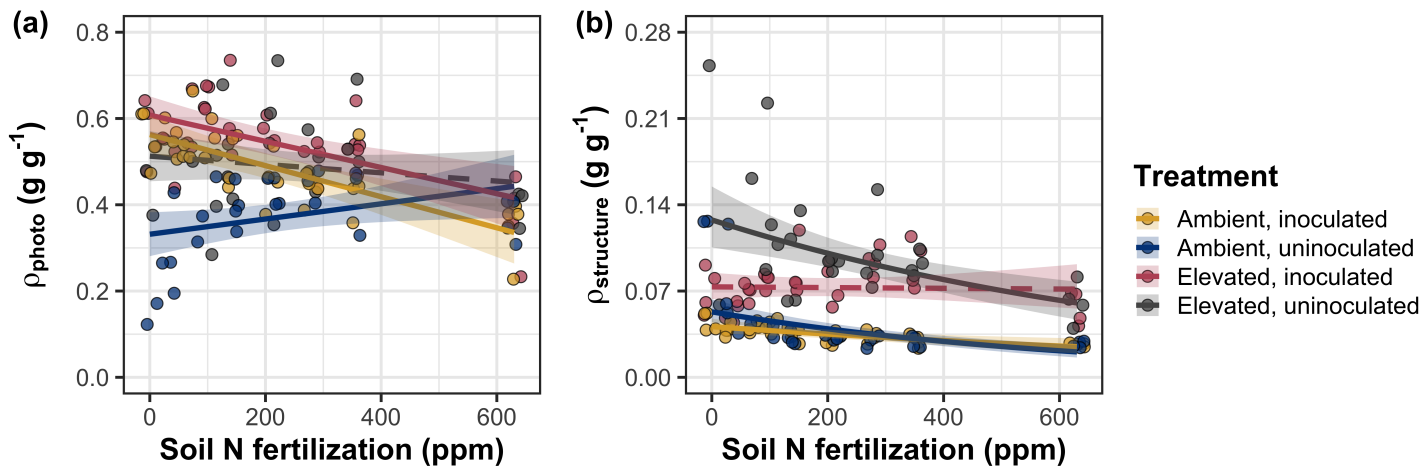


Figure 5.3. Effects of CO_2 , fertilization, and inoculation on the relative fraction of leaf nitrogen allocated to photosynthesis (a) and the fraction of leaf nitrogen allocated to structure (b). Soil nitrogen fertilization is represented on the x-axis in both panels. Colored points and trendlines are as explained in Figure 5.1.

2290 5.3.4 *Whole plant traits*

2291 Total leaf area and total biomass were 51% and 102% greater under elevated CO₂,
2292 respectively ($p<0.001$ in both cases; Table 5.4). The stimulation in total leaf area
2293 and total biomass under elevated CO₂ was enhanced by increasing fertilization
2294 (CO₂-by-fertilization interaction: $p<0.001$ in both cases; Table 5.4; Figs. 5.4a,
2295 5.4b) but was not modified across inoculation treatments (CO₂-by-inoculation
2296 interaction: $p_{total_leaf_area}=0.151$, $p_{total_biomass}=0.472$; Table 5.4). The positive
2297 effect of increasing fertilization on total leaf area and total biomass was modified by
2298 inoculation treatment (fertilization-by-inoculation interaction: $p<0.001$ in both
2299 cases; Table 5.4), indicating a stronger positive effect of increasing fertilization in
2300 uninoculated pots (Tukey: $p_{total_leaf_area}=0.002$, $p_{total_biomass}=0.001$, Figs. 5.4a,
2301 5.4b).

2302 A 62% stimulation in N_{cost} under elevated CO₂ was modified through a
2303 strong three-way interaction between CO₂, fertilization, and inoculation (CO₂-
2304 by-inoculation-by-fertilization interaction: $p<0.001$; Table 5.4; Fig. 5.4). This
2305 interaction revealed a general negative effect of increasing fertilization on N_{cost}
2306 ($p<0.001$; Table 5.4) that was observed in all treatment combinations (Tukey:
2307 $p<0.001$ in all cases) except for inoculated pots grown under elevated CO₂ (Tukey:
2308 $p=0.779$; Fig. 5.4c). This response also resulted in stronger negative effects of in-
2309 creasing fertilization on N_{cost} in uninoculated pots grown under elevated CO₂ than
2310 uninoculated pots grown under ambient CO₂ (Tukey: $p=0.001$) and inoculated
2311 pots grown under either ambient CO₂ (Tukey: $p<0.001$) or elevated CO₂ (Tukey:
2312 $p<0.001$), while uninoculated pots grown under ambient CO₂ had stronger nega-
2313 tive effects of increasing fertilization on N_{cost} than inoculated pots grown under

2314 elevated CO₂ (Tukey: $p=0.002$), but not inoculated pots grown under ambient
2315 CO₂ (Tukey: $p=0.216$; Fig. 5.4). The reduction in N_{cost} with increasing fertiliza-
2316 tion and in uninoculated pots were driven by a stronger positive effect of increasing
2317 fertilization on N_{wp} (denominator of N_{cost}) than C_{bg} (numerator of N_{cost}), while
2318 the stimulation in N_{cost} under elevated CO₂ was driven by a stronger positive
2319 effect of elevated CO₂ on C_{bg} than N_{wp} (Table 5.4).

Table 5.4. Effects of CO₂, fertilization, and inoculation on total leaf area (cm²), whole plant biomass (g), carbon costs to acquire nitrogen (N_{cost} ; gC gN⁻¹), belowground carbon biomass (C_{bg} ; gC), and whole plant nitrogen biomass (N_{wp} ; gN)*

	Total leaf area			Total biomass ^b			<i>N</i> _{cost}			
	df	Coefficient	χ^2	p	Coefficient	χ^2	p	Coefficient	χ^2	p
(Intercept)	-	8.78E+01	-	-	9.96E-01	-	-	8.67E+00	-	-
CO ₂	1	3.36E+01	69.291	<0.001	5.07E-01	131.477	<0.001	8.75E+00	88.189	<0.001
Inoculation (I)	1	1.88E+02	35.715	<0.001	7.96E-01	34.264	<0.001	-1.68E+00	136.343	<0.001
Fertilization (N)	1	9.35E-01	274.199	<0.001	3.14E-03	269.046	<0.001	-8.50E-03	80.501	<0.001
CO ₂ *I	1	6.44E+01	2.064	0.151	-7.69E-02	0.518	0.472	-8.38E+00	85.237	<0.001
CO ₂ *N	1	5.05E-01	18.655	<0.001	1.61E-03	16.877	<0.001	-9.17E-03	1.050	0.306
I*N	1	-3.84E-01	10.804	0.001	-1.45E-03	15.779	<0.001	4.20E-03	46.489	<0.001
CO ₂ *I*N	1	-2.97E-03	<0.001	0.990	-1.14E-04	0.023	0.880	1.32E-02	18.125	<0.001

	C_{bg}^{a}		N_{wp}^{b}				
	df	Coefficient	χ^2	p	Coefficient	χ^2	p
(Intercept)	-	-1.70E+00	-	-	1.24E-01	-	-
CO ₂	1	9.21E-01	84.134	<0.001	-3.41E-03	23.890	<0.001
Inoculation (I)	1	1.18E+00	41.030	<0.001	1.68E-01	134.460	<0.001
N fertilization (N)	1	3.38E-03	152.248	<0.001	6.69E-04	529.021	<0.001
CO ₂ * I	1	-6.18E-01	8.965	0.003	3.68E-02	1.190	0.275
CO ₂ * N	1	-3.66E-05	1.188	0.276	1.58E-04	5.915	0.015
I * N	1	-2.22E-03	22.648	<0.001	-3.20E-04	55.562	<0.001
CO ₂ * I * N	1	8.09E-04	1.109	0.292	-7.54E-05	0.620	0.431

2320 *Significance determined using Type II Wald χ^2 tests ($\alpha=0.05$). *P*-values less than 0.05 are in bold. Superscripts
2321 included after trait labels indicate if models were fit with natural log (^a) or square root (^b) transformed response
2322 variables. Key: df=degrees of freedom; χ^2 =Wald Type II chi-square test statistic.

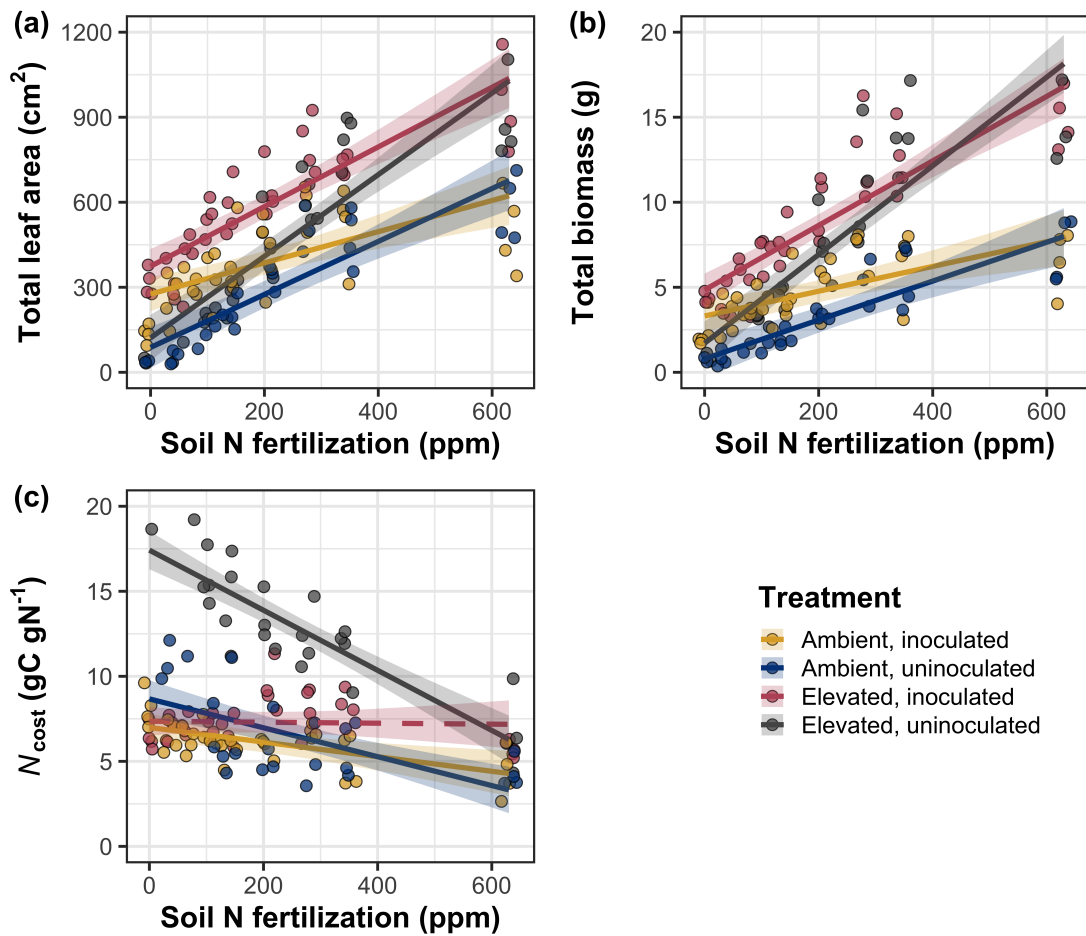


Figure 5.4. Effects of CO_2 , fertilization, and inoculation on total leaf area (a), total biomass (b), and structural carbon costs to acquire nitrogen (c). Soil nitrogen fertilization is represented on the x-axis in all panels. Colored points and trendlines are as explained in Figure 5.1.

2323 5.3.5 *Nitrogen fixation*

2324 Nodule biomass was stimulated by 30% under elevated CO₂ ($p<0.001$; Table 5.5),
2325 a pattern that was modified across the fertilization gradient (CO₂-by-fertilization
2326 interaction: $p=0.479$; Table 5.5), but not between inoculation treatments (CO₂-
2327 by-inoculation interaction: $p=0.404$; Table 5.5). Specifically, the negative effect
2328 of increasing fertilization on nodule biomass ($p<0.001$; Table 5.5) was stronger
2329 under elevated CO₂ (Tukey: $p<0.001$; Fig. 5.5a). An interaction between fertil-
2330 ization and inoculation (fertilization-by-inoculation interaction: $p<0.001$; Table
2331 5.5) indicated a stronger negative effect of increasing fertilization in inoculated
2332 pots (Tukey: $p<0.001$; Fig. 5.5a).

2333 There was no effect of CO₂ on nodule: root biomass ($p=0.767$; Table 5.5),
2334 although an interaction between CO₂ and inoculation (CO₂-by-inoculation in-
2335 teraction: $p<0.001$; Table 5.5) indicated that the positive effect of inoculation
2336 on nodule: root biomass ($p<0.001$; Table 5.5) was stronger under ambient CO₂
2337 (3129% increase; Tukey: $p<0.001$) than elevated CO₂ (379% increase; Tukey:
2338 $p<0.001$; Fig. 5.5b). The null effect of CO₂ on nodule: root biomass was consis-
2339 tently observed across the fertilization gradient (CO₂-by-fertilization interaction:
2340 $p=0.183$; Table 5.5; Fig. 5.5b). An interaction between fertilization and inocula-
2341 tion (fertilization-by-inoculation interaction: $p<0.001$; Table 5.5) indicated that
2342 the negative effect of increasing fertilization on nodule: root biomass ($p<0.001$;
2343 Table 5.5) was stronger in inoculated pots (Tukey: $p<0.001$; Fig. 5.5b).

2344 There was no effect of CO₂ on %N_{dfa} ($p=0.472$; Table 5.5), a pattern
2345 that was not modified by inoculation (CO₂-by-inoculation interaction: $p=0.156$;
2346 Table 5.5) or fertilization (CO₂-by-fertilization interaction: $p=0.099$; Table 5.5).

- 2347** An interaction between fertilization and inoculation (fertilization-by-inoculation
2348 interaction: $p<0.001$; Table 5.5) indicated that the negative effect of increasing
2349 fertilization on $\%N_{dfa}$ ($p<0.001$; Table 5.5) was only observed in inoculated pots
2350 (Tukey: $p<0.001$; Fig. 5.5c).

Table 5.5. Effects of CO₂, fertilization, and inoculation on root nodule biomass (g), plant investments in symbiotic nitrogen fixation (unitless), and percent nitrogen fixed from the atmosphere (%N_{dfa}; unitless)*

	Root nodule biomass ^b			Root nodule: root biomass ^b			%N _{dfa} ^b			
	df	Coefficient	χ^2	p	Coefficient	χ^2	p	Coefficient	χ^2	p
(Intercept)	-	9.41E-03	-	-	1.33E-02	-	-	7.48E-01	-	-
CO ₂	1	1.20E-01	19.258	<0.001	9.94E-02	0.087	0.768	-1.00E-01	0.518	0.472
Inoculation (I)	1	5.74E-01	755.020	<0.001	5.40E-01	903.691	<0.001	9.01E+00	955.570	<0.001
Fertilization (N)	1	7.71E-06	84.376	<0.001	-5.99E-06	258.099	<0.001	3.64E-04	292.938	<0.001
CO ₂ *I	1	-4.68E-02	0.950	0.330	-1.38E-01	20.614	<0.001	-1.44E-01	2.010	0.156
CO ₂ *N	1	-1.59E-04	2.106	0.147	-1.73E-04	1.773	0.183	-6.21E-05	2.716	0.099
I*N	1	-5.82E-04	44.622	<0.001	-7.45E-04	133.918	<0.001	-1.58E-02	231.290	<0.001
CO ₂ *I*N	1	7.26E-05	0.196	0.658	1.76E-04	2.359	0.125	2.77E-03	2.119	0.145

2351 *Significance determined using Type II Wald χ^2 tests ($\alpha=0.05$). P-values less than 0.05 are in bold, while p-values
2352 between 0.05 and 0.1 are italicized. Superscript letters indicate model coefficients fit to square-root (^b) transformed
2353 data. Key: df=degrees of freedom; χ^2 =Wald Type II chi-square test statistic.

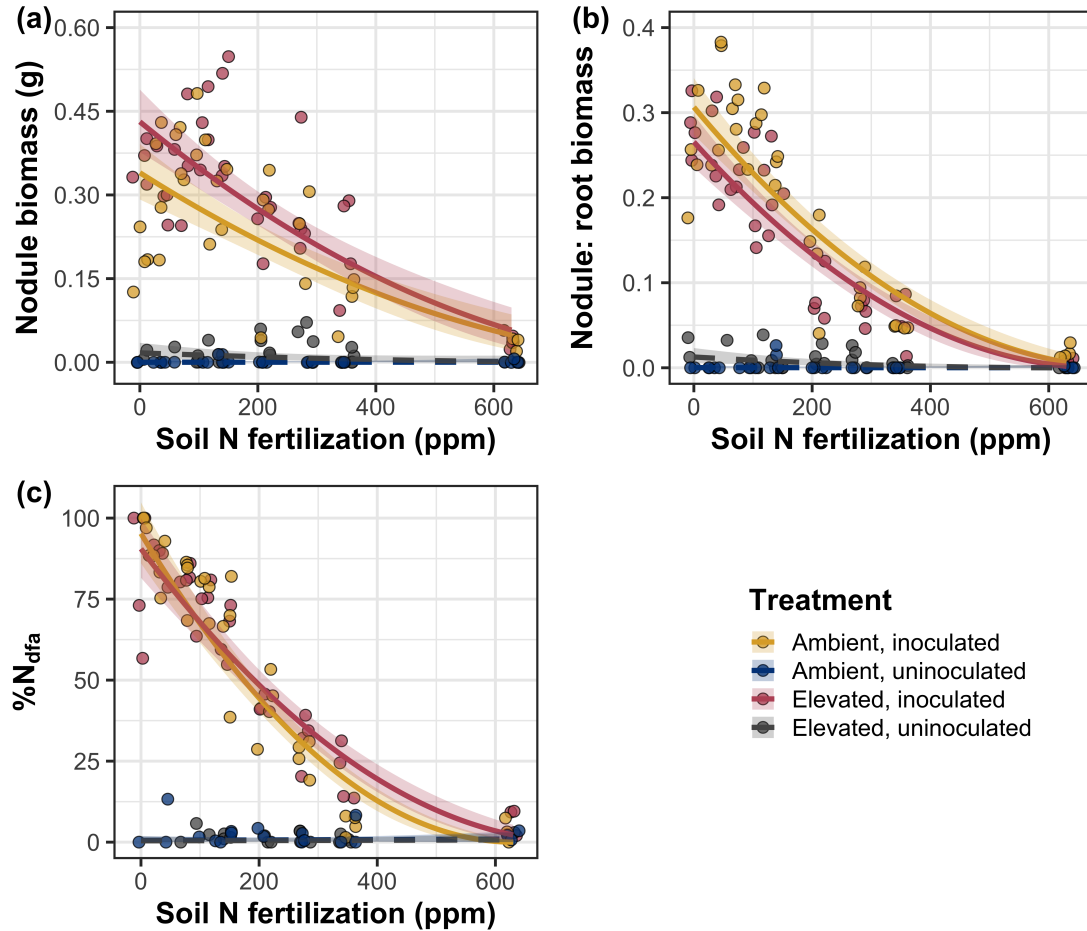


Figure 5.5. Effects of CO₂, fertilization, and inoculation on nodule biomass (a), nodule biomass: root biomass (b), and percent nitrogen fixed from the atmosphere (c). Soil nitrogen fertilization is represented on the x-axis. Colored points and trendlines are as explained in Figure 5.1. Curvilinear trendlines occur as a result of back-transforming models where response variables received either a natural log or square root transformation prior to fitting.

2354 5.4 Discussion

2355 In this study, I determined leaf and whole plant acclimation responses of 7-week *G.*
2356 *max* seedlings grown under two CO₂ concentrations, two inoculation treatments,
2357 and nine soil nitrogen fertilization treatments in a full-factorial growth chamber
2358 experiment. In support of hypotheses and patterns expected from theory, elevated
2359 CO₂ reduced N_{area} , V_{cmax25} , and J_{max25} . The relatively stronger downregulation in
2360 V_{cmax25} than J_{max25} under elevated CO₂ resulted in a stimulation in $J_{\text{max25}}:V_{\text{cmax25}}$
2361 under elevated CO₂. The downregulation of V_{cmax25} and J_{max25} under elevated
2362 CO₂ was similar across fertilization and inoculation treatments, indicating that
2363 the CO₂ responses were not associated with nitrogen limitation. Interestingly,
2364 results indicate that elevated CO₂ increased the fraction of leaf nitrogen allocated
2365 to photosynthesis and structure, leading to a stimulation in nitrogen use efficiency
2366 under elevated CO₂ despite the apparent downregulation in N_{area} , V_{cmax25} , and
2367 J_{max25} .

2368 The downregulation in leaf photosynthetic processes under elevated CO₂
2369 corresponded with a strong stimulation in total leaf area and total biomass. Strong
2370 stimulations in whole plant growth due to elevated CO₂ were generally enhanced
2371 with increasing fertilization and were negatively related to structural carbon costs
2372 to acquire nitrogen. Inoculation generally did not modify whole plant responses
2373 to elevated CO₂ across the fertilization gradient, likely due to a strong reduc-
2374 tion in root nodulation with increasing fertilization. However, strong positive
2375 effects of inoculation on whole plant growth were observed under low fertilization,
2376 consistent with hypotheses. Overall, observed leaf and whole plant acclimation
2377 responses to CO₂ support hypotheses and patterns expected from photosynthetic

2378 least-cost theory, showing that leaf acclimation responses to CO₂ were decoupled
2379 from soil nitrogen availability and ability to acquire nitrogen via symbiotic nitro-
2380 gen fixation. Instead, leaf and whole plant acclimation responses to CO₂ were
2381 driven by optimal resource investment to photosynthetic capacity, where optimal
2382 resource investment at the leaf level maximized nitrogen allocation to structures
2383 that support whole plant growth.

2384 5.4.1 *Soil nitrogen fertilization has divergent effects on leaf and whole plant*
2385 *acclimation responses to CO₂*

2386 Elevated CO₂ reduced N_{area} , V_{cmax25} , J_{max25} , and stomatal conductance by 29%,
2387 16%, 10%, and 20%, respectively. The larger downregulation of V_{cmax25} than
2388 J_{max25} led to an 8% stimulation in $J_{\text{max25}}:V_{\text{cmax25}}$, while the larger downregulation
2389 of N_{area} than V_{cmax25} resulted in a 21% stimulation in the fraction of leaf nitro-
2390 gen allocated to photosynthesis under elevated CO₂. These acclimation responses
2391 are directionally consistent with previous studies that have investigated or re-
2392 viewed leaf acclimation responses to CO₂ (Drake et al. 1997; Makino et al. 1997;
2393 Ainsworth et al. 2002; Ainsworth and Long 2005; Ainsworth and Rogers 2007;
2394 Smith and Dukes 2013; Smith and Keenan 2020; Poorter et al. 2022), and fol-
2395 low patterns expected from photosynthetic least-cost theory (Wright et al. 2003;
2396 Prentice et al. 2014; Smith et al. 2019; Smith and Keenan 2020). Together, the
2397 stimulation in $J_{\text{max25}}:V_{\text{cmax25}}$ and the fraction of leaf nitrogen allocated to pho-
2398 tosynthesis under elevated CO₂ provide strong support for the idea that leaves
2399 were downregulating V_{cmax25} in response to elevated CO₂ in order to optimally co-
2400 ordinate photosynthesis such that net photosynthesis rates approached becoming

2401 equally co-limited by Rubisco carboxylation and RuBP regeneration (Chen et al.
2402 1993; Maire et al. 2012) while optimizing resource use efficiency.

2403 Increasing fertilization and inoculation induced strong positive effects on
2404 N_{area} , $V_{\text{cmax}25}$, $J_{\text{max}25}$. The general positive response of N_{area} to increasing fertiliza-
2405 tion and in inoculated pots was enhanced under ambient CO₂, which, paired with
2406 the general downregulation of N_{area} under elevated CO₂, resulted in a stronger
2407 downregulation of N_{area} under elevated CO₂ with increasing fertilization and in
2408 inoculated pots. These patterns suggest that N_{area} responses to CO₂ were at least
2409 partially dependent on soil nitrogen fertilization and nitrogen acquisition strat-
2410 egy. However, the general stimulation in the fraction of leaf nitrogen allocated to
2411 Rubisco, bioenergetics, or photosynthesis under elevated CO₂ was not modified
2412 across the fertilization gradient and was only marginally enhanced in inoculated
2413 pots. These patterns suggest that the increased downregulation of N_{area} under
2414 elevated CO₂ with increasing fertilization was not necessarily associated with a
2415 change in relative investment to photosynthetic tissue, providing another line of
2416 evidence suggesting that leaf acclimation responses to CO₂ are decoupled from
2417 changes in soil nitrogen availability.

2418 Leaf acclimation responses to elevated CO₂ corresponded with a 62% and
2419 100% stimulation in total leaf area and total biomass, respectively. The stimula-
2420 tion in total leaf area and total biomass under elevated CO₂ corresponded with
2421 generally larger structural carbon costs to acquire nitrogen, a pattern driven by
2422 a stimulation in belowground carbon biomass and reduction in whole plant ni-
2423 trogen biomass. This result suggests that elevated CO₂ reduces plant nitrogen
2424 uptake efficiency, which does not explain why plants grown under elevated CO₂

2425 generally had higher biomass and total leaf area, unless growth stimulations un-
2426 der elevated CO₂ were driven by reductions in per-tissue nitrogen demand (Dong
2427 et al. 2022). Interestingly, strong negative effects of increasing fertilization on
2428 structural carbon costs to acquire nitrogen, which were generally similar between
2429 CO₂ concentrations, were driven by stronger increases in whole plant nitrogen
2430 biomass than belowground carbon biomass. This response allowed plants to in-
2431 crease nitrogen uptake efficiency with increasing fertilization, which could be the
2432 mechanism that drove the enhanced growth stimulation under elevated CO₂ with
2433 increasing fertilization.

2434 Interestingly, results indicate that the stimulation in total leaf area and
2435 whole plant growth under elevated CO₂ was not modified by inoculation despite
2436 an apparent general negative effect of inoculation on N_{cost} . This response could
2437 have been due to strong negative effect of increasing fertilization on nodulation,
2438 which may have caused the strong increase in the positive effect of elevated CO₂ on
2439 whole plant growth with increasing fertilization to mask any increase in the posi-
2440 tive effect of elevated CO₂ on whole plant growth due to inoculation. Reductions
2441 in nodulation with increasing fertilization are commonly observed patterns that
2442 have been inferred to be a response that allows species optimize nitrogen uptake
2443 efficiency as costs to acquire nitrogen via direct uptake become more similar (Gib-
2444 son and Harper 1985; Rastetter et al. 2001). In this study, pairwise comparisons
2445 indicated strong positive effects of inoculation on total leaf area and total biomass
2446 (158% increase in total leaf area, 119% increase in total biomass) under elevated
2447 CO₂ at 0 ppm N ($p < 0.05$ in both cases), but no observable inoculation effect on
2448 total leaf area or total biomass under elevated CO₂ at 350 ppm N or 630 ppm N

2449 ($p>0.05$ in both cases). While these responses did not generally differ from those
2450 observed under ambient CO₂, they do confirm the hypothesis that positive effects
2451 of inoculation on whole plant growth responses to elevated CO₂ would decrease
2452 with increasing fertilization.

2453 Combined, results reported here suggest that soil nitrogen availability plays
2454 divergent roles in shaping leaf and whole plant acclimation responses to CO₂. Leaf
2455 acclimation responses were generally decoupled from fertilization, while whole
2456 plant acclimation responses relied heavily on an increase in nitrogen uptake ef-
2457 ficiency and consequent reduction in costs of acquiring nitrogen associated with
2458 increasing fertilization. Whole plant responses to CO₂ indicated that fertilization
2459 may play a more important role in determining whole plant acclimation responses
2460 to CO₂ than nitrogen acquisition strategy, although any inoculation effect was
2461 likely masked by the strong reduction in root nodulation with increasing fertil-
2462 ization. These results suggest that plants acclimate to CO₂ in nitrogen-limited
2463 systems by minimizing the number of optimally coordinated leaves, and that
2464 downregulations in leaf nitrogen content under elevated CO₂ are not driven by
2465 changes in soil nitrogen availability as has been previously implied.

2466 5.4.2 *Implications for future model development*

2467 Many terrestrial biosphere models predict photosynthetic capacity through plant
2468 functional group-specific linear regressions between N_{area} and V_{cmax} (Rogers 2014;
2469 Rogers et al. 2017), which assumes that leaf nitrogen-photosynthesis relation-
2470 ships are constant across growing environments. These results build on previ-
2471 ous work suggesting that leaf nitrogen-photosynthesis relationships dynamically
2472 change across growing environments (Luo et al. 2021; Dong et al. 2022), showing

2473 that CO₂ concentration increases the fraction of leaf nitrogen content allocated to
2474 photosynthesis independent of fertilization or acquisition strategy. Additionally,
2475 increasing fertilization strongly decreased the fraction of leaf nitrogen allocated
2476 to photosynthesis, a response that was largely determined by acquisition strategy.
2477 Specifically, reductions in the fraction of leaf nitrogen allocated to photosynthesis
2478 with increasing fertilization were only observed in inoculated pots that had less
2479 finite access to nitrogen, suggesting that constant leaf nitrogen-photosynthesis
2480 relationships may only be apparent in environments where nitrogen is limiting.
2481 Terrestrial biosphere models that parameterize photosynthetic capacity through
2482 linear relationships between N_{area} and V_{cmax} (Rogers 2014; Rogers et al. 2017) may
2483 therefore be overestimating photosynthetic capacity in systems where nitrogen is
2484 not as limiting. Such models are also not capable of detecting stimulations in the
2485 fraction of leaf nitrogen allocated to photosynthesis with increasing CO₂ concen-
2486 tration. The inability of models to predict these responses likely contributes to the
2487 widespread divergence of model simulations under future environmental scenarios
2488 (Friedlingstein et al. 2014; Davies-Barnard et al. 2020), and should therefore be
2489 a target for resolving in future generations of terrestrial biosphere models.

2490 These results demonstrate that optimal resource investment to photosyn-
2491 thetic capacity defines leaf acclimation responses to elevated CO₂, and that these
2492 responses were independent of fertilization or inoculation treatment. Current
2493 model approaches for simulating photosynthetic responses to CO₂ generally invoke
2494 patterns expected from progressive nitrogen limitation, where the downregulation
2495 in N_{area} , and therefore photosynthetic capacity, due to elevated CO₂ is formu-
2496 lated as a function of progressive reductions in soil nitrogen availability. Results

2497 reported here contradict this formulation, suggesting that the leaf acclimation re-
2498 sponse is driven by optimal resource investment to photosynthetic capacity and
2499 is independent of soil resource supply. Optimality models that leverage prin-
2500 ciples from optimal coordination and photosynthetic least-cost theories (Wang
2501 et al. 2017; Stocker et al. 2020; Scott and Smith 2022) are capable of capturing
2502 such acclimation responses to CO₂ (Smith and Keenan 2020), suggesting that the
2503 implementation of these models may improve the simulation of photosynthetic
2504 processes in terrestrial biosphere models under increasing CO₂ concentrations.

2505 5.4.3 *Study limitations and future directions*

2506 There are two study limitations that must be addressed to contextualize patterns
2507 observed in this study. First, restricting the volume of belowground substrate
2508 via a potted experiment does not adequately replicate belowground environments
2509 of natural systems, and therefore may modify effects of soil resource availability
2510 and inoculation on plant nitrogen uptake. This limitation may be particularly
2511 relevant if pot size limits whole plant growth (Poorter et al. 2012). I attempted
2512 to minimize the extent of pot size limitation experienced in the first experimen-
2513 tal chapter while accounting for the expected stimulation in whole plant growth
2514 under elevated CO₂ by using 6-liter pots. Despite attempts to minimize growth
2515 limitation imposed by pot volume, fertilization and CO₂ treatments increased the
2516 biomass: pot volume ratio such that all treatment combinations to exceed 1 g L⁻¹
2517 biomass: pot volume under high fertilization (Table D3; Fig. D2). The 1 g L⁻¹
2518 biomass: pot volume recommendation from Poorter et al. (2012) was designated
2519 to avoid growth limitation imposed by pot volume. However, if pot size limita-

2520 tion indeed limited whole plant growth, then structural carbon costs to acquire
2521 nitrogen, belowground carbon biomass, whole plant nitrogen biomass, and whole
2522 plant biomass should each exhibit strong saturation points with increasing fertil-
2523 ization, which was not observed here. Importantly, leaf acclimation responses to
2524 CO₂ observed in this study are consistent with findings reported in (Smith and
2525 Keenan 2020), who used data from field manipulation experiments that did not
2526 have any belowground space limitation.

2527 Second, this study evaluated leaf and whole plant responses to CO₂ in 7-
2528 week seedlings. Given the long-term scale of the progressive nitrogen limitation
2529 hypothesis, patterns observed here should be validated in longer-term nitrogen
2530 manipulation experiments. Previous work in free air CO₂ enrichment experiments
2531 show some support for patterns expected from the progressive nitrogen limitation
2532 hypothesis (Reich et al. 2006; Norby et al. 2010), although results are not consis-
2533 tent across experimental sites (Finzi et al. 2006; Moore et al. 2006; Liang et al.
2534 2016). I found some support for patterns expected by the progressive nitrogen
2535 limitation hypothesis, namely the increase in plant nitrogen uptake under elevated
2536 CO₂ (Luo et al. 2004), though leaf acclimation responses to CO₂ were strongly
2537 indicative of optimal resource investment to photosynthetic capacity as expected
2538 from photosynthetic least-cost theory (Prentice et al. 2014; Smith et al. 2019;
2539 Smith and Keenan 2020).

2540 5.4.4 *Conclusions*

2541 This study provides strong evidence suggesting that leaf acclimation responses
2542 to elevated CO₂ did not vary with soil nitrogen fertilization or ability to acquire
2543 nitrogen through symbiotic nitrogen fixation. However, whole plant acclimation

2544 responses to CO₂ were dependent on fertilization, where increasing fertilization
2545 increased the positive effect of whole plant growth under elevated CO₂. Results
2546 also indicate that fertilization played a relatively more important role in modify-
2547 ing whole plant responses to CO₂ than inoculation with symbiotic nitrogen-fixing
2548 bacteria, perhaps due to a reduction in nodulation across the fertilization gra-
2549 dient. These patterns strongly support the hypothesis that leaf and whole plant
2550 acclimation responses are driven by optimal resource investment to photosynthetic
2551 capacity, and that leaf acclimation responses to CO₂ were not modified by changes
2552 in soil nitrogen availability. These results build on previous work suggesting that
2553 constant leaf nitrogen-photosynthesis relationships are dynamic and change across
2554 growing environments, calling the current formulation of photosynthetic processes
2555 used in many terrestrial biosphere models into question.

2556

Chapter 6

2557

Conclusions

2558 The experiments included in this dissertation test mechanisms that drive patterns
2559 expected from photosynthetic least-cost theory across various edaphic and climatic
2560 gradients. Specifically, I investigate environmental drivers of carbon costs to ac-
2561 quire nitrogen, tradeoffs between nitrogen and water use, and plant acclimation
2562 responses to CO₂. These experiments provide important empirical data needed to
2563 test assumptions made in optimality models that leverage photosynthetic least-
2564 cost frameworks, and are among the first manipulative experiments to show sup-
2565 port for patterns expected from theory. Below, I summarize main findings of each
2566 chapter, synthesize common patterns observed across experiments, and conclude
2567 with a few study ideas that I think will help refine our understanding of plant
2568 nutrient acquisition and allocation responses to environmental change leveraging
2569 patterns predicted by photosynthetic least-cost theory.

2570 In the first experimental chapter, I quantified carbon costs to acquire ni-
2571 trogen in a species capable of forming associations with symbiotic nitrogen-fixing
2572 bacteria (*Glycine max*) and a species not capable of forming such associations
2573 (*Gossypium hirsutum*) grown under four soil nitrogen fertilization treatments and
2574 four light availability treatments in a full factorial greenhouse experiment. Sup-
2575 porting hypotheses, increasing light availability increased carbon costs to acquire
2576 nitrogen in both species due to a larger increase in belowground carbon biomass
2577 than whole plant nitrogen biomass. In further support of hypotheses, increasing
2578 fertilization decreased carbon costs to acquire nitrogen due to a larger increase in

2579 whole plant nitrogen biomass than belowground carbon biomass. Root nodulation
2580 data indicated that *G. max* shifted relative carbon allocation from nitrogen fixa-
2581 tion to direct uptake with increasing fertilization, which may explain the reduced
2582 responsiveness of *G. max* carbon costs to acquire nitrogen across the fertilization
2583 gradient.

2584 Despite evidence that reductions in the response of *G. max* carbon costs
2585 to acquire nitrogen to increasing fertilization may have been driven by shifts away
2586 from nitrogen fixation with increasing fertilization, I urge caution in assigning
2587 causality to the differential response of carbon costs to acquire nitrogen between
2588 species. This is because *G. max* and *G. hirsutum* are not phylogenetically related
2589 and have different life histories. Differences in life history between the two species
2590 limit my ability to assess whether reductions in the negative effect of increasing
2591 fertilization on carbon costs to acquire nitrogen in *G. max* were driven by shifts
2592 to direct uptake with increasing fertilization. However, these patterns were later
2593 confirmed in the fourth experimental chapter, where similar weaker negative ef-
2594 fects of increasing fertilization on carbon costs to acquire nitrogen were observed
2595 in *G. max* that were inoculated with symbiotic nitrogen-fixing bacteria compared
2596 to *G. max* that were left uninoculated across a similar soil nitrogen fertilization
2597 gradient.

2598 In the second experimental chapter, I assessed whether changes in soil
2599 nitrogen availability or soil pH drove changes in nitrogen-water use tradeoffs pre-
2600 dicted by photosynthetic least-cost theory. I measured leaf traits of mature upper
2601 canopy deciduous trees growing in a nine-year nitrogen-by-sulfur field manipula-
2602 tion experiment, where experimental sulfur additions were added with intent to

2603 acidify plots. Following patterns expected from the theory, increasing soil nitrogen
2604 availability was associated with increased leaf nitrogen content, but not net photo-
2605 synthesis, resulting in an increase in photosynthetic nitrogen use efficiency. In
2606 further support of theory, increasing soil nitrogen availability exhibited slight, but
2607 nonsignificant, decreases in leaf $C_i:C_a$ and increases in measures of photosynthetic
2608 capacity. Perhaps the strongest evidence for the theory was a strong negative
2609 relationship between leaf nitrogen content and leaf $C_i:C_a$, of which increased with
2610 increasing soil nitrogen availability through a stronger increase in leaf nitrogen
2611 content than leaf $C_i:C_a$.

2612 I found no effect of soil pH on nitrogen-water use tradeoffs aside from a
2613 marginal reduction in net photosynthesis rates that marginally reduced photosyn-
2614hetic nitrogen use efficiency with increasing soil pH. Directionally, reductions in
2615 photosynthetic nitrogen use efficiency with increasing soil pH were expected per
2616 theory; however, this response was driven by no change in leaf nitrogen content
2617 and a reduction in net photosynthesis. Theory predicts that these tradeoffs should
2618 be driven by no change in net photosynthesis and an increase in leaf nitrogen con-
2619tent. The general null leaf response to changing soil pH may have been due to
2620 experimental treatments directly increased soil nitrogen availability and affected
2621 soil pH in opposite patterns, suggesting that soil nitrogen availability may be more
2622 important in dictating nitrogen-water use tradeoffs than soil pH per se.

2623 In the third experimental chapter, I quantified variance in leaf nitrogen
2624 content across a precipitation and soil resource availability gradient in Texan
2625 grasslands. Specifically, I measured area-based leaf nitrogen content, components
2626 of area-based leaf nitrogen content (leaf mass per unit leaf area, leaf nitrogen per

2627 unit dry biomass), leaf $C_i:C_a$, and the unit cost of acquiring nitrogen relative to
2628 water in 520 individuals comprising 57 species. I found that variance in area-
2629 based leaf nitrogen content was positively associated with increasing soil nitrogen
2630 availability, soil moisture, vapor pressure deficit, and was negatively related to
2631 increasing leaf $C_i:C_a$. Following patterns expected from theory, a path analysis
2632 revealed that the positive soil nitrogen-leaf nitrogen relationship was driven by a
2633 positive relationship between soil nitrogen availability and the unit cost of acquir-
2634 ing and using nitrogen relative to water, a positive relationship between the unit
2635 cost of acquiring and using nitrogen relative to water, and negative relationship
2636 between leaf $C_i:C_a$ and leaf mass per unit leaf area. Interestingly, there was no
2637 effect of $C_i:C_a$ on leaf nitrogen content per unit dry biomass, indicating that vari-
2638 ance in area-based leaf nitrogen content across the environmental gradient was
2639 driven by a change in leaf morphology and not leaf chemistry.

2640 In the fourth experimental chapter, I quantified leaf and whole plant accli-
2641 mation responses in *G. max* grown under two atmospheric CO₂ levels, with and
2642 without inoculation with *Bradyrhizobium japonicum*, and across nine nitrogen fer-
2643 tilization treatments in a full factorial growth chamber experiment. I found strong
2644 evidence that leaf nitrogen content, V_{cmax} , and J_{max} were each downregulated un-
2645 der elevated CO₂. A stronger downregulation in V_{cmax} than J_{max} and stronger
2646 downregulation in leaf nitrogen content than V_{cmax} or J_{max} provided strong sup-
2647 port suggesting that leaves were acclimating to elevated CO₂ by optimizing leaf
2648 photosynthetic resource use efficiency to achieve optimal coordination. In striking
2649 support of my hypotheses, I find strong evidence suggesting that leaf acclimation
2650 responses to elevated CO₂ were decoupled from soil nitrogen fertilization and in-

2651 oculation treatment, despite apparent strong increases in leaf nitrogen content,
2652 V_{cmax} , and J_{max} with increasing fertilization and in inoculated pots. These find-
2653 ings contrast the current formulation of photosynthetic processes in terrestrial
2654 biosphere models, where many models simulate downregulations in leaf nitrogen
2655 content under elevated CO₂ as a function of progressive nitrogen limitation.

2656 There are currently two iterations of optimality models that employ the
2657 use of patterns expected from photosynthetic least-cost theory, one for C₃ species
2658 (Wang et al. 2017; Smith et al. 2019; Stocker et al. 2020) and one more recently
2659 developed for C₄ species (Scott and Smith 2022). In both model variants, costs
2660 to acquire and use nitrogen relative to water are held constant using a global
2661 dataset of δ¹³C (Cornwell et al. 2018). Throughout experiments, I show strong
2662 evidence suggesting that costs to acquire and use nitrogen are dynamic and vary
2663 predictably across environmental gradients, and that changes in these costs scale
2664 to alter leaf nitrogen-water use tradeoffs and acclimation responses to changing
2665 environments in ways predicted through photosynthetic least-cost theory. Thus,
2666 while optimality model simulations show good agreement with measured data
2667 (Smith et al. 2019; Stocker et al. 2020), such models may not be capturing an
2668 important source of variability in leaf nitrogen-water use tradeoffs by holding costs
2669 of resource use constant across environmental gradients.

2670 First principles of photosynthetic least-cost theory suggest that, in a given
2671 environment, plants optimize photosynthesis rates by sacrificing inefficient use of
2672 a relatively more abundant (and less costly to acquire) resource for more efficient
2673 use of a relatively less abundant (and more costly to acquire) resource. Through-
2674 out experimental chapters, I show strong support for these patterns across ex-

2675 periments, where increasing soil nitrogen fertilization generally decreased the cost
2676 of acquiring nitrogen relative to water, a pattern that scaled to influence leaf
2677 nitrogen-water use tradeoffs. I did not find evidence to suggest that soil moisture
2678 influenced nitrogen-water use tradeoffs, though this was due to strong covariation
2679 between soil moisture and soil nitrogen availability. Overall, findings across exper-
2680 iments provide empirical validation of photosynthetic least-cost theory needed to
2681 further develop optimality models and eventually implement such models in ter-
2682 restrial biosphere model products. Many terrestrial biosphere model products do
2683 not include robust frameworks for simulating acclimation responses to changing
2684 environmental conditions, and empirical findings shown here provide some support
2685 that optimality models that leverage photosynthetic least-cost theory predictions
2686 may improve the ability of terrestrial biosphere models to accurately simulate
2687 photosynthetic processes.

2688 Many terrestrial biosphere models predict photosynthetic capacity through
2689 plant functional group-specific linear regressions between area-based leaf nitrogen
2690 content and V_{cmax} (Rogers 2014; Rogers et al. 2017), which assumes that leaf
2691 nitrogen-photosynthesis relationships are constant across growing environments.
2692 I found constant leaf nitrogen-photosynthesis relationships with increasing soil ni-
2693 trogen availability in the nitrogen-by-sulfur field manipulation experiment. How-
2694 ever, results from the CO₂-by-nitrogen-by-inoculation manipulation experiment
2695 indicated that leaf nitrogen-photosynthesis responses to soil nitrogen availability
2696 were dependent on whether nitrogen was limiting. Further investigation regard-
2697 ing the effect of soil nitrogen availability in modifying leaf nitrogen-photosynthesis
2698 relationships is warranted to better understand the generality of leaf nitrogen pho-

2699 tosynthesis relationships across environmental gradients. However, findings from
2700 these experiments suggest that representing photosynthetic processes through pos-
2701 itive relationships between soil nitrogen availability, leaf nitrogen, and photosyn-
2702 thetic capacity are likely contributing to erroneous errors in model simulations and
2703 may explain the high degree of divergence in simulated processes across terrestrial
2704 biosphere models (Friedlingstein et al. 2014; Davies-Barnard et al. 2020).

2705 The experiments included in this dissertation have provided a strong foun-
2706 dation for me to continue growing as a plant physiological ecologist. I envision
2707 five primary avenues for future research that build on the work presented here,
2708 which are briefly summarized below:

- 2709** 1. Manipulative and environmental gradient experiments included here were
2710 designed to provide empirical data needed to test photosynthetic least-cost
2711 theory assumptions. While these results show promising patterns for pat-
2712 terns expected from photosynthetic least-cost theory, they do not necessarily
2713 address whether these patterns follow those simulated by optimality models
2714 that leverage photosynthetic least-cost principles. Thus, a clear future di-
2715 rection of these experiments would be to conduct model-data comparisons
2716 using data collected here (or similar experiments) to compare against opti-
2717 mality model simulations.

- 2718** 2. Experiments included here explicitly quantify effects of symbiotic nitrogen
2719 fixation on carbon costs to acquire nitrogen, nitrogen-water use tradeoffs,
2720 and leaf nitrogen-photosynthesis relationships. However, carbon costs to ac-
2721 quire nitrogen also vary in species that associate with different mycorrhizal
2722 types (Brzostek et al. 2014; Terrer et al. 2018), and dominant mycorrhizal

2723 type in an ecosystem has been shown to determine net biogeochemical cycle
2724 dynamics in deciduous forests of the northeastern United States (Phillips
2725 et al. 2013). Thus, future work should consider conducting similar experi-
2726 ments while manipulating mycorrhizal association to better understand how
2727 microbial symbioses modify leaf and whole plant acclimation responses to
2728 changing environments.

2729 3. Recent work indicates a high degree of variance in symbiotic nitrogen fixa-
2730 tion rates across terrestrial biosphere models (Meyerholt et al. 2016; Davies-
2731 Barnard et al. 2020), perhaps due to nitrogen fixation rates that are im-
2732 plemented across terrestrial biosphere models as a function of temperature
2733 (Houlton et al. 2008). While energetic costs of nitrogen fixation are de-
2734 pendent on temperature, I show that structural carbon costs to acquire
2735 nitrogen via symbiotic nitrogen fixation are driven by factors that influence
2736 demand to acquire nitrogen (i.e. CO₂, light) and are modified by soil ni-
2737 tragen supply. The light-by-nitrogen greenhouse experiment was published
2738 in *Journal of Experimental Botany*, and a reviewer encouraged future work
2739 to include a model-data comparison comparing structural carbon costs to
2740 acquire nitrogen measured in the experiment to carbon costs to acquire ni-
2741 tragen simulated by the FUN biogeochemical model (Fisher et al. 2010;
2742 Brzostek et al. 2014; Allen et al. 2020). Conveniently, FUN calculates car-
2743 bon costs to acquire nitrogen following the same calculation used in the first
2744 and fourth experimental chapter. Conducting such a model-data comparison
2745 would be a useful step toward identifying biases in the FUN biogeochemi-
2746 cal model, which is currently coupled to several terrestrial biosphere models

2747 (Clark et al. 2011; Shi et al. 2016; Lawrence et al. 2019; Davies-Barnard
2748 et al. 2020).

2749 4. Carbon costs to acquire nitrogen relative to water were quantified at the
2750 leaf level as a function of $\delta^{13}\text{C}$ and vapor pressure deficit, while structural
2751 carbon costs to acquire nitrogen were quantified at the whole plant level
2752 as the ratio of belowground carbon allocation per unit whole plant nitro-
2753 gen biomass. As increasing soil nitrogen availability decreases both leaf and
2754 whole plant estimates of costs to acquire and use nitrogen, one might expect
2755 leaf and whole plant carbon cost to acquire nitrogen estimates to covary. Fu-
2756 ture work should consider investigating if leaf and whole plant estimates of
2757 carbon costs to acquire nitrogen covary and evaluate whether environmental
2758 conditions (or species acquisition strategy) modifies any of this possible co-
2759 variance. Strong covariance between leaf and whole plant costs of nitrogen
2760 acquisition could be a possible avenue to implement frameworks for allowing
2761 costs of nitrogen acquisition to vary in optimality models, as the FUN model
2762 calculates carbon costs of nitrogen acquisition at the whole plant level.

2763 5. While experiments included here target effects of soil nitrogen availability
2764 on carbon costs to acquire nitrogen and associated leaf nitrogen-water use
2765 tradeoffs, photosynthetic least-cost theory predicts that plants acclimate
2766 their photosynthetic processes by minimizing the summed cost of nutrient
2767 (not just nitrogen) and water use. Therefore, the theory would predict
2768 similar leaf acclimation responses across soil phosphorus or other nutrient
2769 availability gradients. Recent iterations of the FUN biogeochemical cycle
2770 includes a framework for determining the carbon and nitrogen cost of ac-

2771 quiring and using phosphorus, which similarly varies in species with different
2772 nutrient acquisition strategies (Allen et al. 2020). The implementation of
2773 this model in a terrestrial biosphere model (E3SM) was also recently shown
2774 to improve model performance of ecosystem nutrient limitation (Braghieri
2775 et al. 2022). As nitrogen and phosphorus commonly co-limit leaf photo-
2776 synthesis and primary productivity, extending experiments reported here to
2777 investigate carbon and nitrogen costs of phosphorus use, and whether these
2778 patterns scale to leaf nutrient-water use tradeoffs would be a useful next
2779 step in understanding extensions and limitations of photosynthetic least-
2780 cost theory.

2781 The experiments included in this dissertation and the proposed experiments sum-
2782 marized above provide a snapshot view of the things that I have learned through-
2783 out my time as a graduate student. I am excited to continue learning and growing
2784 as a plant ecophysiologicalist, ecologist, and scientist, and look forward to continuing
2785 along my journey of investigating nutrient acquisition and allocation responses to
2786 global change.

2787

References

- 2788** Abrams, M. D. and S. A. Mostoller (1995). Gas exchange, leaf structure and
2789 nitrogen in contrasting successional tree species growing in open and under-
2790 story sites during a drought. *Tree Physiology* 15(6), 361–370.
- 2791** Adams, M. A., T. L. Turnbull, J. I. Sprent, and N. Buchmann (2016). Legumes
2792 are different: Leaf nitrogen, photosynthesis, and water use efficiency. *Pro-
2793 ceedings of the National Academy of Sciences of the United States of Amer-
2794 ica* 113(15), 4098–4103.
- 2795** Ainsworth, E. A., P. A. Davey, C. J. Bernacchi, O. C. Dermody, E. A. Heaton,
2796 D. J. Moore, P. B. Morgan, S. L. Naidu, H. S. Y. Ra, X. G. Zhu, P. S. Curtis,
2797 and S. P. Long (2002). A meta-analysis of elevated [CO₂] effects on soybean
2798 (*Glycine max*) physiology, growth and yield. *Global Change Biology* 8(8),
2799 695–709.
- 2800** Ainsworth, E. A. and S. P. Long (2005). What have we learned from 15 years of
2801 free-air CO₂ enrichment (FACE)? A meta-analytic review of the responses
2802 of photosynthesis, canopy properties and plant production to rising CO₂.
2803 *New Phytologist* 165(2), 351–372.
- 2804** Ainsworth, E. A. and A. Rogers (2007). The response of photosynthesis and
2805 stomatal conductance to rising [CO₂]: mechanisms and environmental in-
2806 teractions. *Plant, Cell and Environment* 30(3), 258–270.
- 2807** Allen, K., J. B. Fisher, R. P. Phillips, J. S. Powers, and E. R. Brzostek (2020).
2808 Modeling the carbon cost of plant nitrogen and phosphorus uptake across
2809 temperate and tropical forests. *Frontiers in Forests and Global Change* 3,

- 2810 1–12.
- 2811 Allison, S. D., C. I. Czimczik, and K. K. Treseder (2008). Microbial activity
2812 and soil respiration under nitrogen addition in Alaskan boreal forest. *Global
2813 Change Biology* 14(5), 1156–1168.
- 2814 Andersen, M. K., H. Hauggaard-Nielsen, P. Ambus, and E. S. Jensen (2005).
2815 Biomass production, symbiotic nitrogen fixation and inorganic N use in dual
2816 and tri-component annual intercrops. *Plant and Soil* 266(1-2), 273–287.
- 2817 Andrews, M., E. K. James, J. I. Sprent, R. M. Boddey, E. Gross, and F. B. dos
2818 Reis (2011). Nitrogen fixation in legumes and actinorhizal plants in natural
2819 ecosystems: Values obtained using ^{15}N natural abundance. *Plant Ecology
2820 and Diversity* 4(2-3), 117–130.
- 2821 Arndal, M. F., A. Tolver, K. S. Larsen, C. Beier, and I. K. Schmidt (2018). Fine
2822 root growth and vertical distribution in response to elevated CO₂, warming
2823 and drought in a mixed heathland–grassland. *Ecosystems* 21(1), 15–30.
- 2824 Arnone, J. A. (1997). Indices of plant N availability in an alpine grassland under
2825 elevated atmospheric CO₂. *Plant and Soil* 190(1), 61–66.
- 2826 Arora, V. K., A. Katavouta, R. G. Williams, C. D. Jones, V. Brovkin,
2827 P. Friedlingstein, J. Schwinger, L. Bopp, O. Boucher, P. Cadule, M. A.
2828 Chamberlain, J. R. Christian, C. Delire, R. A. Fisher, T. Hajima, T. Ilyina,
2829 E. Joetzjer, M. Kawamiya, C. D. Koven, J. P. Krasting, R. M. Law, D. M.
2830 Lawrence, A. Lenton, K. Lindsay, J. Pongratz, T. Raddatz, R. Séférian,
2831 K. Tachiiri, J. F. Tjiputra, A. Wiltshire, T. Wu, and T. Ziehn (2020).
2832 Carbon-concentration and carbon-climate feedbacks in CMIP6 models and
2833 their comparison to CMIP5 models. *Biogeosciences* 17(16), 4173–4222.

- 2834 Bae, K., T. J. Fahey, R. D. Yanai, and M. Fisk (2015). Soil nitrogen availability affects belowground carbon allocation and soil respiration in northern
2835 hardwood forests of New Hampshire. *Ecosystems* 18(7), 1179–1191.
- 2836
- 2837 Barber, S. A. (1962). A diffusion and mass-flow concept of soil nutrient availability. *Soil Science* 93(1), 39–49.
- 2838
- 2839 Barnes, J. D., L. Balaguer, E. Manrique, S. Elvira, and A. W. Davison (1992).
2840 A reappraisal of the use of DMSO for the extraction and determination
2841 of chlorophylls a and b in lichens and higher plants. *Environmental and
2842 Experimental Botany* 32(2), 85–100.
- 2843 Bates, D., M. Mächler, B. Bolker, and S. Walker (2015). Fitting linear mixed-
2844 effects models using lme4. *Journal of Statistical Software* 67(1), 1–48.
- 2845 Beaudette, D., J. Skovlin, S. Roeker, and A. Brown (2022). soilDB: Soil
2846 Database Interface.
- 2847 Bengtson, P., J. Barker, and S. J. Grayston (2012). Evidence of a strong cou-
2848 pling between root exudation, C and N availability, and stimulated SOM
2849 decomposition caused by rhizosphere priming effects. *Ecology and Evolu-
2850 tion* 2(8), 1843–1852.
- 2851 Bernacchi, C. J., E. L. Singsaas, C. Pimentel, A. R. Portis, and S. P. Long
2852 (2001). Improved temperature response functions for models of Rubisco-
2853 limited photosynthesis. *Plant, Cell and Environment* 24(2), 253–259.
- 2854 Bialic-Murphy, L., N. G. Smith, P. Voothuluru, R. M. McElderry, M. D.
2855 Roche, S. T. Cassidy, S. N. Kivlin, and S. Kalisz (2021). Invasion-induced
2856 root–fungal disruptions alter plant water and nitrogen economies. *Ecology*

- 2857** *Letters* 24(6), 1145–1156.
- 2858** Bloom, A. J., F. S. Chapin, and H. A. Mooney (1985). Resource limitation
2859 in plants - an economic analogy. *Annual Review of Ecology and Systemat-*
2860 *ics* 16(1), 363–392.
- 2861** Bloomfield, K. J., B. D. Stocker, T. F. Keenan, and I. C. Prentice (2023).
2862 Environmental controls on the light use efficiency of terrestrial gross primary
2863 production. *Global Change Biology* 29(4), 0–2.
- 2864** Bonan, G. B., M. D. Hartman, W. J. Parton, and W. R. Wieder (2013). Eval-
2865 uating litter decomposition in earth system models with long-term litter
2866 bag experiments: an example using the Community Land Model version 4
2867 (CLM4). *Global Change Biology* 19(3), 957–974.
- 2868** Bonan, G. B., P. J. Lawrence, K. W. Oleson, S. Levis, M. Jung, M. Reich-
2869 stein, D. M. Lawrence, and S. C. Swenson (2011). Improving canopy pro-
2870 cesses in the Community Land Model version 4 (CLM4) using global flux
2871 fields empirically inferred from FLUXNET data. *Journal of Geophysical Re-*
2872 *search* 116(G2), G02014.
- 2873** Booth, B. B. B., C. D. Jones, M. Collins, I. J. Totterdell, P. M. Cox, S. Sitch,
2874 C. Huntingford, R. A. Betts, G. R. Harris, and J. Lloyd (2012). High sen-
2875 sitivity of future global warming to land carbon cycle processes. *Environ-*
2876 *mental Research Letters* 7(2), 024002.
- 2877** Borer, E. T., W. S. Harpole, P. B. Adler, E. M. Lind, J. L. Orrock, E. W.
2878 Seabloom, and M. D. Smith (2014). Finding generality in ecology: A model
2879 for globally distributed experiments. *Methods in Ecology and Evolution* 5(1),
2880 65–73.

- 2881** Braghieri, R. K., J. B. Fisher, K. Allen, E. Brzostek, M. Shi, X. Yang, D. M.
- 2882** Ricciuto, R. A. Fisher, Q. Zhu, and R. P. Phillips (2022). Modeling global
- 2883** carbon costs of plant nitrogen and phosphorus acquisition. *Journal of Ad-*
- 2884** *vances in Modeling Earth Systems* 14(8), 1–23.
- 2885** Brix, H. (1971). Effects of nitrogen fertilization on photosynthesis and respi-
- 2886** ration in Douglas-fir. *Forest Science* 17(4), 407–414.
- 2887** Brzostek, E. R., J. B. Fisher, and R. P. Phillips (2014). Modeling the carbon
- 2888** cost of plant nitrogen acquisition: Mycorrhizal trade-offs and multipath
- 2889** resistance uptake improve predictions of retranslocation. *Journal of Geo-*
- 2890** *physical Research: Biogeosciences* 119, 1684–1697.
- 2891** Bubier, J. L., R. Smith, S. Juutinen, T. R. Moore, R. Minocha, S. Long, and
- 2892** S. Minocha (2011). Effects of nutrient addition on leaf chemistry, morphol-
- 2893** ogy, and photosynthetic capacity of three bog shrubs. *Oecologia* 167(2),
- 2894** 355–368.
- 2895** Cernusak, L. A., N. Ubierna, K. Winter, J. A. M. Holtum, J. D. Marshall, and
- 2896** G. D. Farquhar (2013). Environmental and physiological determinants of
- 2897** carbon isotope discrimination in terrestrial plants. *New Phytologist* 200(4),
- 2898** 950–965.
- 2899** Chen, J.-L., J. F. Reynolds, P. C. Harley, and J. D. Tenhunen (1993). Coor-
- 2900** dination theory of leaf nitrogen distribution in a canopy. *Oecologia* 93(1),
- 2901** 63–69.
- 2902** Clark, D. B., L. M. Mercado, S. Sitch, C. D. Jones, N. Gedney, M. J. Best,
- 2903** M. Pryor, G. G. Rooney, R. L. H. Essery, E. Blyth, O. Boucher, R. J.
- 2904** Harding, C. Huntingford, and P. M. Cox (2011). The Joint UK Land Envi-

- 2905 ronment Simulator (JULES), model description. Part 2: Carbon fluxes and
2906 vegetation dynamics. *Geoscientific Model Development* 4(3), 701–722.
- 2907 Cornwell, W. K., J. H. C. Cornelissen, K. Amatangelo, E. Dorrepaal, V. T.
2908 Eviner, O. Godoy, S. E. Hobbie, B. Hoorens, H. Kurokawa, N. Pérez-
2909 Harguindeguy, H. M. Quested, L. S. Santiago, D. A. Wardle, I. J. Wright,
2910 R. Aerts, S. D. Allison, P. van Bodegom, V. Brovkin, A. Chatain, T. V.
2911 Callaghan, S. Díaz, E. Garnier, D. E. Gurvich, E. Kazakou, J. A. Klein,
2912 J. Read, P. B. Reich, N. A. Soudzilovskaia, M. V. Vaieretti, and M. Westoby
2913 (2008). Plant species traits are the predominant control on litter decompo-
2914 sition rates within biomes worldwide. *Ecology Letters* 11(10), 1065–1071.
- 2915 Cornwell, W. K., I. J. Wright, J. Turner, V. Maire, M. M. Barbour, L. A.
2916 Cernusak, T. E. Dawson, D. S. Ellsworth, G. D. Farquhar, H. Griffiths,
2917 C. Keitel, A. Knohl, P. B. Reich, D. G. Williams, R. Bhaskar, J. H. C. Cor-
2918 nelissen, A. Richards, S. Schmidt, F. Valladares, C. Körner, E.-D. Schulze,
2919 N. Buchmann, and L. S. Santiago (2018). Climate and soils together regulate
2920 photosynthetic carbon isotope discrimination within C₃ plants worldwide.
2921 *Global Ecology and Biogeography* 27(9), 1056–1067.
- 2922 Cramer, W. and I. C. Prentice (1988). Simulation of regional soil moisture
2923 deficits on a European scale. *Norsk Geografisk Tidsskrift - Norwegian Jour-*
2924 *nal of Geography* 42(2-3), 149–151.
- 2925 Curtis, P. S. (1996). A meta-analysis of leaf gas exchange and nitrogen in trees
2926 grown under elevated carbon dioxide. *Plant, Cell and Environment* 19(2),
2927 127–137.
- 2928 Daly, C., M. Halbleib, J. I. Smith, W. P. Gibson, M. K. Doggett, G. H. Taylor,

- 2929 J. Curtis, and P. P. Pasteris (2008). Physiographically sensitive mapping
2930 of climatological temperature and precipitation across the conterminous
2931 United States. *International Journal of Climatology* 28(15), 2031–2064.
- 2932 Davies-Barnard, T., J. Meyerholt, S. Zaehle, P. Friedlingstein, V. Brovkin,
2933 Y. Fan, R. A. Fisher, C. D. Jones, H. Lee, D. Peano, B. Smith, D. Wårlind,
2934 and A. J. Wiltshire (2020). Nitrogen cycling in CMIP6 land surface models:
2935 progress and limitations. *Biogeosciences* 17(20), 5129–5148.
- 2936 Davis, T. W., I. C. Prentice, B. D. Stocker, R. T. Thomas, R. J. Whitley,
2937 H. Wang, B. J. Evans, A. V. Gallego-Sala, M. T. Sykes, and W. Cramer
2938 (2017). Simple process-led algorithms for simulating habitats (SPLASH
2939 v.1.0): robust indices of radiation, evapotranspiration and plant-available
2940 moisture. *Geoscientific Model Development* 10, 689–708.
- 2941 Delaire, M., E. Frak, M. Sigogne, B. Adam, F. Beaujard, and X. Le Roux
2942 (2005). Sudden increase in atmospheric CO₂ concentration reveals strong
2943 coupling between shoot carbon uptake and root nutrient uptake in young
2944 walnut trees. *Tree Physiology* 25(2), 229–235.
- 2945 Doane, T. A. and W. R. Horwáth (2003). Spectrophotometric determination of
2946 nitrate with a single reagent. *Analytical Letters* 36(12), 2713–2722.
- 2947 Dong, N., I. C. Prentice, B. J. Evans, S. Caddy-Retalic, A. J. Lowe, and I. J.
2948 Wright (2017). Leaf nitrogen from first principles: field evidence for adaptive
2949 variation with climate. *Biogeosciences* 14(2), 481–495.
- 2950 Dong, N., I. C. Prentice, I. J. Wright, B. J. Evans, H. F. Togashi, S. Caddy-
2951 Retalic, F. A. McInerney, B. Sparrow, E. Leitch, and A. J. Lowe (2020).
2952 Components of leaf-trait variation along environmental gradients. *New Phy-*

- 2953** *tologist* 228(1), 82–94.
- 2954** Dong, N., I. C. Prentice, I. J. Wright, H. Wang, O. K. Atkin, K. J. Bloomfield,
- 2955** T. F. Domingues, S. M. Gleason, V. Maire, Y. Onoda, H. Poorter, and N. G.
- 2956** Smith (2022). Leaf nitrogen from the perspective of optimal plant function.
- 2957** *Journal of Ecology* 110(11), 2585–2602.
- 2958** Dong, N., I. J. Wright, J. M. Chen, X. Luo, H. Wang, T. F. Keenan, N. G.
- 2959** Smith, and I. C. Prentice (2022). Rising CO₂ and warming reduce global
- 2960** canopy demand for nitrogen. *New Phytologist* 235(5), 1692–1700.
- 2961** Dovrat, G., H. Bakhshian, T. Masci, and E. Sheffer (2020). The nitrogen eco-
- 2962** nomic spectrum of legume stoichiometry and fixation strategy. *New Phytol-*
- 2963** *ogist* 227(2), 365–375.
- 2964** Dovrat, G., T. Masci, H. Bakhshian, E. Mayzlish Gati, S. Golan, and E. Shef-
- 2965** fer (2018). Drought-adapted plants dramatically downregulate dinitrogen
- 2966** fixation: Evidences from Mediterranean legume shrubs. *Journal of Ecol-*
- 2967** *ogy* 106(4), 1534–1544.
- 2968** Drake, B. G., M. A. Gonzàlez-Meler, and S. P. Long (1997). More efficient
- 2969** plants: a consequence of rising atmospheric CO₂? *Annual Review of Plant*
- 2970** *Biology* 48, 609–639.
- 2971** Duursma, R. A. (2015). Plantecophys - An R package for analyzing and mod-
- 2972** elling leaf gas exchange data. *PLOS ONE* 10(11), e0143346.
- 2973** Eastman, B. A., M. B. Adams, E. R. Brzostek, M. B. Burnham, J. E. Carrara,
- 2974** C. Kelly, B. E. McNeil, C. A. Walter, and W. T. Peterjohn (2021). Altered
- 2975** plant carbon partitioning enhanced forest ecosystem carbon storage after 25

- 2976 years of nitrogen additions. *New Phytologist* 230(4), 1435–1448.
- 2977 Ellsworth, D. S. and P. B. Reich (1996). Photosynthesis and leaf nitrogen in five
2978 Amazonian tree species during early secondary succession. *Ecology* 77(2),
2979 581–594.
- 2980 Espelta, J. M., P. Cortés, M. Mangirón, and J. Retana (2005). Differences
2981 in biomass partitioning, leaf nitrogen content, and water use efficiency δ^{13}
2982 result in similar performance of seedlings of two Mediterranean oaks with
2983 contrasting leaf habit. *Ecoscience* 12(4), 447–454.
- 2984 Evans, J. R. (1989). Photosynthesis and nitrogen relationships in leaves of C₃
2985 plants. *Oecologia* 78(1), 9–19.
- 2986 Evans, J. R. and V. C. Clarke (2019). The nitrogen cost of photosynthesis.
2987 *Journal of Experimental Botany* 70(1), 7–15.
- 2988 Evans, J. R. and H. Poorter (2001). Photosynthetic acclimation of plants to
2989 growth irradiance: the relative importance of specific leaf area and nitrogen
2990 partitioning in maximizing carbon gain. *Plant, Cell and Environment* 24(8),
2991 755–767.
- 2992 Evans, J. R. and J. R. Seemann (1989). The allocation of protein nitrogen in
2993 the photosynthetic apparatus: costs, consequences, and control. *Photosyn-*
2994 *thesis* 8, 183–205.
- 2995 Exbrayat, J.-F., A. A. Bloom, P. Falloon, A. Ito, T. L. Smallman, and
2996 M. Williams (2018). Reliability ensemble averaging of 21st century projec-
2997 tions of terrestrial net primary productivity reduces global and regional
2998 uncertainties. *Earth System Dynamics* 9(1), 153–165.

- 2999** Farquhar, G. D., J. R. Ehleringer, and K. T. Hubick (1989). Carbon isotope
3000 discrimination and photosynthesis. *Annual Review of Plant Physiology and*
3001 *Plant Molecular Biology* 40(1), 503–537.
- 3002** Farquhar, G. D. and T. D. Sharkey (1982). Stomatal conductance and photo-
3003 synthesis. *Annual Review of Plant Physiology* 33(1), 317–345.
- 3004** Farquhar, G. D., S. von Caemmerer, and J. A. Berry (1980). A biochemical
3005 model of photosynthetic CO₂ assimilation in leaves of C₃ species.
3006 *Planta* 149(1), 78–90.
- 3007** Fay, P. A., S. M. Prober, W. S. Harpole, J. M. H. Knops, J. D. Bakker, E. T.
3008 Borer, E. M. Lind, A. S. MacDougall, E. W. Seabloom, P. D. Wragg, P. B.
3009 Adler, D. M. Blumenthal, Y. M. Buckley, C. Chu, E. E. Cleland, S. L.
3010 Collins, K. F. Davies, G. Du, X. Feng, J. Firn, D. S. Gruner, N. Hagenah,
3011 Y. Hautier, R. W. Heckman, V. L. Jin, K. P. Kirkman, J. A. Klein, L. M.
3012 Ladwig, Q. Li, R. L. McCulley, B. A. Melbourne, C. E. Mitchell, J. L. Moore,
3013 J. W. Morgan, A. C. Risch, M. Schütz, C. J. Stevens, D. A. Wedin, and
3014 L. H. Yang (2015). Grassland productivity limited by multiple nutrients.
3015 *Nature Plants* 1(7), 15080.
- 3016** Feng, X. (1999). Trends in intrinsic water-use efficiency of natural trees for the
3017 past 100-200 years: A response to atmospheric CO₂ concentration. *Geochim-
ica et Cosmochimica Acta* 63(13-14), 1891–1903.
- 3019** Field, C. B. and H. A. Mooney (1986). The photosynthesis-nitrogen relationship
3020 in wild plants. In T. J. Givnish (Ed.), *On the Economy of Plant Form and
Function*, pp. 25–55. Cambridge: Cambridge University Press.
- 3022** Finzi, A. C., D. J. P. Moore, E. H. DeLucia, J. Lichter, K. S. Hofmockel, R. B.

- 3023 Jackson, H. S. Kim, R. Matamala, H. R. McCarthy, R. Oren, J. S. Pippen,
3024 and W. H. Schlesinger (2006). Progressive nitrogen limitation of ecosystem
3025 processes under elevated CO₂ in a warm-temperate forest. *Ecology* 87(1),
3026 15–25.
- 3027 Firn, J., J. M. McGree, E. Harvey, H. Flores Moreno, M. Schutz, Y. M. Buckley,
3028 E. T. Borer, E. W. Seabloom, K. J. La Pierre, A. M. MacDougall, S. M.
3029 Prober, C. J. Stevens, L. L. Sullivan, E. Porter, E. Ladouceur, C. Allen,
3030 K. H. Moromizato, J. W. Morgan, W. S. Harpole, Y. Hautier, N. Eisen-
3031 hauer, J. P. Wright, P. B. Adler, C. A. Arnillas, J. D. Bakker, L. Biederman,
3032 A. A. D. Broadbent, C. S. Brown, M. N. Bugalho, M. C. Caldeira, E. E. Cle-
3033 land, A. Ebeling, P. A. Fay, N. Hagenah, A. R. Kleinhesselink, R. Mitchell,
3034 J. L. Moore, C. Nogueira, P. L. Peri, C. Roscher, M. D. Smith, P. D. Wragg,
3035 and A. C. Risch (2019). Leaf nutrients, not specific leaf area, are consistent
3036 indicators of elevated nutrient inputs. *Nature Ecology and Evolution* 3(3),
3037 400–406.
- 3038 Fisher, J. B., S. Sitch, Y. Malhi, R. A. Fisher, C. Huntingford, and S.-Y. Tan
3039 (2010). Carbon cost of plant nitrogen acquisition: A mechanistic, globally
3040 applicable model of plant nitrogen uptake, retranslocation, and fixation.
3041 *Global Biogeochemical Cycles* 24(1), 1–17.
- 3042 Fox, J. and S. Weisberg (2019). *An R companion to applied regression* (Third
3043 edit ed.). Thousand Oaks, California: Sage.
- 3044 Franklin, O., R. E. McMurtrie, C. M. Iversen, K. Y. Crous, A. C. Finzi, D. Tis-
3045 sue, D. S. Ellsworth, R. Oren, and R. J. Norby (2009). Forest fine-root
3046 production and nitrogen use under elevated CO₂: contrasting responses

- 3047** in evergreen and deciduous trees explained by a common principle. *Global
3048 Change Biology* 15(1), 132–144.
- 3049** Friedlingstein, P., M. Meinshausen, V. K. Arora, C. D. Jones, A. Anav, S. K.
3050 Liddicoat, and R. Knutti (2014). Uncertainties in CMIP5 climate projections
3051 due to carbon cycle feedbacks. *Journal of Climate* 27(2), 511–526.
- 3052** Friel, C. A. and M. L. Friesen (2019). Legumes modulate allocation to rhizobial
3053 nitrogen fixation in response to factorial light and nitrogen manipulation.
3054 *Frontiers in Plant Science* 10, 1316.
- 3055** Fujikake, H., A. Yamazaki, N. Ohtake, K. Sueoshi, S. Matsuhashi, T. Ito,
3056 C. Mizuniwa, T. Kume, S. Hoshimoto, N.-S. Ishioka, S. Watanabe, A. Osa,
3057 T. Sekine, H. Uchida, A. Tsuji, and T. Ohyama (2003). Quick and reversible
3058 inhibition of soybean root nodule growth by nitrate involves a decrease in
3059 sucrose supply to nodules. *Journal of Experimental Botany* 54(386), 1379–
3060 1388.
- 3061** Ghannoum, O., J. R. Evans, and S. von Caemmerer (2011). Nitrogen and water
3062 use efficiency of C₄ plants. In A. S. Raghavendra and R. F. Sage (Eds.), *C₄
3063 Photosynthesis and Related CO₂ Concentrating Mechanisms*, Chapter 8, pp.
3064 129–146. Springer.
- 3065** Ghimire, B., W. J. Riley, C. D. Koven, J. Kattge, A. Rogers, P. B. Reich, and
3066 I. J. Wright (2017). A global trait-based approach to estimate leaf nitrogen
3067 functional allocation from observations:. *Ecological Applications* 27(5),
3068 1421–1434.
- 3069** Giardina, C. P., M. D. Coleman, J. E. Hancock, J. S. King, E. A. Lilleskov,
3070 W. M. Loya, K. S. Pregitzer, M. G. Ryan, and C. C. Trettin (2005). The

- 3071** response of belowground carbon allocation in forests to global change. In
3072 D. Binkley and O. Manyailo (Eds.), *Tree Species Effects on Soils: Implica-*
3073 *tions for Global Change* (Volume 55 ed.), Chapter Chapter 7, pp. 119–154.
3074 Berlin/Heidelberg: Springer-Verlag.
- 3075** Gibson, A. H. and J. E. Harper (1985). Nitrate effect on nodulation of soybean
3076 by *Bradyrhizobium japonicum*. *Crop Science* 25(3), 497–501.
- 3077** Gill, A. L. and A. C. Finzi (2016). Belowground carbon flux links biogeochemical
3078 cycles and resource-use efficiency at the global scale. *Ecology Letters* 19(12),
3079 1419–1428.
- 3080** Goll, D. S., V. Brovkin, B. R. Parida, C. H. Reick, J. Kattge, P. B. Reich, P. M.
3081 van Bodegom, and Ü. Niinemets (2012). Nutrient limitation reduces land
3082 carbon uptake in simulations with a model of combined carbon, nitrogen
3083 and phosphorus cycling. *Biogeosciences Discussions* 9(3), 3173–3232.
- 3084** Gregory, L. M., A. M. McClain, D. M. Kramer, J. D. Pardo, K. E. Smith, O. L.
3085 Tessmer, B. J. Walker, L. G. Ziccardi, and T. D. Sharkey (2021, oct). The
3086 triose phosphate utilization limitation of photosynthetic rate: Out of global
3087 models but important for leaf models. *Plant, Cell and Environment* 44(10),
3088 3223–3226.
- 3089** Grossiord, C., T. N. Buckley, L. A. Cernusak, K. A. Novick, B. Poulter, R. T. W.
3090 Siegwolf, J. S. Sperry, and N. G. McDowell (2020). Plant responses to rising
3091 vapor pressure deficit. *New Phytologist* 226(6), 1550–1566.
- 3092** Gulmon, S. L. and C. C. Chu (1981). The effects of light and nitrogen on pho-
3093 tosynthesis, leaf characteristics, and dry matter allocation in the chaparral
3094 shrub, *Diplacus aurantiacus*. *Oecologia* 49(2), 207–212.

- 3095** Gutschick, V. P. (1981). Evolved strategies in nitrogen acquisition by plants.
- 3096** *The American Naturalist* 118(5), 607–637.
- 3097** Hallik, L., Ü. Niinemets, and I. J. Wright (2009). Are species shade and drought
- 3098** tolerance reflected in leaf-level structural and functional differentiation in
- 3099** Northern Hemisphere temperate woody flora? *New Phytologist* 184(1), 257–
- 3100** 274.
- 3101** Harrison, M. T., E. J. Edwards, G. D. Farquhar, A. B. Nicotra, and J. R.
- 3102** Evans (2009). Nitrogen in cell walls of sclerophyllous leaves accounts for
- 3103** little of the variation in photosynthetic nitrogen-use efficiency. *Plant, Cell*
- 3104** and *Environment* 32(3), 259–270.
- 3105** Harrison, S. P., W. Cramer, O. Franklin, I. C. Prentice, H. Wang,
- 3106** Å. Bränström, H. de Boer, U. Dieckmann, J. Joshi, T. F. Keenan,
- 3107** A. Lavergne, S. Manzoni, G. Mengoli, C. Morfopoulos, J. Peñuelas,
- 3108** S. Pietsch, K. T. Rebel, Y. Ryu, N. G. Smith, B. D. Stocker, and I. J.
- 3109** Wright (2021). Eco-evolutionary optimality as a means to improve vegeta-
- 3110** tion and land-surface models. *New Phytologist* 231(6), 2125–2141.
- 3111** Henneron, L., P. Kardol, D. A. Wardle, C. Cros, and S. Fontaine (2020). Rhizo-
- 3112** sphere control of soil nitrogen cycling: a key component of plant economic
- 3113** strategies. *New Phytologist* 228(4), 1269–1282.
- 3114** Hijmans, R. J. (2022). terra: Spatial Data Analysis.
- 3115** Hikosaka, K. and A. Shigeno (2009). The role of Rubisco and cell walls in the
- 3116** interspecific variation in photosynthetic capacity. *Oecologia* 160(3), 443–
- 3117** 451.

- 3118** Hoagland, D. R. and D. I. Arnon (1950). The water culture method for growing
3119 plants without soil. *California Agricultural Experiment Station: 347* 347(2),
3120 1–32.
- 3121** Hobbie, E. A. (2006). Carbon allocation to ectomycorrhizal fungi correlates
3122 with belowground allocation in culture studies. *Ecology* 87(3), 563–569.
- 3123** Hobbie, E. A. and J. E. Hobbie (2008). Natural abundance of ^{15}N in nitrogen-
3124 limited forests and tundra can estimate nitrogen cycling through mycorrhizal
3125 fungi: a review. *Ecosystems* 11(5), 815–830.
- 3126** Hoek, T. A., K. Axelrod, T. Biancalani, E. A. Yurtsev, J. Liu, and J. Gore
3127 (2016). Resource availability modulates the cooperative and competitive na-
3128 ture of a microbial cross-feeding mutualism. *PLOS Biology* 14(8), e1002540.
- 3129** Höglberg, M. N., M. J. I. Briones, S. G. Keel, D. B. Metcalfe, C. Campbell, A. J.
3130 Midwood, B. Thornton, V. Hurry, S. Linder, T. Näsholm, and P. Höglberg
3131 (2010). Quantification of effects of season and nitrogen supply on tree below-
3132 ground carbon transfer to ectomycorrhizal fungi and other soil organisms in
3133 a boreal pine forest. *New Phytologist* 187(2), 485–493.
- 3134** Höglberg, P., M. N. Höglberg, S. G. Göttlicher, N. R. Betson, S. G. Keel, D. B.
3135 Metcalfe, C. Campbell, A. Schindlbacher, V. Hurry, T. Lundmark, S. Linder,
3136 and T. Näsholm (2008). High temporal resolution tracing of photosynthate
3137 carbon from the tree canopy to forest soil microorganisms. *New Phytolo-*
3138 *gist* 177(1), 220–228.
- 3139** Houlton, B. Z., Y.-P. Wang, P. M. Vitousek, and C. B. Field (2008). A uni-
3140 fying framework for dinitrogen fixation in the terrestrial biosphere. *Na-*
3141 *ture* 454(7202), 327–330.

- 3142** Huber, M. L., R. A. Perkins, A. Laesecke, D. G. Friend, J. V. Sengers, M. J.
3143 Assael, I. N. Metaxa, E. Vogel, R. Mareš, and K. Miyagawa (2009). New
3144 international formulation for the viscosity of H₂O. *Journal of Physical and*
3145 *Chemical Reference Data* 38(2), 101–125.
- 3146** Hungate, B. A., J. S. Dukes, M. R. Shaw, Y. Luo, and C. B. Field (2003).
3147 Nitrogen and climate change. *Science* 302(5650), 1512–1513.
- 3148** IPCC (2021). *Climate Change 2021: The Physical Science Basis. Contribution*
3149 *of Working Group I to the Sixth Assessment Report of the Intergovernmental*
3150 *Panel on Climate Change*, Volume In Press. Cambridge, United Kingdom
3151 and New York, NY, USA: Cambridge University Press.
- 3152** Johnson, N. C., J. H. Graham, and F. A. Smith (1997). Functioning of mycor-
3153 rhizal associations along the mutualism-parasitism continuum. *New Phytol-*
3154 *ogist* 135(4), 575–585.
- 3155** Kachurina, O. M., H. Zhang, W. R. Raun, and E. G. Krenzer (2000). Simul-
3156 taneous determination of soil aluminum, ammonium- and nitrate- nitrogen
3157 using 1 M potassium chloride. *Communications in Soil Science and Plant*
3158 *Analysis* 31(7-8), 893–903.
- 3159** Kaiser, C., M. R. Kilburn, P. L. Clode, L. Fuchsleger, M. Koranda, J. B. Cliff,
3160 Z. M. Solaiman, and D. V. Murphy (2015). Exploring the transfer of recent
3161 plant photosynthates to soil microbes: mycorrhizal pathway vs direct root
3162 exudation. *New Phytologist* 205(4), 1537–1551.
- 3163** Katabuchi, M. (2015). LeafArea: An R package for rapid digital analysis of leaf
3164 area. *Ecological Research* 30(6), 1073–1077.

- 3165** Kattge, J. and W. Knorr (2007). Temperature acclimation in a biochemical
3166 model of photosynthesis: a reanalysis of data from 36 species. *Plant, Cell*
3167 and *Environment* 30(9), 1176–1190.
- 3168** Kattge, J., W. Knorr, T. Raddatz, and C. Wirth (2009). Quantifying photosyn-
3169 thetic capacity and its relationship to leaf nitrogen content for global-scale
3170 terrestrial biosphere models. *Global Change Biology* 15(4), 976–991.
- 3171** Kayler, Z., A. Gessler, and N. Buchmann (2010). What is the speed of link
3172 between aboveground and belowground processes? *New Phytologist* 187(4),
3173 885–888.
- 3174** Kayler, Z., C. Keitel, K. Jansen, and A. Gessler (2017). Experimental evidence
3175 of two mechanisms coupling leaf-level C assimilation to rhizosphere CO₂
3176 release. *Environmental and Experimental Botany* 135, 21–26.
- 3177** Keeling, C. D., W. G. Mook, and P. P. Tans (1979, jan). Recent trends in the
3178 ¹³C:¹²C ratio of atmospheric carbon dioxide. *Nature* 277(5692), 121–123.
- 3179** Keeney, D. R. and D. W. Nelson (1983). Nitrogen—Inorganic Forms. In A. L.
3180 Page (Ed.), *Methods of Soil Analysis* (2nd ed.), Chapter 33, pp. 643–698.
3181 Madison, WI, USA: ASA and SSSA.
- 3182** Kenward, M. G. and J. H. Roger (1997). Small sample inference for fixed effects
3183 from restricted maximum likelihood. *Biometrics* 53(3), 983.
- 3184** Knapp, A. K., M. L. Avolio, C. Beier, C. J. W. Carroll, S. L. Collins, J. S.
3185 Dukes, L. H. Fraser, R. J. Griffin-Nolan, D. L. Hoover, A. Jentsch, M. E.
3186 Loik, R. P. Phillips, A. K. Post, O. E. Sala, I. J. Slette, L. Yahdjian, and
3187 M. D. Smith (2017). Pushing precipitation to the extremes in distributed

- 3188 experiments: recommendations for simulating wet and dry years. *Global
3189 Change Biology* 23(5), 1774–1782.
- 3190 Knorr, W. (2000). Annual and interannual CO₂ exchanges of the
3191 terrestrial biosphere: process-based simulations and uncertainties. *Global
3192 Ecology and Biogeography* 9(3), 225–252.
- 3193 Knorr, W. and M. Heimann (2001). Uncertainties in global terrestrial biosphere
3194 modeling: 1. A comprehensive sensitivity analysis with a new photosynthesis
3195 and energy balance scheme. *Global Biogeochemical Cycles* 15(1), 207–225.
- 3196 Kulmatiski, A., P. B. Adler, J. M. Stark, and A. T. Tredennick (2017). Water
3197 and nitrogen uptake are better associated with resource availability than
3198 root biomass. *Ecosphere* 8(3), e01738.
- 3199 Lavergne, A., D. Sandoval, V. J. Hare, H. Graven, and I. C. Prentice (2020).
3200 Impacts of soil water stress on the acclimated stomatal limitation of pho-
3201 tosynthesis: Insights from stable carbon isotope data. *Global Change Biol-
3202 ogy* 26(12), 7158–7172.
- 3203 Lawrence, D. M., R. A. Fisher, C. D. Koven, K. W. Oleson, S. C. Swen-
3204 son, G. B. Bonan, N. Collier, B. Ghimire, L. Kampenhout, D. Kennedy,
3205 E. Kluzek, P. J. Lawrence, F. Li, H. Li, D. L. Lombardozzi, W. J. Riley,
3206 W. J. Sacks, M. Shi, M. Vertenstein, W. R. Wieder, C. Xu, A. A. Ali,
3207 A. M. Badger, G. Bisht, M. Broeke, M. A. Brunke, S. P. Burns, J. Buzan,
3208 M. Clark, A. Craig, K. M. Dahlin, B. Drewniak, J. B. Fisher, M. Flanner,
3209 A. M. Fox, P. Gentine, F. M. Hoffman, G. Keppel-Aleks, R. Knox, S. Ku-
3210 mar, J. Lenaerts, L. R. Leung, W. H. Lipscomb, Y. Lu, A. Pandey, J. D.
3211 Pelletier, J. Perket, J. T. Randerson, D. M. Ricciuto, B. M. Sanderson,

- 3212** A. Slater, Z. M. Subin, J. Tang, R. Q. Thomas, M. Val Martin, and X. Zeng
3213 (2019). The Community Land Model Version 5: description of new features,
3214 benchmarking, and impact of forcing uncertainty. *Journal of Advances in*
3215 *Modeling Earth Systems* 11(12), 4245–4287.
- 3216** LeBauer, D. S. and K. K. Treseder (2008). Nitrogen limitation of net primary
3217 productivity. *Ecology* 89(2), 371–379.
- 3218** Lefcheck, J. S. (2016). piecewiseSEM: Piecewise structural equation modelling
3219 in r for ecology, evolution, and systematics. *Methods in Ecology and Evolu-*
3220 *tion* 7(5), 573–579.
- 3221** Lenth, R. (2019). emmeans: estimated marginal means, aka least-squares
3222 means.
- 3223** Li, W., H. Zhang, G. Huang, R. Liu, H. Wu, C. Zhao, and N. G. McDowell
3224 (2020). Effects of nitrogen enrichment on tree carbon allocation: A global
3225 synthesis. *Global Ecology and Biogeography* 29(3), 573–589.
- 3226** Liang, J., X. Qi, L. Souza, and Y. Luo (2016). Processes regulating progressive
3227 nitrogen limitation under elevated carbon dioxide: a meta-analysis. *Biogeosciences*
3228 13(9), 2689–2699.
- 3229** Liang, X., T. Zhang, X. Lu, D. S. Ellsworth, H. BassiriRad, C. You, D. Wang,
3230 P. He, Q. Deng, H. Liu, J. Mo, and Q. Ye (2020). Global response patterns of
3231 plant photosynthesis to nitrogen addition: A meta-analysis. *Global Change*
3232 *Biology* 26(6), 3585–3600.
- 3233** López, J., D. A. Way, and W. Sadok (2021). Systemic effects of rising atmo-
3234 spheric vapor pressure deficit on plant physiology and productivity. *Global*

- 3235** *Change Biology* 27(9), 1704–1720.
- 3236** Lu, J., J. Yang, C. Keitel, L. Yin, P. Wang, W. Cheng, and F. A. Dijkstra
- 3237** (2022). Belowground carbon efficiency for nitrogen and phosphorus acqui-
- 3238** sition varies between *Lolium perenne* and *Trifolium repens* and depends on
- 3239** phosphorus fertilization. *Frontiers in Plant Science* 13, 1–9.
- 3240** Luo, X., T. F. Keenan, J. M. Chen, H. Croft, I. C. Prentice, N. G. Smith,
- 3241** A. P. Walker, H. Wang, R. Wang, C. Xu, and Y. Zhang (2021). Global
- 3242** variation in the fraction of leaf nitrogen allocated to photosynthesis. *Nature*
- 3243** *Communications* 12(1), 4866.
- 3244** Luo, Y., W. S. Currie, J. S. Dukes, A. C. Finzi, U. A. Hartwig, B. A. Hungate,
- 3245** R. E. McMurtrie, R. Oren, W. J. Parton, D. E. Pataki, R. M. Shaw, D. R.
- 3246** Zak, and C. B. Field (2004). Progressive nitrogen limitation of ecosystem
- 3247** responses to rising atmospheric carbon dioxide. *BioScience* 54(8), 731–739.
- 3248** Maire, V., P. Martre, J. Kattge, F. Gastal, G. Esser, S. Fontaine, and J.-F.
- 3249** Soussana (2012). The coordination of leaf photosynthesis links C and N
- 3250** fluxes in C₃ plant species. *PLoS ONE* 7(6), e38345.
- 3251** Makino, A. (2003). Rubisco and nitrogen relationships in rice: leaf photosyn-
- 3252** thesis and plant growth. *Soil Science and Plant Nutrition* 49(3), 319–327.
- 3253** Makino, A., M. Harada, T. Sato, H. Nakano, and T. Mae (1997). Growth and N
- 3254** Allocation in Rice Plants under CO₂ Enrichment. *Plant Physiology* 115(1),
- 3255** 199–203.
- 3256** Markham, J. H. and C. Zekveld (2007). Nitrogen fixation makes biomass al-
- 3257** location to roots independent of soil nitrogen supply. *Canadian Journal of*

- 3258** *Botany* (9), 787–793.
- 3259** Marschner, H. and B. Dell (1994). Nutrient uptake in mycorrhizal symbiosis.
- 3260** *Plant and Soil* 159(1), 89–102.
- 3261** Matamala, R. and W. H. Schlesinger (2000). Effects of elevated atmospheric
- 3262** CO₂ on fine root production and activity in an intact temperate forest
- 3263** ecosystem. *Global Change Biology* 6(8), 967–979.
- 3264** Medlyn, B. E., E. Dreyer, D. S. Ellsworth, M. Forstreuter, P. C. Harley,
- 3265** M. U. F. Kirschbaum, X. Le Roux, P. Montpied, J. Strassmeyer, A. Wal-
- 3266** croft, K. Wang, and D. Loustau (2002). Temperature response of parameters
- 3267** of a biochemically based model of photosynthesis. II. A review of experimen-
- 3268** tal data. *Plant, Cell and Environment* 25(9), 1167–1179.
- 3269** Menge, D. N. L., S. A. Levin, and L. O. Hedin (2008). Evolutionary tradeoffs can
- 3270** select against nitrogen fixation and thereby maintain nitrogen limitation.
- 3271** *Proceedings of the National Academy of Sciences* 105(5), 1573–1578.
- 3272** Menne, M. J., I. Durre, R. S. Vose, B. E. Gleason, and T. G. Houston (2012).
- 3273** An overview of the global historical climatology network-daily database.
- 3274** *Journal of Atmospheric and Oceanic Technology* 29(7), 897–910.
- 3275** Meyerholt, J., K. Sickel, and S. Zaehle (2020). Ensemble projections elucidate
- 3276** effects of uncertainty in terrestrial nitrogen limitation on future carbon up-
- 3277** take. *Global Change Biology* 26(7), 3978–3996.
- 3278** Meyerholt, J., S. Zaehle, and M. J. Smith (2016). Variability of projected ter-
- 3279** restrial biosphere responses to elevated levels of atmospheric CO₂ due to
- 3280** uncertainty in biological nitrogen fixation. *Biogeosciences* 13(5), 1491–1518.

- 3281 Minocha, R., S. Long, A. H. Magill, J. D. Aber, and W. H. McDowell (2000).
- 3282 Foliar free polyamine and inorganic ion content in relation to soil and soil
3283 solution chemistry in two fertilized forest stands at the Harvard Forest,
3284 Massachusetts. *Plant and Soil* 222(1-2), 119–137.
- 3285 Moore, D. J., S. Aref, R. M. Ho, J. S. Pippen, J. G. Hamilton, and E. H. De
3286 Lucia (2006). Annual basal area increment and growth duration of *Pinus*
3287 *taeda* in response to eight years of free-air carbon dioxide enrichment. *Global
3288 Change Biology* 12(8), 1367–1377.
- 3289 Morgan, J. A., D. E. Pataki, C. Körner, H. Clark, S. J. Del Grosso, J. M.
3290 Grünzweig, A. K. Knapp, A. R. Mosier, P. C. D. Newton, P. A. Niklaus,
3291 J. B. Nippert, R. S. Nowak, W. J. Parton, H. W. Polley, and M. R. Shaw
3292 (2004). Water relations in grassland and desert ecosystems exposed to ele-
3293 vated atmospheric CO₂. *Oecologia* 140(1), 11–25.
- 3294 Muñoz, N., X. Qi, M. W. Li, M. Xie, Y. Gao, M. Y. Cheung, F. L. Wong, and
3295 H.-M. Lam (2016). Improvement in nitrogen fixation capacity could be part
3296 of the domestication process in soybean. *Heredity* 117(2), 84–93.
- 3297 Nadelhoffer, K. J. and J. W. Raich (1992). Fine root production estimates and
3298 belowground carbon allocation in forest ecosystems. *Ecology* 73(4), 1139–
3299 1147.
- 3300 Niinemets, Ü. and J. D. Tenhunen (1997). A model separating leaf structural
3301 and physiological effects on carbon gain along light gradients for the shade-
3302 tolerant species *Acer saccharum*. *Plant, Cell and Environment* 20(7), 845–
3303 866.
- 3304 Norby, R. J., J. Ledford, C. D. Reilly, N. E. Miller, and E. G. O'Neill

- 3305 (2004). Fine-root production dominates response of a deciduous forest to
3306 atmospheric CO₂ enrichment. *Proceedings of the National Academy of Sci-*
3307 *ences* 101(26), 9689–9693.
- 3308 Norby, R. J., J. M. Warren, C. M. Iversen, B. E. Medlyn, and R. E. Mc-
3309 Murtrie (2010). CO₂ enhancement of forest productivity constrained by
3310 limited nitrogen availability. *Proceedings of the National Academy of Sci-*
3311 *ences* 107(45), 19368–19373.
- 3312 Novick, K. A., D. L. Ficklin, P. C. Stoy, C. A. Williams, G. Bohrer, A. C.
3313 Oishi, S. A. Papuga, P. D. Blanken, A. Noormets, B. N. Sulman, R. L.
3314 Scott, L. Wang, and R. P. Phillips (2016). The increasing importance of
3315 atmospheric demand for ecosystem water and carbon fluxes. *Nature Climate
3316 Change* 6(11), 1023–1027.
- 3317 Noyce, G. L., M. L. Kirwan, R. L. Rich, and J. P. Megonigal (2019). Asyn-
3318 chronous nitrogen supply and demand produce nonlinear plant allocation re-
3319 sponds to warming and elevated CO₂. *Proceedings of the National Academy
3320 of Sciences* 116(43), 21623–21628.
- 3321 Onoda, Y., K. Hikosaka, and T. Hirose (2004). Allocation of nitrogen to
3322 cell walls decreases photosynthetic nitrogen-use efficiency. *Functional Ecol-
3323 ogy* 18(3), 419–425.
- 3324 Onoda, Y., I. J. Wright, J. R. Evans, K. Hikosaka, K. Kitajima, Ü. Niinemets,
3325 H. Poorter, T. Tosens, and M. Westoby (2017). Physiological and structural
3326 trade-offs underlying the leaf economics spectrum. *New Phytologist* 214(4),
3327 1447–1463.
- 3328 Oren, R., J. S. Sperry, G. G. Katul, D. E. Pataki, B. E. Ewers, N. Phillips,

- 3329 and K. V. R. Schäfer (1999). Survey and synthesis of intra- and interspecific
3330 variation in stomatal sensitivity to vapor pressure deficit. *Plant, Cell and*
3331 *Environment* 22(12), 1515–1526.
- 3332 Oreskes, N., K. Shrader-Frechette, and K. Belitz (1994). Verification, vali-
3333 dation, and confirmation of numerical models in the Earth sciences. *Sci-*
3334 *ence* 263(5147), 641–646.
- 3335 Paillassa, J., I. J. Wright, I. C. Prentice, S. Pepin, N. G. Smith, G. Ethier,
3336 A. C. Westerband, L. J. Lamarque, H. Wang, W. K. Cornwell, and V. Maire
3337 (2020). When and where soil is important to modify the carbon and water
3338 economy of leaves. *New Phytologist* 228(1), 121–135.
- 3339 Parvin, S., S. Uddin, S. Tausz Posch, R. Armstrong, and M. Tausz (2020). Car-
3340 bon sink strength of nodules but not other organs modulates photosynthesis
3341 of faba bean (*Vicia faba*) grown under elevated [CO₂] and different water
3342 supply. *New Phytologist* 227(1), 132–145.
- 3343 Paul, K. I., P. J. Polglase, A. M. O'Connell, J. C. Carlyle, P. J. Smethurst, and
3344 P. K. Khanna (2003). Defining the relation between soil water content and
3345 net nitrogen mineralization. *European Journal of Soil Science* 54(1), 39–48.
- 3346 Peng, Y., K. J. Bloomfield, L. A. Cernusak, T. F. Domingues, and I. C. Pren-
3347 tice (2021). Global climate and nutrient controls of photosynthetic capacity.
3348 *Communications Biology* 4(1), 462.
- 3349 Perkowski, E. A., E. F. Waring, and N. G. Smith (2021). Root mass carbon
3350 costs to acquire nitrogen are determined by nitrogen and light availabil-
3351 ity in two species with different nitrogen acquisition strategies. *Journal of*
3352 *Experimental Botany* 72(15), 5766–5776.

- 3353** Phillips, R. P., E. R. Brzostek, and M. G. Midgley (2013). The mycorrhizal-
3354 associated nutrient economy: a new framework for predicting carbon-
3355 nutrient couplings in temperate forests. *New Phytologist* 199(1), 41–51.
- 3356** Phillips, R. P., A. C. Finzi, and E. S. Bernhardt (2011). Enhanced root ex-
3357 udation induces microbial feedbacks to N cycling in a pine forest under
3358 long-term CO₂ fumigation. *Ecology Letters* 14(2), 187–194.
- 3359** Pinheiro, J. and D. Bates (2022). nlme: linear and nonlinear mixed effects
3360 models.
- 3361** Poggio, L., L. M. De Sousa, N. H. Batjes, G. B. M. Heuvelink, B. Kempen,
3362 E. Ribeiro, and D. Rossiter (2021). SoilGrids 2.0: Producing soil information
3363 for the globe with quantified spatial uncertainty. *Soil* 7(1), 217–240.
- 3364** Pons, T. L. and R. W. Pearcy (1994). Nitrogen reallocation and photosynthetic
3365 acclimation in response to partial shading in soybean plants. *Physiologia*
3366 *Plantarum* 92(4), 636–644.
- 3367** Poorter, H., J. Bühler, D. Van Dusschoten, J. Climent, and J. A. Postma (2012).
3368 Pot size matters: A meta-analysis of the effects of rooting volume on plant
3369 growth. *Functional Plant Biology* 39(11), 839–850.
- 3370** Poorter, H., O. Knopf, I. J. Wright, A. A. Temme, S. W. Hogewoning, A. Graf,
3371 L. A. Cernusak, and T. L. Pons (2022). A meta-analysis of responses of C₃
3372 plants to atmospheric CO₂: dose-response curves for 85 traits ranging from
3373 the molecular to the whole-plant level. *New Phytologist* 233(4), 1560–1596.
- 3374** Prentice, I. C., N. Dong, S. M. Gleason, V. Maire, and I. J. Wright (2014).
3375 Balancing the costs of carbon gain and water transport: testing a new theo-

- 3376** retical framework for plant functional ecology. *Ecology Letters* 17(1), 82–91.
- 3377** Prentice, I. C., X. Liang, B. E. Medlyn, and Y.-P. Wang (2015). Reliable, ro-
- 3378** bust and realistic: The three R’s of next-generation land-surface modelling.
- 3379** *Atmospheric Chemistry and Physics* 15, 5987–6005.
- 3380** Priestley, C. H. B. and R. J. Taylor (1972). On the Assessment of Surface
- 3381** Heat Flux and Evaporation Using Large-Scale Parameters. *Monthly Weather*
- 3382** *Review* 100(2), 81–92.
- 3383** Querejeta, J. I., I. Prieto, C. Armas, F. Casanoves, J. S. Diémé, M. Diouf,
- 3384** H. Yossi, B. Kaya, F. I. Pugnaire, and G. M. Rusch (2022). Higher leaf
- 3385** nitrogen content is linked to tighter stomatal regulation of transpiration
- 3386** and more efficient water use across dryland trees. *New Phytologist* 235(4),
- 3387** 1351–1364.
- 3388** R Core Team (2021). R: A language and environment for statistical computing.
- 3389** Raich, J. W., D. A. Clark, L. Schwendenmann, and T. E. Wood (2014). Above-
- 3390** ground tree growth varies with belowground carbon allocation in a tropical
- 3391** rainforest environment. *PLoS ONE* 9(6), e100275.
- 3392** Rastetter, E. B., P. M. Vitousek, C. B. Field, G. R. Shaver, D. Herbert, and
- 3393** G. I. Ågren (2001). Resource optimization and symbiotic nitrogen fixation.
- 3394** *Ecosystems* 4(4), 369–388.
- 3395** Reich, P. B. (2014). The world-wide ‘fast-slow’ plant economics spectrum: a
- 3396** traits manifesto. *Journal of Ecology* 102(2), 275–301.
- 3397** Reich, P. B., S. E. Hobbie, T. Lee, D. S. Ellsworth, J. B. West, D. Tilman,
- 3398** J. M. H. Knops, S. Naeem, and J. Trost (2006). Nitrogen limitation con-

- 3399 strains sustainability of ecosystem response to CO₂. *Nature* 440(7086), 922–
3400 925.
- 3401 Reichman, G. A., D. L. Grunes, and F. G. Viets (1966). Effect of soil moisture
3402 on ammonification and nitrification in two Northern Plains soils. *Soil Science
3403 Society of America Journal* 30(3), 363–366.
- 3404 Rhine, E. D., R. L. Mulvaney, E. J. Pratt, and G. K. Sims (1998). Improving
3405 the Berthelot reaction for determining ammonium in soil extracts and water.
3406 *Soil Science Society of America Journal* 62(2), 473.
- 3407 Rogers, A. (2014). The use and misuse of V_{cmax} in Earth System Models. *Photo-
3408 synthesis Research* 119(1-2), 15–29.
- 3409 Rogers, A., B. E. Medlyn, J. S. Dukes, G. B. Bonan, S. Caemmerer, M. C.
3410 Dietze, J. Kattge, A. D. B. Leakey, L. M. Mercado, Ü. Niinemets, I. C.
3411 Prentice, S. P. Serbin, S. Sitch, D. A. Way, and S. Zaehle (2017). A roadmap
3412 for improving the representation of photosynthesis in Earth system models.
3413 *New Phytologist* 213(1), 22–42.
- 3414 Saathoff, A. J. and J. Welles (2021). Gas exchange measurements in the un-
3415 steady state. *Plant Cell and Environment* 44(11), 3509–3523.
- 3416 Sage, R. F. and R. W. Pearcy (1987). The nitrogen use efficiency of C₃ and C₄
3417 plants: I. Leaf nitrogen, growth, and biomass partitioning in *Chenopodium
3418 album* (L.) and *Amaranthus retroflexus* (L.). *Plant Physiology* 84(3), 954–
3419 958.
- 3420 Saleh, A. M., M. Abdel-Mawgoud, A. R. Hassan, T. H. Habeeb, R. S. Yehia,
3421 and H. AbdElgawad (2020). Global metabolic changes induced by arbuscular

- 3422** mycorrhizal fungi in oregano plants grown under ambient and elevated levels
3423 of atmospheric CO₂. *Plant Physiology and Biochemistry* 151, 255–263.
- 3424** Saxton, K. E. and W. J. Rawls (2006). Soil water characteristic estimates by
3425 texture and organic matter for hydrologic solutions. *Soil Science Society of*
3426 *America Journal* 70(5), 1569–1578.
- 3427** Schaefer, K., C. R. Schwalm, C. Williams, M. A. Arain, A. Barr, J. M. Chen,
3428 K. J. Davis, D. Dimitrov, T. W. Hilton, D. Y. Hollinger, E. Humphreys,
3429 B. Poulter, B. M. Racza, A. D. Richardson, A. Sahoo, P. Thornton, R. Var-
3430 gas, H. Verbeeck, R. Anderson, I. Baker, T. A. Black, P. Bolstad, J. Chen,
3431 P. S. Curtis, A. R. Desai, M. C. Dietze, D. Dragoni, C. M. Gough, R. F.
3432 Grant, L. Gu, A. K. Jain, C. Kucharik, B. E. Law, S. Liu, E. Lokipitiya,
3433 H. A. Margolis, R. Matamala, J. H. McCaughey, R. Monson, J. W. Munger,
3434 W. Oechel, C. Peng, D. T. Price, D. Ricciuto, W. J. Riley, N. Roulet,
3435 H. Tian, C. Tonitto, M. Torn, E. Weng, and X. Zhou (2012). A model-
3436 data comparison of gross primary productivity: Results from the North
3437 American Carbon Program site synthesis. *Journal of Geophysical Research:*
3438 *Biogeosciences* 117(G3), G03010.
- 3439** Schmitt, M. R. and G. E. Edwards (1981). Photosynthetic capacity and nitrogen
3440 use efficiency of maize, wheat, and rice: A comparison between C₃ and C₄
3441 photosynthesis. *Journal of Experimental Botany* 32(3), 459–466.
- 3442** Schneider, C. A., W. S. Rasband, and K. W. Eliceiri (2012). NIH Image to
3443 ImageJ: 25 years of image analysis. *Nature Methods* 9(7), 671–675.
- 3444** Scott, H. G. and N. G. Smith (2022). A Model of C₄ photosynthetic acclima-
3445 tion based on least-cost optimality theory suitable for Earth system model

- 3446** incorporation. *Journal of Advances in Modeling Earth Systems* 14(3), 1–16.
- 3447** Shi, M., J. B. Fisher, E. R. Brzostek, and R. P. Phillips (2016). Carbon cost
- 3448** of plant nitrogen acquisition: Global carbon cycle impact from an improved
- 3449** plant nitrogen cycle in the Community Land Model. *Global Change Biology*
- 3450** 22(3), 1299–1314.
- 3451** Shi, M., J. B. Fisher, R. P. Phillips, and E. R. Brzostek (2019). Neglecting
- 3452** plant–microbe symbioses leads to underestimation of modeled climate im-
- 3453** pacts. *Biogeosciences* 16(2), 457–465.
- 3454** Smith, B., D. Wärllind, A. Arneth, T. Hickler, P. Leadley, J. Siltberg, and
- 3455** S. Zaehle (2014). Implications of incorporating N cycling and N limitations
- 3456** on primary production in an individual-based dynamic vegetation model.
- 3457** *Biogeosciences* 11(7), 2027–2054.
- 3458** Smith, N. G. and J. S. Dukes (2013). Plant respiration and photosynthesis in
- 3459** global-scale models: incorporating acclimation to temperature and CO₂.
- 3460** *Global Change Biology* 19(1), 45–63.
- 3461** Smith, N. G. and J. S. Dukes (2018). Drivers of leaf carbon exchange capacity
- 3462** across biomes at the continental scale. *Ecology* 99(7), 1610–1620.
- 3463** Smith, N. G. and T. F. Keenan (2020). Mechanisms underlying leaf photosyn-
- 3464** thetic acclimation to warming and elevated CO₂ as inferred from least-cost
- 3465** optimality theory. *Global Change Biology* 26(9), 5202–5216.
- 3466** Smith, N. G., T. F. Keenan, I. C. Prentice, H. Wang, I. J. Wright, Ü. Niinemets,
- 3467** K. Y. Crous, T. F. Domingues, R. Guerrieri, F. oko Ishida, J. Kattge, E. L.
- 3468** Kruger, V. Maire, A. Rogers, S. P. Serbin, L. Tarvainen, H. F. Togashi,

- 3469 P. A. Townsend, M. Wang, L. K. Weerasinghe, and S.-X. Zhou (2019).
3470 Global photosynthetic capacity is optimized to the environment. *Ecology*
3471 *Letters* 22(3), 506–517.
- 3472 Smith, N. G., D. L. Lombardozzi, A. Tawfik, G. B. Bonan, and J. S. Dukes
3473 (2017). Biophysical consequences of photosynthetic temperature acclimation
3474 for climate. *Journal of Advances in Modeling Earth Systems* 9(1), 536–547.
- 3475 Smith, N. G., S. L. Malyshev, E. Shevliakova, J. Kattge, and J. S. Dukes
3476 (2016). Foliar temperature acclimation reduces simulated carbon sensitivity
3477 to climate. *Nature Climate Change* 6(4), 407–411.
- 3478 Smith, S. E. and D. J. Read (2008). *Mycorrhizal Symbiosis*. Academic Press.
- 3479 Soil Survey Staff (2022). Web Soil Survey.
- 3480 Soudzilovskaia, N. A., J. C. Douma, A. A. Akhmetzhanova, P. M. van Bode-
3481 gom, W. K. Cornwell, E. J. Moens, K. K. Treseder, and J. H. C. Cornelissen
3482 (2015). Global patterns of plant root colonization intensity by mycorrhizal
3483 fungi explained by climate and soil chemistry. *Global Ecology and Biogeog-
3484 raphy* 24(3), 371–382.
- 3485 Stark, J. M. and M. K. Firestone (1995). Mechanisms for soil moisture ef-
3486 fects on activity of nitrifying bacteria. *Applied and Environmental Microbi-
3487 ology* 61(1), 218–221.
- 3488 Stocker, B. D., H. Wang, N. G. Smith, S. P. Harrison, T. F. Keenan, D. San-
3489 doval, T. Davis, and I. C. Prentice (2020). P-model v1.0: An optimality-
3490 based light use efficiency model for simulating ecosystem gross primary pro-
3491 duction. *Geoscientific Model Development* 13(3), 1545–1581.

- 3492 Stocker, B. D., J. Zscheischler, T. F. Keenan, I. C. Prentice, J. Peñuelas, and
3493 S. I. Seneviratne (2018). Quantifying soil moisture impacts on light use
3494 efficiency across biomes. *New Phytologist* 218(4), 1430–1449.
- 3495 Sulman, B. N., D. T. Roman, K. Yi, L. Wang, R. P. Phillips, and K. A.
3496 Novick (2016). High atmospheric demand for water can limit forest car-
3497 bon uptake and transpiration as severely as dry soil. *Geophysical Research*
3498 *Letters* 43(18), 9686–9695.
- 3499 Sulman, B. N., E. Shevliakova, E. R. Brzostek, S. N. Kivlin, S. L. Malyshev,
3500 D. N. L. Menge, and X. Zhang (2019). Diverse mycorrhizal associations
3501 enhance terrestrial C storage in a global model. *Global Biogeochemical Cy-*
3502 *cles* 33(4), 501–523.
- 3503 Sweet, S. K., D. W. Wolfe, A. DeGaetano, and R. Benner (2017). Anatomy
3504 of the 2016 drought in the Northeastern United States: Implications for
3505 agriculture and water resources in humid climates. *Agricultural and Forest*
3506 *Meteorology* 247, 571–581.
- 3507 Taylor, B. N. and D. N. L. Menge (2018). Light regulates tropical symbiotic
3508 nitrogen fixation more strongly than soil nitrogen. *Nature Plants* 4(9), 655–
3509 661.
- 3510 Terrer, C., S. Vicca, B. A. Hungate, R. P. Phillips, and I. C. Prentice (2016).
3511 Mycorrhizal association as a primary control of the CO₂ fertilization effect.
3512 *Science* 353(6294), 72–74.
- 3513 Terrer, C., S. Vicca, B. D. Stocker, B. A. Hungate, R. P. Phillips, P. B. Reich,
3514 A. C. Finzi, and I. C. Prentice (2018). Ecosystem responses to elevated CO₂
3515 governed by plant–soil interactions and the cost of nitrogen acquisition. *New*

- 3516** *Phytologist* 217(2), 507–522.
- 3517** Thieurmel, B. and A. Elmarhraoui (2019). suncalc: Compute sun position,
- 3518** sunlight phases, moon position, and lunar phase.
- 3519** Thomas, R. Q., E. N. J. Brookshire, and S. Gerber (2015). Nitrogen limita-
- 3520** tion on land: how can it occur in Earth system models? *Global Change*
- 3521** *Biology* 21(5), 1777–1793.
- 3522** Thomas, R. Q., S. Zaehle, P. H. Templer, and C. L. Goodale (2013). Global pat-
- 3523** terns of nitrogen limitation: confronting two global biogeochemical models
- 3524** with observations. *Global Change Biology* 19(10), 2986–2998.
- 3525** Thornton, P. E., J.-F. Lamarque, N. A. Rosenbloom, and N. M. Mahowald
- 3526** (2007). Influence of carbon-nitrogen cycle coupling on land model response
- 3527** to CO₂ fertilization and climate variability. *Global Biogeochemical Cy-*
- 3528** *cles* 21(4), GB4018.
- 3529** Tingey, D. T., D. L. Phillips, and M. G. Johnson (2000). Elevated CO₂ and
- 3530** conifer roots: effects on growth, life span and turnover. *New Phytolo-*
- 3531** *gist* 147(1), 87–103.
- 3532** Udvardi, M. and P. S. Poole (2013). Transport and metabolism in legume-
- 3533** rhizobia symbioses. *Annual Review of Plant Biology* 64, 781–805.
- 3534** USDA NRCS (2022). The PLANTS Database.
- 3535** Uselman, S. M., R. G. Qualls, and R. B. Thomas (2000). Effects of increased
- 3536** atmospheric CO₂, temperature, and soil N availability on root exudation
- 3537** of dissolved organic carbon by an N-fixing tree (*Robinia pseudoacacia* L.).
- 3538** *Plant and Soil* 222, 191–202.

- 3539 van Diepen, L. T. A., E. A. Lilleskov, K. S. Pregitzer, and R. M. Miller (2007).
- 3540 Decline of arbuscular mycorrhizal fungi in northern hardwood forests ex-
- 3541 posed to chronic nitrogen additions. *New Phytologist* 176(1), 175–183.
- 3542 Vance, C. P. and G. H. Heichel (1991). Carbon in N₂ fixation: Limitation or
- 3543 exquisite adaptation. *Annual Review of Plant Physiology and Plant Molec-*
- 3544 *ular Biology* 42(1), 373–392.
- 3545 Viet, H. D., J.-H. Kwak, K.-S. Lee, S.-S. Lim, M. Matsushima, S. X. Chang,
- 3546 K.-H. Lee, and W.-J. Choi (2013). Foliar chemistry and tree ring δ¹³C of
- 3547 *Pinus densiflora* in relation to tree growth along a soil pH gradient. *Plant*
- 3548 *and Soil* 363(1-2), 101–112.
- 3549 Vitousek, P. M., K. Cassman, C. C. Cleveland, T. Crews, C. B. Field, N. B.
- 3550 Grimm, R. W. Howarth, R. Marino, L. Martinelli, E. B. Rastetter, and
- 3551 J. I. Sprent (2002). Towards an ecological understanding of biological nitro-
- 3552 gen fixation. In *The Nitrogen Cycle at Regional to Global Scales*, pp. 1–45.
- 3553 Springer Netherlands.
- 3554 Vitousek, P. M. and R. W. Howarth (1991). Nitrogen limitation on land and in
- 3555 the sea: How can it occur? *Biogeochemistry* 13(2), 87–115.
- 3556 Vitousek, P. M., S. Porder, B. Z. Houlton, and O. A. Chadwick (2010).
- 3557 Terrestrial phosphorus limitation: mechanisms, implications, and nitro-
- 3558 gen–phosphorus interactions. *Ecological Applications* 20(1), 5–15.
- 3559 Walker, A. P., A. P. Beckerman, L. Gu, J. Kattge, L. A. Cernusak, T. F.
- 3560 Domingues, J. C. Scales, G. Wohlfahrt, S. D. Wullschleger, and F. I. Wood-
- 3561 ward (2014). The relationship of leaf photosynthetic traits - V_{cmax} and J_{max}
- 3562 - to leaf nitrogen, leaf phosphorus, and specific leaf area: a meta-analysis

- 3563 and modeling study. *Ecology and Evolution* 4(16), 3218–3235.
- 3564 Walker, A. P., A. L. Johnson, A. Rogers, J. Anderson, R. A. Bridges, R. A.
- 3565 Fisher, D. Lu, D. M. Ricciuto, S. P. Serbin, and M. Ye (2021). Multi-
- 3566 hypothesis comparison of Farquhar and Collatz photosynthesis models re-
- 3567 veals the unexpected influence of empirical assumptions at leaf and global
- 3568 scales. *Global Change Biology* 27(4), 804–822.
- 3569 Wang, H., I. C. Prentice, T. F. Keenan, T. W. Davis, I. J. Wright, W. K.
- 3570 Cornwell, B. J. Evans, and C. Peng (2017). Towards a universal model for
- 3571 carbon dioxide uptake by plants. *Nature Plants* 3(9), 734–741.
- 3572 Wang, H., I. C. Prentice, I. J. Wright, D. I. Warton, S. Qiao, X. Xu, J. Zhou,
- 3573 Kikuzawa, and N. C. Stenseth (2023). Leaf economics fundamentals ex-
- 3574 plained by optimality principles. *Science Advances* 9(3), eadd566.
- 3575 Wang, J., J. M. Knops, C. E. Brassil, and C. Mu (2017). Increased productivity
- 3576 in wet years drives a decline in ecosystem stability with nitrogen additions
- 3577 in arid grasslands. *Ecology* 98(7), 1779–1786.
- 3578 Wang, W., Y. Wang, G. Hoch, Z. Wang, and J. Gu (2018). Linkage of root mor-
- 3579 phology to anatomy with increasing nitrogen availability in six temperate
- 3580 tree species. *Plant and Soil* 425(1-2), 189–200.
- 3581 Weatherburn, M. W. (1967). Phenol-hypochlorite reaction for determination of
- 3582 ammonia. *Analytical Chemistry* 39(8), 971–974.
- 3583 Wellburn, A. R. (1994). The spectral determination of chlorophylls a and b, as
- 3584 well as total carotenoids, using various solvents with spectrophotometers of
- 3585 different resolution. *Journal of Plant Physiology* 144(3), 307–313.

- 3586 Wen, Z., P. J. White, J. Shen, and H. Lambers (2022). Linking root exuda-
3587 tion to belowground economic traits for resource acquisition. *New Phytolo-*
3588 *gist* 233(4), 1620–1635.
- 3589 Westerband, A. C., I. J. Wright, V. Maire, J. Paillassa, I. C. Prentice, O. K.
3590 Atkin, K. J. Bloomfield, L. A. Cernusak, N. Dong, S. M. Gleason, C. Guil-
3591 herme Pereira, H. Lambers, M. R. Leishman, Y. Malhi, and R. H. Nolan
3592 (2023). Coordination of photosynthetic traits across soil and climate gradi-
3593 ents. *Global Change Biology* 29(3), 1–29.
- 3594 Wieder, W. R., C. C. Cleveland, W. K. Smith, and K. Todd-Brown (2015).
3595 Future productivity and carbon storage limited by terrestrial nutrient avail-
3596 ability. *Nature Geoscience* 8(6), 441–444.
- 3597 Wieder, W. R., D. M. Lawrence, R. A. Fisher, G. B. Bonan, S. J. Cheng, C. L.
3598 Goodale, A. S. Grandy, C. D. Koven, D. L. Lombardozzi, K. W. Oleson,
3599 and R. Q. Thomas (2019). Beyond static benchmarking: using experimental
3600 manipulations to evaluate land model assumptions. *Global Biogeochemical*
3601 *Cycles* 33(10), 1289–1309.
- 3602 Wright, I. J., P. B. Reich, and M. Westoby (2003). Least-cost input mixtures
3603 of water and nitrogen for photosynthesis. *The American Naturalist* 161(1),
3604 98–111.
- 3605 Wright, I. J., P. B. Reich, M. Westoby, D. D. Ackerly, Z. Baruch, F. Bongers,
3606 J. Cavender-Bares, T. Chapin, J. H. C. Cornelissen, M. Diemer, J. Flexas,
3607 E. Garnier, P. K. Groom, J. Gulias, K. Hikosaka, B. B. Lamont, T. Lee,
3608 W. Lee, C. Lusk, J. J. Midgley, M.-L. Navas, Ü. Niinemets, J. Oleksyn,
3609 N. Osada, H. Poorter, P. Poot, L. Prior, V. I. Pyankov, C. Roumet, S. C.

- 3610** Thomas, M. G. Tjoelker, E. J. Veneklaas, and R. Villar (2004). The world-
3611 wide leaf economics spectrum. *Nature* 428(6985), 821–827.
- 3612** Xu-Ri and I. C. Prentice (2017). Modelling the demand for new nitrogen fixation
3613 by terrestrial ecosystems. *Biogeosciences* 14(7), 2003–2017.
- 3614** Yahdjian, L., L. A. Gherardi, and O. E. Sala (2011). Nitrogen limitation in
3615 arid-subhumid ecosystems: A meta-analysis of fertilization studies. *Journal*
3616 *of Arid Environments* 75(8), 675–680.
- 3617** Zaehle, S., B. E. Medlyn, M. G. De Kauwe, A. P. Walker, M. C. Dietze, T. Hick-
3618 ler, Y. Luo, Y. P. Wang, B. El-Masri, P. Thornton, A. Jain, S. Wang,
3619 D. Warlind, E. Weng, W. Parton, C. M. Iversen, A. Gallet-Budynek, H. Mc-
3620 carthy, A. C. Finzi, P. J. Hanson, I. C. Prentice, R. Oren, and R. J. Norby
3621 (2014). Evaluation of 11 terrestrial carbon-nitrogen cycle models against
3622 observations from two temperate Free-Air CO₂ Enrichment studies. *New*
3623 *Phytologist* 202(3), 803–822.
- 3624** Zaehle, S., S. Sitch, B. Smith, and F. Hatterman (2005). Effects of parame-
3625 ter uncertainties on the modeling of terrestrial biosphere dynamics. *Global*
3626 *Biogeochemical Cycles* 19(3), GB3020.
- 3627** Zhu, Q., W. J. Riley, J. Tang, N. Collier, F. M. Hoffman, X. Yang, and G. Bisht
3628 (2019). Representing nitrogen, phosphorus, and carbon interactions in the
3629 E3SM land model: development and global benchmarking. *Journal of Ad-*
3630 *vances in Modeling Earth Systems* 11(7), 2238–2258.
- 3631** Ziegler, C., M. E. Dusenge, B. Nyirambangutse, E. Zibera, G. Wallin, and
3632 J. Uddling (2020). Contrasting dependencies of photosynthetic capacity on
3633 leaf nitrogen in early- and late-successional tropical montane tree species.

- 3634** *Frontiers in Plant Science* 11, 1–12.
- 3635** Ziehn, T., J. Kattge, W. Knorr, and M. Scholze (2011). Improving the pre-
3636 dictability of global CO₂ assimilation rates under climate change. *Geophys-
3637 ical Research Letters* 38(10), L10404.

3638 Appendix A: Supplemental material for "Structural carbon costs to
3639 acquire nitrogen are determined by nitrogen and light availability in
3640 two species with different nitrogen acquisition strategies"

Table A1. Summary table containing volumes of compounds used to create modified Hoagland's solutions for each soil nitrogen fertilization treatment. All volumes are expressed as milliliters per liter (mL/L)

Compound	0 ppm N	70 ppm N	210 ppm N	630 ppm N
1 M NH ₄ H ₂ PO ₄	0	0.33	1	1
2 M KNO ₃	0	0.67	2	2
2 M Ca(NO ₃) ₂	0	0.67	2	2
1 M NH ₄ NO ₃	0	0.33	1	0
8 M NH ₄ NO ₃	0	0	0	2
1 M KH ₂ PO ₄	1	0.67	0	0
1 M KCl	4	1.33	0	0
1 M CaCO ₃	4	3	0	0
2 M MgSO ₄	1	1	1	1
10% Fe-EDTA	1	1	1	1
Trace Elements	1	1	1	1

Table A2. Analysis of variance results exploring species-specific effects of light availability, nitrogen fertilization, and their interactions on the ratio of whole plant biomass to pot volume (g L⁻¹)*

	df	Coefficient	χ^2	p
<i>G. hirsutum</i>				
Intercept		0.740	-	-
Light (L)	1	-4.23E-03	189.581	<0.001
Nitrogen (N)	1	7.86E-04	17.927	<0.001
L*N	1	-6.61E-06	4.709	0.030
<i>G. max</i>				
Intercept		-0.233	-	-
Light (L)	1	-1.12E-02	69.500	<0.001
Nitrogen (N)	1	8.29E-04	40.297	<0.001
L*N	1	-8.51E-06	5.548	0.019

3641 *Significance determined using Wald's χ^2 tests ($p=0.05$). *P*-values less than 0.05
3642 are in bold and *p*-values between 0.05 and 0.1 are italicized. Negative coefficients
3643 for light treatments indicate a positive effect of increasing light availability on
3644 all response variables, as light availability is treated as percent shade cover in all
3645 linear mixed-effects models.

Table A3. Slopes of the regression line describing the relationship between each dependent variable and nitrogen fertilization at each light level*

Shade cover	Slope
<i>G. hirsutum</i>	
0%	8.29E-04^a
30%	5.74E-04^a
50%	4.03E-04^a
80%	1.48E-04 ^a
<i>G. max</i>	
0%	7.86E-04
30%	5.87E-04
50%	4.55E-04
80%	<i>2.57E-05</i>

3646 *Slopes represent estimated marginal mean slopes from linear mixed-effects models described in the Methods. Slopes
3647 were calculated using the ‘emmeans’ R package (Lenth 2019). Superscripts indicate slopes fit to natural-log (^a) or
3648 square root (^b) transformed data. Slopes statistically different from zero (Tukey: $p < 0.05$) are indicated in bold.
3649 Marginally significant slopes (Tukey: $0.05 < p < 0.1$) are italicized.

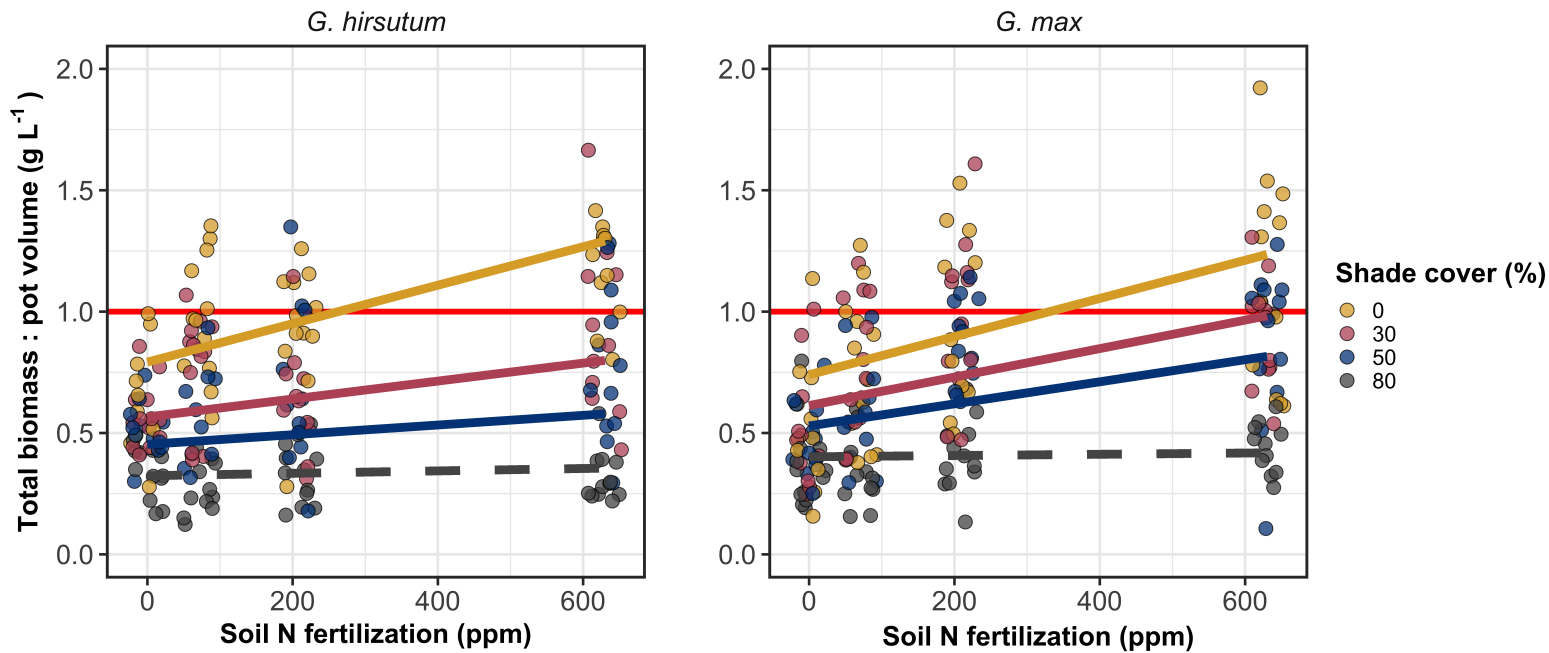


Figure A1. Effects of shade cover and nitrogen fertilization on the ratio of plant biomass to rooting volume in *G. hirsutum* (left panel) and *G. max* (right panel). The red horizontal line indicates the recommended 1 g L^{-1} threshold for BVR recommended by Poorter et al. (2012) to avoid pot size-induced growth limitation. Nitrogen fertilization treatments are represented on the x-axis. Shade cover treatments are represented through colored points and trendlines. Points are jittered for visibility. Yellow points and trendlines represent the 0% shade cover treatment, blue points and trendlines represent the 30% shade cover treatment, green points and trendlines represent the 50% shade cover treatment, and purple points and trendlines represent the 80% shade cover treatment. Solid trendlines indicate slopes that are significantly different from zero (Tukey: $p < 0.05$), while dashed trendlines indicate slopes that are not statistically different from zero.

3650 Appendix B: Supplemental material for "Soil nitrogen availability
3651 modifies leaf nitrogen economies in mature temperate deciduous
3652 forests: a direct test of photosynthetic least-cost theory"

Table B1. Sample sizes of each species, abbreviated by their USDA NRCS PLANTS database code, within each plot at each site*

	ACRU	ACSA	FAGR	FRAM	QURU	N_{plot}
Bald Hill						
+N; +S	0	6	1	0	1	8
+N; -S	1	2	2	0	1	6
-N; +S	2	2	0	0	2	6
-N; -S	2	3	3	0	2	10
Carter Creek						
+N; +S	0	6	1	2	0	9
+N; -S	0	4	0	2	0	6
-N; +S	0	5	1	4	0	10
-N; -S	0	7	0	0	0	7
Mount Pleasant						
+N; +S	3	2	1	0	3	9
+N; -S	0	5	4	1	0	10
-N; +S	1	2	4	0	0	7
-N; -S	3	3	1	2	1	10
N_{spp}	12	47	18	11	10	98

3653 *Plots within each site are represented based on nitrogen and sulfur addition
3654 status. The final column on the right depicts total sample size per plot in each
3655 site (N_{plot}) and the final row on the bottom represents cumulative species sample
3656 size across all plots and all sites (N_{spp}). Key: ACRU = *A. rubrum*; ACSA = *A.*
3657 *saccharum*; FAGR = *F. grandifolia*; FRAM = *F. americana*; QURU = *Q. rubra*

Table B2. Analysis of variance results exploring the linear effect of leaf temperature on net photosynthesis rate (A_{net} ; $\mu\text{mol m}^{-2} \text{s}^{-1}$) and stomatal conductance (g_{sw} ; $\mu\text{mol m}^{-2} \text{s}^{-1}$) measured at $400 \mu\text{mol mol}^{-1} \text{CO}_2$

	df	A_{net}		g_{sw}	
		χ^2	p	χ^2	p
Leaf temperature	1	1.287	0.257	1.716	0.190

3658 *Results detail linear mixed effects model where temperature was regressed against
3659 net photosynthesis or stomatal conductance, with site and species designated as
3660 random intercept terms. Significance was determined using Type II Wald χ^2 tests
3661 ($\alpha=0.05$).

Table B3. Second order log-polynomial regression coefficients that described the effect of leaf temperature on net photosynthesis (A_{net} ; $\mu\text{mol m}^{-2} \text{s}^{-1}$) and stomatal conductance (g_s ; $\mu\text{mol m}^{-2} \text{s}^{-1}$) measured at 400 $\mu\text{mol mol}^{-1} \text{CO}_2$ *

	a	b	c
A_{net}	9.422	-0.573	0.010
g_s	-0.170	-0.186	0.003

3662 *Net photosynthesis and stomatal conductance values were fit to the log-polynomial
3663 equation $\log(y) = a + bx + cx^2$, where x is leaf temperature in °C.

Table B4. Mean, standard error, and 95% confidence interval ranges of soil nitrogen availability estimates across all measured plots. All units are expressed as $\mu\text{g N g}^{-1}$ resin d^{-1}

Site	Treatment	Mean	SE	Lower 95% CI	Upper 95% CI
Bald Hill	Ammonium sulfate	27.11	6.14	15.08	39.13
Bald Hill	Control	14.41	5.02	4.56	24.26
Bald Hill	Sodium nitrate	20.65	3.15	14.46	26.83
Bald Hill	Sulfur	6.33	2.19	2.04	10.62
Carter Creek	Ammonium sulfate	26.94	5.36	16.43	37.44
Carter Creek	Control	19.87	1.92	16.10	23.64
Carter Creek	Sodium nitrate	15.51	4.16	7.36	23.65
Carter Creek	Sulfur	5.50	1.40	2.75	8.25
Mount Pleasant	Ammonium sulfate	8.02	2.31	3.49	12.56
Mount Pleasant	Control	2.00	0.57	0.89	3.11
Mount Pleasant	Sodium nitrate	2.52	0.68	1.19	3.85
Mount Pleasant	Sulfur	2.42	0.39	1.66	3.17

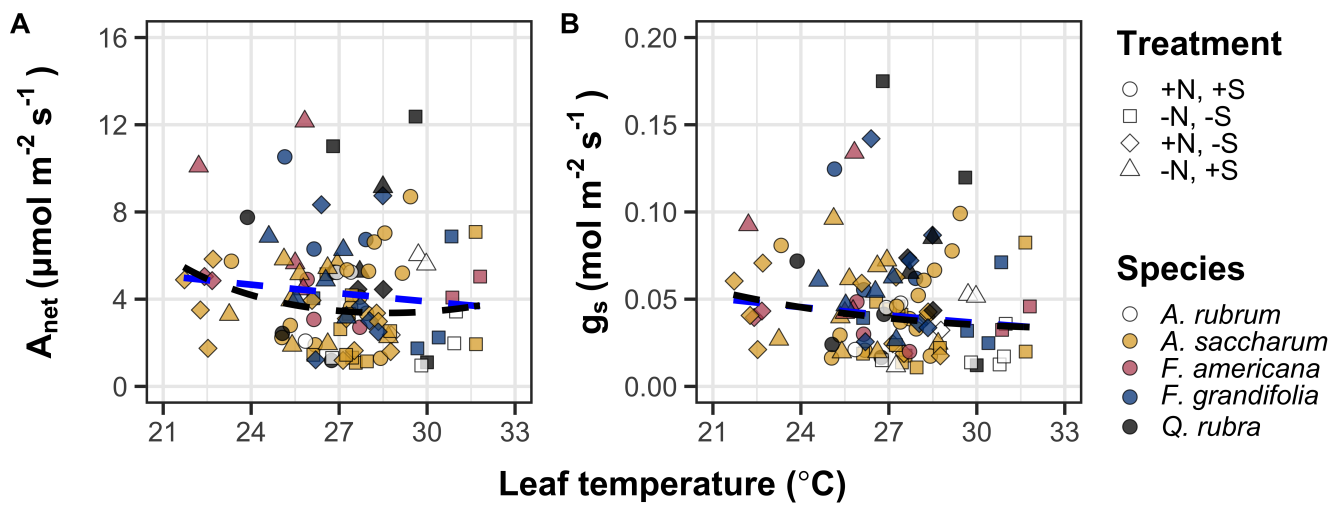


Figure B1. Effects of leaf temperature on net photosynthesis rate (A) and stomatal conductance (B) values when measured at $400 \mu\text{mol mol}^{-1} \text{CO}_2$. Leaf temperature is represented on the x-axis, while species are represented as colored points. Colored points and shapes are as explained in Figure 3.1. The dashed blue trendline describes the linear relationship between leaf temperature and each response variable, while the dashed black trendline describes the same relationship with a log-polynomial regression equation.

**3664 Appendix C: Supplemental material for "The relative cost of resource
3665 use for photosynthesis drives variance in leaf nitrogen content across a
3666 climate and soil resource availability gradient"**

3667 C.1 Calculations for soil water holding capacity

3668 Water holding capacity (θ_{WHC} ; mm) was calculated as a function of the volumetric
3669 soil water storage at field capacity (W_{FC} ; m³ m⁻³), and the volumetric soil water
3670 storage at wilting point (W_{PWP} ; m³ m⁻³):

$$\theta_{WHC} = (W_{FC} - W_{PWP})(1 - f_{gravel}) * \min(z_{bedrock}, z_{max}) \quad (\text{C4.1})$$

3671 where f_{gravel} (%) is the fraction of gravel content in soil, $z_{bedrock}$ (mm) is the
3672 distance to bedrock, and z_{max} (mm) is the maximum allowable distance to bedrock,
3673 set to 2000mm. W_{FC} is calculated as:

$$\theta_{FC} = k_{fc} + (1.283 * (k_{fc})^2 - 0.374 * k_{fc} - 0.015) \quad (\text{C4.2})$$

3674 where

$$\begin{aligned} k_{fc} = & -0.251 * f_{sand} + 0.195 * f_{clay} + 0.011 * f_{OM} \\ & + 0.006 * (f_{sand} * f_{OM}) - 0.027 * (f_{clay} \\ & * f_{OM}) + 0.452 * (f_{sand} * f_{clay}) + 0.299 \end{aligned} \quad (\text{C4.3})$$

3675 W_{PWP} is calculated as:

$$W_{PWP} = k_{pwp} + (0.14 * k_{pwp} - 0.02) \quad (\text{C4.4})$$

3676 where

$$\begin{aligned} k_{pwp} = & -0.024 * f_{sand} + 0.487 * f_{clay} + 0.006 * f_{OM} \\ & + 0.005 * (f_{sand} * f_{OM}) - 0.013 * (f_{clay} \\ & * f_{OM}) + 0.068 * (f_{sand} * f_{clay}) + 0.031 \end{aligned} \quad (\text{C4.5})$$

3677 In Equations C4.4 and C4.5, f_{sand} (%) is the fraction of sand content in soil

3678 (%), f_{clay} (%) is the fraction of clay content in soil (%), and f_{OM} is the fraction of

3679 organic matter in soil (%). Organic matter in the soil was calculated by converting

3680 soil organic carbon data extracted from SoilGrids 2.0 to soil organic matter using

3681 the van Bemmelen factor (1.724 conversion factor).

Table C1. List of sampled species and their plant functional group assignment

Symbol	Species	Photo. pathway	Growth duration	Growth habit	N-fixer?	Plant functional group	Number sampled
ACAN11	<i>Acaciella angustissima</i>	c3	perennial	forb	yes	c3_legume	3
AMAR2	<i>Ambrosia artemisiifolia</i>	c3	annual	forb	no	c3_nonlegume	25
AMPS	<i>Ambrosia psilostachya</i>	c3	perennial	forb	no	c3_nonlegume	32
ARAL3	<i>Argemone albiflora</i>	c3	annual	forb	no	c3_nonlegume	3
ARPU9	<i>Aristida purpurea</i>	c4	perennial	graminoid	no	c4_nonlegume	2
ASAS	<i>Asclepias asperula</i>	c3	perennial	forb	no	c3_nonlegume	3
ASLA4	<i>Asclepias latifolia</i>	c3	perennial	forb	no	c3_nonlegume	3
ASSY	<i>Asclepias syriaca</i>	c3	perennial	forb	no	c3_nonlegume	18
BASA	<i>Baccharis salicina</i>	c3	perennial	shrub	no	c3_nonlegume	3
BOIS	<i>Bothriochloa ischaemum</i>	c4	perennial	graminoid	no	c4_nonlegume	6
BOSA	<i>Bothriochloa saccharoides</i>	c4	perennial	graminoid	no	c4_nonlegume	6
CAAM2	<i>Callicarpa americana</i>	c3	perennial	shrub	no	c3_nonlegume	3
CAPL3	<i>Carex planostachys</i>	c4	perennial	graminoid	no	c4_nonlegume	3
CAREX	<i>Carex</i> spp.	c4	perennial	graminoid	no	c4_nonlegume	16
CHFE3	<i>Chamaesyce fendleri</i>	c3	perennial	forb	no	c3_nonlegume	2
CHPI8	<i>Chrysopsis pilosa</i>	c3	annual	forb	no	c3_nonlegume	3
COCO13	<i>Conoclinium coelestinum</i>	c3	perennial	forb	no	c3_nonlegume	3
COER	<i>Commelina erecta</i>	c3	perennial	forb	no	c3_nonlegume	3
CRGLL	<i>Croton glandulosus</i>	c3	annual	forb	no	c3_nonlegume	22
CYDA	<i>Cynodon dactylon</i>	c4	perennial	graminoid	no	c4_nonlegume	15
DATE3	<i>Dasyllirion texanum</i>	c3	perennial	shrub	no	c3_nonlegume	3
DIAN	<i>Dichanthium annulatum</i>	c4	perennial	graminoid	no	c4_nonlegume	8
ENPE4	<i>Engelmannia peristenia</i>	c3	perennial	forb	no	c3_nonlegume	6
EUMA8	<i>Euphorbia marginata</i>	c3	annual	forb	no	c3_nonlegume	6
GAPU	<i>Gaillardia pulchella</i>	c3	annual	forb	no	c3_nonlegume	16
GLGO	<i>Glandularia gooddingii</i>	c3	perennial	forb	no	c3_nonlegume	2
HEAN3	<i>Helianthus annuus</i>	c3	annual	forb	no	c3_nonlegume	6

Table C2. List of sampled species and their plant functional group assignment (cont.)

Symbol	Species	Photo. pathway	Growth duration	Growth habit	N-fixer?	Plant functional group	Number sampled
HECA8	<i>Heterotheca canescens</i>	c3	perennial	forb	no	c3_nonlegume	2
HETE3	<i>Heliotropium tenellum</i>	c3	annual	forb	no	c3_nonlegume	3
IVAX	<i>Iva axillaris</i>	c3	perennial	forb	no	c3_nonlegume	4
LIAT	<i>Lilaeopsis attenuata</i>	c3	perennial	forb	no	c3_nonlegume	3
LIPU	<i>Liatris punctata</i>	c3	perennial	forb	no	c3_nonlegume	3
LOPE	<i>Lolium perenne</i>	c3	perennial	graminoid	no	c3_nonlegume	9
MIQU2	<i>Mimosa quadrivalvis</i>	c3	perennial	forb	yes	c3_legume	15
NALE3	<i>Nassella leucotricha</i>	c3	perennial	graminoid	no	c3_nonlegume	19
OECU2	<i>Oenothera curtiflora</i>	c3	annual	forb	no	c3_nonlegume	3
OENOT	<i>Oenothera</i> spp.	c3	annual	forb	no	c3_nonlegume	1
PAVI2	<i>Panicum virgatum</i>	c4	perennial	graminoid	no	c4_nonlegume	12
PRGL2	<i>Prosopis glandulosa</i>	c3	perennial	shrub	yes	c3_legume	33
QUHA3	<i>Quercus harvardii</i>	c3	perennial	shrub	no	c3_nonlegume	3
QUMO	<i>Quercus mohriana</i>	c3	perennial	shrub	no	c3_nonlegume	1
RACO3	<i>Ratibida columnifera</i>	c3	perennial	forb	no	c3_nonlegume	40
RHAM	<i>Rhamnus</i> spp.	c3	perennial	shrub	yes	c3_legume	1
RHSET	<i>Rhynchosia senna</i>	c3	perennial	forb	yes	c3_legume	1
RUHI2	<i>Rudbeckia hirta</i>	c3	perennial	forb	no	c3_nonlegume	3
RUNU	<i>Ruellia nudiflora</i>	c3	perennial	forb	no	c3_nonlegume	15
RUTR	<i>Rubus trivialis</i>	c3	perennial	vine	no	c3_nonlegume	3
SAFA2	<i>Salvia farinacea</i>	c3	perennial	forb	no	c3_nonlegume	7
SCHIZ4	<i>Schizachyrium</i> spp.	c4	perennial	graminoid	no	c4_nonlegume	8
SCSC	<i>Schizachyrium scoparium</i>	c4	perennial	graminoid	no	c4_nonlegume	3
SODI	<i>Solanum dimidiatum</i>	c3	perennial	forb	no	c3_nonlegume	1
SOEL	<i>Solanum elaeagnifolium</i>	c3	perennial	forb	no	c3_nonlegume	53
SOHA	<i>Sorghum halapense</i>	c4	perennial	graminoid	no	c4_nonlegume	38
STTE3	<i>Stillingia texana</i>	c3	perennial	forb	no	c3_nonlegume	3

Table C3. List of sampled species and their plant functional group assignment (cont.)

Symbol	Species	Photo. pathway	Growth duration	Growth habit	N-fixer?	Plant functional group	Number sampled
VEOC	<i>Verbesina occidentalis</i>	c3	perennial	forb	no	c3_nonlegume	3
VEST	<i>Verbena stricta</i>	c3	perennial	forb	no	c3_nonlegume	3
WEAC	<i>Wedelia acapulcensis</i>	c3	perennial	shrub	no	c3_nonlegume	6

Table C4. Model selection results for soil moisture and vapor pressure deficit. Soil moisture was used in a bivariate regression against log-transformed β , while vapor pressure deficit was used in bivariate regressions against leaf $C_l:C_a$

Day	Soil moisture		VPD	
	AICc	RMSE	AICc	RMSE
1	1431.77	0.8400	-772.71	0.0853
2	1431.76	0.8400	-775.47	0.0849
3	1431.78	0.8400	-770.86	0.0854
4	1431.79	0.8401	-793.49	0.0839
5	1431.79	0.8401	-771.66	0.0853
6	1431.78	0.8401	-771.66	0.0853
7	1431.78	0.8401	-771.05	0.0854
8	1431.76	0.8401	-770.94	0.0854
9	1431.75	0.8401	-770.11	0.0854
10	1431.74	0.8401	-770.08	0.0855
15	1431.54	0.8401	-768.64	0.0856
20	1431.40	0.8401	-769.77	0.0855
30	1431.23	0.8400	-772.18	0.0853
60	1429.84	0.8391	-779.06	0.0848
90	1429.14	0.8385	-773.99	0.0852

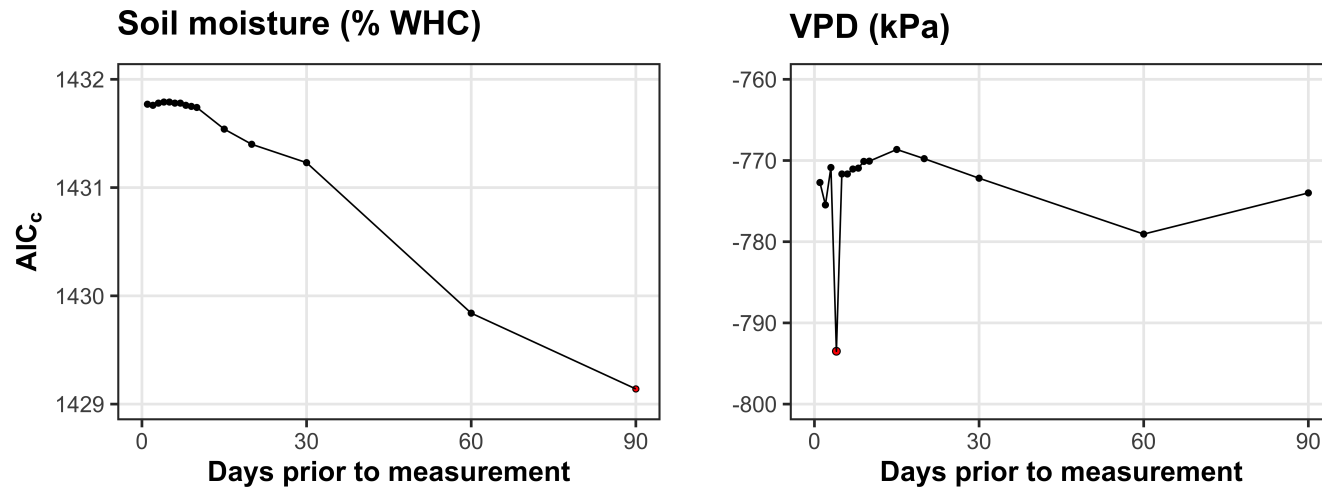


Figure C1. Model selection results exploring relevant timescales for soil moisture (left panel) and vapor pressure deficit (right panel). The x-axis indicates the number of days before each site visit and the y-axis notes the corrected Akaike Information Criterion value. The timescale with the lowest AICc value, and therefore most relevant timescale to include in statistical models, is noted as a red point.

**3682 Appendix D: Supplemental material for "Optimal resource investment
 3683 to photosynthetic capacity maximizes nutrient allocation to whole
 3684 plant growth under elevated CO₂"**

Table D1. Summary table containing volumes of compounds used to create modified Hoagland's solutions for each soil nitrogen fertilization treatment. All volumes are expressed as milliliters per liter (mL/L)

Compound	0 ppm N	35 ppm N	70 ppm N	105 ppm N	140 ppm N
1 M NH ₄ H ₂ PO ₄	0	0.165	0.33	0.5	0.67
2 M KNO ₃	0	0.335	0.67	1	1.33
2 M Ca(NO ₃) ₂	0	0.335	0.67	1	1.33
1 M NH ₄ NO ₃	0	0.165	0.33	0.5	0.67
8 M NH ₄ NO ₃	0	0	0	0	0
1 M KH ₂ PO ₄	1	0.85	0.67	0.5	0.33
1 M KCl	3	2.45	2	1.5	1
1 M CaCO ₃	4	3.33	2.67	2	1.33
2 M MgSO ₄	1	1	1	1	1
10% Fe-EDTA	1	1	1	1	1
Trace elements	1	1	1	1	1

Compound	210 ppm N	280 ppm N	350 ppm N	630 ppm N
1 M NH ₄ H ₂ PO ₄	1	1	1	1
2 M KNO ₃	2	2	2	2
2 M Ca(NO ₃) ₂	2	2	2	2
1 M NH ₄ NO ₃	1	3.5	0	0
8 M NH ₄ NO ₃	0	0	0.75	2
1 M KH ₂ PO ₄	0	0	0	0
1 M KCl	0	0	0	0
1 M CaCO ₃	0	0	0	0
2 M MgSO ₄	1	1	1	1
10% Fe-EDTA	1	1	1	1
Trace elements	1	1	1	1

Table D2. Summary of the daily growth chamber growing condition program

Time	Air temperature (°C)	Light (%)
09:00	21	25
09:45		50
10:30	25	75
11:15		100
22:45	21	75
23:30		50
00:15	17	25
01:00		0

Table D3. Effects of CO₂, fertilization, and inoculation on whole plant biomass: pot volume (BVR; g L⁻¹)*

	df	Coefficient	χ^2	p
(Intercept)	-	1.33E-01	-	-
CO ₂	1	1.53E-01	146.004	<0.001
Inoculation (I)	1	4.19E-01	19.320	<0.001
Fertilization (N)	1	1.90E-03	279.387	<0.001
CO ₂ *I	1	1.03E-01	0.007	0.934
CO ₂ *N	1	2.44E-03	49.725	<0.001
I*N	1	-6.90E-04	9.006	0.003
CO ₂ *I*N	1	-4.95E-04	0.640	0.424

3685 *Significance determined using Type II Wald χ^2 tests ($\alpha=0.05$). P-values less
3686 than 0.05 are in bold. Key: df=degrees of freedom; χ^2 =Wald Type II chi-square
3687 test statistic.

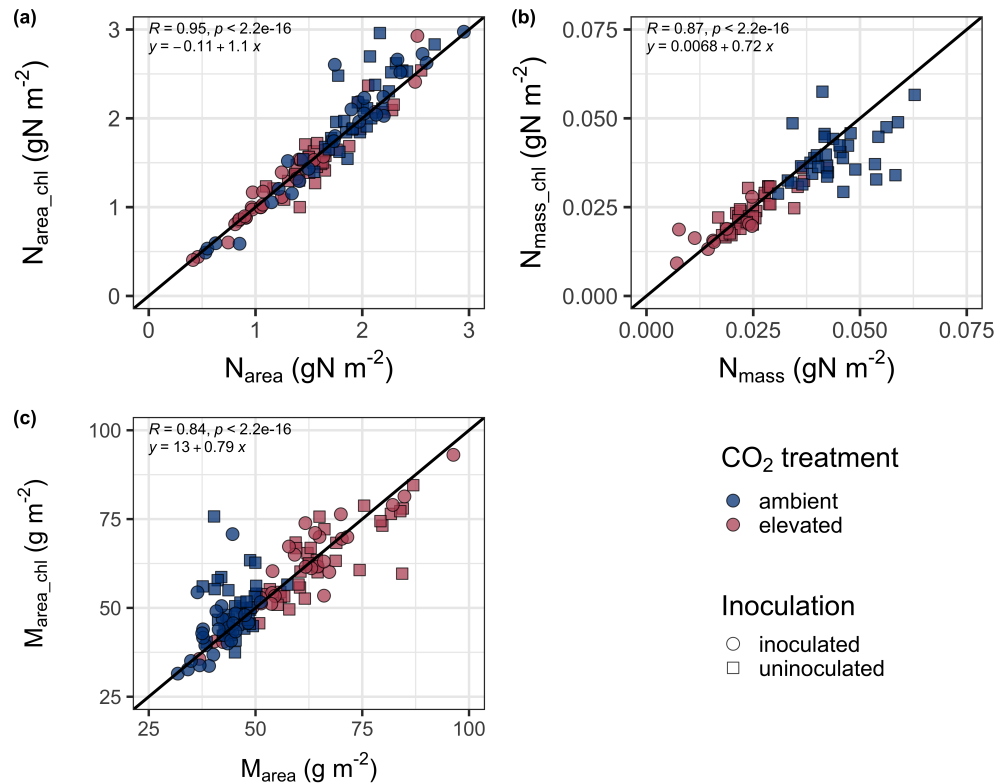


Figure D1. Relationships between area-based leaf nitrogen content (a), mass-based leaf nitrogen content (b), and leaf mass per unit leaf area (c) measured on the focal leaf used to generate A_{net}/C_i curves (x-axis) and leaf nitrogen content measured on the leaf used for chlorophyll extractions (y-axis). Blue points refer to leaves grown under ambient CO₂ and red points refer leaves grown under elevated CO₂. Square points indicate uninoculated pots and circular points indicate inoculated pots. Pearson's correlation coefficient, associated *p*-values, and the line of the regression line that described each bivariate are included in the top left corner of each plot. The solid black line visualizes the trend given a 1:1 bivariate relationship.

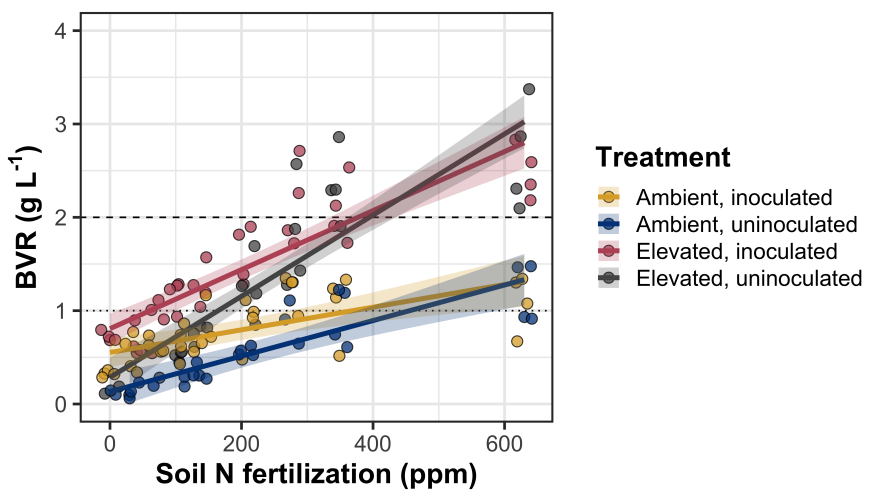


Figure D2. Effects of CO₂, fertilization, and inoculation on the ratio of whole plant biomass to pot volume. Soil nitrogen fertilization is represented on the x-axis in all panels. Yellow points and trendlines indicate inoculated individuals grown under ambient CO₂, blue points and trendlines indicate uninoculated individuals grown under ambient CO₂, red points and trendlines indicate inoculated individuals grown under elevated CO₂, and grey points indicate uninoculated individuals grown under elevated CO₂. Solid trendlines indicate regression slopes that are different from zero ($p<0.05$). The dotted horizontal line indicates the point where biomass:pot volume exceeds 1 g L⁻¹, and the dashed line indicates the point where biomass:pot volume exceeds 2 g L⁻¹.